I O N O S P H E R I C S T U D I E S

O F

T H E S O L A R E C L I P S E

25 D E C E M B E R, 1 9 5 4

Being a Thesis for the degree of
Doctor of Philosophy of Rhodes University
by

M. W. McELHINNY, B.Sc. (Hons)(Rhodes)

September, 1958

TO M

who suffered through most of it.

CONTENTS

Acknowledgements.

It is a pleasure here to acknowledge the help and assistance of Dr. M. E. Szendrei, who directed the initial part of this work during 1954 and 1955. Part I of this thesis was done entirely in collaboration with Dr. Szendrei. To him I must express my sincere thanks.

It will be noted that the ionosphere sounder was already partly completed but construction was abandoned several years before the start of this work in 1954. My thanks are due to Dr. J. W. King who was mainly responsible for this initial work.

The author wishes to thank Mr. A. P. Dale, B.Sc., who helped with some running repairs on the sounder, and Mr. A. R. Scanlen for his advice and the construction of the mechanical parts of the switching system.

Thanks are also due to:-

Dr. A. K. Das of the Astrophysical Observatory, Kodaikanal, India, for supplying sketches of the sun from spectroheliogram and other observations.

Mr. C. M. Minnis of the D.S.I.R. Radio Research Station, Slough, England for forwarding the coronal data.

Mr. A. M. van Wyk of the Magnetic Observatory, Hermanus, for sending the magnetic data for the period of the measurements.

and to:-

The South African Council for Scientific and Industrial Research, for a substantial grant towards the building of the automatic ionosphere sounder and for a maintenance bursary during 1954 and 1955.

The author wishes to tender his thanks and appreciation to Professor J. A. Gledhill, who directed this work from afar since 1955, for his advice and encouragements, and for supplying the scaled values of the critical frequencies during the eclipse at Cape Town and Johannesburg.

Finally, I should like to thank my wife, who has had to perservere with the typing of the thesis.

Publications.

As a result of this work, the following papers have been published or read at various conferences.

1. "The Ionospheric Solar Eclipse of 25 December, 1954" by M. E. Szendrei and M. W. McElhinny.
(Paper read at conference of South African Association for the Advance of Science, Grahamstown, July 1955).

2. "Preliminary results of the ionospheric solar eclipse, 25 December, 1954". by M. E. Szendrei and M. W. McElhinny.
(J. Atmos. Terr. Phys., 8, 108, 1956)

3. "The Behaviour of the E_1 layer during the solar eclipse of 25 December, 1954". by M. E. Szendrei and M. W. McElhinny. (Solar Eclipses and the Ionosphere, p.74, Pergamon Press, London).

4. "Recombination and attachment in the F_1 and F_2 layers during the solar eclipse of 25 December, 1954", by M. E. Szendrei and M. W. McElhinny. (J. Atmos. Terr. Phys., 9, 118, 1956).

5. "Some further analyses of E layer measurements in South Africa during the solar eclipse of 25 December, 1954" by M. W. McElhinny. (Paper read at conference of South African Institute of Physics, July, 1958). (Also in press J. Atmos. Terr. Phys.)

HISTORICAL OUTLINE

The structure of the ionosphere.

Since the Kennelly-Heaviside hypothesis in 1902 of the existence of a partially conducting layer in the upper atmosphere was proved to be true by the experiments of APPLETON and BARNETT (1925) and BREIT and TUVE (1926), this region has become known as the ionosphere.

The ionosphere was soon discovered to consist of, not one but several layers (Fig. 1)

(i) A layer at a height of just over 100 km. called the E layer.

(ii) A layer at a height of approximately 300km. called the F_2 layer.

(iii) A layer at a height of approximately 200 km. called the F_1 layer; this layer differs from the other two in that it is only present during the day time in Summer.

(iv) Occasional intense reflections from a height of about 100 km. are found - these cannot be attributed to the normal E layer and have received the name "Sporadic E".

The presence of two E layers (E_1 and E_2) has been suggested by HALLIDAY (1936) and BEST and RATCLIFFE (1938), but until recently most workers still seem to attribute these

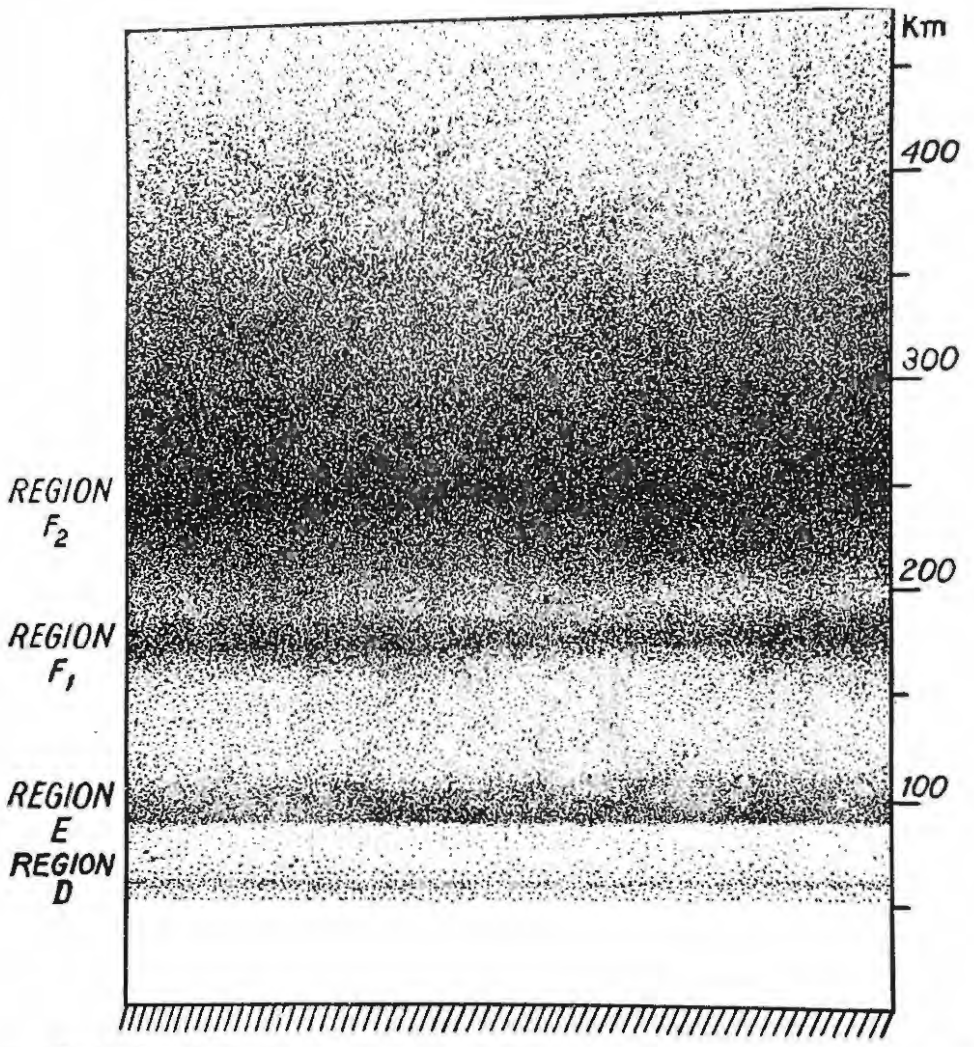

FIG. 1. Ionized regions of the upper atmosphere. The relative density of ionization is roughly indicated by the depth of shading. During daytime another region of ionization E_2 is sometimes formed immediately above E; this is not shown. Region D is mainly an absorbing region. At night this region disappears and also F_1 and F_2 coalesce to form a single Region F.

reflections to Sporadic E. Recent measurement by rockets of the electron density at E layer heights still do not confirm whether such bifurcation exists in the E region. The diurnal and seasonal variations of the first three layers indicate that the sun is the chief agent in their production. It is generally agreed that these layers consist of ionised molecules or atoms and free electrons produced by radiation from the sun.

The origin of Sporadic E ionisation is still obscure, but it is thought that these sudden increases in ionisation which occur at E layer heights are due to passing meteors. Recently it has also been suggested by SEDDON, PICKAR and JACKSON (1954) from rocket measurements that Sporadic E might be due to a steep electron density gradient above the E layer.

Propagation of electro-magnetic waves in the ionosphere.

APPLETON (1932) has worked out the theory of the propagation and reflection of electro-magnetic waves in an ionised layer. The theory shows that reflection of an electro-magnetic wave will take place provided that the electron density is sufficiently high. The higher the electron density, the higher the frequency that will be reflected. The presence of the free ions and electrons has the effect of reducing the effective refractive index of the medium. If the electron density is sufficiently high, the refractive index may be reduced to zero, which is the condition for the reflection of an incident electro-magnetic wave. Depending on the maximum electron

density of a layer, there will naturally be a certain maximum frequency which can be reflected - this is called the critical frequency. The layer will reflect all frequencies below the critical and none above it.

Owing to the fact that the electro-magnetic wave is being propagated in the earth's magnetic field, the wave is split into two components elliptically polarised with opposite rotation. Each of the polarised components has its own critical frequency and for the ordinary waves this critical frequency f^o is related to the maximum electron density, N, by the formula:

$$N = \frac{\pi m}{e} (f^o)^2 \qquad \ldots\ (1)$$

where 'm' and 'e' are the electronic mass and charge in e.s.u., and 'f^o' is the critical frequency when measured at vertical incidence. Substituting the numerical values for $e = 4.80 \times 10^{-11}$ e.s.u. and $e/m = 5.27 \times 10^{17}$ e.s.u., and expressing f^o in Mc/sec. this becomes:

$$N = 1.24 \times 10^4 (f^o)^2 \qquad \ldots\ (2)$$

The critical frequency for the extraordinary wave f^x is found to differ from f^o by an amount which depends on the strength and direction of the magnetic field. Since at any given place these are practically constant, the separation between the two critical frequencies is also constant.

Considerable discussion has taken place by TONKS (1933), NORTON (1933), HARTREE (1933), DARWIN (1934), (1943) and RATCLIFFE (1939) on the advisability of applying the Lorentz

theory of electrons to this theory. If this is done the general results of Appleton's theory are not altered but the numerical values obtained differ by as much as 50% in some cases. Recent measurements by rockets of the electron density up to 220 km. (SEDDON, PICKAR and JACKSON, 1954) indicate that the Lorentz term can in all probability be neglected. In view of this, the Lorentz term has not been included in the present work.

Methods of determining the apparent or virtual height of the layers have been developed by APPLETON and BARNETT (1925) BREIT and TUVE (1926), and APPLETON and RATCLIFFE (1927), but these will be discussed later.

Appleton's theory states that the presence of the free ions and electrons has the effect of reducing the effective refractive index of the medium, and hence the group velocity (i.e. the velocity with which the energy is propagated). In calculating the apparent height of the layer from time delay measurements, it is assumed that the energy is propagated everywhere with the velocity of light; thus the apparent height is always greater than the true height by an amount depending on the density of ionisation at all points along the path. This apparent height so measured is normally termed the "virtual height".

Methods of deducing the true height from the virtual height have been proposed by APPLETON (1930) (1937), MURRAY

and HOAG (1937), BOOKER and SEATON (1940), MANNING (1947) and KELSO (1952). Up to the present wide scale deductions of true heights from virtual heights have not been undertaken and most workers have confined their attention to virtual height readings. This is mainly due to the long and time consuming procedure involved.

Ionosphere stations have been in operation over almost all parts of the world for the past 25 years. The diurnal and seasonal variations of the maximum electron density and virtual height of the layers are now well established.

The formation of the ionised layers.

The basic theory of layer formation under the action of the sun's radiation is that of CHAPMAN (1931). This theory has many simplifying assumptions, which are probably not true for the conditions prevailing in the ionosphere. It has, however, served as an important basis for the theoretical study of the formation of the ionised layers. Both the E and F_1 layers approximate fairly closely to "Chapman" layers.

From the regular observations made on the E and F_1 layers it is noted that their ionisation follows the rise and fall of the sun very closely. It is thus natural to assume that ultra-violet radiation is the ionising agent for these two layers. The morphology of the F_2 region, however, exhibits many complexities and anomalies in time and space which cannot be accounted for by simple Chapman theory.

It has also been suggested by CHAPMAN (1932) that the ionised layers might be produced by neutral particles emitted from the sun with a limiting velocity of 1600 km/sec. Various factors have been introduced to account for the observed variations of F_2 ionisations. GLEDHILL and SZENDREI (1950) and NICOLET (1951) considered an atmosphere with a linear temperature gradient rejecting Chapman's assumption of an isothermal atmosphere. It was considered that the departure from the Chapman theory was due to expansion due to heating. The drift theory of MARTYN (1947 a, b) has received increasing attention in the post-war years. According to this theory, the abnormal daily, seasonal and latitude variations of f^0F_2 and of the maximum height of F_2 are due to the polarisation S (electrostatic) field, associated with the production of the current in the "dynamo" region of the ionosphere responsible for the observed magnetic variations on both magnetically "quiet" and magnetically "disturbed" days.

RATCLIFFE (1951) has recently evaluated $\int Ndh$, thus determining the total number of electrons in a vertical column of one square centimetre through the F_2 region below its maximum. In this way it was possible to eliminate any effect of expansion or movements. He showed that the total number of electrons calculated this way behaved in quite a regular manner with respect to the sun. This provided

support for the ultra-violet origin of the F_2 layer.

Early measurements made during solar eclipses.

Information as to the controlling effect of the sun's radiation on the ionised layers can be obtained by observing the changes in ionisation produced by a solar eclipse.

Radio measurements made during solar eclipses as early as 1925 and 1927 established that appreciable effects were produced within those regions which were responsible for long distance radio transmission (i.e. the ionosphere). The Breit and Tuve pulse or echo-sounding technique, which could determine changes produced within the ionosphere was not available until the total solar eclipse of August 31, 1932. The study of ionisation changes during an eclipse afforded an ideal opportunity for testing the two hypotheses regarding the origin of the ionospheric layers, namely as to whether ultra-violet radiation or neutral corpuscles were the ionising agent. The eclipse for corpuscles - ("corpuscular eclipse") occurs several hours before the optical or ultra-violet eclipse.

During the 1932 eclipse extensive observations were made in America. Marked decreases in the ionisation of the E and F_1 layers were observed, coinciding with the time of the optical eclipse. This provided evidence for the ultra-violet origin of these two layers. No positive evidence at all was obtained that any change in ionisation was produced in the

F_2 region. Further measurements were made during subsequent eclipses in 1935, 1936, 1937 and during the partial eclipse of April 7, 1940. Further and conclusive evidence was obtained during these eclipses in favour of the ultra-violet origin of the E and F_1 layers. The observations also showed that the ionisation changes were closely in equilibrium with the source. Uncertainty still prevailed whether solar ultra-violet radiation or corpuscles or both were active in the formation of the F_2 region.

The interpretation of eclipse effects in the F_2 region has been by no means an easy task. During the middle part of the day large and irregular fluctuations are likely to occur. Thus many observers (KIRBY, GILLILAND and JUDSON, 1935, SCHAFER and GOODALL, 1936) have been forced to admit that what appeared to have been an eclipse effect in the F_2 region might just as well have been an everyday fluctuation. In addition, it is well known that increased magnetic activity affects the ionised layers, particularly the F_2 layer. The eclipse of June 19, 1936 was accompanied by a severe magnetic storm. KIRBY et al (1936), NAISMITH (1937) and other observers were thus unable to decide whether the observed effects were due to the eclipse or the magnetic storm.

The advent of the Second World War prevented large numbers of readings being taken during eclipses until 1945. However, a total eclipse of the sun occured on October,1, 1940

over parts of Brazil and South Africa. A party under GILLILAND (1942) made observations in Brazil, and three parties under HIGGS (1942), PIERCE (1948) and HALLIDAY (PIERCE, HIGGS and HALLIDAY, 1940a, b, 1942) undertook readings in South Africa. These three parties in South Africa were placed some distance apart along the belt of totality. Although Higgs was not sure that there was an eclipse effect on the F_2, comparing with Pierce's results, he states that any eclipse effect was certainly an ultra-violet effect and not corpuscular.

Now that it had been established that ultra-violet radiation was at least responsible for the E and F_1 layers, it was interesting to see whether this radiation was emitted uniformly from the sun's disc. From the known relationship between radio fade-outs and chromospheric erruptions, local and important "hot spots" are known to exist at certain times; but the regular behaviour of the E region from day to day, in contrast with the much bigger variations, for example in the areas of bright hydrogen patches visible on the sun, suggest that these locally enriched areas are of only temporary importance. The fact that Higgs and Pierce were so placed along the belt of totality was of particular use in determining whether there was any such non-uniformity in the radiation from the solar disc. It appeared that the radiation responsible for the E region was not emitted uniformly from the sun's disc, but was coming at least mainly from groups of calcium flocculi.

Large groups of observers took observations in Scandinavia during the eclipse of July 9, 1945. RYDBECK (1946) found a correlation with radiation emitted from hydrogen faculae. Later WALDMEIER (1947) showed that in fact a better fit to Rydbeck's readings could be obtained by correlating with the intensities of the 5303A^{o} coronal radiation. Since the main emitting regions of coronal radiation were closely connected with the faculae regions such an analysis was not conclusive.

Recently MINNIS (1955) from E layer measurements also found a correlation with sources of intense green coronal radiation.

The electron-loss processes in the ionosphere.

If the formation of each of the ionised regions is attributed to the ionisation of some particular atom or molecule, then the rate of increase of electron density N, is given by the equation:-

$$\frac{dN}{dt} = q - k \qquad \ldots\ 3$$

where q is the rate of production of electrons or positive-ions per cm^3 due to photoionisation and k is the rate of loss of electrons per cm^3 due to some process (e.g. recombination etc.) APPLETON and NAISMITH (1932) inclined to the view that electrons disappeared mainly by attachment to neutral particles, and the subsequent mutual neutralisation of positive and negative ions took place. ECKERSLEY (1933) however, favoured

a process of recombination between electrons and positive-ions. Later APPLETON and NAISMITH (1935) adduced their arguments in favour of the main process being recombination in both the E and F regions. MARTYN and PULLEY (1936) then suggested that recombination and attachment followed by the subsequent breaking up of the negative ions all occurred together. MASSEY (1937) and BATES et al (1939) have shown that this is probably a satisfactory picture of what occurs and that it does account generally for the observed variations, in particular for the apparent behaviour according to a recombination law, when in fact important attachment and detachment processes are occuring together.

For a simple recombination process, the ionospheric continuity equation becomes:-

$$\frac{dN}{dt} = q - \alpha_e N^2 \qquad \ldots\ 4$$

where α_e is the radiative recombination coefficient. For a predominantly attachment process the equation becomes:-

$$\frac{dN}{dt} = q - \beta N_o N \qquad \ldots\ 5$$

where β is the attachment coefficient and N_o is the number of neutral particles per cm^3.

On the theory of Massey and his collaborators the equation would be:-

$$\frac{dN}{dt} = q - \alpha' N^2 \qquad \ldots\ 6$$

where α' is the "effective" recombination coefficient, which

includes factors due to attachment etc.

Measurements made during solar eclipses also provide information as to the electron-loss coefficients, whether they be due to attachment alone or due to an effective recombination process.

HULBURT (1939) suggested that if the ionospheric continuity equation were of the form say of equation 6, then during an eclipse this would reduce to:-

$$\frac{dN}{dt} = fq - \alpha' N^2 \qquad \ldots\ldots 7$$

where f is the unobscured fraction of the solar disc. In order to determine the likely value of α' for any particular layer a value of α' is assumed and q calculated from control day data using equation 6. Using these values of q, the expected or "theoretical" variation of N is then calculated from point to point during the eclipse using equation 7. The process is then repeated for different values of α' until the best fit with the experimental curves is obtained.

Using this method, values of α' have been calculated from many eclipse measurements. The values differ considerably from eclipse to eclipse, but in general the following values are approximately those found for each of the three main layers.

$$\alpha'_E = 1 \times 10^{-8} \text{cm}^3\text{sec}^{-1}$$
$$\alpha'_{F_1} = 5 \times 10^{-9} \text{cm}^3\text{sec}^{-1}$$
$$\alpha'_{F_2} = 1 \times 10^{-10} \text{cm}^3\text{sec}^{-1}$$

Some observers (e.g. KIRBY, GILLILAND and JUDSON, 1936;

SAVITT, 1950) have concluded that attachment is the predominant electron-loss process in the F_2 region. They found that equation 5 with q replaced by fq during the eclipse provided a much better fit to experimental observations than the effective recombination law of equation 6. At the present time the electron-loss processes are still a matter of some considerable discussion.

BATES et al (1939) have calculated that α_e the radiative recombination coefficient is of the order of $10^{-12} cm^3 sec^{-1}$. Clearly from the values of α' obtained from eclipses - and other means - this process is too slow to account for the observed values of α'. Massey and his collaborators (MASSEY, 1937; BATES et al, 1939) have shown that:-

$$\alpha' = \alpha_e + \lambda\alpha_i \qquad \ldots\ 8$$

where λ is the ratio of the number of negative-ions to the number of electrons, and α_i is the ionic recombination coefficient. Since $\alpha_e \ll \alpha'$, $\alpha' \simeq \lambda\alpha_i$ 9

In this way it was possible to explain the large values of α' deduced from experiment.

Later, however, BATES and MASSEY (1943, 1946) have shown that in fact their negative-ion theory of the recombination coefficient still does not account for the large values of α' since the theoretical values of λ and α_i are still too small.

In order to overcome this difficulty BATES and MASSEY (1947) have proposed a new recombination theory in

which it is supposed that positive molecular ions recombine due to dissociative recombination (in the E layer) and positive atomic ions transfer their charge to molecules with subsequent dissociative recombination (in the F region). The theoretical value of the dissociative recombination coefficient is about $10^{-8}cm^3sec^{-1}$ and this readily accounts for the observed values of α'. On this theory α' would decrease with height as the molecular concentration decreases with height.

The theory shows that lower down at E and F_1 heights the electron loss rate would be proportional to N^2 (recombination-like) and higher up at F_2 heights it would be proportional to N (attachment-like). This would seem to account for the fact that some observers have concluded from eclipse measurements that the loss of electrons in the F_2 layer follows an apparent attachment law, although this point has not yet been mentioned in the literature.

Origin of the F_2 layer.

It was first suggested by BRADBURY (1938) that the F_2 layer might have the same origin as the F_1 layer due to the ionisation of the same ionisable constituent by the same source of radiation, but being formed because of the much slower electron loss rate at F_2 heights.

The consequences of this hypothesis have been considered by MITRA (1952), RATCLIFFE et al (1956) and RATCLIFFE

(1956). In particular RATCLIFFE (1956) has shown that this hypothesis is also consistent with the dissociative recombination theory of Bates and Massey. He shows that this accounts for the formation of the F_1 layer only during the daytime in Summer and in particular at sunspot minimum. In addition, it is pointed out that an F_1 peak should be more enhanced during a solar eclipse. This has in fact been observed on several occasions as the formation of an additional layer ($F_{1\frac{1}{2}}$) between the F_1 and F_2 regions. (e.g. LEDIG et al, 1946; ESTRABAUD, 1952; MINNIS, 1955). The $F_{1\frac{1}{2}}$ layer so formed later merged with the F_2 again, when the F_1 layer recovered its normal ionisation towards the end of the eclipse.

The eclipse of December 25, 1954.

The work presented in this thesis contains an analysis of ionospheric records obtained during December 1954 and January 1955, including an annular solar eclipse which occurred on December 25, 1954.

In spite of investigations over twenty-five years, including investigations at over fifteen eclipses, a large number of problems still remain unsolved, in particular regarding the behaviour of the F_2 region. The normal ionospheric records obtained by the pulse sounding method at most recording stations do not lend themselves to particularly accurate measurement of critical frequency or of the virtual height. It must be remembered that if

quantities like N^2 are to be calculated this involves the evaluation of $(f^o)^4$, and clearly the accurate measurement of critical frequency is very important. For the purpose of this investigation a specially designed automatic ionosphere sounder of high resolution was constructed in order to achieve this end.

The great majority of workers in this field, in analysing daily ionospheric records have limited their calculations and conclusions to the observation of critical frequencies and virtual heights. It is admitted that the conversion of virtual heights to true heights by any of the earlier methods presented in the literature (e.g. BOOKER and SEATON, 1940) involves a considerable amount of additional computation. In addition, until recently the methods are usually based on the assumption of a parabolic layer which is generally not true, except near the maximum in the layer. However, it must be stressed that any results based entirely on virtual height observations can hardly give even a qualitative explanation of the processes which take place in the ionosphere. Recent methods of computing the true height from the virtual height (MANNING, 1947; KELSO, 1952) are based on fewer assumptions and the electron density - height distribution can be calculated fairly simply. Observations at only two eclipses (SAVITT, 1950; MINNIS, 1955) have made use of these methods. The complete scaling of all the records taken during this

investigation, using the method of KELSO (1952), was thus undertaken. A thorough and complete picture of the control conditions were thus obtained for comparison with eclipse observations.

Clearly, ionospheric readings during solar eclipses offer unique opportunities for studying the many factors which influence the ionised layers and which could not so easily be deduced from the normal diurnal and seasonal variation. It is hoped that the observations and deductions produced in this thesis will make some contribution to a clearer understanding of the processes which take place in the ionosphere.

PART 1

(a) Experimental Methods.

Introduction.

The Experiments of APPLETON and BARNETT (1925) and BREIT and TUVE (1926) were able to prove the existence of a conducting layer in the upper atmosphere. Appleton and Barnett varied the frequency of a transmitter linearly by a small amount, and were able to produce interference fringes at a receiving station some distance away; these could only be attributed to interference between a "ground ray" coming straight from the transmitter and a "sky wave" reflected from the conducting layer. By counting the number of fringes they were able to calculate the apparent path difference and hence the virtual height of the layer.

Breit and Tuve modulated a transmitter with a series of pulses of 500 microseconds duration. They coupled an oscillograph to the receiver and this showed two received pulses - again, one due to the ground wave and one due to the sky wave. By measuring the time interval between the two received pulses the virtual height could be calculated.

APPLETON and RATCLIFFE (1927) devised a third method of measuring the virtual height. Using a directional receiving antenna system they were able to measure the angle of incidence of the down-coming sky wave.

The Breit and Tuve method has proved to be preferable for further investigation, and has been improved and developed.

At Rhodes University, ionospheric measurements had previously been made by manually operated equipment (GLEDHILL and SZENDREI, 1947a). This method is laborious and time consuming, and it is obviously an advantage to construct a sounder which will take readings automatically at definite intervals.

Completely automatic equipment has been devised by BERKNER, WELLS and SEATON (1936) and others, and the Carnegie Institute maintains such apparatus in continuous operation for recording conditions in the ionosphere at a number of stations throughout the world. Whilst this apparatus operates very satisfactorily a large number of engineering problems had to be overcome. A transmitter and receiver had to be designed to cover the large frequency range, say from 0 to 15 Mc/sec. Obviously no oscillator can cover this range in one band, and apparatus such as that used by the Carnegie Institute becomes very intricate when three or four bands are required. Not only do the transmitter and receiver have to be bandswitched automatically, but the receiver has to be kept tuned to the transmitter at all stages. The apparatus becomes very bulky with the additional mechanical equipment necessary to carry out these operations.

WADLEY (1949) brilliantly overcame this necessity for bandswitching by employing the heterodyne principle. A single oscillator is required operating between 30 Mc/sec and 50 Mc/sec; this can be done in a single band.

To produce an output of 0 to 20 Mc/sec the oscillator is mixed with a fixed oscillator at 30 Mc/sec, the difference in frequency (0 - 20 Mc/sec) being amplified through a system of wide-band amplifiers. The variable oscillator 30 to 50 Mc/sec is also used as the local oscillator of a superheterodyne receiver giving an intermediate frequency of 30 Mc/sec, with the incoming signals of 0 to 20 Mc/sec.

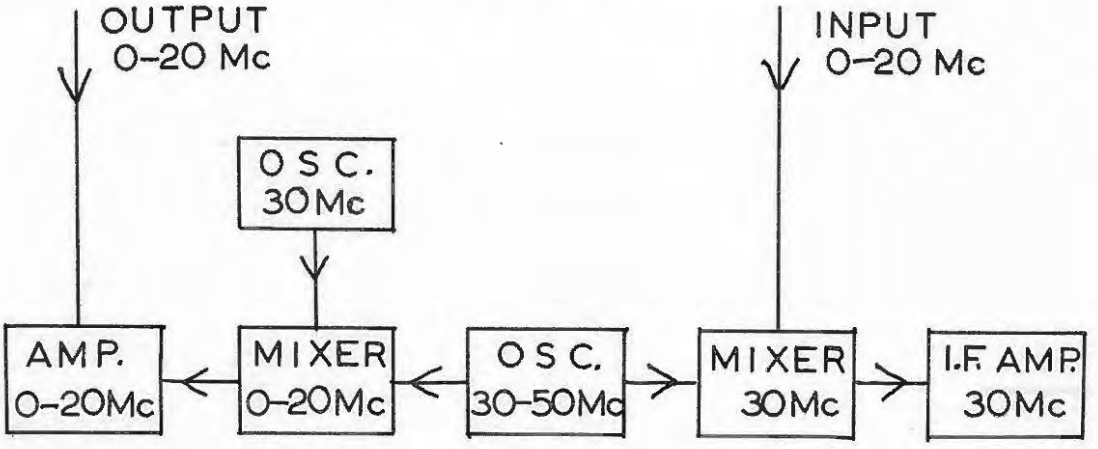

Block diagram of Wadley's heterodyne technique.

In this manner the transmitter and receiver are at all times tuned to one another and the complete operation can be performed by the rotation of a single condenser. Using this principle a completely automatic ionosphere sounder was constructed and readings were taken over two months centring on an annular eclipse of the sun which occured over South Africa on December 25, 1954.

Design of Automatic Ionosphere equipment.

As has been stated above, the method consists of sending out short pulsesof suitable length, varying the frequency of the transmitter and receiving both the ground wave and the sky wave on a special receiver whose output is coupled to a recording device. In this case a cathode ray oscillograph was used. At any moment the oscillograph will indicate the virtual height of the reflected ray corresponding to the time delay between the ground ray and the reflected ray. Accurate measurement is required of (i) the frequency of the transmitter and (ii) the virtual height of the reflecting medium corresponding to this frequency. Height calibration is obtained by applying suitable "pips" to the oscillograph corresponding to 50 km. height marks. Frequency calibration is obtained by applying the height pips at ½ Mc/sec intervals. This is done through a calibration "gate" stage.

For the purpose of description the equipment may thus be divided into the following sections:

(a) Pulse generator

(b) Transmitter

(c) Aerial system

(d) Receiver

(e) Height Calibrator

(f) Frequency Calibrator

(g) Calibration Gate stage

(h) Recording and Monitoring Oscillographs

(i) Power Supplies

(j) Automatic Switching

(k) Recording Camera

In order to arrange for the system to be independent of the stability of high frequency oscillators the use of double heterodyne in both the transmitter and receiver is employed. The fixed frequency of 30 Mc/sec is obtained by taking the fourth harmonic of a 7.275 Mc/sec crystal oscillator, giving a frequency of 29.1 Mc/sec. This is then mixed with a pulsed oscillator of 900 Kc/sec, giving the desired output of 30 Mc/sec. The 29.1 Mc/sec so derived is also used as the second local oscillator of the receiver. It is mixed with the first I.F. of 30 Mc/sec and a second I.F. of 900 Kc/sec is produced. This is much more suitable for amplification in the receiver than the 30 Mc/sec I.F. Fig. (2) shows a block diagram of the apparatus.

The apparatus was constructed on five chassis, each approximately 2 feet 6 inches by 1 foot 6 inches, housed in a framework of racks about 6 feet high. (Fig. 3).

The construction of the apparatus, which is described here, was actually started several years previously but was abandoned after only Chassis 1 and part of Chassis 2 had been completed. After some modifications to these two chassis the construction of the remainder of the five chassis was completed by October 1954 in preparation for readings relating

FIG: 2 BLOCK DIAGRAM OF IONOSPHERE SOUNDER

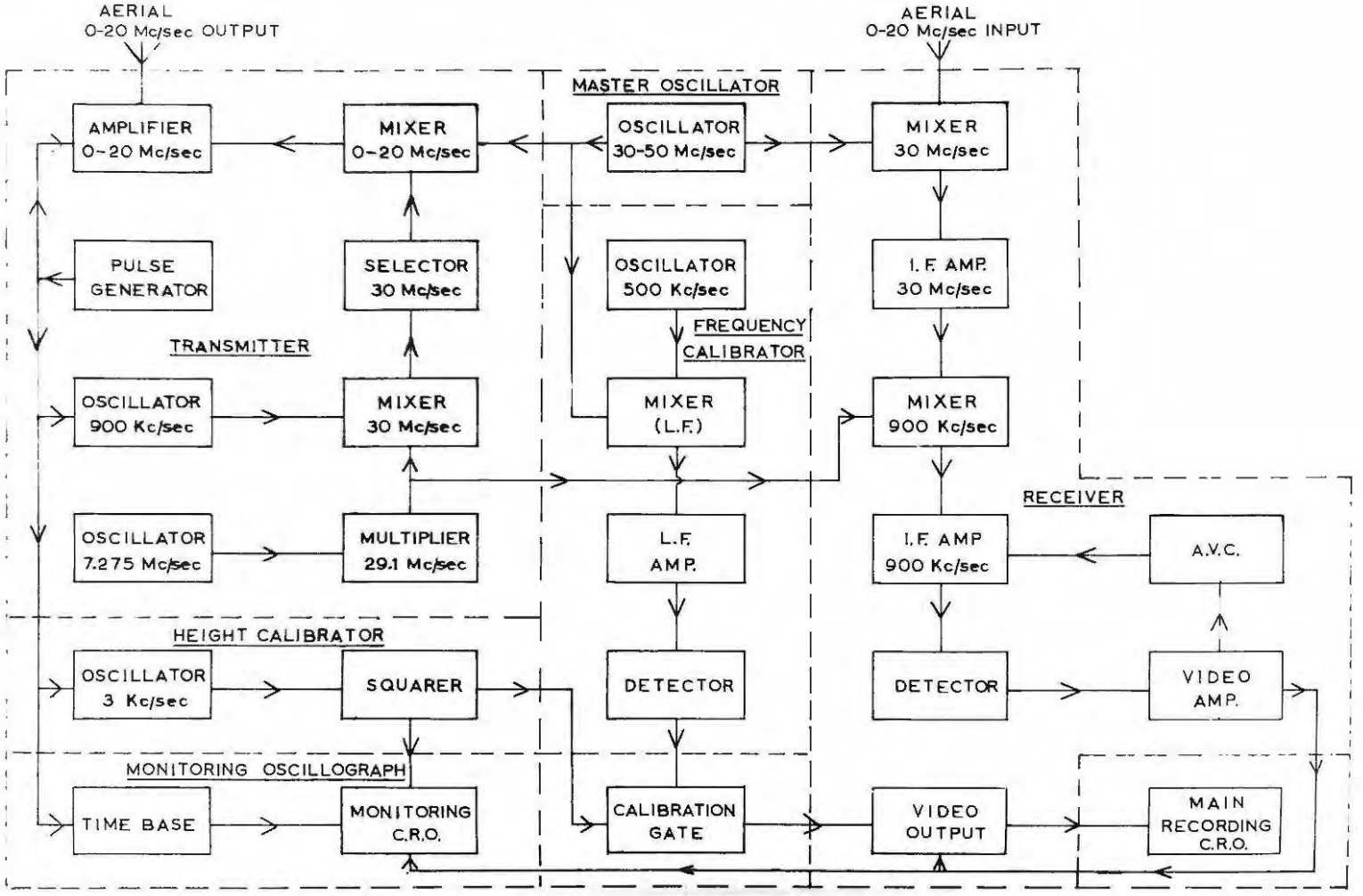

FIG: 3 AUTOMATIC IONOSPHERE SOUNDER

to the eclipse.

Each chassis comprised the following parts of the equipment:

Chassis I — Main Power Supplies - (Figs. 4 and 5)

Chassis II — Automatic Switching for filaments and H.T. supplies, frequency calibrator - (Figs. 6 and 7)

Chassis III — Monitoring oscillograph, pulse generator, height calibrator, calibration gate stage video output and AVC stages of the receiver - (Figs. 8 and 9)

Chassis IV — Transmitter driver, receiver, automatic switching for recording camera and condenser drive motor - (Figs. 10 and 11)

Chassis V — Transmitter amplifiers and output stage (Figs. 12 and 13)

The recording oscillograph and its power supply are seen in Figs. 14 and 15, and the recording camera in Fig. 16

(a) Pulse generator and modulator.

Using the pulse sounding method for ionosphere investigation, certain limits must naturally be attached to the pulse length and pulse rate. The duration of the pulse must be sufficiently short not to overlap the leading edge of the reflection from the lowest layer. As the height of the E layer is about 100 km. the length of the forward and return path at vertical incidence is 200 km. If the signal travels with the speed of light (3×10^5km/sec) then:-

FIG:5 CHASSIS No.1

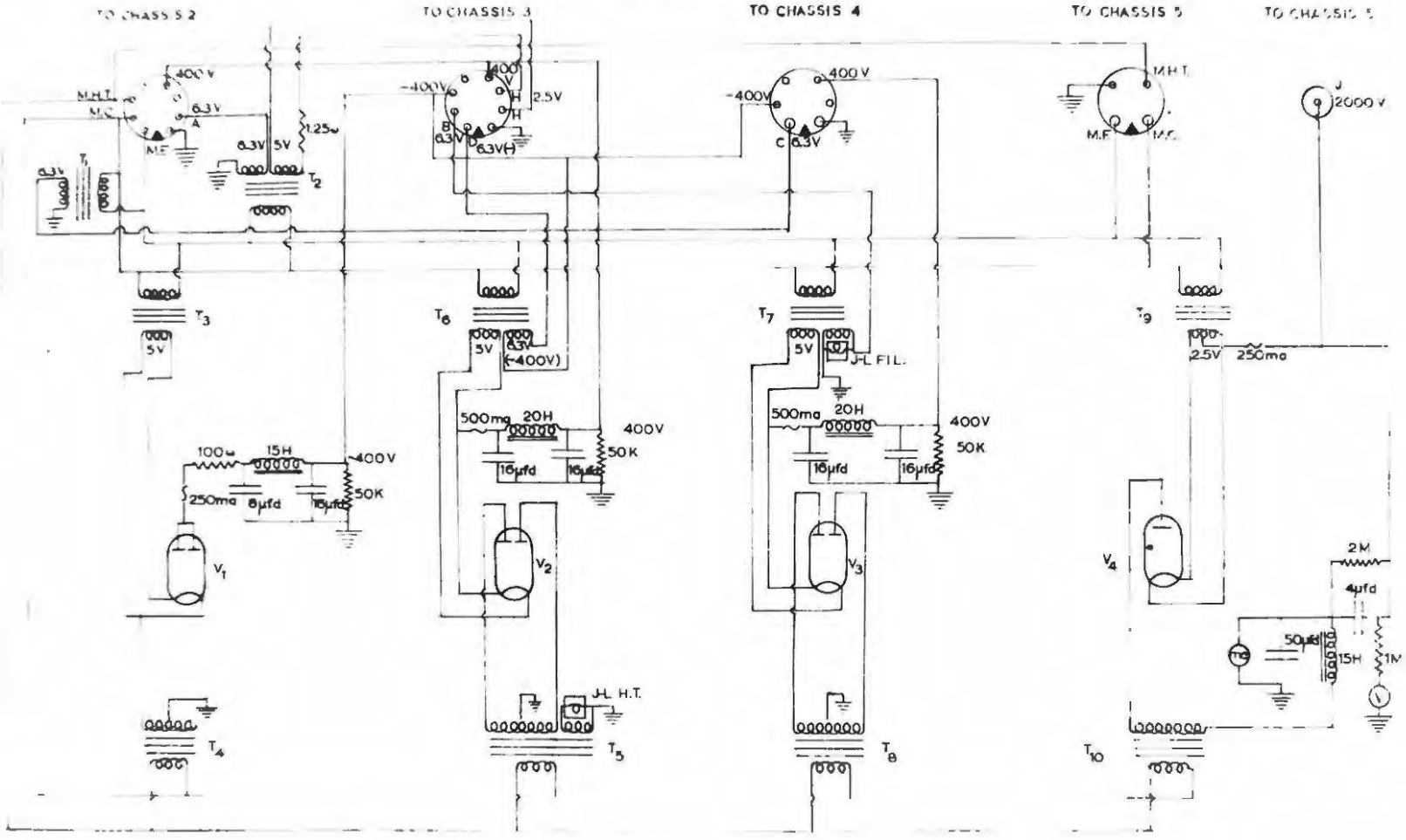

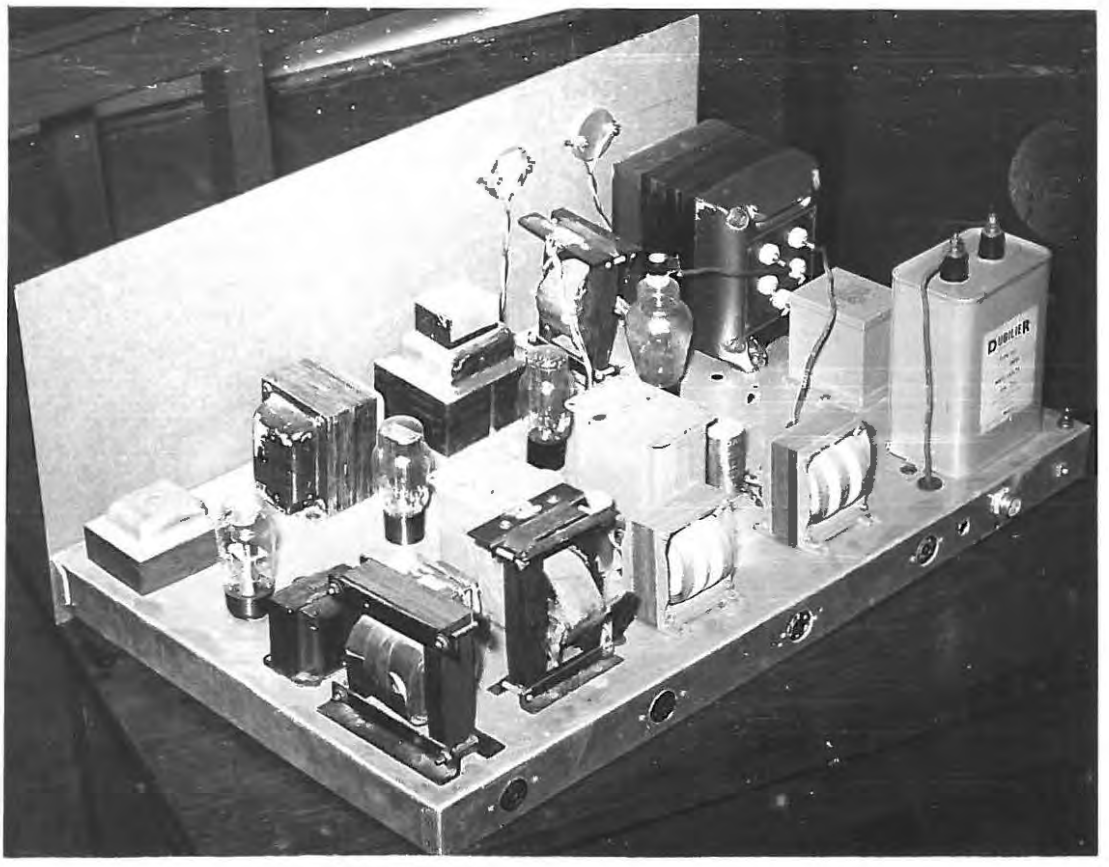

FIG: 4 CHASSIS No.1

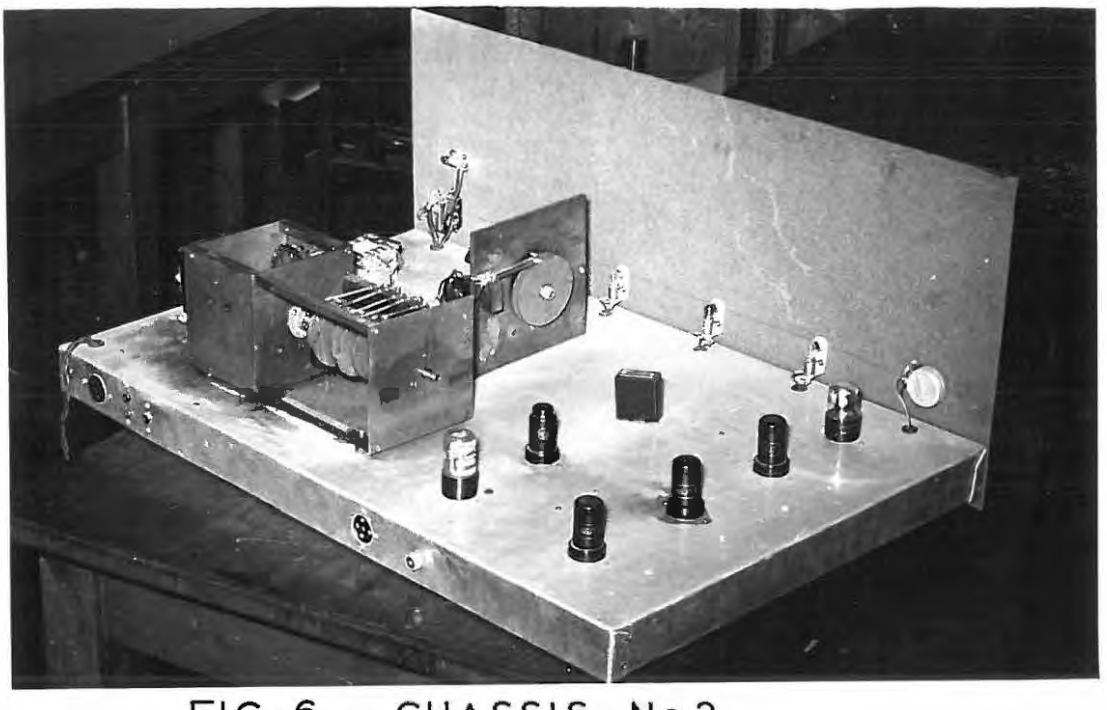

FIG: 6 CHASSIS No.2

FIG. 7 CHASSIS No. 2

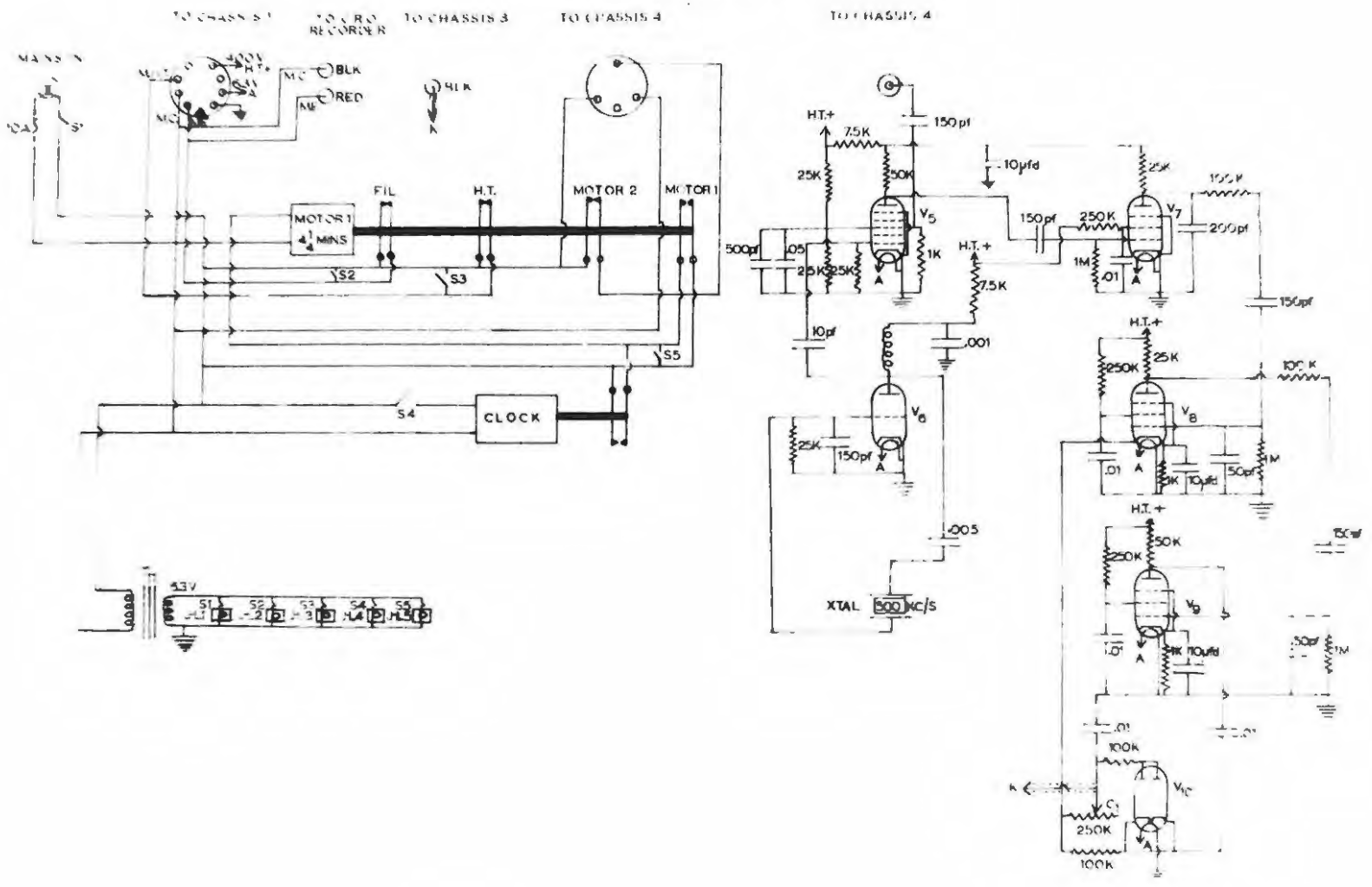

FIG: 9 CHASSIS No.3

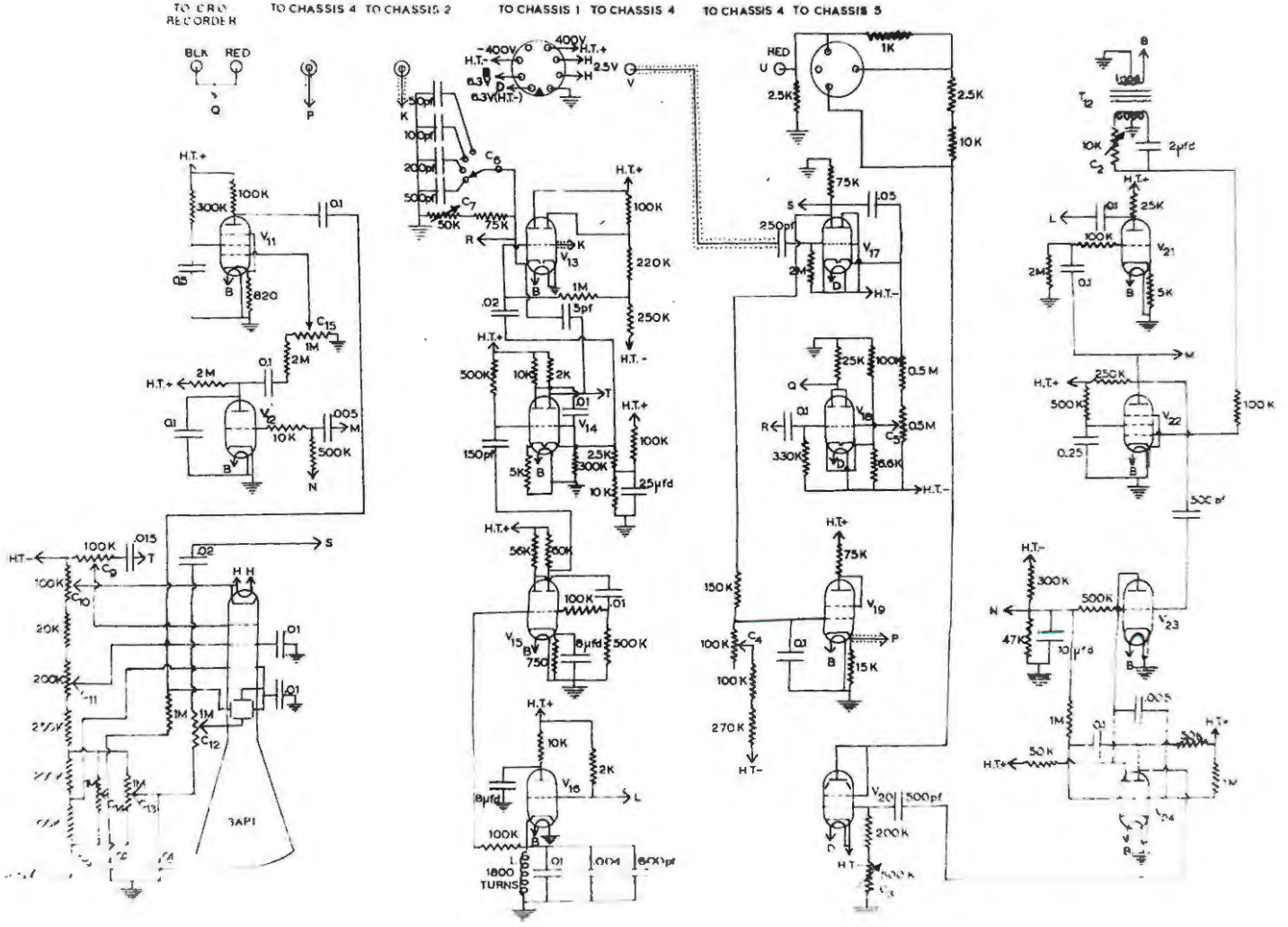

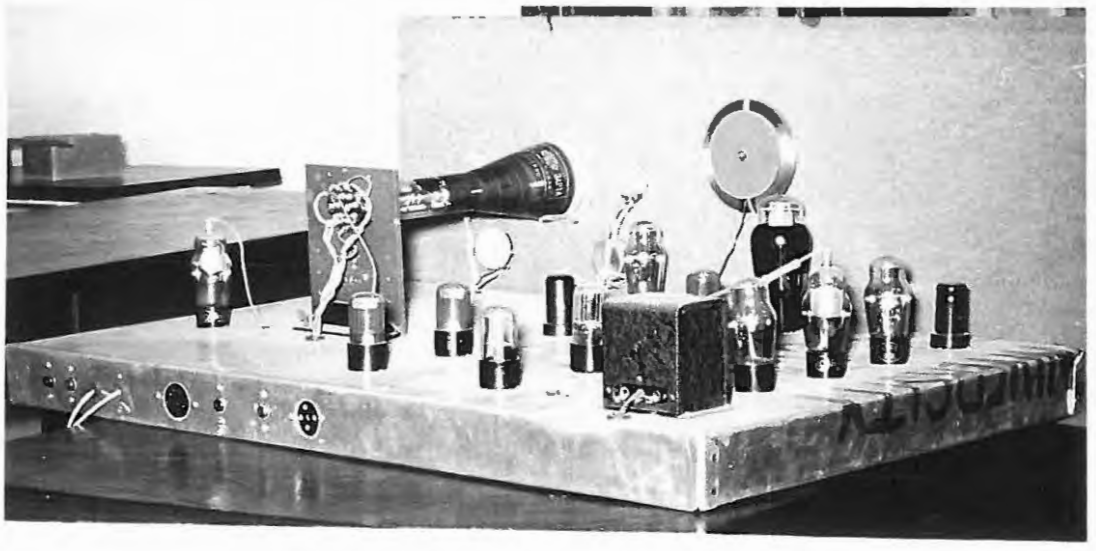

FIG: 8 CHASSIS No.3

FIG: 10 CHASSIS No.4

$$\text{Time delay of echo} = \frac{200}{3 \times 10^5} = 667\ \mu\text{secs.}$$

However, the pulse should not be very short because the amount of energy which can be radiated with a given transmitter decreases as the pulses are shortened. Practically, a length of 100 to 200 micro-seconds is found to be suitable.

In addition, the interval between pulses must be large compared with the time delay of an echo from the highest layer. Virtual heights of 1,000 km. are not uncommon in the pulse sounding of the F_2 layers, particularly near the critical frequency. By a similar calculation to the above this gives a time delay of about 7,000 micro-seconds. Thus the pulse rate should not exceed 150 per second. The lower limit is set by the persistence of the glow on the CRO screen. In a town supplied with 50 c/sec A.C. mains, it is very convenient to control the pulse rate from the mains. The method offers the advantage that other apparatus may easily be synchronised with the pulse rate and will not go out of synchronisation even if the mains frequency fluctuates somewhat.

The pulse generator is located on Chassis 3, and comprises valves V_{22}, V_{23}, V_{24} and V_{20}. The 50 c/sec A.C. mains is applied to the grid of V_{22} from the 6.3 volts filament potential through the step-up transformer T_{12} and the phase-shifting circuit $2\mu fd$ and 10K. V_{22} squares and limits the wave which is then differentiated by the 500 pf

and 500K at the grid of V_{23}. At this stage it was found that the pulse was not sharp enough due to insufficient squaring in V_{22}. In order to obtain a sharper pulse a double triode V_{24} was used as a multivibrator. Normally the multivibrator is in a quiescent state, since its first grid is returned to a point 50 volts negative and its second grid is returned to H.T. positive. A negative going square wave from V_{23} applied to the second grid of V_{24} thus sets one cycle of the multivibrator in motion. The multivibrator is designed to give a very sharp negative slope and this is differentiated by the RC circuit at the grid of V_{20} which therefore determines the duration of the pulse.

V_{20} is the pulse modulator and is normally drawing heavy current since its grid is leaked to ground (i.e. H.T. positive relative to the cathode). Corresponding negative voltages are thus developed across the various sections 2.5K, 1K and 12.5K in the plate load. These voltages are sufficient to cut off each of the various transmitter amplifier stages to which they are applied as grid bias. The negative going square wave from the multi-vibrator causes the tube to cut off sharply, and the transmitter amplifiers thus become conducting. The duration of the pulse is controlled by C_3 which alters the RC time constant at the grid of V_{20} by varying the 500K resistor.

(b) Transmitter.

This is divided into two sections, the transmitter driver which comprises valves V_{33} to V_{43} inclusive on Chassis 4, and the transmitter amplifiers which comprise the whole of Chassis 5. (V_{44} to V_{49}). V_{43} is a crystal controlled oscillator operating at 7.275 Mc/sec. This drives a multiplier stage V_{42}, whose plate circuit is tuned to the fourth harmonic (29.1 Mc/sec). This frequency of 29.1 Mc/sec is then fed into the first transmitter mixer stage V_{41}. The signal grid of V_{41} is fed with a pulsed 900 Kc/sec wave from V_{40}. Normally V_{40} is biased beyond cut off through the 20K grid leak resistor to the pulse modulator plate load via cross connected U to Chassis 3. Thus V_{40} is caused to produce a pulsed oscillation of 900 Kc/sec in synchronism with the pulse generator. The 2M resistor from the grid of V_{40} to H.T. positive ensures that the grid is brought to ground potential at the start of the pulse and not somewhere negative.

The mixer stage V_{41} has its output sharply tuned to 30 Mc/sec and a pulse of this frequency is developed across it. V_{39} and V_{37} are stages similarly tuned to 30 Mc/sec. Their purpose is not to amplify but to select the 30 Mc/sec pulse and suppress the original 29.1 Mc/sec. Hence the feed to the grid of each stage is tapped down the previous tuned circuit.

The output of V_{37}, suitably matched down to low

FIG: 11 CHASSIS No. 4

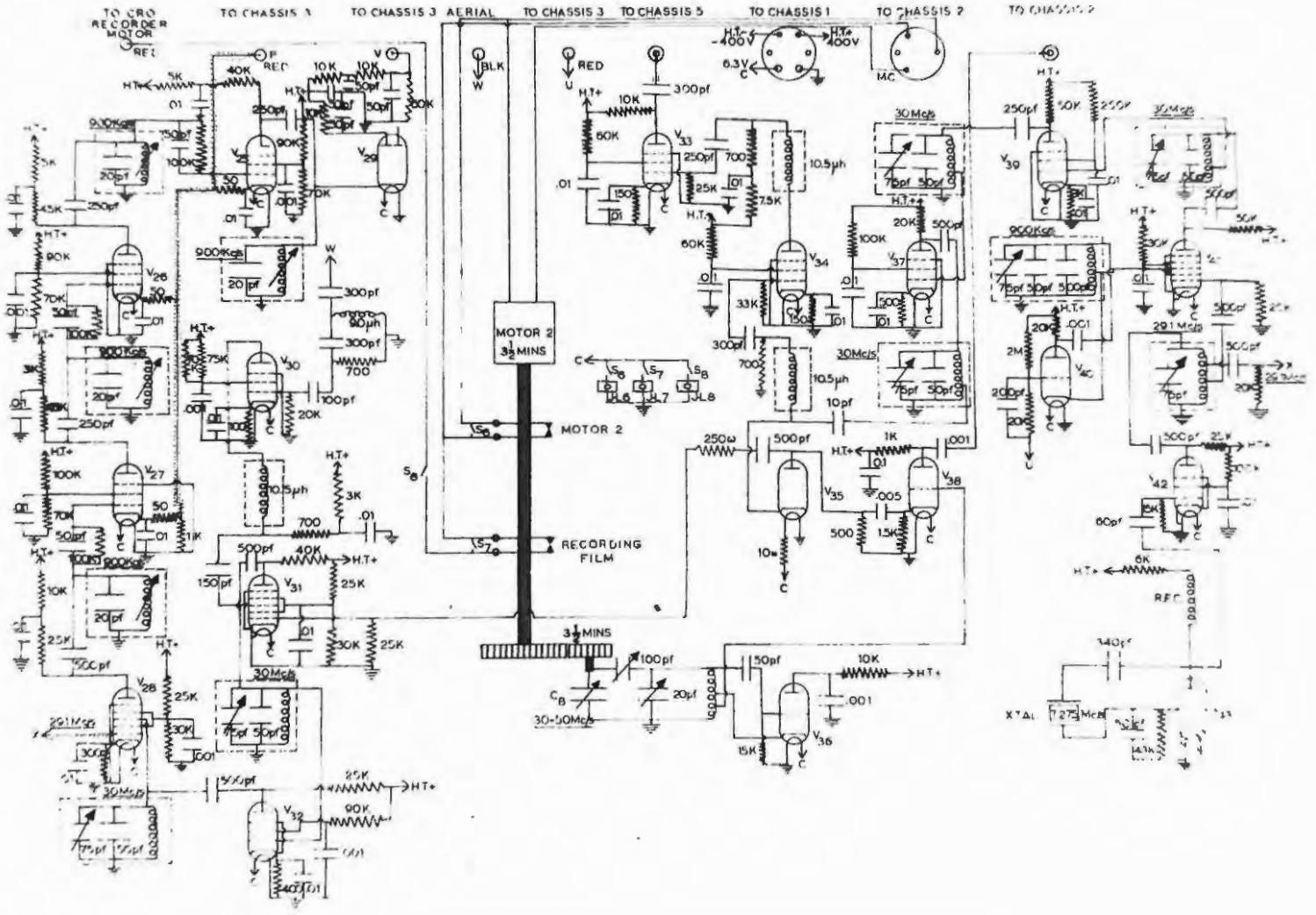

FIG:13 CHASSIS No.5

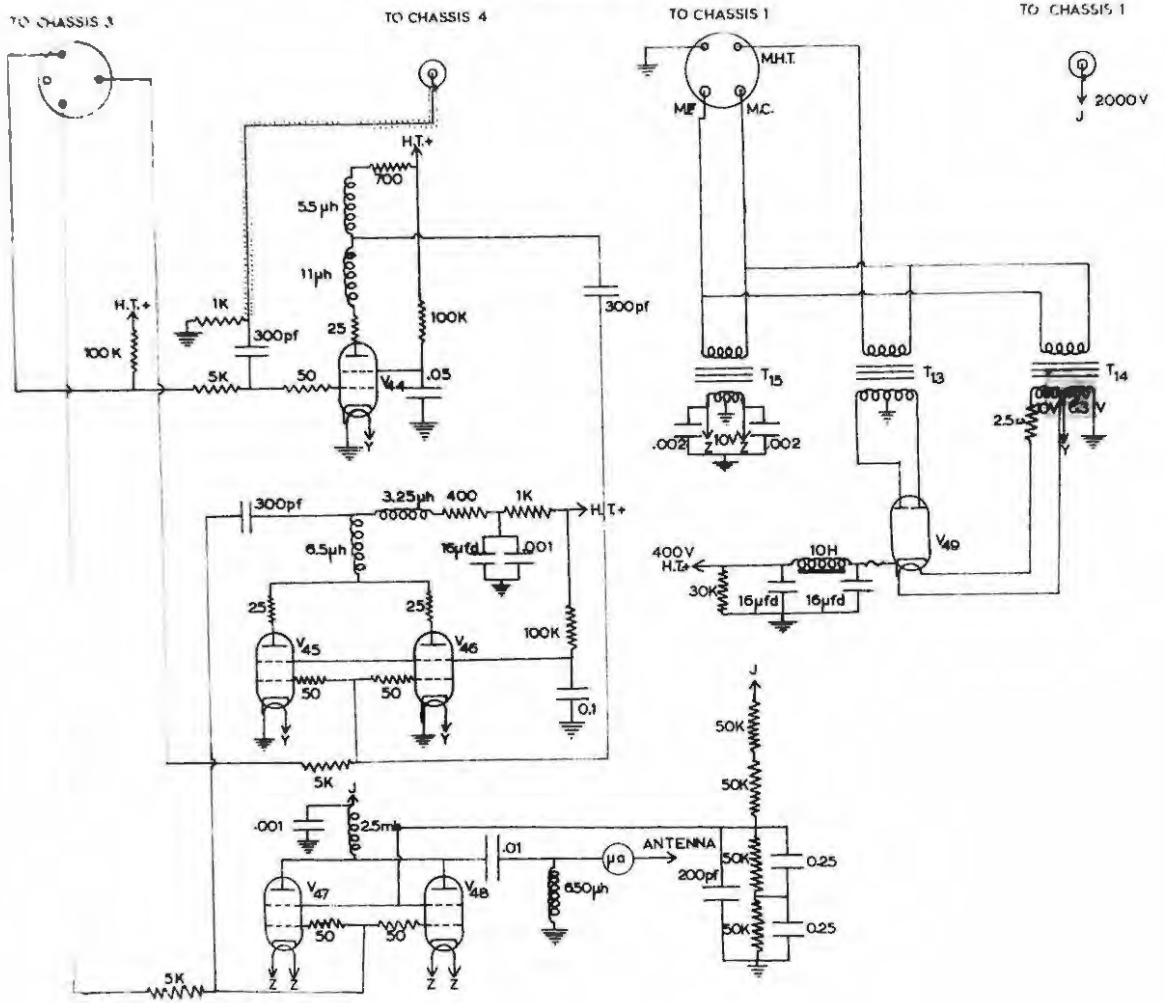

FIG : 12 CHASSIS No.5

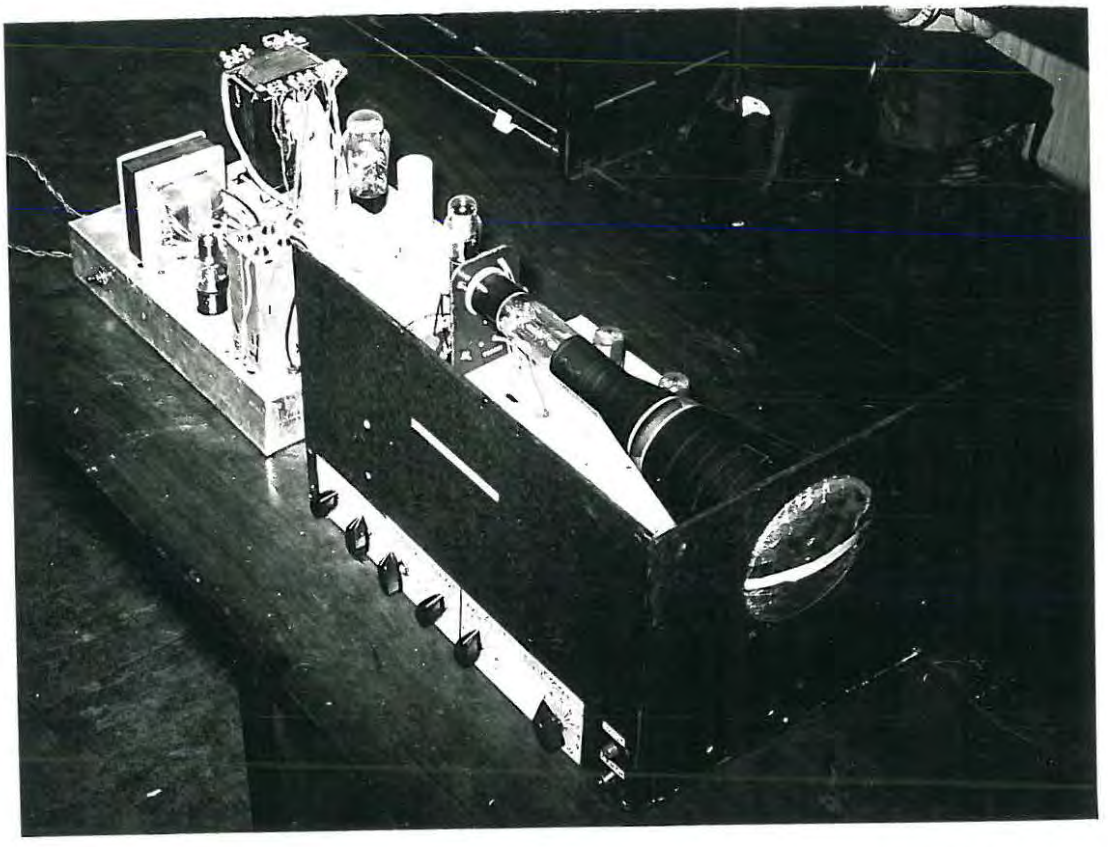

FIG : 14 RECORDING OSCILLOGRAPH

impedance is coupled via the 10 pf condenser to the cathode of V_{35}, a low-impedance diode which is the second transmitter mixer stage.

V_{36} is the main oscillator operating from 30 to 50 Mc/sec. The upper frequency limit can be set by the 20 pf trimmer, and the lower limit by the 100 pf padder condenser. The output of this oscillator is applied to the cathode follower V_{38} to match down to low impedance and then fed to the plate of the mixer V_{35}. The difference in frequency of 0 to 20 Mc/sec appears across the cathode coupling condenser of 10 pf. This 10 pf condenser forms the mid-shunt input component of a low pass filter terminated in 700 ohms. The 10.5 microhenries inductance is the series element, whilst the grid capacity of V_{34} acts as the mid-shunt terminating element. This is a low-pass filter corresponding to type I in Fig. 17. This and all the subsequent coupling filters cut off at 20 Mc/sec. V_{34} is the first wide-band amplifier. At this stage there would normally have been enough output to feed V_{44}, the first of the three transmitter amplifier stages located on Chassis 5. However, the output from Chassis 4 had to be fed through coaxial-cable to Chassis 5 to avoid pick-up, radiation etc. Since the cable had a characteristic impedance of 100 ohms, it would have been impossible to employ a suitable filter to couple from Chassis 4 to Chassis 5. The output from Chassis 4 to Chassis 5 would be partly attenuated in the cable. It was found that

there was insufficient input to V_{44} on Chassis 5. This called for an additional amplifier V_{33}, on Chassis 4 to compensate for the attenuation in the cable. The output from V_{34} was fed into the grid of V_{33} through the same type of filter terminated in 700 ohms, using the fact that the output capacity of V_{34} and the input capacity of V_{33} were both about 10 pf. The output from V_{33} was then fed through the coaxial cable to Chassis 5 which contains the three transmitter amplifier stages.

These three stages are all pulsed into class A condition in synchronism with the pulse as described in (a). The output from V_{44} is fed into V_{45} and V_{46} in parallel through the low pass filter terminated in 700 ohms. This filter is mid-shunt input as before, but is mid series terminated since the combined grid capacities of $V_{45}$and V_{46} in parallel is about twice the output capacity of V_{44}. This corresponds to the low pass filter of type II in Fig. 17. The output of V_{45} and V_{46} is finally fed into a 400 ohm filter, also of type II, feeding the final amplifier consisting of V_{47} and V_{48} in parallel.

On each of the three transmitter amplifier stages the 300 pf and 5K grid coupling circuit is designed to couple the R.F. satisfactorily down to at least 1 Mc/sec and at the same time, to apply the bias to the grids without distortion due to the by-passing effect of the coupling condenser.

It will be noted that the grid and plate circuit

of the three stages contain small resistors of 50 and 25 ohms respectively. This is to damp out any parasitic self-oscillations which are likely to occur when two valves are operated in parallel.

The final amplifier stage operates at a screen voltage of 1,000 volts, derived from the H.T. voltage of 2, 000 volts which is applied to the plate through the R.F. choke of 2 millihenries. This stage presents a plate impedance of about 600 ohms, and the output from the plate is coupled via the 0.01 fd D.C. blocking condenser, and the 650 microhenries R.F. choke to the aerial. This aerial should present an R.F. impedance of about 600 ohms to the final stage. The R.F. power level in the aerial is about 2 kw.

It may seem surprising that so many states of amplification are required. It must be remembered that (i) the stages are untuned, and (ii) with the system of wide band coupling utilising low pass filters, a small load resistance has to be used in each stage corresponding to the terminating resistance of the filter. This means that with loads of 400 and 700 ohms a gain of only 4 or 5 is realised at each stage, hence the need for several stages of amplification.

(c) Aerials.

The design of a suitable aerial or aerial system presents a considerable problem. The system must be able

to radiate the whole frequency band from 1.5 to 15 Mc/sec. This was the frequency range used during the readings. Many systems have been suggested, the most popular of which is a system of two vertical rhombics. With the space available at Rhodes University this was impracticable, and resort had to be made to a simpler type of aerial. Any aerial usually has its characteristic resonant frequency, and at this frequency maximum output from the transmitter is registered and radiated. The output and the amount radiated falls off rapidly on either side of the resonant frequency. Unless resort is made to a system of several aerials of differing resonant frequency the obvious solution seems to be to try and construct a non-resonant aerial. The ordinary straight-wire above ground has a certain characteristic impedance, and if terminated in this impedance would have no resonant points at all. It will behave as a pure resistance to all frequencies. At a height of about 100 feet above ground this characteristic impedance is about 600 ohms, and this is the correct impedance value which the aerial should present to the final stage. Such an aerial was constructed about 120 feet above ground, 30^0 feet long, and terminated to ground by 600 ohms pure resistance. The resistance was made weather proof by setting it in paraffin-wax and enclosing it in a metal shield.

The power to the aerial never varied by more than a factor of 3 over the whole range. It decreased most at the

higher frequencies. This was not, however, characteristic of the aerial but rather of the output of the amplifier.

A 150 feet long wire aerial was used for the receiver. It was unnecessary to terminate this in 600 ohms, since the input to the receiver contained a high-pass filter terminated in 700 ohms.

(d) Receiver.

The main section of the receiver is located on Chassis 4, only the AVC and the video output stages being located on Chassis 3.

The input from the aerial is fed through a high-pass filter terminated in 700 ohms which cuts off all frequencies below 1 Mc/sec. This is a filter corresponding to type 3 in Fig. 17 and eliminates interference from nearby broadcast stations. It is coupled to the grid of a wide-band R.F. amplifier stage V_{30}, through a short time constant R.C. coupling circuit of 100 pf and 20K. This is important since the circuit must recover quickly from the initial pulse corresponding to the ground wave in order to receive the reflected wave effectively. The time-constant is 2 micro-seconds and it thus takes perhaps 20 micro-seconds for this circuit to recover completely. The output of V_{30} is coupled via a 700 ohm low pass filter of type 1 (Fig. 17), to the signal grid of V_{31}, which is fed with the 30 to 50 Mc/sec signal from V_{38} in the transmitter section. The first I.F. of 30 Mc/sec is thus derived and applied via a

tuned circuit to V_{32}, the first I.F. amplifier. The output of V_{32} is similarly tuned to 30 Mc/sec and applied to the signal grid of V_{28}, which is the second mixer stage. The oscillator grid of this stage is supplied with a 29.1 Mc/sec signal from V_{42} via cross-connection X. The second I.F. of 900 Kc/sec is thus derived. This 900 Kc/sec is exactly equal to the original pulsed 900 Kc/sec at V_{40} in the transmitter. The second I.F. has three amplifier stages, V_{27}, V_{26} and V_{25}, all of which are similar. The grid of each stage has a series R.C. circuit of 100K and 50 pf. This enables the amplifiers to work through strong CW signals as the grid current drawn by each stage increases the bias voltage to prevent the amplifier saturating. The output of the last of the three stages is applied to the diode detector V_{29}, whose output passes through an I.F. filter consisting of three RC sections of 10K and 50 pf. At this point the signals are negative going and are applied via cross-connection V to the grid of the first section of V_{17}, a double triode, located on Chassis 3. This section acts as a video amplifier. The pulses are separated from any D.C. level which may be present due to interfering stations by the RC circuit of 250 pf and 2M on the grid of V_{17}. The pulses and noise voltages are D.C. restored by the grid current of V_{17} which operates at zero bias. The signals on the plate are positive going and the mean D.C. level at this point is a measure of the noise voltages present. This level is used to control the AVC

circuit to maintain a more or less constant noise level. The pulse amplitudes have relatively little effect on the AVC as they are of short duration. This mean D.C. level is applied to the grid of the AVC tube V_{19}, the D.C. being filtered out by the RC circuit of 150K and 0.1μfd. This grid is leaked to H.T. negative via the gain control C_4. V_{19} is a cathode follower with its cathode connected to all the cathodes of the second I.F. amplifiers through the screened lead P between Chassis 3 and 4. The gain control C_4 is adjusted so that, with no noise present the grid of V_{19} is somewhere behind cut off. The presence of noise causes the grid to rise positive and V_{19} begins to draw current. The I.F. cathodes consequently rise positive and reduce the gain of the receiver. A more or less constant noise level is maintained determined by the initial bias applied to V_{19} by the setting of the gain control C_4. The common cathode resistor of 1K of V_{19} and the three I.F. amplifiers V_{25}, V_{26}, and V_{27} are located on Chassis 3. An additional cathode resistance of 15K, large compared with 1K, has been inserted in the cathode of V_{19} on Chassis 4 in parallel with the 1K resistor. This acts as a protective resistance in case Chassis 3 and 4 are disconnected, otherwise the cathode of V_{19} would be "floating".

The positive going output from the plate of the first section of V_{17} is now applied to the grid of one

section of V_{18}, the video output stage. After coupling over from the first section of V_{17}, the signal is D.C. restored by the second section which operates as a diode restoring the signals to H.T. negative. C_5 serves to control the level of the output from the receiver at the grid of V_{18}. The other section of V_{18} contains the signal from the calibration gate stage. This signal and the output from the receiver are both developed across the combined plate load of 25K as negative going signals and are applied to the grid of the CRO.

(e) Height Calibrator.

This is located on Chassis 3. V_{16} has a tuned circuit of 3 Kc/sec in its cathode. The tube is normally conducting since its grid is leaked to H.T. positive. V_{27} supplies a negative going square wave from the pulse generator which causes the current in V_{16} to cut off sharply in synchronism with the transmitter pulse.

The inductance L discharges into the capacity of the tuned circuit and a damped oscillation of 3 Kc/sec is produced. V_{15}, a double triode, amplifies, squares and limits the wave. The series grid resistors in each stage allow the voltage to swing positive without drawing excessive grid current. This ensures that the squaring takes place in the correct phase relative to the square synchronising wave. The output of V_{15} is then differentiated by the 150 pf and 500 K RC circuit to give pips. The

latter are then amplified and limited by the first half of V_{14} and are then applied to the second half. This is a cathode follower which operates with its bias beyond cut off. Its function is to remove the negative going pips and pass the positive ones only. The time delay between the pips of a 3 Kc/sec wave is 1/3,000 sec. For a wave travelling at 3×10^5 km/sec this corresponds to a distance of $\frac{3 \times 10^5 \text{km}}{3,000}$. i.e. 100 km. distance. Thus each pip represents a 50 km. height mark when projected on the CRO trace with the reflected pulses. The cathode output is applied to the calibration gate stage V_{13}. Negative going pips from the plate are also applied to V_{13} for neutralising purposes as will be described later.

(f) Frequency Calibrator.

This is located on Chassis 2. V_6 is a crystal oscillator operating at 500 Kc/sec. The full output across the plate circuit is applied to the oscillator grid of V_5, a mixer stage, through the 10 pf coupling condenser. This grid draws heavy current on positive swings charging the 10 pf condenser. The condenser discharges on negative swings and a highly distorted wave form is produced containing a fair distribution of 500 Kc/sec harmonies up to at least 50 Mc/sec. The signal grid of this mixer stage is fed with the 30 to 50 Mc/sec signal from the main oscillator on Chassis 4 through coaxial cable. Audio beats thus occur at 500 Kc/sec increments of the main

variable oscillator frequency as follows:-

60th harmonic of 500 Kc/sec produces zero beat with 30 Mc/sec

61st " " " " " " " " 30.5 "

62nd " " " " " " " " 31 "

and so on.

These audio beats are amplified by the three stages V_7, V_8 and V_9. The band-pass of these stages is restricted to 10 Kc/sec. by the RC coupling filters between stages. The output of these amplifiers is coupled to the double-diode V_{10}. The two diode sections are connected in parallel and the audio beat is rectified to give a negative going calibrating pulse. This pulse is coupled to the calibration gate stage through a screened lead K to Chassis 3. The duration of the pulse is determined by the RC circuit of 0.01 μfd and the 250K variable resistor. It is thus of about 1/500 sec. duration with the middle of the pulse corresponding to the 500 Kc/sec division.

It was found that in fact, pulses were produced every 250 Kc/sec. This was due to the 500 Kc/sec oscillator being sufficiently rich in harmonics to be able to produce audio beats with the second harmonic of the main 30 to 50 Mc/sec variable oscillator. These audio beats occured as follows:-

121st. harmonic of 500 Kc/sec produced zero beat with the second harmonic of 30.25 Mc/sec.

123rd. harmonic of 500 Kc/sec produced zero beat with the

second harmonic of 30.75 Mc/sec., and so on. These pulses at 250 Kc/sec were noticeable up to about 6 Mc/sec (i.e. 36 Mc/sec on the main oscillator). As these provided useful additional frequency marks, no attempt was made to eliminate them.

(g) Calibration Gate Stage

This is situated on Chassis 3 and is the double triode V_{13}. The second section of this triode (the right hand one in the diagram) has the calibrating pulse from the frequency calibrator on Chassis 2 connected to its grid via the screened lead K. This grid has a standing positive bias which is supplied from the cathode of V_8, also via K. This positive bias prevents the tube from responding to noise and small spurious pulses from the frequency calibrator. This tube is thus normally conducting, its plate being connected to a point on the bleeder between H.T. positive and H.T. negative. The grid of the first section of V_{13} is returned to a point on the same bleeder so that this section is biased beyond cut off. The positive going height calibration pips are also supplied to this grid, the bias not normally allowing the pips to appear across the cathode load.

The negative going calibrating pulse from the frequency calibrator via K causes the second section to cut off completely, the section stops conducting causing a rise in potential at the plate, and a corresponding rise in the grid potential of the first section. The bias of this

grid is now brought to just behind cut off. This triode acts as a cathode follower and the height calibration pips now appear across the cathode load. This cathode load is by-passed by a series of condensers through C_6. The RC time constant of this cathode circuit controls the length of the pips. The selection of one of the capacities from C_6 provides coarse adjustment and the 50K variable resistor provides fine adjustment for controlling the pip length.

Even though the stage is normally biased well below cut off, the grid-cathode capacity tends to allow the height calibration pips still to appear on the cathode. This is due to the cathode resistor being unavoidable high. A 5 pf condenser from the plate V_{14} supplies negative going pips to the cathode to neutralise the height pips which still appear when the stage is biased well back.

The positive pips developed on the cathode with each calibration pulse are fed in one section of the double triode V_{18}, and negative going pips are developed in the common plate load of 25K together with the negative pulses from the receiver. These are then fed to the main CRO via cross-connection Q.

(h) Recording and monitoring oscillographs.

The recording oscillograph is a 5LPIA type CR tube with a blue short persistence screen suitable for photographic purposes. It has been mentioned previously

that it is very convenient to control apparatus from the A.C. mains frequency. The pulse rate has already been controlled from this source. It is therefore very convenient to control the time-base of the recording oscillograph from this source as well, since it will thus not go out of synchronisation with the pulse rate should the mains frequency alter at all. A pulse-rate of 50 c/sec. corresponds to an interval of 20 milliseconds between pulses. Thus it is possible to read virtual heights up to 3,000 km. At the most, it is only really necessary to be able to read heights up to 1,500 km. under the usual ionosphere conditions. Hence a fairly large amplifier would be necessary in order that the first half of the time base be spread over the CRO trace. This would affect the linearity of the time base, and in order to avoid this possibility, as well as the need for a large amplifier, a delay-type time base was employed, working over one half of the cycle only.

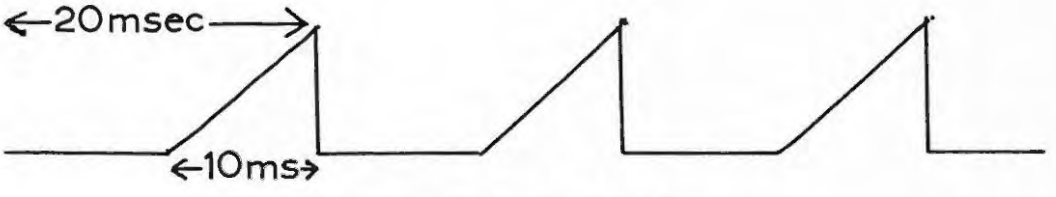

Delay-type time base

The time base comprises V_{52}, V_{53}, V_{54}, V_{55} and V_{56} in the circuit diagram of the recording oscillograph (Fig. 15) The 50c/sec A.C. mains frequency is injected to the grid of V_{54} through the step-up transformer T_{16} and the phase-shifting

FIG:15 RECORDING OSCILLOGRAPH

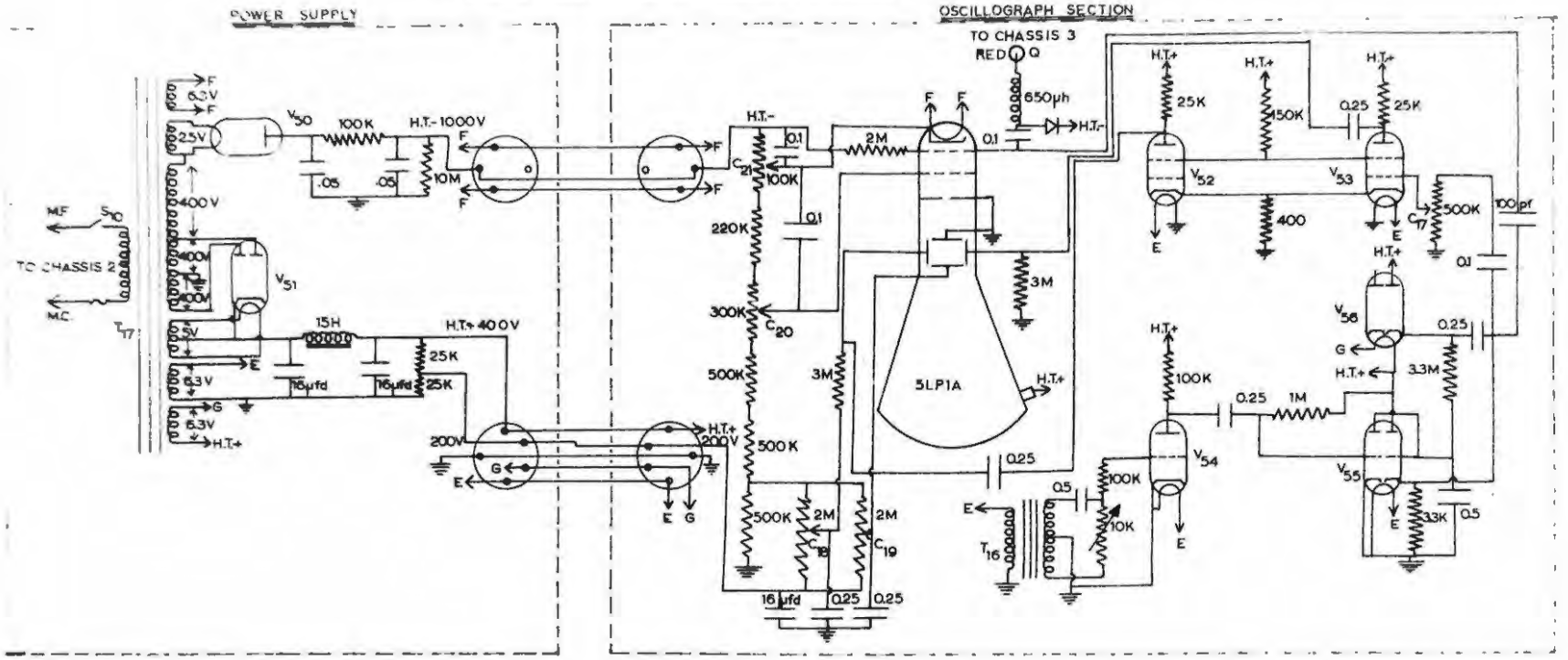

RC circuit of 10K and 0.5 μfd. V_{54} squares and limits the wave which is then fed into the grid of the first section of V_{55}, a double triode. This section is an electronic clamp; it has its plate connected directly to the grid of the second section. Without any input of its grid the first section is normally conducting since its grid is returned to H.T. positive. Consequently the potential on the grid of the second section is low. When a negative going square wave is applied to the grid of the first section from V_{54}, it ceases to conduct and its plate potential begins to rise, and as it does so the potential across the 0.5 μfd condenser also rises. This automatically raises the cathode potential of the second section (since it now starts to conduct) and this higher potential is applied through the 0.25 μfd condenser to the cathode of V_{56}, a diode. The difference in potential across the 3.3 M resistance is thus kept constant (within the limitations of the cathode follower), and therefore the current through it is also constant. Since this current flows through the 0.5 μfd condenser, the rate of charge of this condenser is also constant. The purpose of the diode V_{56} is to allow its cathode (which is also the top of the 3.3 M resistor) to rise well above the H.T. potential during charging peaks. The advent of a positive going square wave at the grid of the first section of V_{55} causes the valve to conduct more and the grid of the second section to drop and hence the second section cuts off until

the next negative going square wave appears at the grid of the first section. Thus the desired wave-form is produced at the cathode of the second section of V_{55} - a linear time base working over one half of the cycle only. The output from the cathode is then fed to the push-pull amplifier V_{52} and V_{53} and is then applied to the X deflecting plates of the CR tube. Part of the output from the cathode is also fed through the 100 pf condenser to the grid of the CR tube to black out the fly back of the time-base on the trace.

The grid of the CR tube operates at about 1,000 volts negative and has a grid leak resister of 2M to the H.T. negative supply. The bias on the cathode can be adjusted by the control C_{21} on the H.T. bleeder and this controls the tube intensity. Position control is obtained by varying C_{18} and C_{19}, the 2M resistors in the X and Y plate circuits. The anode operates at ground potential, and the intensifying electrode is supplied with 400 volts positive from the H.T. supplying the time-base tubes.

The receiver output and calibrating pips from Chassis 3 are fed via cross-connection Q on to the grid of the CR tube through the 0.1 μfd D.C. blocking condenser. These signals are all negative going and cause black-outs spots on the CRT trace. As the CRO was situated in a dark-room, a fairly long lead had to be taken from the main equipment. This lead tended to pick up the pulse modulated R.F.

signals from the transmitter and apply it to the grid of the CR tube. This caused a blurring of the trace, since a positive signal would increase the trace intensity. It was particularly important to eliminate this since the oscillograph was to be photographed. Hence an R.F. choke of 650 microhenries and a crystal diode returned to H.T. negative were inserted in the coupling circuit. The crystal diode served to by-pass any positive going pulses which occured in this lead.

The monitoring oscillograph is situated on Chassis 3. The time base is provided by V_{12}. It is normally cut off since its grid is returned to a point about 50 volts negative via cross-connection N. The 0.1μfd condenser across the valve is charged up to the H.T. positive potential through the 2M resistor. A positive going square pulse from the pulse generator circuit via cross-connection M is applied to the grid. This causes the valve to conduct and the condenser discharges through the valve. The condenser then begins to charge up slowly through the 2M resistor, until the arrival of the next positive pulse when it discharges again. A saw-tooth voltage is thus produced at the plate of V_{12} and amplified through V_{11} before being applied to the X plates of the CR tube. The output of the time base amplifier is controlled by C_{15}. Output from the receiver is supplied from the plate of V_{17} via cross-connection S, and applied to the Y deflecting plates.

Height calibration pips are applied to the grid via cross-connection T from V_{14}. These are not "gated" by the calibrating pulse, but appear permanently as black-out spots on the trace.

The monitoring tube works off the 400 volts H.T. negative and the 400 volts H.T. positive supply. Its cathode is biased positively by being returned to a point on the bleeder. C_{13} and C_{14} are the position controls which vary the potential on the X and Y plates. C_{12} and C_9 control the receiver output and the pip length respectively.

(i) Power Supplies.

Chassis 1 contains four H.T. supplies, with V_1, V_2, V_3 and V_4 as rectifiers. V_1 rectifiers the voltage from T_4, supplying an H.T. voltage of - 400 volts to Chassis 3 and 4. T_3 supplies the 5 volts filament potential to V_1. V_2 and V_3 are retifiers for two H.T. positive supplies of 400 volts at 200 ma. The rectifying voltage comes from T_5 and T_3 respectively. The filaments are supplied from T_6 and T_7 respectively. V_2 supplies Chassis 2 and 3 and V_3 supplies Chassis 4. V_4 is a mercury vapour rectifier, which provides a D.C. potential of 2,000 volts from T_{10}, at 50 Ma. This supplies the final transmitter amplifier on Chassis 5. The filament supplies to the various chassis are as follows:-

T_1 supplies 6.3 volts at 12 amps to Chassis 4.

T_2 supplies 6.3 volts at 2 amps to Chassis 2, and 2.5 volts

at 2 amps to Chassis 3; this runs the filament of the monitoring oscillograph, the original 5 volts being dropped through the 1.25 ohm resistor.

T_6 supplies 6.3 volts at 5 amps, at H.T. negative potential to Chassis 3.

T_7 supplies 6.3 volts at 5 amps to Chassis 3.

T_9 supplies 2.5 volts at 5 amps to V_4.

T_{11} (on Chassis 2) supplies 6.3 volts at 2 amps to the five jewel lights. On Chassis 5, the rectifier V_{49}, supplies the H.T. positive potential of 400 volts at 120 ma to V_{44}, V_{45} and V_{46}, the A.C. potential being supplied from T_{13}.

T_{14} supplies 6.3 volts at 5 amps to V_{44}, V_{45}, and V_{46} and 5 volts at 5 amps to V_{49}. (The 10 volts from T_{14} is dropped through the 2.5 ohm resistor).

T_{15} supplies 10 volts at 10 amps to V_{47} and V_{48}.

T_{17} is the recording oscillograph transformer.

V_{51} supplies 400 volts H.T. positive to the oscillograph time base tubes and the intensifying electrode.

V_{50} produces a negative supply of 1000 volts for the main CRO. There are three filament supplies:-

6.3 volts (FF) to the CRO, 6.3v. (E) at ground potential, and 6.3 volts operating at H.T. positive to run V_{56}.

(f) Automatic Switching.

Two electric gramophone motors on Chassis 2 and 4 are geared down to one revolution in 4½ minutes and 3⅝

minutes respectively. The various cams on the arms of these motors contain the trip switches. The mains input through the 10 amp. fuse and the main switch S_1 is split into three leads. The grounded side of the mains is a common lead denoted by M.C., and the other lead is split into two - M.F. and M.H.T.

M.F. is the lead providing mains voltages to the filament transformers. It is also the lead which contains the switching system for the filament transformers. Similarly, M.H.T. provides mains voltage to the H.T. transformers, and is also fed through the H.T. switching system. Switches S_1 to S_7 are all double pole single throw, the second section switching the various jewel lights. S_2, S_3, S_5, S_6 and S_7 are all in parallel with the various automatic switches on the cams. This provides a manual switch, should the various sections be operated separately. Normal operation is as follows:- Switches S_1, S_4, S_8 and S_{10} are always left on. Once each hour the clock trips over the switch which starts motor 1 and Chassis 2. The cam switch on the clock is in parallel with S_5. After a few seconds trip switch indicated by Motor 2 (on the Motor 1 shaft) starts Motor 2 an Chassis 4. The latter is also the condenser drive motor, and the condenser starts to rotate. A few seconds later the trip switch in parallel with S_2, switches on all the filaments, and also the H.T. and filaments of the recording oscillograph. The

filaments are given 90 seconds to warm up. The H.T. trip switch, in parallel with S_3, is arranged to work just as the condenser is brought into the zero position, corresponding to the lowest transmitting frequency of 1.5 Mc/sec. Just before this the recording film switch, in parallel with S_7, starts the motor on the recording camera. This provides a small piece of blank film after the previous sweep, before the sweep starts.

In the meanwhile, the switch denoted by Motor 1 (in parallel with S_5) has come on, the trip switch on the clock is now superfluous and switches off sometime later. Similarly, the trip switch denoted by Motor 2 (in parallel with S_6) has also come on, and trip switch on Chassis 2 for Motor 2 is also superfluous. This also switches off sometime later. Thus Motor 1 and 2 are now switched through the trip switches on their own shafts, and will automatically switch themselves off when the cam shaft has completed one revolution.

When the condenser has completed one 180° sweep, the frequency sweep is completed, and the recording film, the H.T., and the filaments switch themselves off in that order. The two motors are then left to complete their revolution and switch themselves off, ready for the start of the next sweep.

Should readings be required at more frequent intervals than once every hour, all that is required is

for S_5 to be switched on until Motor 1 trip switch takes over. It must then be switched off before the end of the sweep. S_8 in series with the switch to the recording film is provided so that the apparatus may be switched on at random without recording a sweep on the film. S_8 must merely be switched off, and the motor in the recording camera will not operate during the sweep.

If it is desired to operate the equipment without working through the automatic switching circuits, the filament switch (S_2) is first switched on and a 90 second warm up period is allowed. The H.T. may now be switched on by S_3 and the sweep may be conducted either by disengaging the gear on the condenser drive motor and rotating the condenser by hand, or alternatively the condenser may be run by Motor 2 by switching on S_6 on Chassis 4. Care should be taken when using this method to see that the condenser is returned to its correct starting position for automatic operation. When running Motor 2 in this way, S_6 should be switched off when the switch on its own cam shaft has "taken over", this is after about half a revolution. The motor will then switch itself off after completing the revolution and thus return to its starting position. When using Motor 2 in this way, S_8, the series switch to the recording film, must be switched off, otherwise the recording camera will operate.

(k) Recording Camera.

The photograph records were made on 35 mm. film, using a home-made camera. (fig 16) A lens with adjustable aperture focussed the image of the oscillograph screen on the film, which was driven in a vertical direction by a synchronous motor. Since the trace of the oscillograph denotes the time delay (or virtual height) of the pube from the ionosphere at each frequency, the film will thus trace out a graph of frequency against virtual height. The calibration pips also appear on the film at $\frac{1}{2}$ Mc/sec intervals at the lower frequencies and every $\frac{1}{4}$ Mc/sec at higher frequencies, as has already been pointed out. Positive type film was used, and as it was rather insensitive, the intensity of the trace had to be kept rather high. This caused the whole screen to glow slightly. In order to prevent over exposure of the film, the screen was covered in lead foil, except for the trace.

The complete frequency sweep took about $1\frac{3}{4}$ minutes and this was recorded on approximately nine inches of film.

FIG:16 RECORDING CAMERA

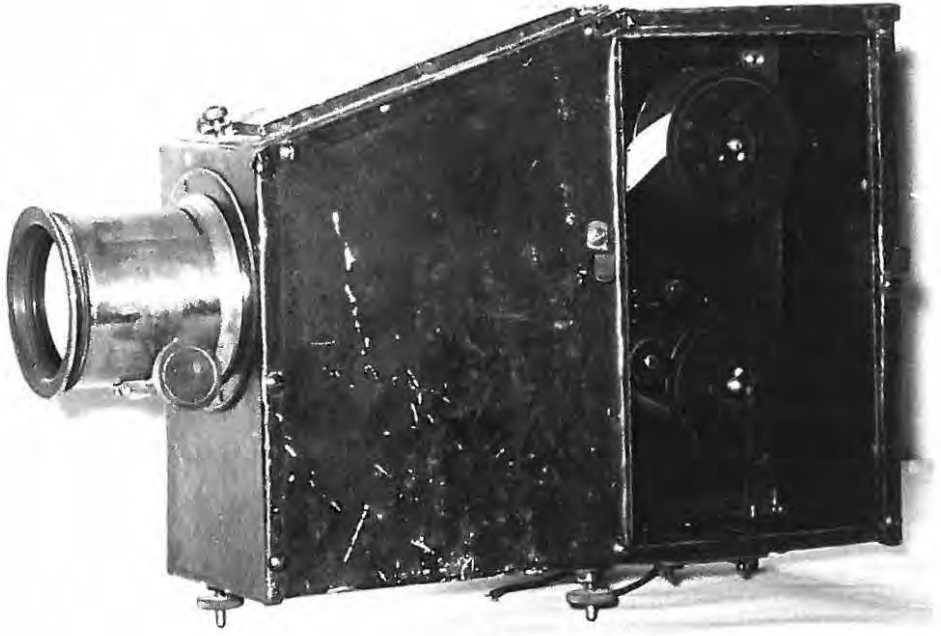

FIG:17 WAVE FILTERS

TYPE 1 : LOW PASS FILTER, $f_c = \frac{1}{\pi\sqrt{LC}}$

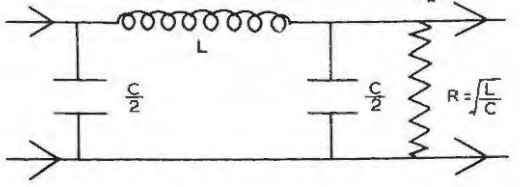

TYPE 2 : LOW PASS FILTER, $f_c = \frac{1}{\pi\sqrt{LC}}$

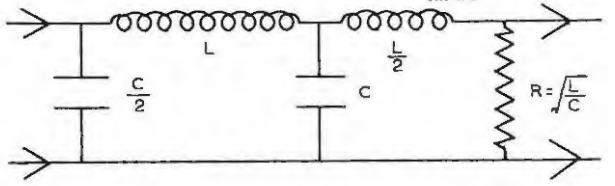

IN BOTH TYPES 1 & 2 THE FIRST CAPACITY IS THE OUTPUT CAPACITY OF THE VALVE AND THE SECOND CAPACITY THE INPUTCAPACITY OF THE NEXT STAGE.

TYPE 3 : HIGH PASS FILTER, $f_c = \frac{1}{4\pi\sqrt{LC}}$

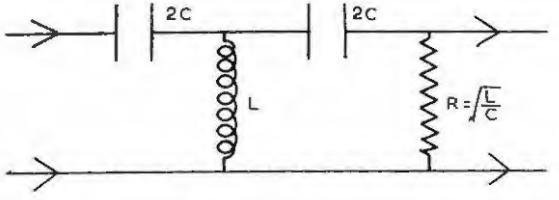

TABLE 1 - VALVES

V_1 - 5Y3	V_{20} - 6L6	V_{39} - 6SJ7
V_2 - 5U4	V_{21} - 6C5	V_{40} - 6J5
V_3 - 5U4	V_{22} - 6J7	V_{41} - 6SA7
V_4 - 866	V_{23} - 6C5	V_{42} - 6AC7
V_5 - 6SA7	V_{24} - 6SC7	V_{43} - 6J5
V_6 - 6C5	V_{25} - 6SK7	V_{44} - 807
V_7 - 6SJ7	V_{26} - 6SK7	V_{45} - 807
V_8 - 6SJ7	V_{27} - 6SK7	V_{46} - 807
V_9 - 6SJ7	V_{28} - 6SA7	V_{47} - 813
V_{10} - 6H6	V_{29} - 6H6	V_{48} - 813
V_{11} - 6J7	V_{30} - 6AC7	V_{49} - 5Y3
V_{12} - 6C5	V_{31} - 6AG7	V_{50} - 2X2
V_{13} - 6SN7	V_{32} - 6SA7	V_{51} - 80
V_{14} - 6SN7	V_{33} - 6SK7	V_{52} - 6V6
V_{15} - 6SN7	V_{34} - 6AC7	V_{53} - 6V6
V_{16} - 6J5	V_{35} - VR78	V_{54} - 6SF5
V_{17} - 6SL7	V_{36} - VR135	V_{55} - 6SN7
V_{18} - 6SN7	V_{37} - 6AC7	V_{56} - 6H6
V_{19} - 6V6	V_{38} - 955	

TABLE 11 - CONTROLS

Sounder Controls

(Unless otherwise stated these appear on the front panel of the apparatus).

C_1 - Calibration pulse-length (Not on outer panel).

C_2 - Transmitter pulse phase

C_3 - Transmitter pulse length

C_4 - AVC setting. (Not on panel)

C_5 - Receiver output

C_6 - Calibration pip length (coarse)

C_7 - Calibration pip length (fine)

C_8 - Frequency change.

Monitoring Oscillograph Controls.

C_9 - Cal. pip length

C_{10} - Intensity

C_{11} - Focus

C_{12} - Y axis amplifier gain (Receiver output)

C_{13} - Y axis positioning control

C_{14} - X axis positioning control

C_{15} - X axis amplifier gain (Time base)

Recording Oscillograph Controls

C_{16} - Time-base phase

C_{17} - X axis amplifier gain (Time base)

C_{18} - X axis position control

C_{19} - Y axis position control

C_{20} - Focus

C_{21} - Intensity.

TABLE iii - Cross-Connections

A - 6.3V filament supply, Chassis 1 supplying Chassis 2.

B - 6.3V filament supply, Chassis 1 supplying Chassis 3.

C - 6.3V filament supply, Chassis 1 supplying Chassis 4.

D - 6.3V filament supply, at H.T. negative, Chassis 1 supplying Chassis 3.

E - 6.3V filament supply, for oscillograph section.

F - 6.3V filament supply, Recording CRO

G - 6.3V filament supply, H.T. positive for V_{56}, oscillograph section.

H - 2.5V filament supply, Chassis 1 to Monitoring Oscillograph, Chassis 3.

J - 2000V H.T. supply, Chassis 1 supplying Chassis 5.

K - V_{10} Chassis 2 to V_{13} Chassis 3

L - V_{21} to V_{16}, Chassis 3.

M - V_{22} to V_{12}, Chassis 3.

N - V_{23} to V_{12}, Chassis 3

P - V_{19} Chassis 3 to V_{25}, V_{26}, V_{27}, Chassis 4 (AVC)

Q - V_{18} Chassis 3 to Recording Oscillograph

R - V_{18} to V_{13}, Chassis 3

S - V_{17} to Monitoring Oscillograph, Chassis 3

T - V_{14} to Monitoring Oscillograph, Chassis 3.

U - V_{20} Chassis 3 to V_{40} Chassis 4.

V - V_{29} Chassis 4 to V_{17} Chassis 3

W - Aerial to V_{30}, Chassis 4

X - V_{42} to V_{28}, Chassis 4

Y - 6.3V filament supply, Chassis 5.

Z - 10V filament supply, Chassis 5 for V_{47} and V_{48}

TABLE 111 cont. - Switches

S_1	- Mains	S_6	- Motor 2
S_2	- Filaments	S_7	- Recording Film, Parallel
S_3	- H.T.	S_8	- Recording Film, Series
S_4	- Clock	S_9	- Monitoring Oscillograph
S_5	- Motor 1.	S_{10}	- Recording Oscillograph.

Reduction and presentation of observations on control days.

(1) Photographic Records.

Fig. 18 shows a typical night time record made with the apparatus. Only one layer is observed, the F_2 layer. Whilst it is possible that the E layer may still be present during the night, its critical frequency fell below the minimum of the frequency range of the apparatus and was not observed.

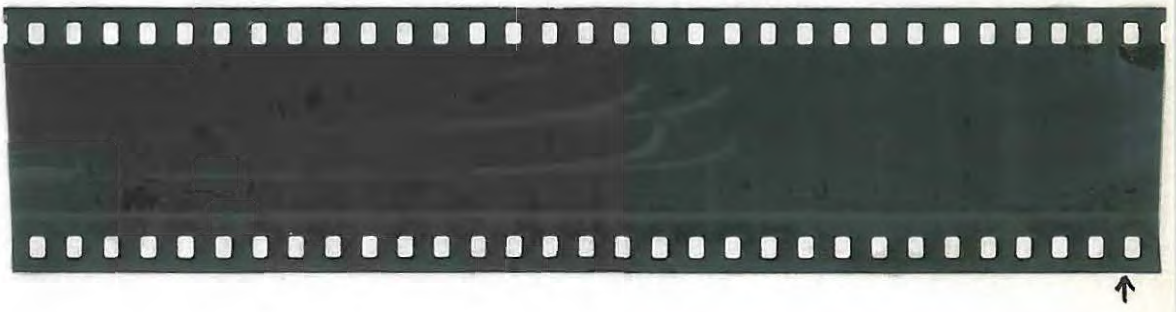

Fig. 18. Typical night-time h'f record @200 hrs. SAST December 5th 1954.

The long height calibrating mark at the beginning of the sweep on the left hand edge of the record, corresponds to 1.5 Mc./sec, the middle of the mark being exactly 1.5 Mc./sec. These height marks are at $\frac{1}{4}$Mc/sec intervals up to about 7 Mc/sec and at $\frac{1}{8}$Mc/sec intervals after that. It will be noticed that there is a distinct line across the film, as indicated by the arrow, just after the 7 Mc./sec mark. At this point the 7.275 Mc/sec oscillator in the transmitter section saturated the receiver, and this provided a useful check for frequency calibration of the

height marks. The splitting of the ray into its ordinary and extraordinary components is very noticeable. The component with the lower critical frequency at 3.75 Mc/sec is the ordinary critical frequency, and the extraordinary critical is observed at about $\frac{1}{2}$ Mc/sec higher. Due to less absorption at night time because of the absence of lower layers, multiple reflections are easily observed occurring at heights which are multiples of the virtual height of the first order reflection (nearest to the ground pulse).

During the post sunrise period, the critical frequency of the F_2 layer increases as does that of the E layer. This E layer critical soon reaches a value above the lowest limit of the apparatus and is observed on the records at a height of about 120 km. It has been noticed that every day the E layer always has two components, the E_1 and E_2, soon after its appearance at sunrise. The E_2, with a higher critical frequency appears first, and soon after the E_1 is observed with a slightly lower critical frequency. Fig. 19 shows a typical early morning record taken with the E_1, E_2 and F_2 layers all present.

Fig. 19. Typical early morning h'f record 0600 hrs. SAST December 5th, 1954.

The E_1 critical occurs at 2.0 Mc/sec, whilst the reflections between 2.0 and 2.25 Mc/sec are interpreted as being due to an E_2 layer with a critical frequency of 2.25 Mc/sec.

The regular occurrence of these reflections from day to day indicates that they cannot be interpreted as Sporadic E. These reflections, particularly just after sunrise, usually exhibit a definite critical frequency which is not observed with Esp. Usually reflections from Esp are still observed even while reflections are also received from the F region making the interpretation of the critical of Esp obscure. It is normal to consider the maximum frequency at which Esp echoes are received to be its critical frequency.

Some sixty to ninety minutes after sunrise a change in slope on the records begins to appear in the region 3.5 to 4.0 Mc/sec. This indicates the beginning of the formation of the F_1. A slight thickening of the trace in Fig. 19 around 3.5 Mc/sec can just be observed, indicating the formation of the F_1 layer. 1½ to 2 hours after sunrise the F_1 layer is observed as a sharp cusp in the records between the E_2 and F_2 criticals. Fig. 20 shows a typical day-time record where all four layers are formed.

Fig. 20. Typical day-time h'f record 0815 hrs. SAST, December 5th, 1954.

The splitting of the ray into its ordinary and extra-ordinary components is easily detectable in both the F_1 and F_2 layers.

The three records shown above were typical of normal conditions undisturbed by Sporadic E. The two records shown below in Figs. 21 and 22 show the effect of the occurrence of Sporadic E.

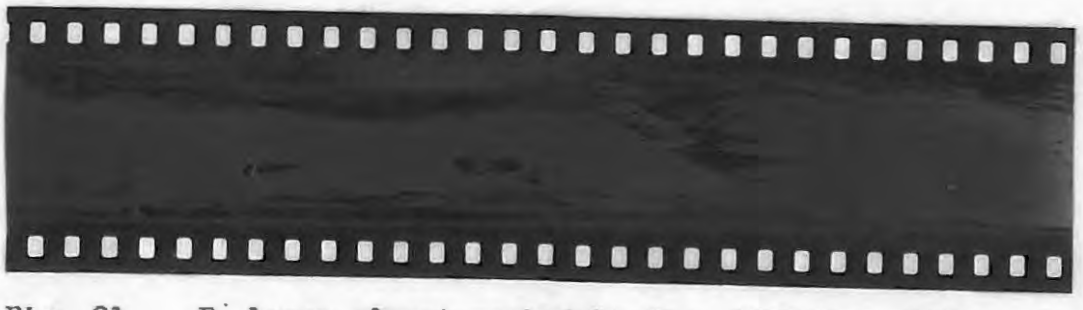

Fig. 21 F_1 layer almost masked by Esp. 1600 hrs. SAST December 3rd, 1954.

In Fig. 21 the F_1 layer critical is only just visible above the Esp, whilst in Fig. 22, the F_1 layer critical is not visible at all, although retardation produced by it on the F_2 indicates it is still present, the density of the Esp being greater than that of the F_1.

Fig. 22. F_1 completely masked by Esp. 1300 hrs. SAST December 3rd, 1954.

In both records it will be noticed that the E_2 is not now visible, probably due to the fact it has now been covered by the Esp. It was only on rare occasions, is at all, that E_2 and Esp were both present at once. The difficulty usually lay in distinguishing between the two. An examination of the records taken showed that any reflection above 4.0 Mc/sec from E layer heights could only be interpreted as Esp. This was taken as a general rule in scaling. Esp is also often characterised by intense multiple order reflections which are rarely seen on E_2 reflections. A sudden jump from the previous record in E_2 critical frequency was also put down to Esp. Where any doubt existed the reflections were usually attributed to Esp.

(2) Determination of time-height electron density distribution

Several methods have been suggested for the deduction of true heights from virtual heights by APPLETON (1930, 1937) and MURRAY and HOAG (1937), but their results lack cases of application. The method proposed by

BOOKER and SEATON (1940) is based on the assumption that the electron density height distribution has a parabolic form. Whilst this may be true near the maximum in a layer, it is doubtful whether this is so at points well below the maximum. The more recent methods of MANNING (1947) and KELSO (1952) contain few assumptions than their predecessors. Kelso's method is fairly simple in its application, although rather laborious and depends on the following argument. The magneto-ionic theory (APPLETON, 1932) shows that, neglecting the earth's magnetic field and the effects of collisions, the index of refraction for a radio wave incident vertically on an ionospheric layer may be written,

$$\mu^2 = 1 - \frac{4\pi N e^2}{mp^2} \qquad \ldots\ 6$$

where μ = index of refraction

$\frac{p}{2\pi}$ = operating frequency

N = electron density

e, m = charge and mass of the electron

Under the conditions noted above the group path P' is given by:-

$$P' = 2\int_0^{hT} \frac{ds}{\mu} \qquad \ldots\ 7$$

where the integral is taken along the path of the ray from the bottom of the layer to the point of reflection h_T, the "true height".

It has been shown (PEKERIS, 1940; MANNING, 1947) that equation 7 may be transformed to give an expression for the height of reflection, h_T, for some frequency f_v, in terms of the group height, $h' = P/2$, and the operating frequency f.

$$h_T(f_v) = \frac{2}{\pi}\int_0^{fv} \frac{h'(f)df}{\sqrt{fv^2 - f^2}} + h_o \qquad \ldots\ 8$$

where h_o is the height from ground level to the bottom of the layer. If the substitution $x = f/_{fv}$ is made equation 8 becomes :-

$$h_T(f_v) = \frac{2}{\pi}\int_0^{1} \frac{h'(x)dx}{\sqrt{1 - x^2}} + h_o \qquad \ldots\ 9$$

This is now the integral which has to be evaluated to determine the true height. The group height (or virtual height) has been measured as a function of frequency so that all the information for the experimental determination of the true height is available.

For the approximate ionospheric conditions defined above, the signal will be reflected at a level given by $\mu = 0$, which from equation 6 gives a value of N as follows:-

$$N(h_T) = \frac{mp^2}{4\pi e^2} \qquad \ldots\ 10$$

Thus for each value of h_T. the true height of reflection determined from equation 9, it is possible to compute from equation 10 the electron density at that height. The applicability of the results in equations 9 and 10 is restricted by the assumptions made,

(i) the earth's magnetic field can be neglected

(ii) the effects of collisions can be neglected

(iii) Ray theory (geometrical optics) is valid

(iv) for each electron density there is a unique height.

In a later papers (KELSO, 1954, 1957) a correction for the earth's magnetic field has been included in Kelso's method. However, results presented here are based on the assumption that the earth's magnetic field can be neglected. The integral in equation 9 is written as:-

$$I = \int_0 \frac{h'(x)dx}{\sqrt{1 - x^2}} \qquad \ldots\ 11$$

Since the group (or virtual) height is defined for positive values of x only, it can be defined for negative values of x so that h'(x) is an even function, then -

$$h'(-x) = h'(x) \qquad \ldots\ 12$$

Equation 11 now becomes -

$$I = \tfrac{1}{2}\int_{-1}^{+1} \frac{h'(x)dx}{\sqrt{1 - x^2}} \qquad \ldots\ 13$$

Writing $x = \cos\theta$, equation 13 may be written

$$I = \tfrac{1}{2}\int_0^{\pi} h'(\cos\theta)d\theta \qquad \ldots\ 14$$

Kelso showed that this can be written in the form:-

$$I = \frac{\pi}{2n}\sum_{k=1}^{n} h'(f_k) \qquad \ldots\ 15$$

where $f_k = x_k f_v$, and $x_k = \cos\theta_k$, and $\theta_k = \frac{(2k - 1)\pi}{2n}$,

$k = 1, 2, 3 \ldots\ldots n$

Substitute in equation 9 and

$$h_T(f_v) = \frac{1}{n} \sum_{k=1}^{n} h'(f_k) \qquad \ldots\ldots 16$$

The procedure, thus involves reading the values of h' corresponding to each value of f_k and averaging them. This gives $h_T(f_v)$. Since h'(f) is an even function, there are only n/2 or $\frac{n+1}{2}$ values to be used in this procedure, according to whether n is even or odd. This is because for positive values of x_k there is a corresponding negative value of the same magnitude.

Thus $$h_T(f_v) = \frac{2}{n} \sum_{k=1}^{n/2} h'(f_k) \qquad \ldots\ldots 17$$

When n = 10, $h_T(f_v) = \frac{1}{5} \sum_{k=1}^{5} h'(f_k)$

k	1	2	3	4	5
x_k	0.988	0.891	0.707	0.454	0.156
f_v	f_1	f_2	f_3	f_4	f_5

When n = 20, $h_T(f_v) = 1/10 \sum_{k=1}^{10} h'(f_k)$

k	1	2	3	4	5	6
x_k	0.997	0.972	0.924	0.853	0.760	0.649
f_v	f_1	f_2	f_3	f_4	f_5	f_6

k	7	8	9	10	
x_k	0.522	0.383	0.233	0.078	
f_v	f_7	f_8	f_9	f_{10}	

When the reflections are not retarded by any intervening layer (i.e. E region in daytime and the F_2 at night), it is only necessary to take 5 points on the curve. When more than one layer is present it is necessary to take 10 points because of the discontinuities and cusps which occur when more than one layer is present.

The method can be simplified by choosing a set of values of f_v in advance and drawing up tables of f_k's for certain fixed values of f_v, which are then always used in the scaling. In this way it is unnecessary to evaluate the f_k's each time for any particular value of f_v chosen at random but always to use one of the values of f_v in the table. Naturally the value of f^o for any layer invariably did not coincide with one of the pre-selected values of f_v. As the true height of the maximum electron density is an important parameter, it was always necessary to evaluate f_k's for f^o in each layer.

For the purpose of measurement the records were enlarged ten times in a microfilm reader. On the base of this was drawn a scale of heights to fit the height calibrating marks on an average record. Owing to the slight variations in the time base of the recording oscillograph, the actual scale rarely fitted the prepared scale accurately and a correction was always applied for this by reading the difference at the nearest 50 km. mark. With this apparatus it was found that the heights could

be read to the nearest 2 km. Fig. 23 shows an enlargement of Fig. 20 by approximately the same amount. It will be seen that the definition is good enough to allow such accuracy. The frequencies were estimated by inspection to the nearest 0.01 Mc/sec. The procedure was as follows: First f^o for each layer was estimated and a set of values of f_v were drawn up for each layer. Usually 5 values were chosen for the F_2 layer, 4 for the F_1 and 3 for the E layers. In each case this included the value of f^o. For each value of f_v thus chosen, the virtual heights h' corresponding to each value of f_k were then read off the record, recorded on an adding machine and the average taken. This average value corresponded to $h_T(f_v)$ as in equation 17.

All data pertaining to a particular record was recorded and reduced on a sheet of the type shown in Fig. 24. This refers to the record shown in Fig. 20. Thus values of f_v,(and hence n, the electron density) were obtained as a function of h_T, the true height. A graph could then be plotted of the true height electron density distribution. Fig. 25 shows the distribution obtained from Fig. 20, corresponding to the values in Fig. 24. The distribution so obtained by Kelso's method compares very favourably with recent rocket measurements of the electron density up to 220 km. by SEDDON, PICKAR and JACKSON (1954).

When the records were marred by Esp a slightly

FIG: 23 ENLARGEMENT OF FIG: 20

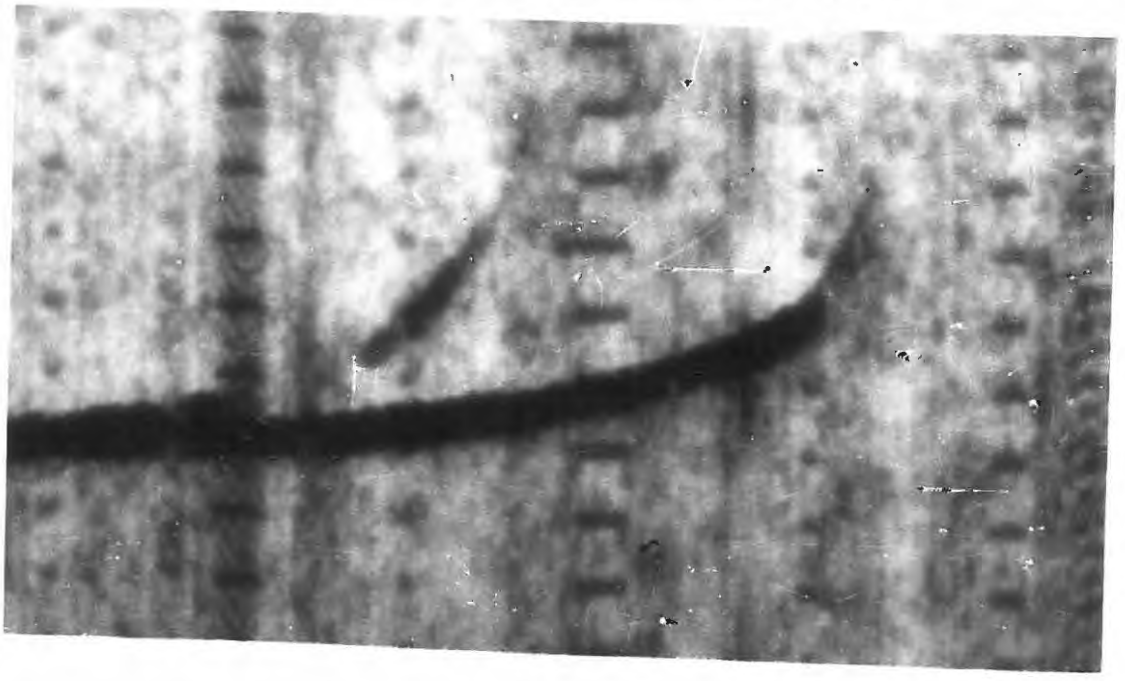

FIG: 24. TYPICAL SCALING SHEET

/S.

IONOSPHERE RESEARCH LABORATORY. DEPARTMENT OF PHYSICS.

SCALING OF RECORDS.

RECORD No: ...367..... DATE 5/12/54. S.M.S.TIME: 08. Hrs 15 Mins...

$f^o(F_2)$ = 6.40	$N(F_2)$ = 5.08	$f^o(E_2)$ = 3.26	$N(E_2)$ = 1.32
$f^o(F_1)$ = 4.13	$N(F_1)$ = 2.11	$f^o(E_1)$ = 3.00	$N(E_1)$ = 1.12
		$f^o(E_{sp})$ = ——	$N(E_{sp})$ = ——

f_v	n	h	f_v	n	h
6.40	5.08	309	3.25	1.31	125
6.25	4.84	282	3.00	1.12	123
6.00	4.45	265	2.75	0.94	119
5.50	3.75	248			
5.00	3.10	233			
4.13	2.11	214			
4.00	1.98	187			
3.75	1.74	160	2.50	0.77	118

Comments:-

different procedure was adopted, as the high density of Esp masked the reflections from the F_1 and sometimes part or the whole of the F_2. Typical records showing the effect of Esp have already been shown in Figs. 21 and 22. Obviously these records cannot be scaled according to Kelso's method using the values of h' from the Esp, as clearly a reading of h' from either the F_1 or F_2 is the correct one. The values of h_T so obtained would be considerably less than the correct value. An estimate was therefore made of h_T, and it will be shown that this approximates fairly closely to the true value.

Fig. 21 is fairly simple and the reflections from the F_1 which are masked by Esp were estimated by extrapolating the F_1 layer curve back to what normally would be the f^oE_2 at that time of day. This was estimated by consulting previous records and taking an average. Around mid-day f^oE_2 was normally about 3.75 Mc/sec. The distribution so obtained from Fig. 21 is shown in Fig. 26. It is obvious that only the f_v at f^oF_1 can be scaled, as any other point would fall too near the extrapolated portion and be largely a matter of guess work. Thus the F_1 is drawn as a dotted line to show that over that portion it has only been estimated.

Fig. 22 has the F_1 layer completely masked by Esp and only part of the F_2 reflections are visible.

In this case the minimum virtual height of the F_2 reflections was assumed up to an average value of f^oF_1 for that particular time of day by consulting previous records etc. This was normally some value between 4.0 and 4.5 Mc/sec. From this assumed value of f^oF_1 the virtual height was usually assumed to be 250 km. (an average value of h' for normal F_1 reflections), back to an estimated value of f^oE_2 for that time of day, as was done for Fig. 21 previously. In this way it was possible to make an estimate of the shape of the F_2 layer near its maximum. The graph obtained from Fig. 22 using this method is shown in Fig. 27. The extrapolated portion of the record is shown by the dotted lines.

To show how nearly this estimate approximates to the true Kelso distribution, it will be assumed that the record in Fig. 20 where there is no Esp, has been masked by Esp up to 5.0 Mc/sec. First an estimate is made of f^oF_1 and f^oE_2. This is done either by interpolating between the previous record and the one proceeding, or by taking an average value for that time of day, In this case they will be supposed to be 4.1 Mc/sec and 3.25 Mc/sec respectively. The minimum virtual height of 320 km. at 5.0 Mc/sec will be assumed to continue back to f^oF_1 (at 4.1 Mc/sec) and a virtual height of 250 km. from f^oF_1 to f^oE_2 (3.25 Mc/sec). Fig. 28 shows the true Kelso distributions as in Fig. 25 together with the

approximate one as suggested above. It is seen that they agree fairly closely near the maximum of the F_2 layer, where the reflections on the record were not masked by Esp.

In general Kelso's method is strictly only applicable to those records where there is one layer, and the record shows no discontinuities and cusps etc. Gross errors occur if a value of f_k falls on or near the F_1 peak and obviously the value of h' which would normally be read off (say 700 - 800 km.) would give a much higher value of h_T for that particular f_v than was correct. Care was thus taken to ensure that any value of f_k did not occur near the F_1 peak by choosing appropriate values of f_v beforehand.

In all about 1200 records were obtained during the control period, covering fifteen days before and fifteen days after the eclipse, from December 10th., 1954 to January 9th., 1955, and all these records were completely scaled where possible by Kelso's method.

(3) Calculation of eclipse circumstances.

It is a simple matter to calculate the circumstances of an eclipse from data given in the Nautical Almanac. The method to be used for annular eclipse of the sun is described in the NAUTICAL ALMANAC (1936). Data for the annular solar eclipse of December 25th., 1954 for use by this method is given in the NAUTICAL ALMANAC

(1954). Fig. 29 shows the path of the eclipse over South Africa and it can be seen that Grahamstown lay practically at the centre of the belt of annularity. The times of the various phases of the eclipse at heights of 100, 200 and 300 kms. are shown below.

Height	1st Contact	2nd Contact	3rd Contact	4th Contact
100 km.	0646 hrs	0800	0807	0935
200 km.	0645	0758	0805	0934
300 km.	0643	0757	0803	0932

Times of contact, S.A. Standard Time = U.T. + 2 hrs.

During annularity 85.8% of the sun's disc was covered.

The path of the moon across the sun is simply found for each of the three heights and is shown in Fig. 30. The revelant data is shown below, where d is the distance from the sun's centre to the moon's centre in terms of the sun's radius, and a is the moon's radius in terms of the sun's radius. P is the position angle of centre of the moon measured from the North Point of the sun in the direction N.E.S.W. (i.e. counter-clockwise).

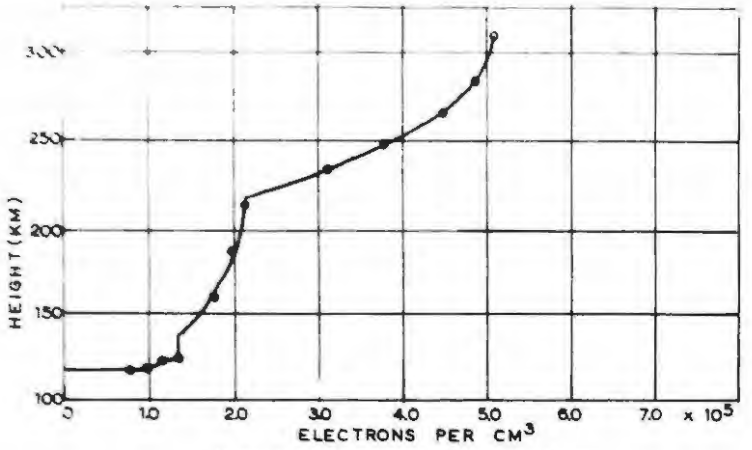

FIG: 25 ELECTRON DISTRIBUTION
0815 HRS 5th DEC, 1954.

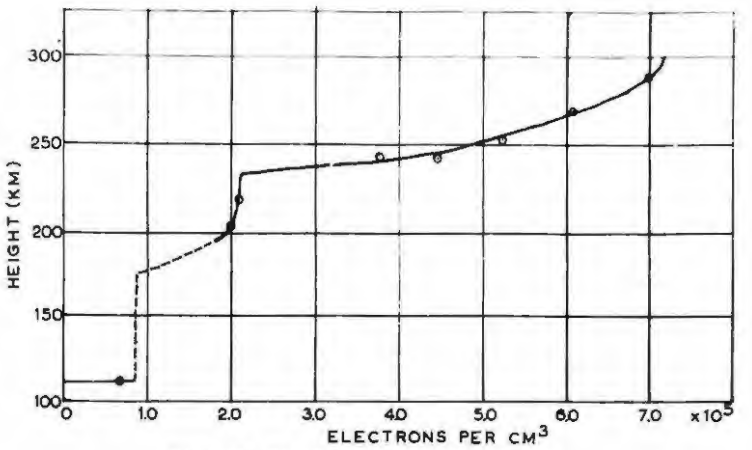

FIG: 26 ELECTRON DISTRIBUTION
1600 HRS 3rd DEC, 1954.

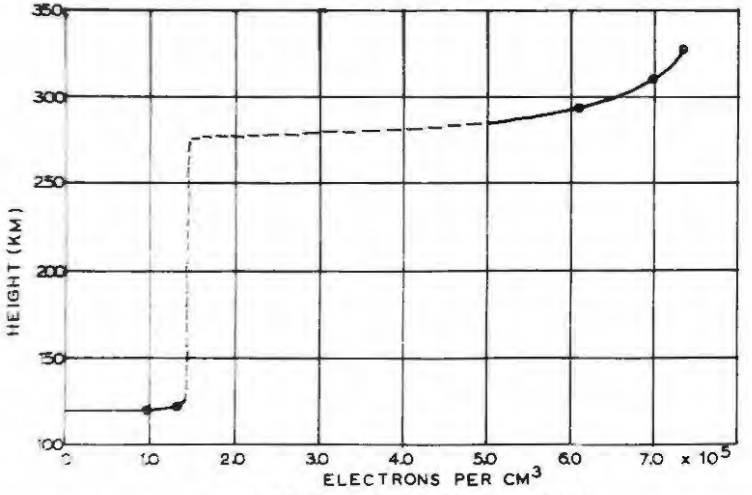

FIG: 27 ELECTRON DISTRIBUTION
1300 HRS 3rd DEC, 1954

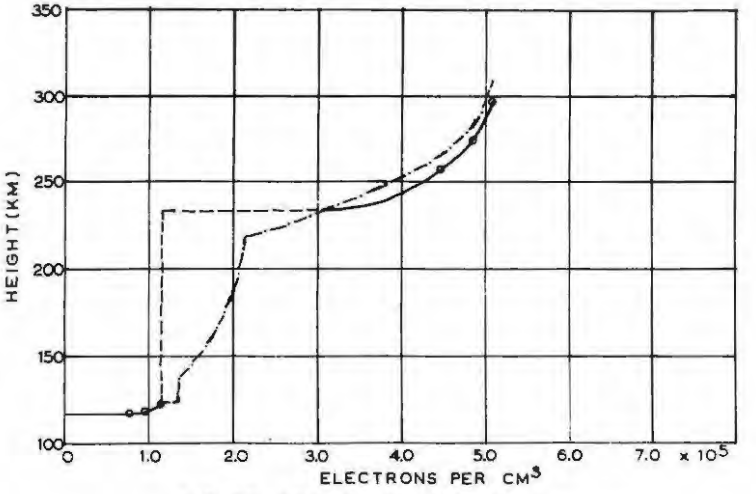

FIG: 28 0815 HRS 3rd DEC, 1954
—·—·— TRUE KELSO DISTRIBUTION
———— ASSUMING $f^{o}Esp = 5$ Mc/s

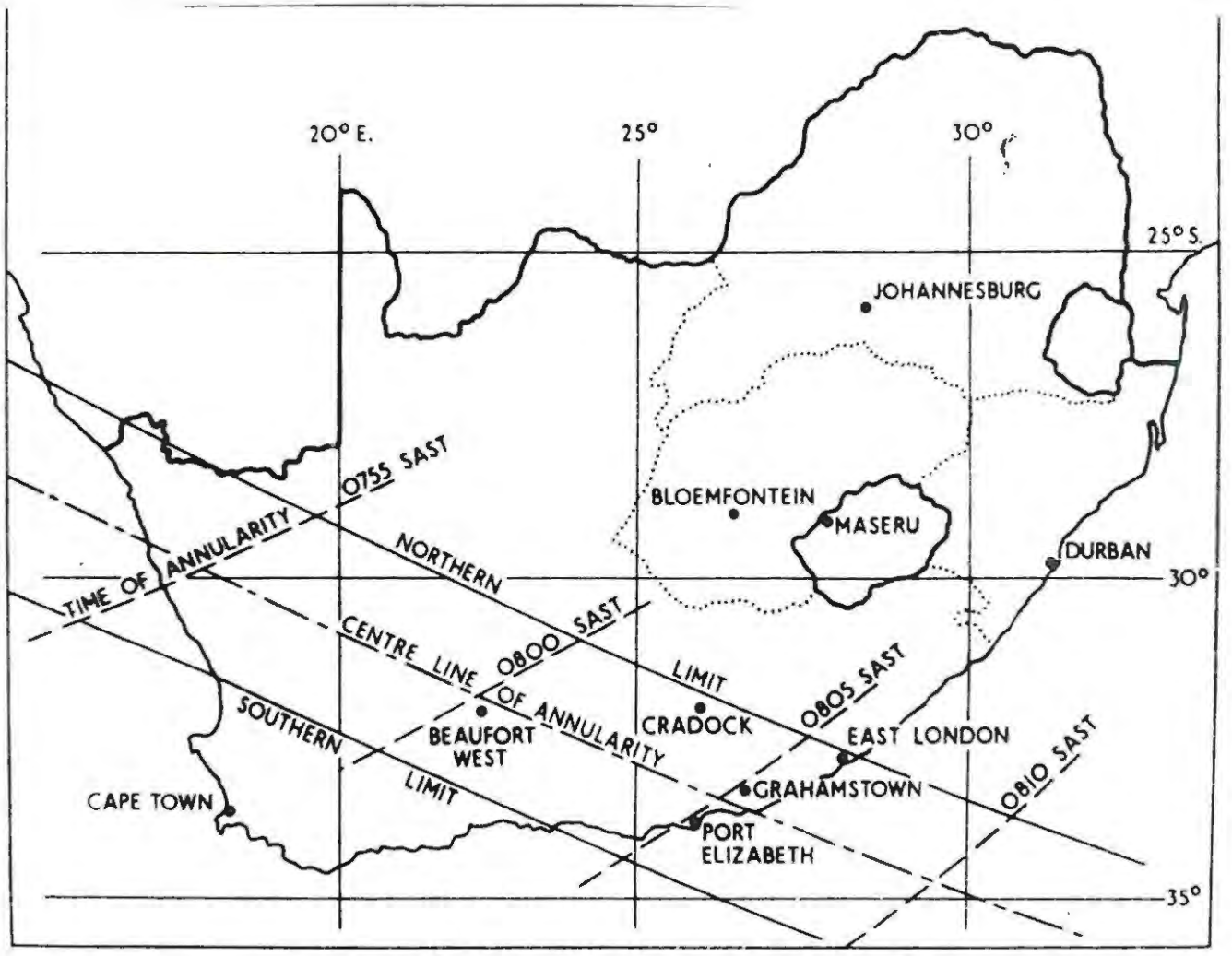

Fig: **29.** Path of annular eclipse over South Africa.

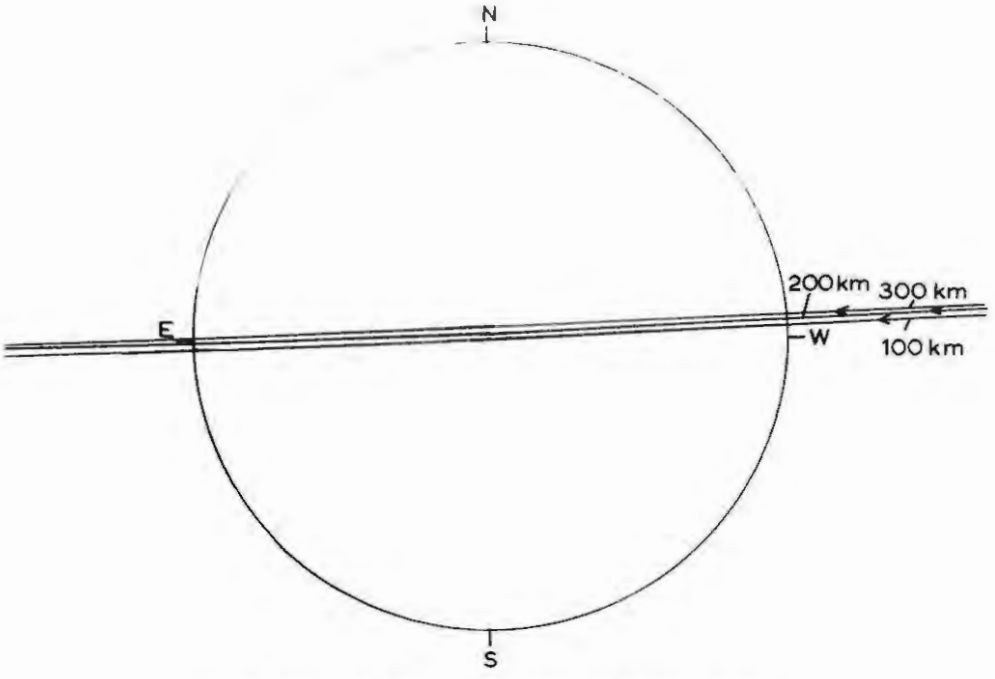

FIG: 30 PATH OF MOON ACROSS SUN AT 100, 200 & 300 km HEIGHT

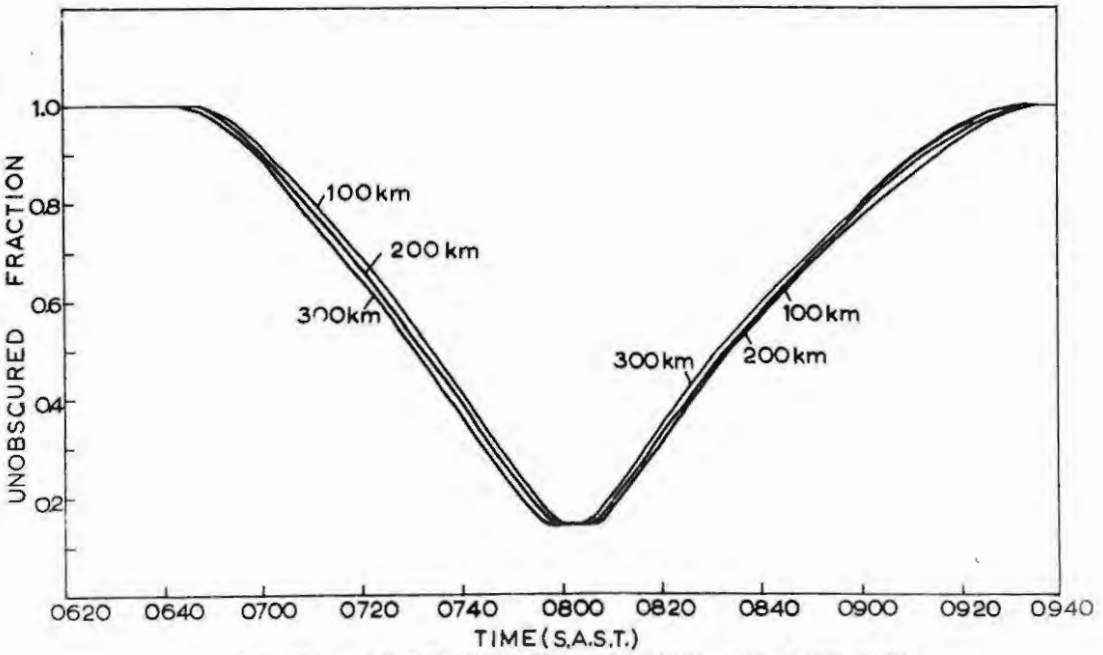

FIG: 31 UNOBSCURED FRACTION OF THE SUN

Time	100 km			200 km			300 km		
SAST	d	a	P	d	a	P	d	a	P
tact	1.924	0.924	272.9°	1.924	0.924	273.7°	1.924	0.924	274.4°
0700	1.560	0.925	272.8°	1.517	0.924	273.7°	1.510	0.924	274.7°
0720	1.050	0.925	272.7°	1.002	0.925	274.1°	0.966	0.925	275.5°
0740	0.554	0.926	272.6°	0.514	0.925	275.1°	0.475	0.925	278.0°
ipse	0.008	0.926	0°0'	0.023	0.926	189.9°	0.044	0.926	2.6°
0820	0.375	0.927	91.7°	0.410	0.926	89.1°	0.449	0.926	87.0°
0840	0.809	0.928	91.6°	0.845	0.927	90.5°	0.880	0.927	89.4°
0900	1.228	0.929	91.4°	1.261	0.928	90.7°	1.293	0.928	90.0°
0920	1.630	0.930	91.0°	1.660	0.929	90.6°	1.692	0.929	90.1°
tact	1.931	0.931	90.8°	1.930	0.930	90.4°	1.930	0.930	90.0°

Data for position of moon during the eclipse.

Calculation of the area of the sun left unobscured at any stage during the eclipse may be performed by the following method. As will be seen later, the unobscured fraction of the solar disc, f, is an important parameter in the analysis of the eclipse data.

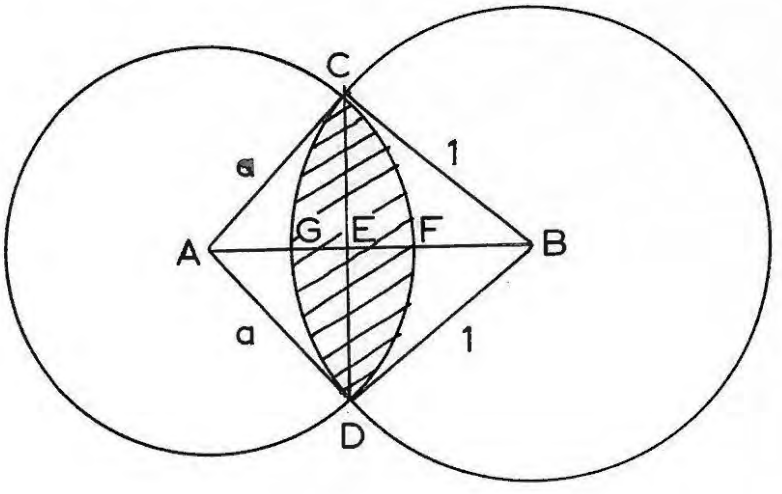

The sun is represented by the circle centre B and radius 1. The moon is represented by the circle centre A and radius a. d = the distance AB as defined previously.

The obscured area is the region enclosed by CGDFC.

Obscured area = area between arc CFD and the centre A +
area between arc CGD and the centre B -
area of quad. ACBD.

Area of Δ ABC = $\sqrt{s(s-d)(s-a)(s-1)}$

where $s = \frac{1}{2}(d+a+1)$

Thus the area of quad ABCD = $2\sqrt{s(s-d)(s-a)(s-1)}$

Area subtended by arc CFD = $\theta_1 a^2$

Area subtended by arc CGD = $\theta_2 1^2 = \theta_2$

Thus obscured area = $\theta_1 a^2 + \theta_2 - 2\sqrt{s(s-d)(s-a)(s-1)}$ ... 18

Now area of Δ ABC = $\frac{1}{2}d.CE = \sqrt{s(s-d)(s-a)(s-1)}$

so that $CE = \frac{2\sqrt{s(s-d)(s-a)(s-1)}}{d}$

$\sin \theta_1 = \frac{CE}{a}$

Thus $\theta_1 = \arcsin \frac{2\sqrt{s(s-d)(s-a)(s-1)}}{a.d.}$

Similarly $\theta_2 = \arcsin \frac{CE}{1} = \arcsin \frac{2\sqrt{s(s-d)(s-a)(s-1)}}{d}$

The unobscured area thus is given by

$$\pi - \theta_1 a^2 + \theta_2 - 2\sqrt{s(s-d)(s-a)(s-1)} \quad \text{... 19}$$

where θ_1 and θ_2

Hence the unobscured fraction of the solar disc f is given by:-

$$f = 1 - \frac{\left[\theta_1 a^2 + \theta_2 - 2\sqrt{s(s-a)(s-d)(s-1)}\right]}{\pi}$$

All that is required is for the value of the term $\sqrt{s(s-d)(s-a)(s-l)}$ to be calculated for each time and the unobscured area is easily found. The table below gives the values of f, the unobscured fraction of the sun's disc, at twenty minute intervals and these are illustrated graphically in Fig. 31.

Time	height		
SAST	100 km.	200 km.	300 km.
0700	0.911	0.896	0.894
0720	0.684	0.658	0.640
0740	0.409	0.387	0.363
0800	0.144	0.142	0.142
0820	0.304	0.325	0.347
0840	0.565	0.574	0.592
0900	0.768	0.785	0.799
0920	0.933	0.944	0.953

Values of "f" at various heights.

(4) Frequency of observations.

While the purpose of this investigation is the study of ionospheric changes during a solar eclipse, such a study cannot be made without reference to control data obtained from normal observations on days before and after the eclipse. The importance of taking control readings over a large number of days has already been stressed. Many previous analyses of eclipse readings suffer from the lack of adequate control data. It is normal in ionosphere work to average out readings

over a month to produce a monthly mean value of ionospheric parameters. If readings are averaged over a period greater than a month it is likely that seasonal variations might affect the mean values so derived. The control readings therefore extended over a period of thirty days, from December 10th, 1954 to January 9th, 1955 inclusive.

The equipment was designed to take automatic readings at hourly intervals during the day and night. While this may have been sufficient for normal day to day ionospheric studies, it was necessary to take more frequent readings on the control days over that part of the day during which the eclipse was due to take place. Mention has already been made of the "corpuscular eclipse" due to occur some two hours before the "optical eclipse". Consequently readings were taken every 15 minutes from 0500 hours to 1000 hours SAST, in addition to the normal hourly readings throughout the rest of the day. This period thus included both the "corpuscular" and "optical" eclipses.

On the eclipse day the equipment was run continuously from 0500 to 1000 hours SAST taking readings every $2\frac{1}{2}$ minutes. From 1000 to 1200 hours readings were taken at 15 minute intervals and every hour for the rest of the day.

In this section consideration will only be given to the control data and its presentation for comparison with the eclipse readings.

(5) Magnetic and sunspot activity.

It is well known that increases in magnetic activity are accompanied by ionospheric disturbances (BERKNER, 1939; SHAPLEY, 1946). I am grateful to Mr. A. M. van Wijk of the Magnetic Observatory, Hermanus, for supplying the magnetic data for the period under observation.

The period occured during the minimum of the sunspot cycle and magnetic activity was very low. It was gratifying to note that December 25th, 1954, the eclipse day, had a magnetic character figure of zero. GLEDHILL and SZENDREI (1947a) in an analysis of ionospheric readings over Grahamstown from November 1945 to February 1946, found a correlation with magnetic data from the Hermanus observatory and rejected all days with magnetic character figure greater than 2. During the thirty day control period there were no days with a magnetic character figure greater than 2 and therefore it seemed unlikely that any magnetically disturbed readings would be included in the mean values for the control period.

(6) Control data

(i) Maximum electron densities and their corresponding heights.

Mean values of the maximum electron density and their heights for each of the four layers for the control period are illustrated in Figs. 32 to 36 inclusive. Figs. 32 to 35 show the mean diurnal variation of the maximum electron densities, whilst Fig. 36 shows the mean diurnial variation of the heights of the maximum electron densities.

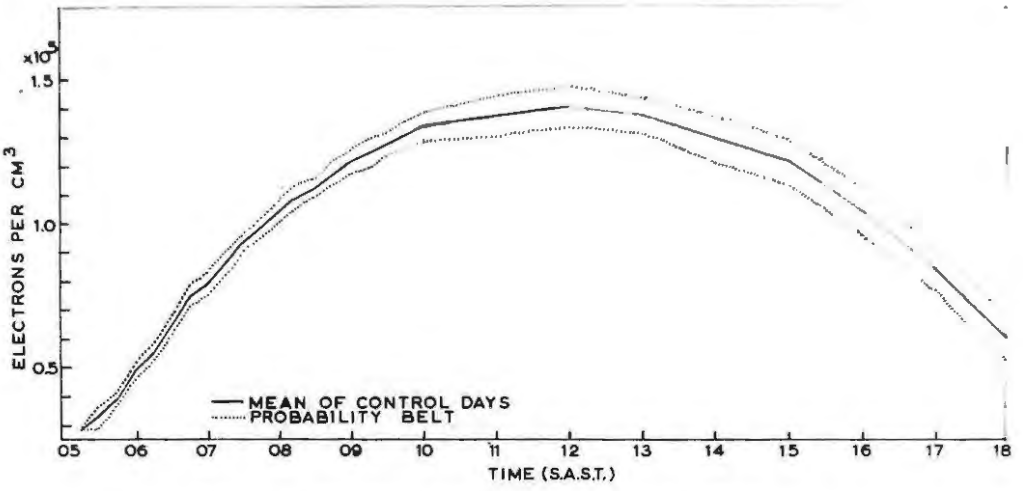

FIG: 32 MAXIMUM ELECTRON DENSITY E_1 LAYER.

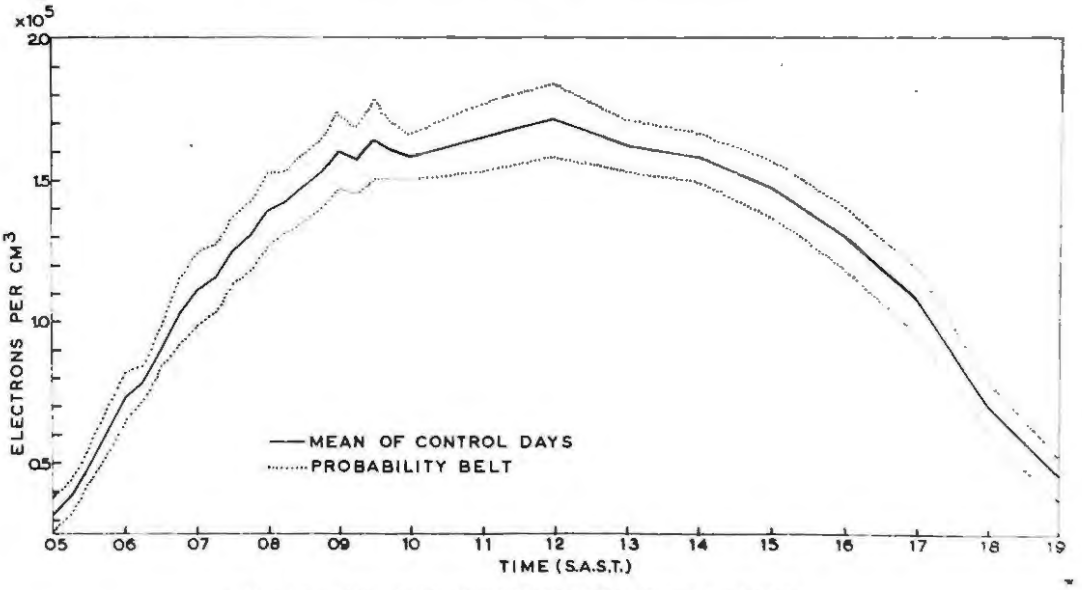

FIG: 33 MAXIMUM ELECTRON DENSITY E_2 LAYER.

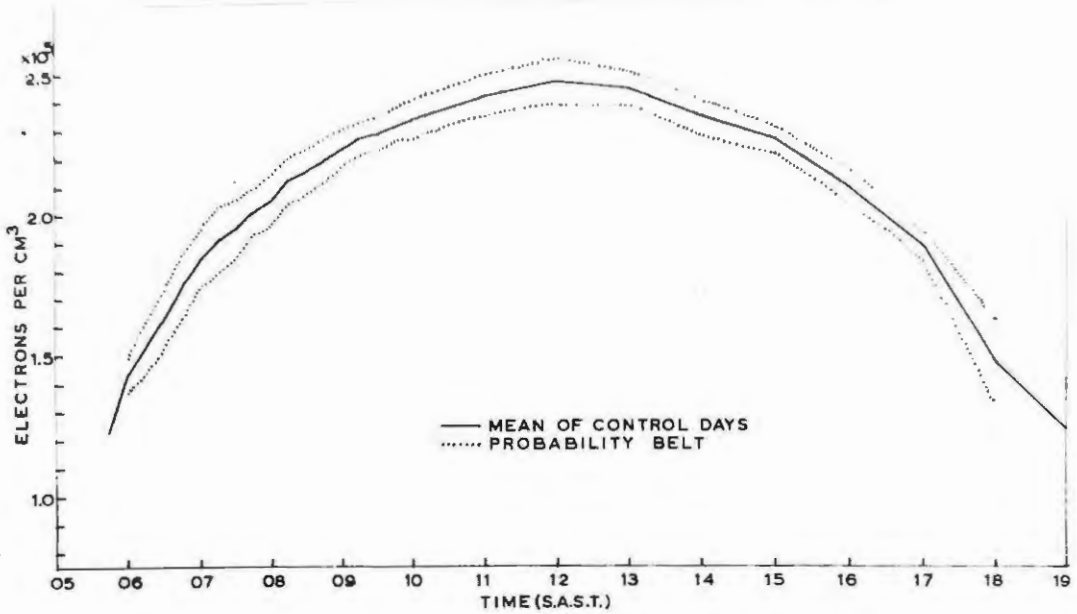

FIG: 34 MAXIMUM ELECTRON DENSITY F_1 LAYER.

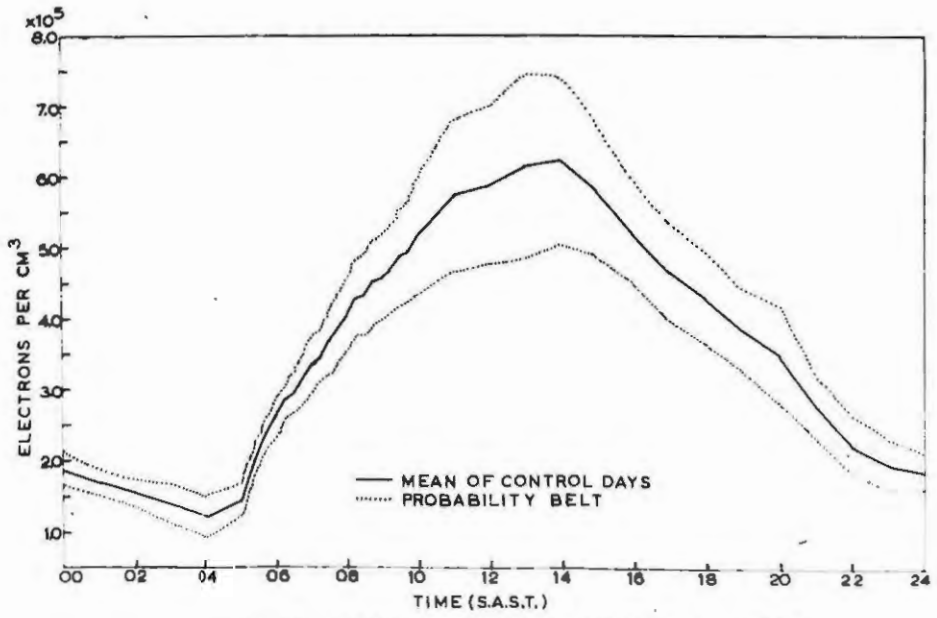

FIG: 35 MAXIMUM ELECTRON DENSITY F_2 LAYER

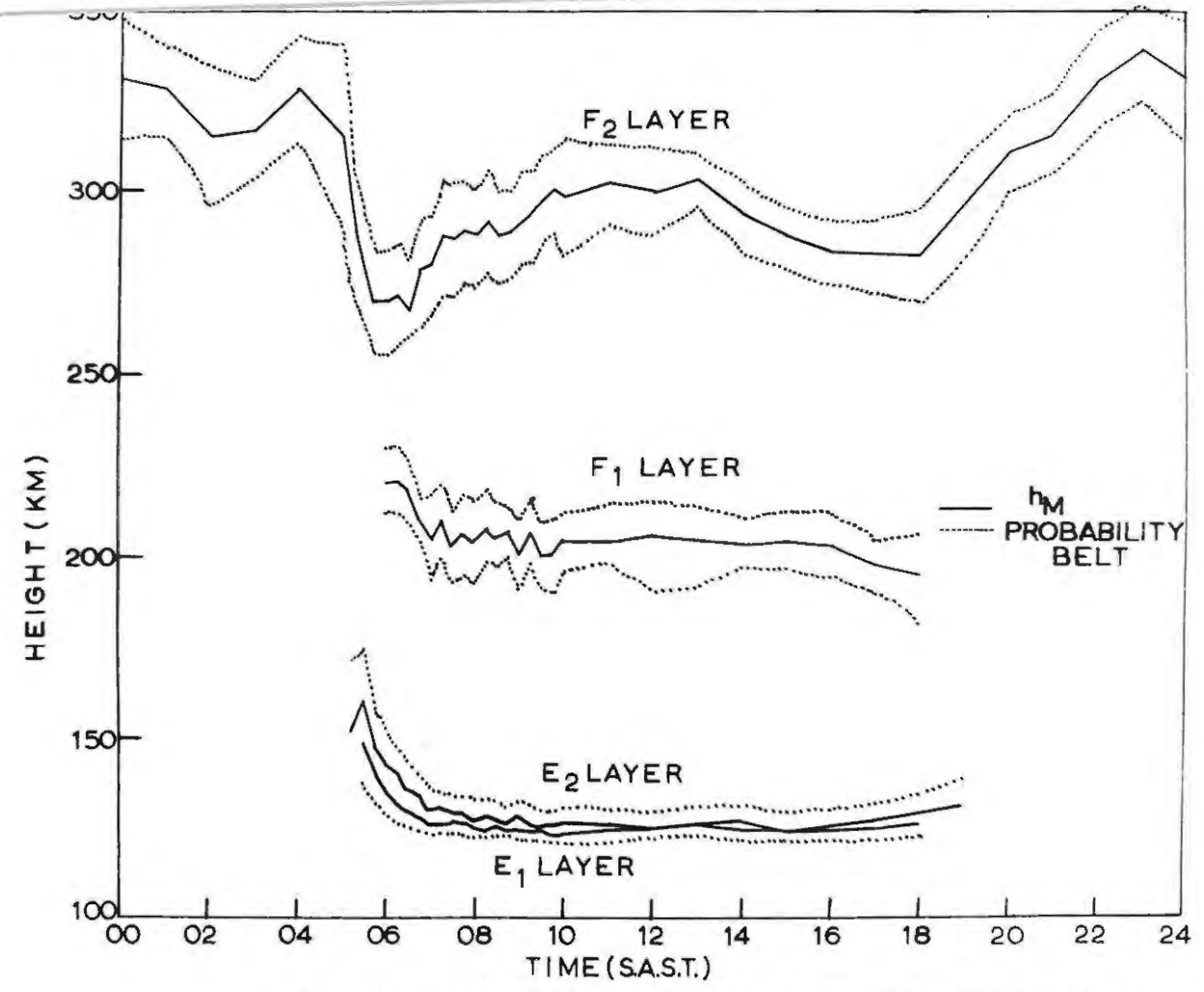

FIG: 36 HEIGHTS OF MAXIMUM ELECTRON DENSITY (h_M)

To gain some idea of the scatter of the individual readings about the mean value, the probably deviation r can be calculated from Peter's formula :-

$$r = 0.845 \frac{\sum d_i}{\sqrt{n(n-1)}} \qquad \ldots\ldots 21$$

where d_i is the deviation of the i th reading from the mean and n is the total number of readings over which the mean is taken. These probable deviations give an index of the scatter of the individual values about the mean. They are included in Figs. 32 to 36. The mean values and probable deviations shown in these figures are tabulated in Tables 4 to 7

Time (hrs SAST)	N	r	h_M	r
0530	0.33	0.036	147	9.7
0545	0.39	0.025	143	7.2
0600	0.49	0.028	135	6.2
0615	0.55	0.034	132	3.8
0630	0.65	0.032	130	3.0
0645	0.75	0.038	128	3.7
0700	0.79	0.038	126	3.7
0715	0.86	0.036	126	2.6
0730	0.93	0.030	127	2.7
0745	0.98	0.030	126	1.9
0800	1.04	0.045	125	3.3
0815	1.09	0.039	124	2.7
0830	1.12	0.029	125	2.4
0845	1.17	0.039	124	3.8
0900	1.21	0.041	125	3.2
0915	1.24	0.052	124	3.4
0930	1.27	0.044	124	3.2
0945	1.30	0.047	123	2.7
1000	1.33	0.052	123	3.4
1100	1.37	0.068	124	3.3
1200	1.40	0.069	124	3.3
1300	1.37	0.065	126	3.3
1400	1.29	0.081	124	4.0
1500	1.21	0.080	124	3.1
1600	1.04	0.079	124	4.1
1700	0.84	0.066	125	3.9
1800	0.60	0.077	126	3.2

Table 4: Mean values of N, the maximum electron density, (electrons per cm^3 x 10^{-5}) and h_M, the height of the maximum (k_m), for the E_1 layer.

Time (hrs SAST)	N	r	h_M	r
0515	0.38	0.065	152	20
0530	0.49	0.060	160	15
0545	0.61	0.084	148	8.6
0600	0.73	0.091	142	8.6
0615	0.78	0.061	140	5.7
0630	0.91	0.068	136	6.3
0645	1.03	0.116	134	5.5
0700	1.11	0.135	130	4.1
0715	1.15	0.117	131	5.3
0730	1.25	0.120	129	3.7
0745	1.30	0.117	129	3.8
0800	1.39	0.133	127	4.2
0815	1.42	0.108	128	3.0
0830	1.47	0.124	127	3.7
0845	1.52	0.120	126	4.4
0900	1.60	0.144	128	4.4
0915	1.57	0.120	126	4.5
0930	1.64	0.138	125	3.5
0945	1.60	0.097	125	3.2
1000	1.58	0.078	126	4.6
1100	1.65	0.121	126	4.4
1200	1.71	0.128	124	4.3
1300	1.62	0.086	125	4.5
1400	1.58	0.089	127	4.8
1500	1.47	0.099	124	4.9
1600	1.30	0.108	126	5.3
1700	1.08	0.119	127	5.1
1800	0.71	0.087	129	6.0
1900	0.46	0.077	131	8.6

Table 5: Mean values of N, the maximum electron density, (electrons per $cm^3 \times 10^{-5}$) and h_M, the height of the maximum (km) for the E_2 layer.

Time (hrs SAST)	N	r	h_M	r
0600	1.43	0.064	221	9.3
0615	1.53	0.093	221	8.9
0630	1.63	0.096	218	8.6
0645	1.75	0.112	210	6.8
0700	1.84	0.096	205	12.0
0715	1.91	0.116	210	10.0
0730	1.95	0.096	203	9.9
0745	2.01	0.079	206	11.0
0800	2.05	0.092	204	11.0
0815	2.12	0.081	208	10.0
0830	2.15	0.080	206	8.8
0845	2.19	0.078	207	6.3
0900	2.23	0.070	201	8.7
0915	2.26	0.064	207	9.0
0930	2.28	0.065	201	8.7
0945	2.31	0.062	200	10.0
1000	2.33	0.066	204	8.3
1100	2.41	0.070	206	8.0
1200	2.46	0.081	203	12.0
1300	2.43	0.065	203	11.0
1400	2.33	0.064	204	7.2
1500	2.25	0.049	204	8.3
1600	2.08	0.061	203	8.7
1700	1.87	0.054	197	7.1
1800	1.47	0.138	194	13

Table 6: Mean values of N, the maximum electron density, (electrons per cm^3 x 10^{-5}) and h_M, the height of the maximum (km) for the F_1 layer.

Time (Hrs SAST)	N	r	h_M	r
0000	1.88	0.242	331	17
0100	1.70	0.176	328	13
0200	1.56	0.192	315	19
0300	1.40	0.276	317	14
0400	1.22	0.294	328	15
0500	1.47	0.222	315	26
0515	1.81	0.199	239	18
0530	2.11	0.211	278	15
0545	2.38	0.224	269	14
0600	2.60	0.279	269	15
0615	2.82	0.255	271	14
0630	2.96	0.284	267	14
0645	3.14	0.348	278	16
0700	3.34	0.388	279	14
0715	3.47	0.365	287	16
0730	3.66	0.458	286	16
0745	3.85	0.470	288	14
0800	4.04	0.517	287	14
0815	4.27	0.526	291	14
0830	4.32	0.583	287	13
0845	4.50	0.603	288	12
0900	4.57	0.601	292	13
0915	4.68	0.595	293	13
0930	4.84	0.687	297	12
0945	4.92	0.687	297	12
1000	5.16	0.810	298	16
1100	5.71	1.070	302	11
1200	5.87	1.117	300	12
1300	6.13	1.305	303	7.9
1400	6.22	1.193	293	9.5
1500	5.80	0.931	287	7.9
1600	5.20	0.696	283	9.1

cont...

Time (Hrs SAST)	N	r	h_M	r
1700	4.66	0.674	282	10
1800	4.29	0.645	282	13
1900	3.84	0.570	295	14
2000	3.50	0.692	310	11
2100	2.78	0.418	316	11
2200	2.24	0.394	331	13
2300	1.99	0.339	339	14

Table 7: Mean values of N, the maximum electron density, (electrons per cm^3 x 10^{-5}), h_M, the height of the maximum (km), and r, the probable deviation, for the F_2 layer.

The regular nature of both the E_1 and F_1 layers is easily seen from the narrow probability belt drawn about the mean. These two layers are only present during the daytime. In both cases the maximum electron density rises to a maximum at noon and falls off evenly on either side of it. The heights of the maximum in the E_1 layer remains fairly constant all day at a height of about 125 kms, as does the F_1 layer at a height of about 205 kms.

The E_2 layer shows more marked variations as can be seen from the somewhat wider probability belt about the mean values of its maximum electron density. The wide variations can however be attributed to the difficulty in distinguishing between sporadic E and E_2. It is inevitable that Esp readingshave been included in the E_2 means. The maximum electron density also rises to a maximum at midday, and the height of this maximum remains fairly constant throughout the day. As in the case of the E_1 layer, the E_2 is only present during the daytime. In both cases the critical frequency fell below the lowest limit of the apparatus during the night. The F_2 layer is the most varied from day to day of all four layers. The wide fluctuations are illustrated vividly by the wide probability around noon. However, the F_2 layer is remarkably consistent in the first two hours after sunset, when it will be noticed that the probability belt is fairly narrow. The maximum electron density rises to its maximum value at about 1400 hours SAST,

probably due to the slow recombination in this layer. The height of the maximum electron density is more varied than the other three layers. It reaches a maximum during the night, and soon after sunrise drops by about 50 km in a period of two hours, thereafter rising to a fairly constant value of about 290 kms during the midday and afternoon period. After sunset the height begins to rise again.

(ii) Electron density - height distribution.

The complete scaling of records by Kelso's method has provided curves of N versus height (N(h) curves) for each time of day. In order to obtain a mean curve for the distribution at any particular time of day, it seems at first sight obvious to plot curves of N versus time(N(t) curves) at constant height. When this is done it is found that the resulting distribution or N(h) curve for a particular time of day has a shape which is somewhat different from the original N(h) curves. The original N(h) curves for each time of day deduced by Kelso's method are smooth curves. Fig. 37(a) shows the resulting N(h) curve deduced by averaging the values of N at constant height from the Kelso curves for one particular time of day. On the same graph is plotted the resulting N(h) curve deduced by a method which will be described below. It seems that the resulting N(h) curve found by averaging the values of N at constant height does not take into account sufficiently the distribution of each individual Kelso scaling. In

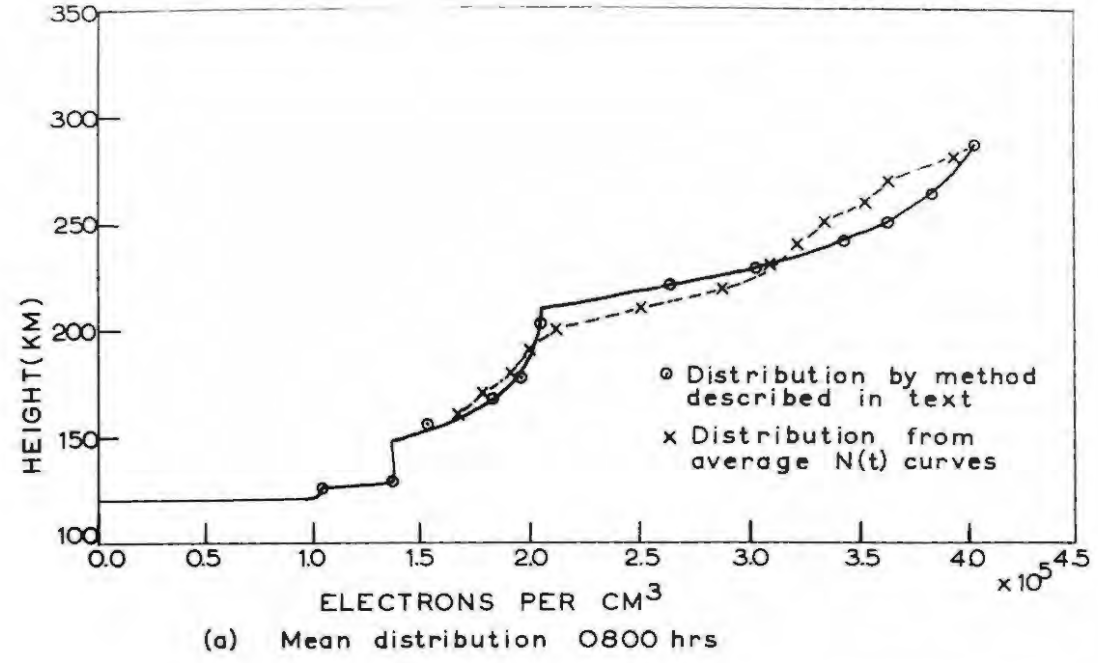

(a) Mean distribution 0800 hrs

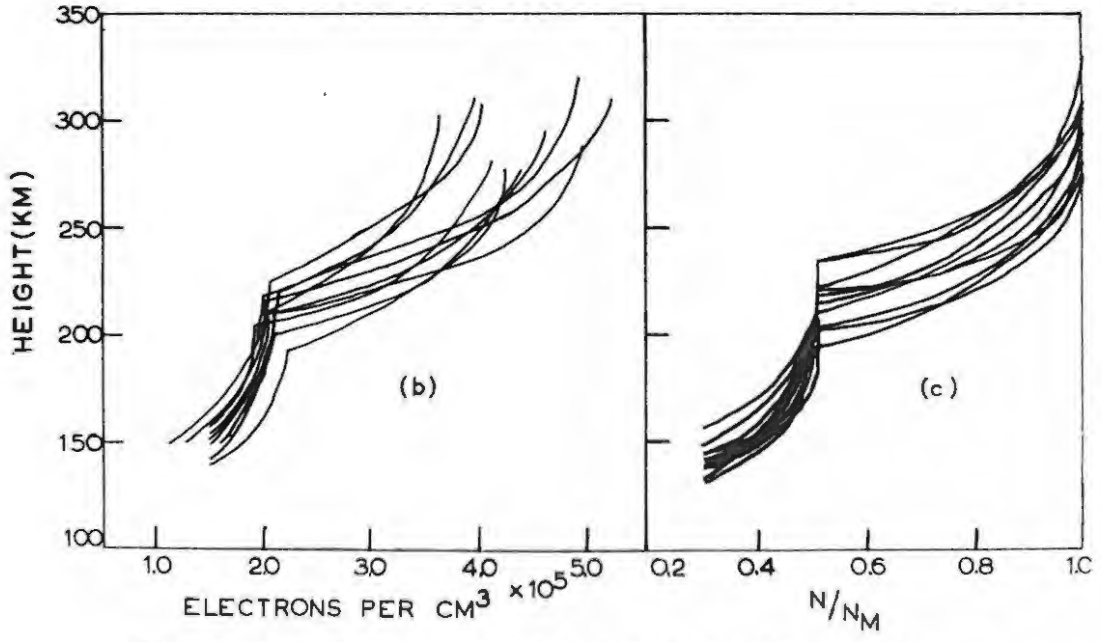

FIG·37. TO ILLUSTRATE THE METHOD OF AVERAVING

other words the curve so deduced is an N(h) curve derived from an N(t) curve and insufficient weight has been given to the individual N(h) distributions.

The method chosen is as follows, and is illustrated in Fig. 37 (b) and (c). For each time of day the mean values of N_M, the maximum electron density and its height h_M were taken from Tables 16 and 17 for the F_1 and F_2 layers. The individual N(h) curves were normalised to the maximum value of N at that particular time and from each record the height, h, corresponding to certain fractions of N_M were read off the individual Kelso distributions. For example, values of h were read for N_M, 0.95, 0.9, 0.85, 0.75 and 0.65 N_M in the F_2 layer, and values of h for N_M, 0.95, 0.9 and 0.75 N_M were read off from the F_1 layer. For each particular time of day, the mean h corresponding to these particular fractions of N_M were then determined. Tables 8 and 9 show a particular computation for the F_1 and F_2 layers at 0800 hours. Figs. 37 (b) and (c) show the method graphically. In Fig. 37 (b) ten of the thirty individual Kelso curves have been drawn for 0800 hours. In Fig. 37 (c) these have been normalised to fixed fractions of N_M (N/N_M), and the evaluations in Tables 8 and 9 are effectively the heights from each individual curve read off at fixed values of N/N_M. The resulting distribution is then shown in Fig 37 (a), together with the distribution evaluated from the values of N at constant height. This type of mean N(h) curve was found to agree

with the individual curves much better than that found by simply averaging an N(t) curve at constant height.

It is interesting to note that quite independently similar Kelso distributions were being deduced at Cambridge, the results of which were presented recently by SCHMERLING and THOMAS (1956). In an attempt to find the distribution of electrons in the "mean quiet F layer", they were forced to conclusions similar to those presented here, namely that to average N(t) curves at constant height, not enough weight is accorded to the individual N(h) distributions. It is pleasing to note that their method of averaging is practically identical to that carried out here, quite independently.

To gain a composite picture of the mean ionospheric conditions for the control period, it is convenient to draw two maps. There are three parameters to be plotted to represent a composite picture of ionosphere, the time of day, the electron density and its height. These can be drawn on two maps. The first, a plot of height versus time of day for constant values of electron density, is an "electron density map" as termed by GLEDHILL and SZENDREI (1950). The second, a graph of electron density versus time of day for constant values of height, is here called a"constant height map". These are shown in Figs 38 and 39 respectively. In Fig 38, the dotted line at the top of the figure represents the height of the maximum electron density,

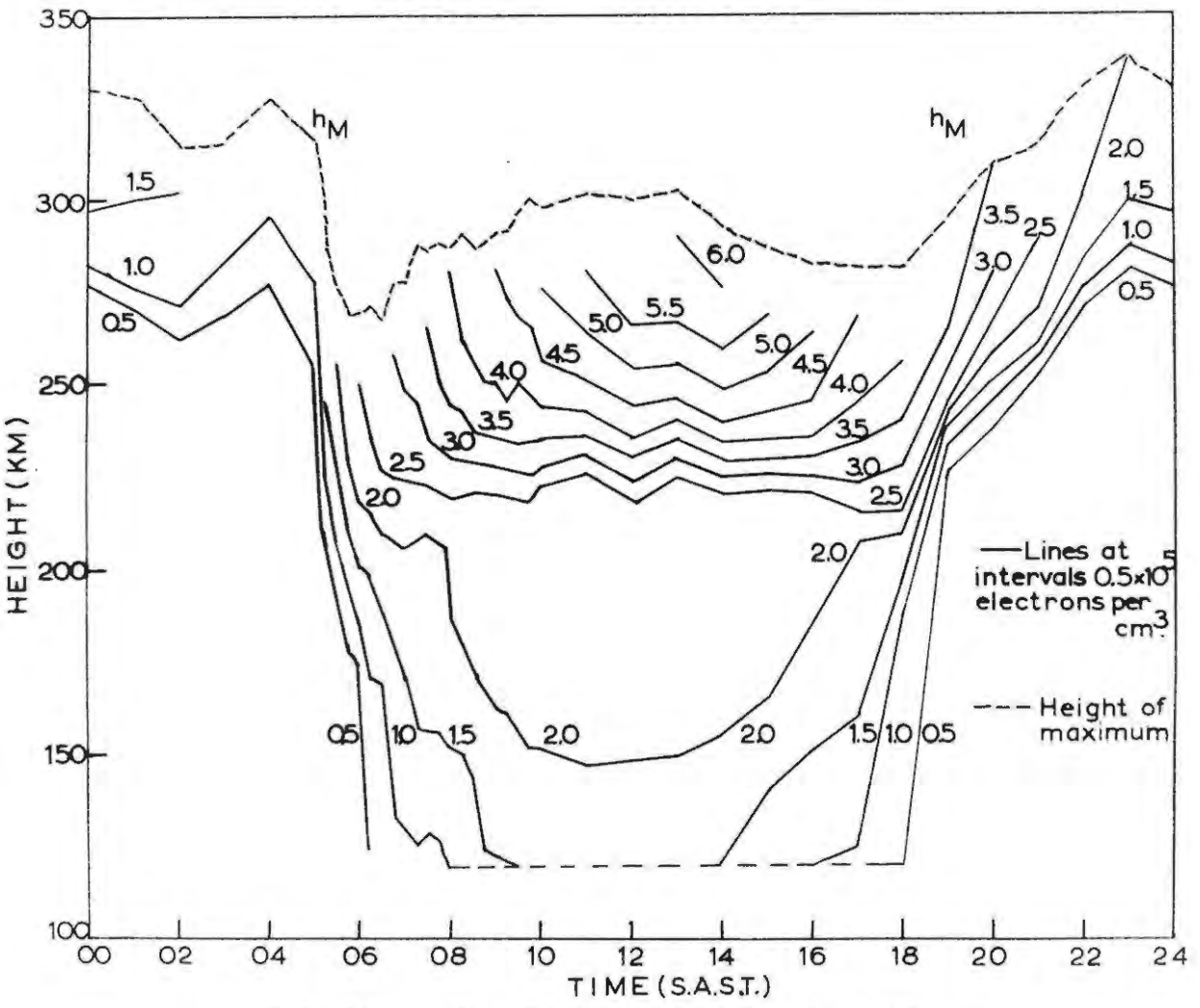

FIG: 38 ELECTRON DENSITY MAP

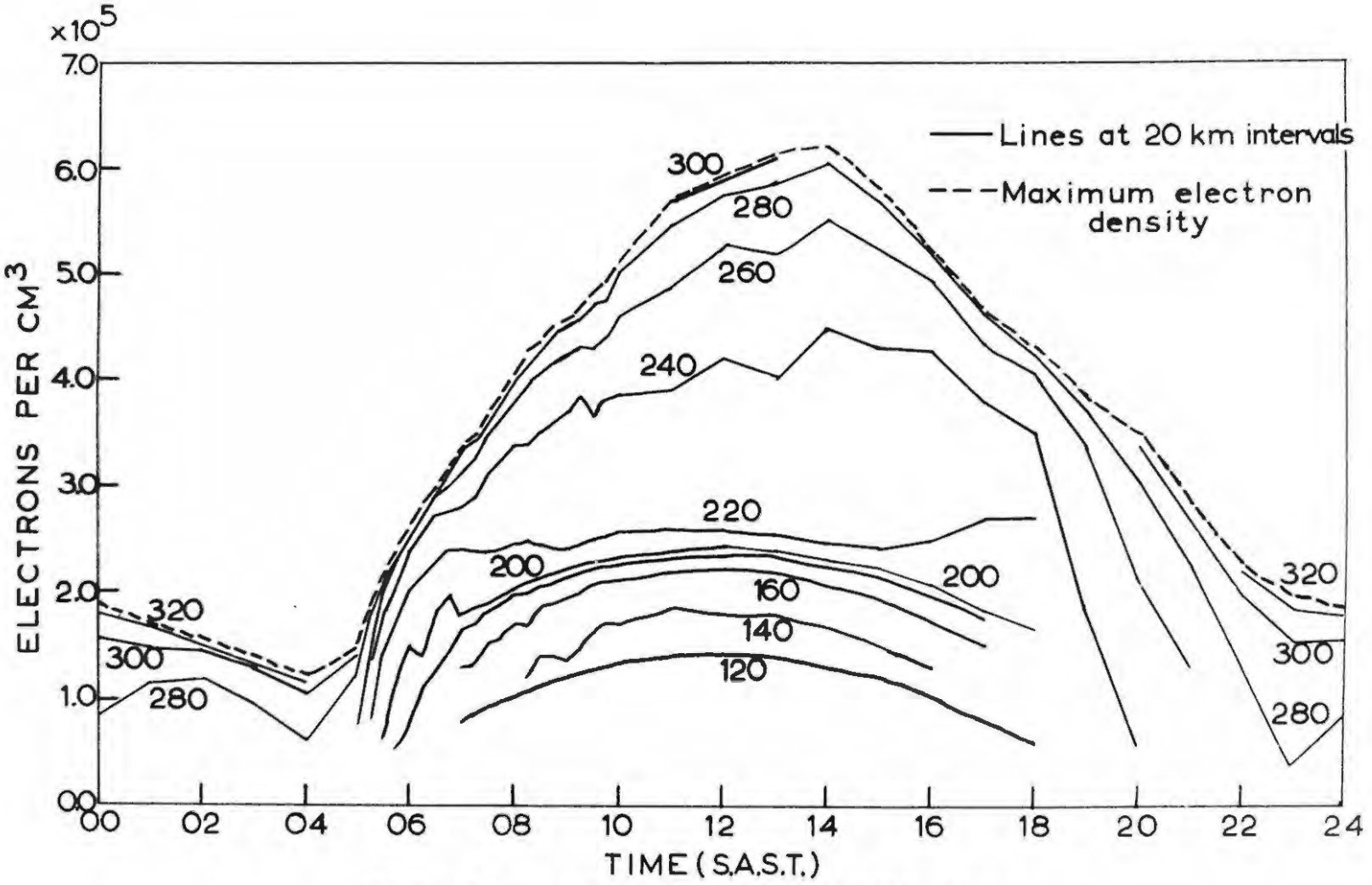

FIG: 39 CONSTANT HEIGHT MAP

and the contours have not been extended above this since the distribution above the maximum cannot be found with the technique used in this work.

This concludes the experimental part of this work. Following the design and construction of the automatic ionosphere sounding apparatus, photographic records of a good standard and fairly high resolution have been obtained over a thirty day control period. A programme of complete scaling has been carried out using the method due to Kelso. This control data has been presented finally in two forms, an electron density map and a constant height map. In the next section these will be compared with the readings taken during the eclipse.

The construction of the ionosonde, the scaling and presentation of the records as has been outlined in Part I here, were carried out in collaboration with the director of this work, Dr. M. P. Szendrei. I am most grateful for his invaluable help and advice.

It is also noted that the recording camera used in this work was that used by GLEDHILL and SZENDREI (1947a).

		F_1 layer			E_2	E_1
Date	h_{NM}	$h_{0.95N}$	$h_{0.9N}$	$h_{0.75N}$	h_M	h_M
Dec 10	-	-	-	-	-	-
11	-	-	-	-	-	130
12	194	183	174	152	134	130
13	199	180	167	144	125	123
14	210	189	179	156	140	130
15	193	181	174	150	127	124
16	216	186	175	155	140	125
17	216	185	174	158	123	-
18	228	189	172	147	123	123
19	212	191	183	164	129	126
20	192	165	156	-	-	-
21	222	185	181	177	129	128
22	231	192	176	155	131	128
23	203	184	170	148	130	130
24	211	188	179	162	129	127
26	-	-	-	-	135	129
27	-	-	-	-	-	130
28	190	155	145	-	121	120
29	180	166	157	-	127	127
30	200	173	158	139	125	125
31	212	160	152	-	125	122
						-

cont...

	F_1 layer				E_2	E_1
Date	h_{NM}	$h_{0.95N}$	$h_{0.9N}$	$h_{0.75N}$	h_M	h_M
Jan 1	186	173	166	-	130	-
2	-	-	-	-	-	128
3	187	159	153	-	125	122
4	196	170	160	150	134	131
5	198	177	165	140	119	119
6	199	172	163	151	125	122
7	188	177	174	169	128	125
8	185	167	161	146	106	102
9	237	201	189	173	122	121
Mean h	203	177	168	154	127	125
Mean n	2.05	1.94	1.84	1.53	1.39	1.04

Table 8: Calculation of mean distribution for F_1 layer 0800 hours SAST

Date	h_{NM}	$h_{0.95N}$	$h_{0.9N}$	$h_{0.85N}$	$h_{0.75N}$	$h_{0.65N}$
Dec 10	-	-	-	-	-	-
11	282	253	240	233	228	225
12	276	244	235	227	217	210
13	275	255	247	239	227	219
14	280	258	245	233	217	-
15	250	235	222	213	198	-
16	301	268	251	242	231	225
17	308	284	272	263	251	242
18	284	259	249	243	235	232
19	310	287	274	263	247	235
20	302	271	254	241	224	212
21	326	302	293	286	276	270
22	292	276	267	260	249	240
23	285	253	245	239	231	225
24	330	285	270	261	246	240
26	271	233	218	213	203	194
27	263	253	247	241	231	224
28	303	280	262	247	228	215
29	294	271	258	248	234	223
30	284	253	237	229	217	211
31	274	255	248	243	230	-

cont...

Date	h_{NM}	$h_{0.95N}$	$h_{0.9N}$	$h_{0.85N}$	$h_{0.75N}$	$h_{0.65N}$
Jan 1	274	250	237	228	212	198
2	-	-	-	-	-	-
3	257	247	240	232	217	206
4	280	200	246	235	220	213
5	274	250	237	227	210	-
6	310	283	267	254	237	225
7	268	246	237	230	217	206
8	276	256	243	233	218	206
9	306	286	273	263	248	-
Mean h	286	264	250	241	229	221
Mean n	4.03	3.83	3.63	3.43	3.03	2.72

Table 9: Calculation of mean distribution for F_2 layer 0800 hours SAST

PART II

The Eclipse Measurements.

(a) The maximum electron density and its height.

Introduction

During a solar eclipse as the moon covers the sun, the source of ionising radiation is gradually removed and then slowly reappears. The resulting effect on the ionosphere is to cause the electron density to decrease from its normal value to a somewhat lower value and finally to recover again after the eclipse, to its usual diurnal variation. Solar eclipses can therefore provide useful information on the controlling effect of the sun's radiation on the ionised layers and the electron-loss processes which take place. Ionospheric measurements during solar eclipses were made as early as 1925. During the eclipse of 29 June 1927, Appleton noticed that the minimum value of the electron density peak occurred about four minutes after the optical centre of totality. At that time it was uncertain whether ultra-violet radiation or corpuscular radiation was the chief cause of ionisation. Appleton noticed the coincidence between the time 4 minutes (240 seconds) and the time it would take for particles travelling at a speed of 1,000 miles per second to traverse the distance from the moon to the earth (240,000 miles). CHAPMAN (1932) therefore considered the possibility of this "corpuscular eclipse" and deduced that such an eclipse would occur about two hours before the optical eclipse. Since

the changes in ionisation in the E layer during the 1927 eclipse occurred during the optical eclipse, it was clear evidence for the ultra-violet origin of the E layer. Further measurements during the eclipses in 1935, 1936 and 1937 proved conclusively that these two layers owed their origin to solar ultra-violet radiation. However the measurements from the F_2 layer were inconclusive. In fact it is often difficult to decide whether an eclipse has any effect on the F_2 layer at all. During the middle part of the day, large and irregular fluctuations occur, as is seen in Fig. 35, where during the period 1000 to 1600 hours SAST the probability belt around the F_2 layer maximum electron density is very wide. If an eclipse occurs during this part of the day, even a considerable deviation from the mean value might lie within the probability belt, and it is inconclusive evidence for the eclipse effect, as such a deviation could just as well be attributed to a normal day to day fluctuation. Many observers (KIRBY, GILLILAND and JUDSON, 1935; SCHAFER and GOODALL, 1936) have been forced to admit that what appeared to have been an eclipse effect might just as well have been an every day fluctuation. It has been mentioned that increased magnetic activity affects the ionosphere, particularly the F_2 layer. KIRBY et al (1936), WAISMITH (1937) and other workers were thus unable to decide whether the observed effects in the F_2 layer were due to the eclipse or to the increased magnetic activity which accompanied the eclipse of 19 June, 1936.

The eclipse of 25 December 1954 was therefore advantageous from two points of view. Firstly the eclipse occurred during the early morning from approximately 0645 to 0930 SAST, during the period in which the F_2 layer is most regular. In fact the "corpuscular eclipse" which occurs some two hours before the "optical eclipse", lies in that part of the F_2 layer curve (Fig. 35.) where the probability belt is its narrowest. The eclipse therefore, was ideal to test the two hypotheses concerning the origin of the F_2 layer. Secondly, as has already been mentioned in Part I, magnetic activity was very low, and in fact the magnetic character figure for the eclipse day was zero. It is unlikely therefore that magnetic activity would have any effect on the F_2 layer.

The effect of the eclipse.

In Figs. 40 to 43, the maximum electron densities as observed during the eclipse have been plotted together with the mean values for the diurnal variation and the probability belts for all the four layers. In the E_1 layer (Fig. 40), there is a marked decrease in electron density coinciding with the optical eclipse, the minimum value of 0.52×10^5 electrons per cm^3 at 0800 hours being only 50% of that observed on control days and lying well outside the probability belt. Clearly there is a considerable effect on the E_1 layer, coinciding with the time of the optical eclipse.

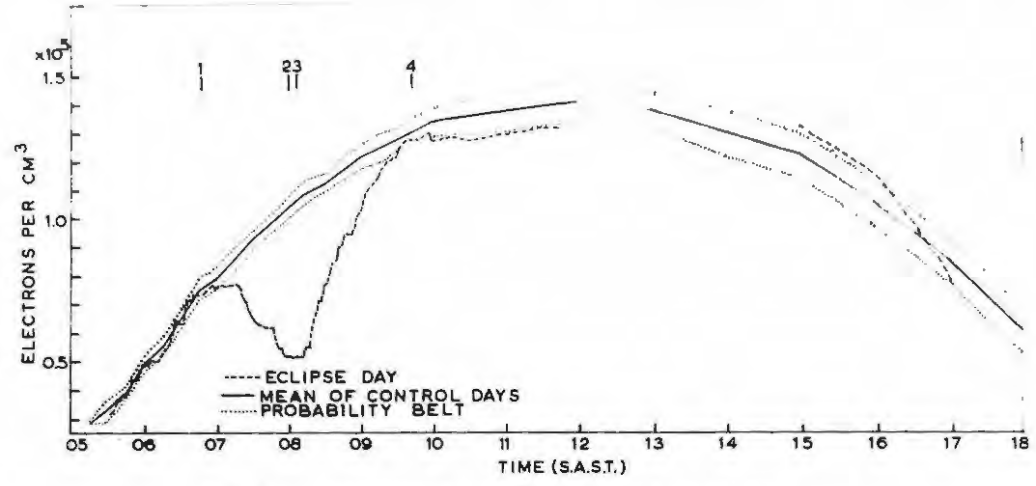

FIG:40 MAXIMUM ELECTRON DENSITY E_1 LAYER.

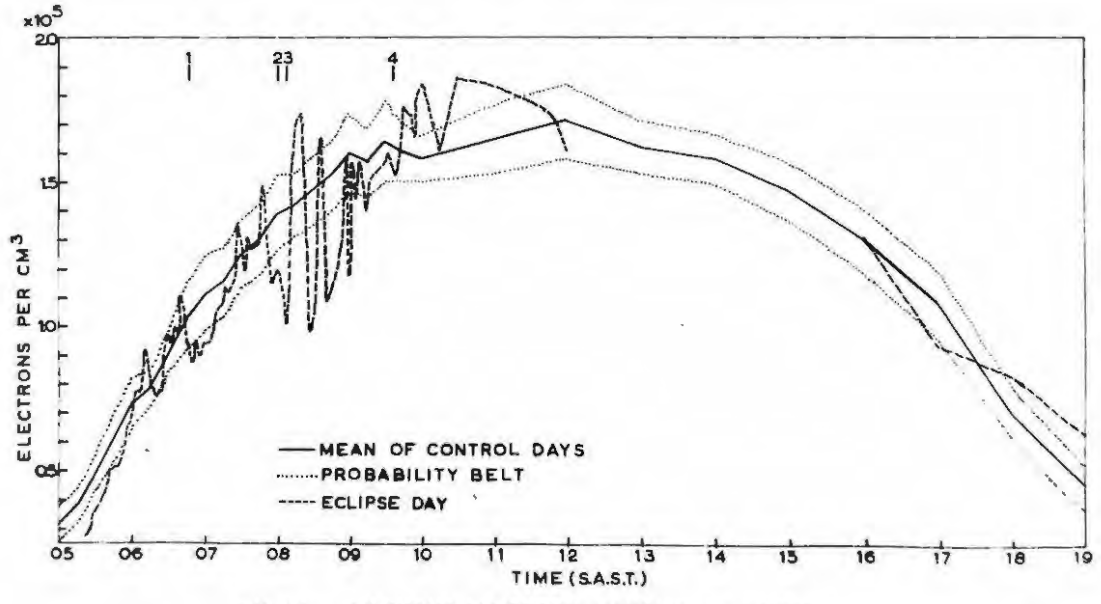

FIG:41 MAXIMUM ELECTRON DENSITY E_2 LAYER.

For the E_2 layer (Fig. 41), there appears to be some evidence for an eclipse effect. However, due to the difficulty of distinguishing between E_2 and Sporadic E, the points which have been plotted probably include some values of Esp. However, if one follows the lowest points on the curve, there is a clear eclipse effect, the minimum value of 0.98×10^5 electrons per cm^3 at 0830 being about 66% of that observed on control days, and lying well outside the probability belt and coinciding with the optical eclipse.

The advent of Sporadic E during the eclipse almost completely masked the F_1 layer during the period 0725 to 0820 SAST (Fig. 42); the critical frequency was not observed during this period. However, from the retardation produced by the F_1 layer on the F_2 reflections during this period it was possible to extrapolate the h'f curve back and estimate that the minimum value of the electron density at the F_1 maximum reached a value of 0.94×10^5 electrons per cm^3 sometime during the annular phase. The F_1 layer curves for the eclipse day have been extrapolated down to this value during the maximum phase of the eclipse. Once again the curves show that there was a considerable effect on the F_1, the electron density falling to an estimated 45% of that observed at the same time on control days. The fall in the electron density once again coinciding with the optical eclipse.

Fig. 43 shows the eclipse curves for the maximum electron density in the F_2 layer. It will be seen that the

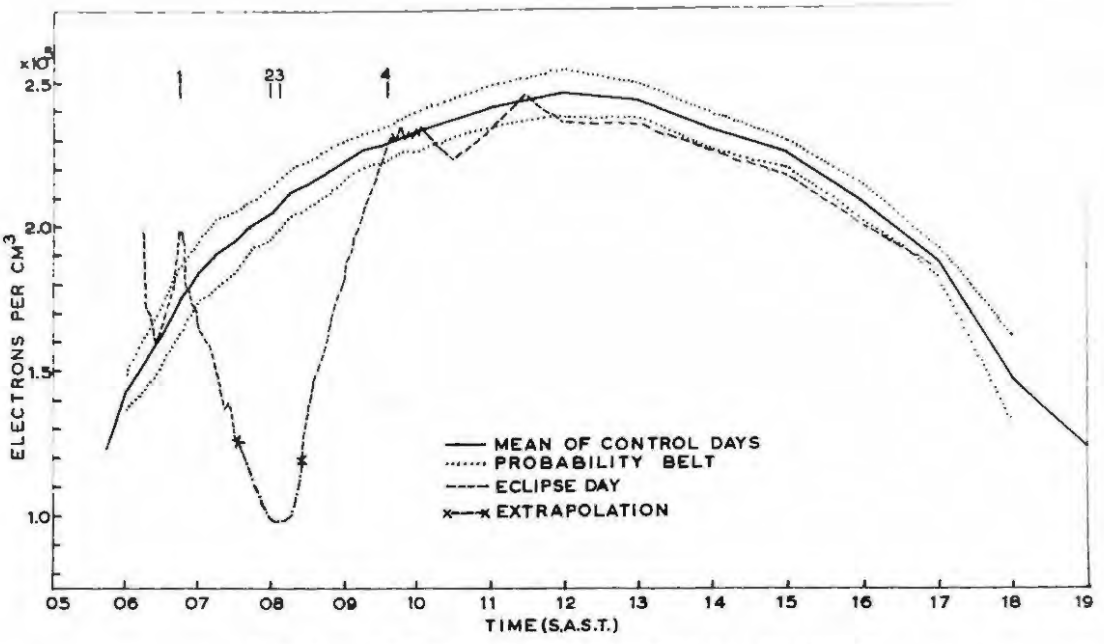

FIG: 42 MAXIMUM ELECTRON DENSITY F_1 LAYER.

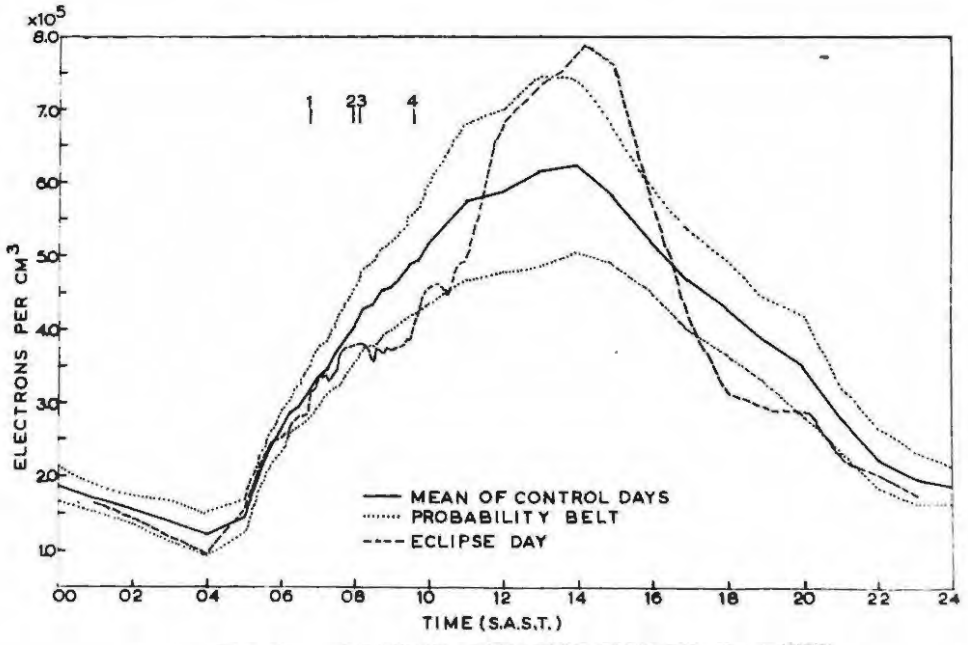

FIG: 43 MAXIMUM ELECTRON DENSITY F_2 LAYER

curve for the eclipse day just begins to fall outside the probability belt during the annular phase and remains outside this belt until about 0945. The result may be interpreted as an eclipse effect, since the curves deviate from the 50% probability belt. In fact the maximum deviation from the mean control values occurs almost one and a half hours after the annular phase and the probability of this deviation from the control curve occurring on any day is 32%. The variation of the height of the maximum electron densities during the eclipse is shown in Fig. 44, on the same figure are included the mean control readings and their probable deviations for all the four layers. There is no significant effect on the E_1, E_2 and F_2 layers. However, it seems likely that there is some evidence for a drop in the height of the F_1 layer maximum during the eclipse. The eclipse values start to deviate from the probability belt before the advent of Sporadic E during the middle of the eclipse, and is still just outside on the reappearance of the F_1 critical frequency after the maximum phase.

The corpuscular eclipse.

CHAPMAN (1932) has considered the effect of the occultation of a stream of corpuscles by the moon during a solar eclipse following the suggestion of Appleton already mentioned. The earth and moon travel round the sun in a slightly elliptical orbit with a speed of 29.80 km per sec. The moon on the other hand, travels in a slightly more

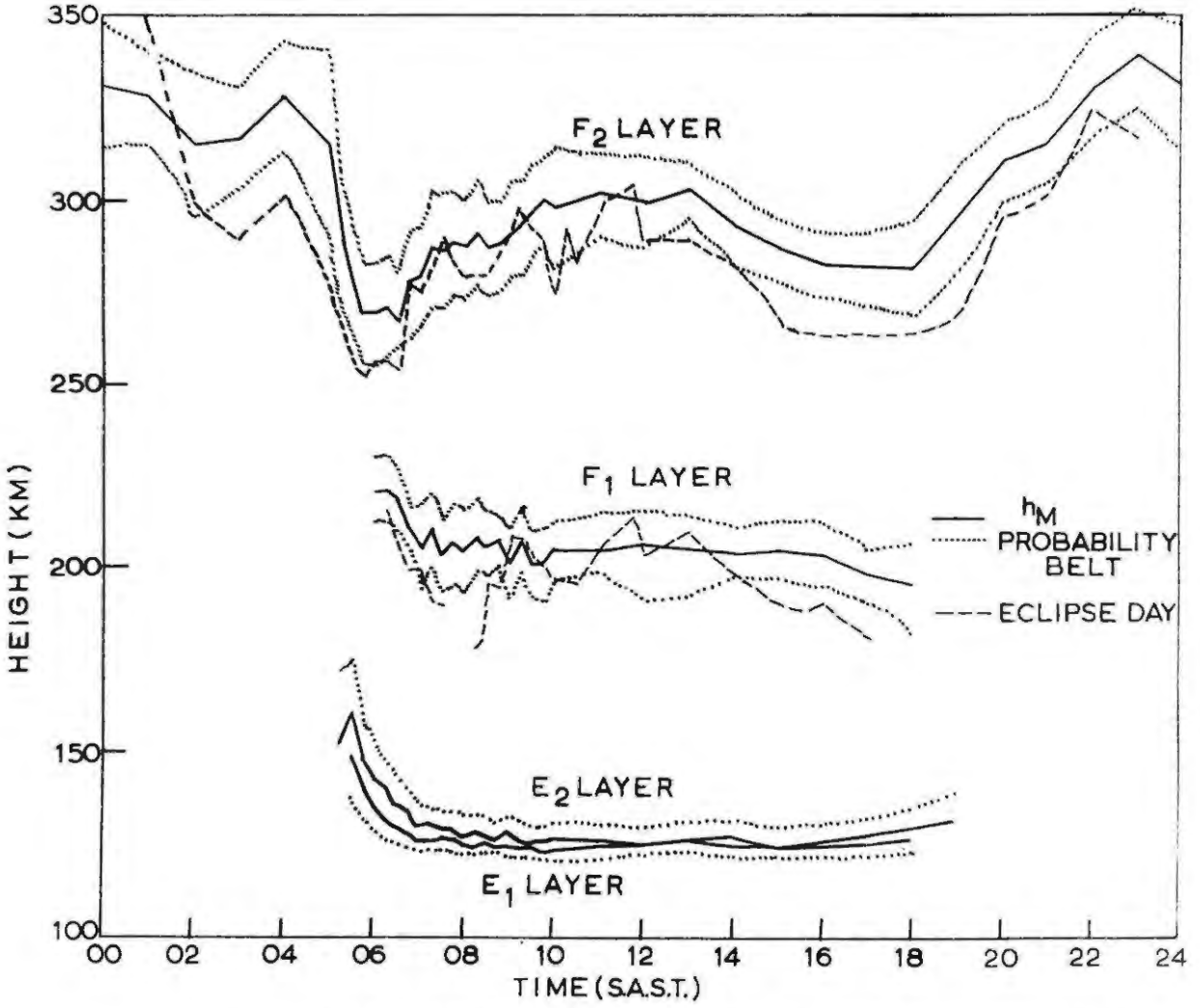

FIG:44 HEIGHTS OF MAXIMUM ELECTRON DENSITY (h_M)

elliptical orbit around the earth at a mean speed of 1.02 km per sec. The result is that even when the moon is on the sunward side of the earth, and relative to the earth is moving backwards, (opposite to the earth-moon system's orbital motion) the moon's motion is still forward. Now if the moon is moving backwards towards a position at new moon when it will cause a solar eclipse, as shown in Fig. 45, the moon will have a mean forward speed of 28.78 km/sec.

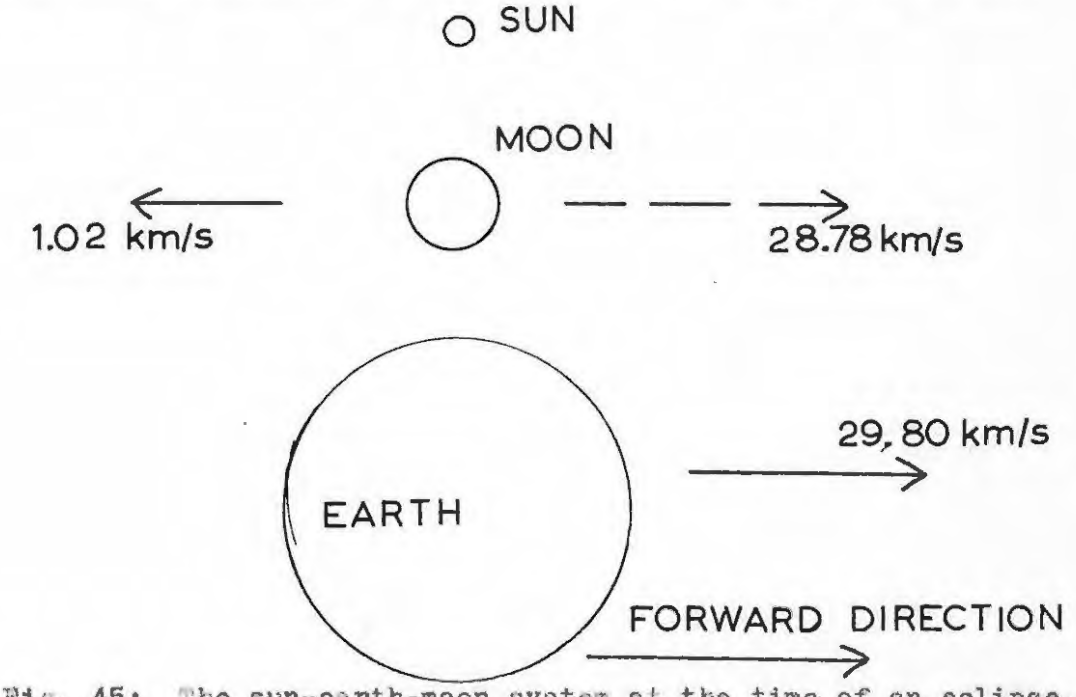

Fig. 45: The sun-earth-moon system at the time of an eclipse.

Since relative to the sun, the moon is moving in the forward direction, it will cast a shadow on the earth devoid of corpuscules sloping backwards due to the time the corpuscles take to travel from the earth to the moon. The shadow for ultra-violet and visible light will lie practically in a

straight line from the sun to the moon to the earth, since the speed of light is so great. The "corpuscular shadow" will thus lag behind the "optical shadow". However, the earth is moving forward relative to the sun faster than the moon. The result is that for an observer on the earth the "corpuscular shadow" will reach him before the "optical shadow". This effect is shown in Fig. 46, where the point P represents an observer on the earth, and as can be seen clearly, the corpuscular eclipse will occur before the optical eclipse.

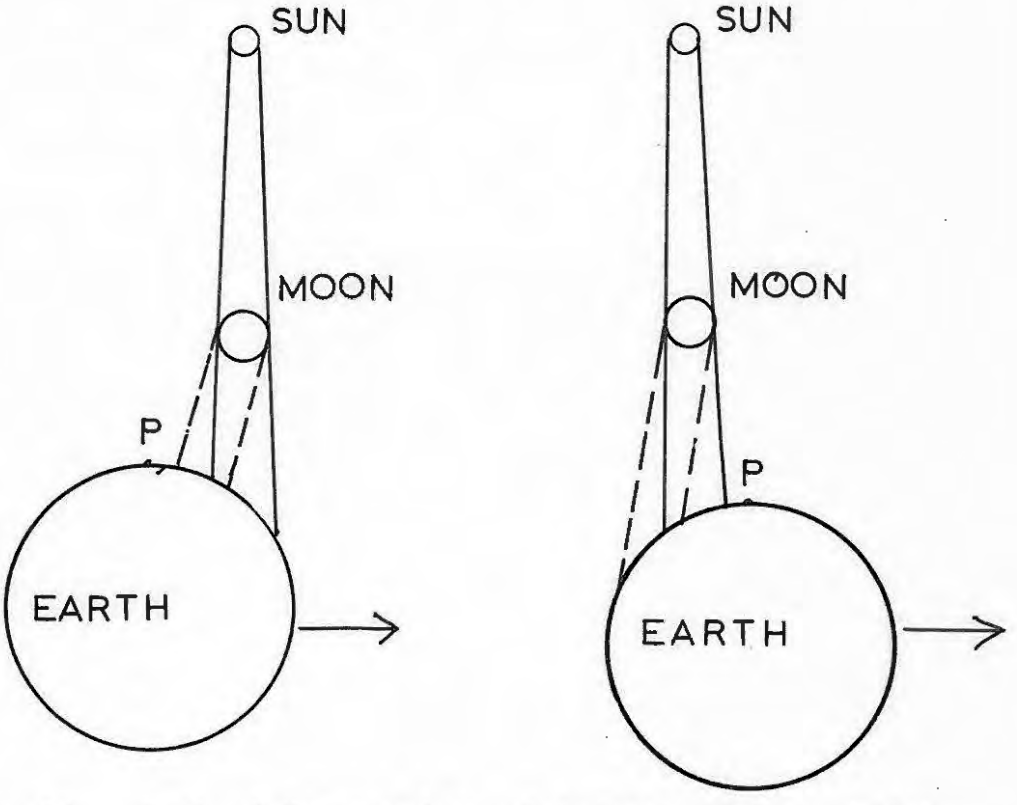

Fig. 46: Path of Corpuscular and Optical eclipse shadow.

For a particle speed of 1,000 miles per sec or 1600 km per sec, the corpuscular shadow will lag by 28.78/1600 radians or 1.03° behind the optical shadow.

The distance between the shadows on the earth's surface (distance 384,400 km from the moon) would thus be $\frac{23.78}{1600} \times 384{,}400 = 6920$ km. As the earth is moving forward at 1.02 km per sec relative to the moon and hence its shadows, this corresponds to a time lag of $\frac{6920}{1.02 \times 60} = 113$ minutes. Thus the corpuscular eclipse will occur about one hour and fifty three minutes before the optical eclipse.

Clearly, the "corpuscular eclipse" whatever the speed of the corpuscules, occurs before the optical eclipse. Examination of Figs. 40 to 43 shows that in no case was there any significant drop in electron density before the optical eclipse. This confirms the previous results of many eclipses for the E and F_1 layers, that quite conclusively the major part of the ionising radiation must be ultra-violet. The conclusion is the same for the F_2 layer. The fact that the significant deviation from the control curve occurs after the annular phase shows that corpuscular radiation cannot play a significant part in the formation of the F_2 layer. If the time lag between the corpuscular and eclipse shadows was only say 45 minutes, corresponding to a corpuscular speed of about 3,500 km per sec, it would probably be impossible to say if part of the ionisation was due to corpuscular radiation since the deviation would closely precede that due to the ultra-violet. This eclipse was particularly well situated for the observation of a corpuscular eclipse on the F_2 layer as it was due to occur during the most regular period of the layer

just after sunrise. No significant effect was observed, and it seems likely that if there is any corpuscular eclipse it must be very weak and is never likely to be observed, as it would be difficult to obtain better circumstances for its observation than during this eclipse.

Uniformly radiating solar disc.

The diurnal variation of the electron density n at any fixed height in the ionosphere may generally be expressed in terms of the simple ionospheric continuity equation

$$\frac{dn}{dt} = q - \alpha n^2 \qquad (22)$$

where q is the rate of electron production per cm^3 per sec, and α is the recombination coefficient.

It is assumed that the electron loss process is a recombination type of process proportional to the square of the electron density. It is usually assumed that the height of the maximum electron density does not vary from its normal value during an eclipse, and that the peak of electron production occurs very near to the maximum in the layer. In this case it can be seen from Fig. 44, that except perhaps for the case of the F_1 layer maximum, the assumption that the height of the layer does not differ from control days is reasonably justified. The diurnal variation of the maximum electron density is then expressed as in equation (22)

$$\frac{dN}{dt} = q - \alpha N^2 \qquad (23)$$

During the eclipse the source of ionising radiation is removed and thus the rate of electron production is decreased. If it is assumed that the sun is a uniformly radiating disc, then the rate of electron production will be proportional to the area of the sun still left uncovered by the moon at any stage. For the eclipse therefore q must be replaced by fq in equation (23) where f is the unobscured fraction of the sun's disc. During the eclipse equation (23) reduces to;

$$\frac{dN}{dt} = fq - \alpha N^2 \qquad (24)$$

Values of f have already been calculated in Part I of this thesis. Numerical solution of equation (24) should thus provide an estimate of the value of α. The numerical solution of the equation is performed by a process of trial and error. A reasonable value of α is chosen and from the diurnal variation established from control data, and using equation (23), values of q can be calculated for various times of day. Using these values of q in equation (24), a theoretical curve for N can be calculated for the eclipse by following the gradient $\frac{dN}{dt}$ from stage to stage throughout the eclipse. The value of α which gives the best fit to the experimental points is then regarded as the correct value.

For the E_1 layer, three values of α have been chosen, 5×10^{-9}, 8×10^{-9}, and 2×10^{-8} $cm^3 sec^{-1}$, and the resulting theoretical curves are shown in Fig. 47. The general shape of the curves agrees fairly well with the

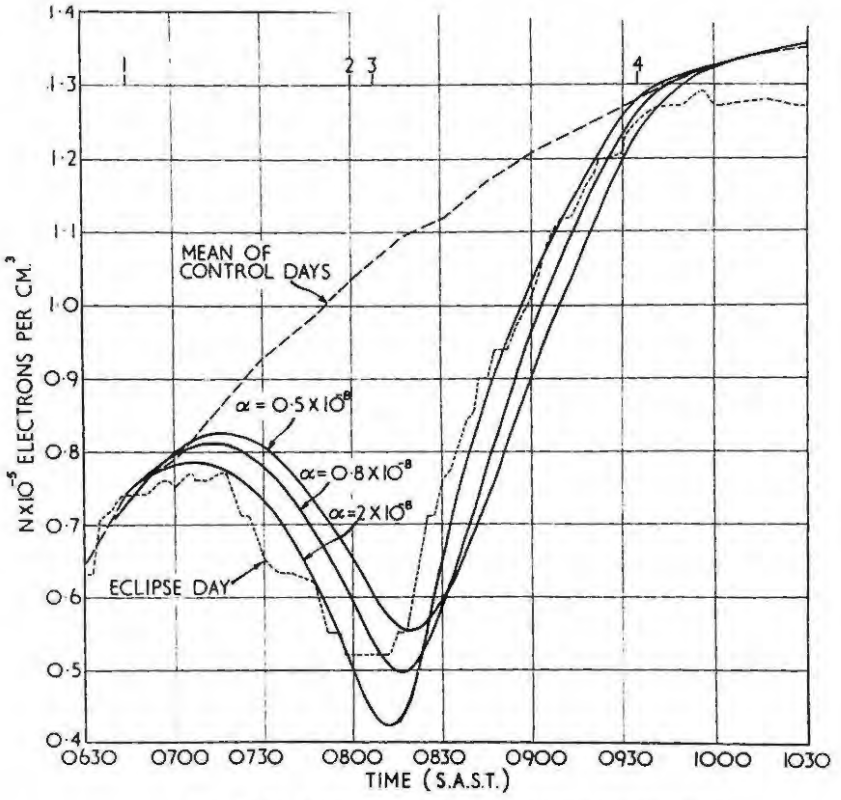

Fig: **47.** *E1* layer; theoretical curves for a uniform sun.

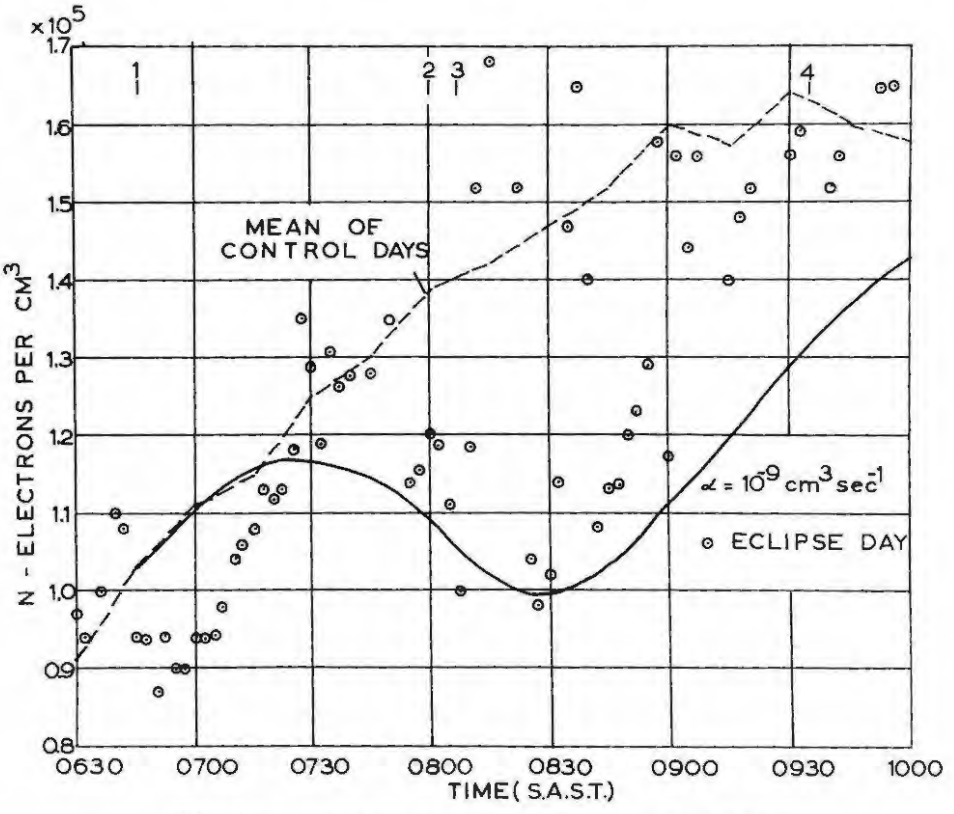

FIG: 48 THEORETICAL CURVES E_2 LAYER

experimental curves, but no perfect fit can be obtained. In all cases the minima occur too late, and if a value of α were chosen to make the minima occur at the same time, the theoretical curve would fall well below the experimental at that stage.

There are two possible criteria on this simple analysis for determining the value of α. If the minimum is taken as the criterion, then $\alpha_E = 0.7 \times 10^{-8} cm^3 sec^{-1}$. However, if the time at which the minimum occurs is the criterion, then $\alpha_E \geqslant 2 \times 10^{-8} cm^3 sec^{-1}$.

The feature of the curves is the fact that it is not possible to reconcile the minimum value of N, N_m, during the eclipse and the time lag δt between the maximum phase and the occurrence of N_m, with the same value of α. In fact this $N_m - \delta t$ anomaly is a feature of almost all eclipses. In addition there invariably seems to be a rapid drop in N after first contact. This has been noticed on several occasions by HARANG (1945), PIERCE (1948) MINNIS (1955) and many others.

Fig. 48 shows the E_2 layer curves, and taking the minimum value as the criterion then $\alpha = 10^{-9} cm^3 sec^{-1}$.

The F_1 layer (Fig. 49) shows features very similar to the E_1 layer, the minima occur too late and if the time of the minima are to agree, the theoretical curve lies well below the experimental. Once again if the minimum N_m is taken as the criterion, $\alpha_{F1} = 5 \times 10^{-9} cm^3 sec^{-1}$, and if the time of occurrence of N_m is used, $\alpha_{F1} > 1 \times 10^{-8} cm^3 sec^{-1}$. A feature similar to the E_1 layer curve is the rapid drop in N at the

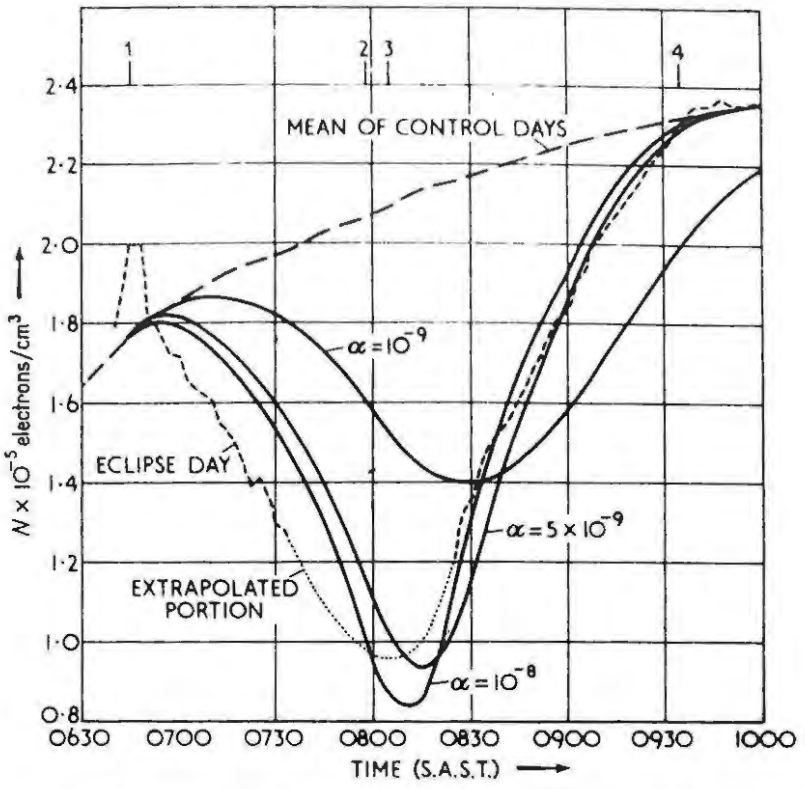

Fig: 49. Experimental and theoretical curves for the F_1-layer.

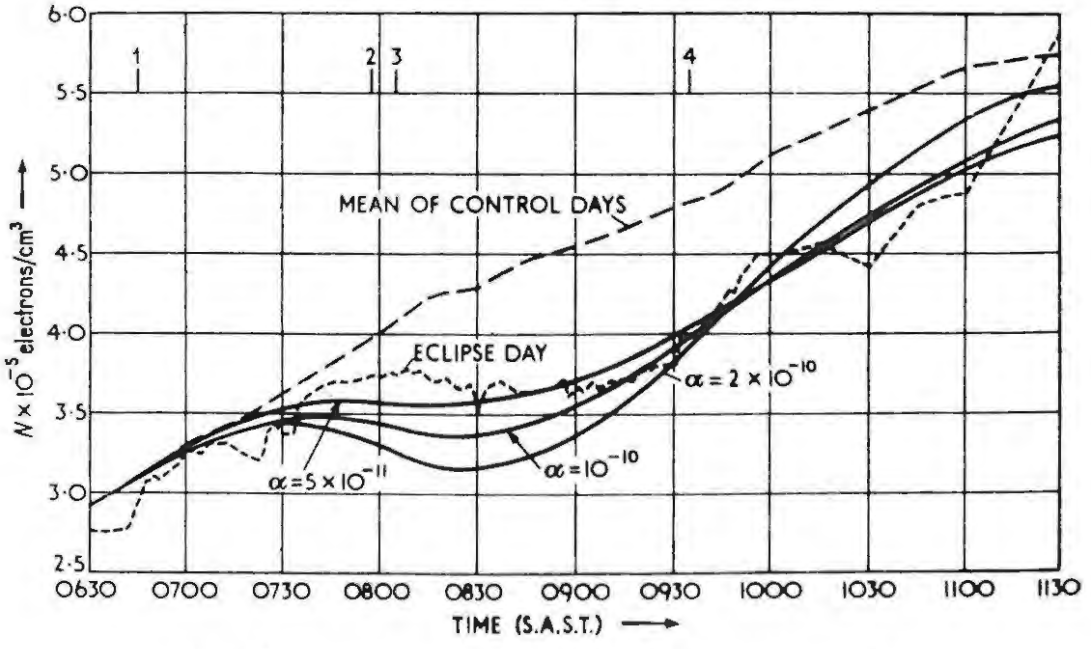

Fig: 50. Experimental and theoretical curves for the F_2-layer.

beginning of the eclipse.

Fig. 50 shows three theoretical curves for the F_2 layer. The feature of the theoretical curves in this case is that the minima all occur too early, and it does not seem possible on this simple theory to plot a theoretical curve such that its time of minimum will agree with the time of the observed N_m. However, the minima agree for $\alpha = 5 \times 10^{-11} cm^3 sec^{-1}$. Because of the obvious difficulty in making a detailed analysis on the E_2 layer, no further analyses are intended on the results from this layer.

To summarise the results obtained, taking the minimum value N_m as the criterion for determining α, the values obtained are shown in Table 10.

LAYER	E_1	E_2	F_1	F_2
$\alpha (cm^3 sec^{-1})$	7×10^{-9}	10^{-9}	5×10^{-9}	5×10^{-11}

Table 10: Values of α for uniformly radiation disc.

Discussion.

Previous workers have usually used the criterion that the minimum value of N during the eclipse approximately determines α. Table 11 shows values obtained by some previous workers using this criterion. Also included are other estimates of α by independent means.

Eclipse and Reference	α_E ($cm^3 sec^{-1}$)	α_{F1} ($cm^3 sec^{-1}$)	α_{F2} ($cm^3 sec^{-1}$)
Oct 1, 1940 Higgs (1942)	1.05×10^{-8}	8.5×10^{-9}	4×10^{-11}
Oct 1, 1940 Gilliland (1942)	72×10^{-8}	10^{-8}	10^{-10}
Oct 1, 1940 Pierce (1948)	1.2×10^{-8}	6×10^{-9}	6×10^{-11}
Feb 4, 1943 Wells & Shapley (1946)	-	-	10^{-9}
Aug 1, 1943 " "	-	-	5 to 10×10^{-10}
Jan 25,1944 " "	-	-	2 to 5×10^{-10}
Jan 14,1945 Gledhill & Szendrei (1947)	-	-	2.8×10^{-10}
July 9, 1945 McLeish (1948)	1.6×10^{-8}	1.4×10^{-8}	10^{-9}
July 9, 1945 Rydbeck (1946)	7×10^{-9}	3×10^{-9}	3×10^{-9}
May 20,1947 Denisse et al (1947)	5×10^{-9}	2×10^{-9}	10^{-10}
May 20,1947 Savitt (1950	-	-	2.5×10^{-10}
May 9, 1948 Nakata (1950)	-	4×10^{-9}	-
Sep 1, 1951 Wells (1952)	-	-	3×10^{-10}
Feb 25, 1952 Minnis (1955)	8×10^{-9}	8×10^{-9}	-
June 30,1954 Stoffregen (1956)	5.1×10^{-8}	1.7×10^{-8}	3×10^{-9}
Other methods.			
Luanr Tides, Martyn (1955)	-	-	6×10^{-11}
Night Values (Grahamstown)	-	-	1.6×10^{-10}
Rockets, Havens et al (1955)	1.5×10^{-8} (100 km)	2.0×10^{-9} (200 km)	1.6×10^{-11} (300 km)

Table 11: Values of α obtained by eclipse and other methods.

A glance at Table 11 shows that the values of α found by this method vary over a wide range whatever the layer. In the E layer, the values vary from 5×10^{-9} to $5 \times 10^{-8} cm^3 sec^{-1}$, by a factor of ten. The median of the values being about $1 \times 10^{-8} cm^3 sec^{-1}$. In the F_1 layer the variation is from 2×10^{-9} to $1.7 \times 10^{-8} cm^3 sec^{-1}$, again by a factor of ten. The F_2 variation is considerable and varies from 1.6×10^{-11} to 10^{-9}, a factor of a hundred. The median values in the last two cases being about 7×10^{-9} and $3 \times 10^{-10} cm^3 sec^{-1}$ respectively. α_{F_2} can also be estimated from the night-time decay of N. At night q = 0, and equation (23) reduces to :

$$\alpha = \frac{-1}{N^2} \cdot \frac{dN}{dt} \qquad (25)$$

Using the values of N from midnight until 0400, this method gave $\alpha = 1.6 \times 10^{-10} cm^3 sec^{-1}$ as indicated in Table 11.

Clearly, to determine the value of α by this method can only give at best the order of magnitude. There are obviously factors which have to be taken into account. A glance at the values shows that in every case the value of decreases from its value in the E region to its value in the F region. As the one goes higher into the ionosphere therefore, the value of α decreases. Most certainly in the F_2 layer, the value of α must depend on the height at which the layer maximum occurs. A glance at Fig. 36 shows that the height of the F_2 layer depends considerably on the time of

day. To take into account the seasonal variation and the time of day, it is best to compare with the solar zenith distance χ, which can be simply determined for any place from the equation:

$$\cos\chi = \sin\delta\cos\theta + \cos\delta\sin\theta\cos\phi$$

where θ = colatitude

δ = sun's declination

$\phi = \frac{2\pi t}{86,400}$ radians where

t = difference in seconds between local mean time and noon.

Table 13 therefore, shows the values of α for the three layers compared with the corresponding values of χ at mid-eclipse at each place. The table also indicates whether the eclipse occurred during morning or afternoon.

Time	χ	Time	χ
0600	80° 08'	1300	14° 10'
0700	68° 16'	1400	25° 16'
0800	55° 57'	1500	37° 36'
0900	43° 28'	1600	50° 05'
1000	30° 56'	1700	62° 31'
1100	19° 01'	1800	74° 38'
1200	10° 25'	1900	86° 16'

Table 12: Values of χ for 25, December, 1954

χ(a.m.)	χ(p.m.)	α_E ($cm^3 sec^{-1}$)	α_{F_1} ($cm^3 sec^{-1}$)	α_{F_2} ($cm^3 sec^{-1}$)
$87^o37'$		-	-	2.8×10^{-10}
	$86^o33'$	-	-	10^{-9}
$86^o32'$		-	-	3.0×10^{-10}
$74^o10'$		1.6×10^{-8}	1.4×10^{-8}	10^{-9}
	$63^o31'$	1.2×10^{-8}	6×10^{-9}	6×10^{-11}
$60^o20'$				2.5×10^{-10}
	$60^o18'$	1.05×10^{-8}	8.5×10^{-9}	4×10^{-11}
$58^o6'$		5×10^{-9}	2×10^{-9}	10^{-10}
$54^o55'$		7×10^{-9}	5×10^{-9}	5×10^{-11}
	$48^o53'$	-	-	$5\text{-}10 \times 10^{-10}$
$41^o44'$		-	-	$2\text{-}5 \times 10^{-10}$
$40^o59'$		2×10^{-8}	10^{-8}	10^{-10}
$26^o42'$		8×10^{-9}	8×10^{-9}	-

Table 13: Values of α compared with solar zenith distance χ.

This does not seem to indicate any general trend, although there is some indication that the values of α are higher for the larger values of χ. One would expect that since in the early morning post-sunrise period, the F_2 is much lower in height, the value of α_{F_2} would consequently be higher.

It is obvious that no picture of the F region can be obtained without studying the variation of electron density at fixed heights.

There are many factors which might complicate the analysis on simple theory. Firstly, the sun may not be a uniformly radiating disc and hence f will not represent the unobscured fraction of the solar radiation. Secondly, the recombination coefficient may be a complex function and vary during an eclipse. Thirdly, there may be termperature variations which will affect the value of q during the eclipse. The prupose of the next sections will be to consider all these points in detail in order to account for the departures from the simple uniform disc theory. In the next section each region will be considered separately.

(b) E Regions.

The evaluation of q.

The basic relation for the variation of the electron density at any point in the atmosphere is that given in equation (22). Chapman (1931) has considered the effect of monochromatic ionising radiation falling on an isothermal atmosphere and being absorbed according to a mass-absorption law by one atmospheric constituent. Chapman obtained the well-known relationship for q, the rate of the electron production at height h,

$$q = q_0 \exp\left(1 - z - e^{-z}\sec\chi\right) \qquad (27)$$

where q_0 = maximum rate of electron production, occurring at height h_0, when $\chi = 0$, and where $z = \frac{h - h_0}{H}$ (28)

H being the "scale height" of the atmospheric constituent which is being ionised.

$$H = \frac{kT}{mg} \qquad (29)$$

where k = Boltzmann's constant

T = absolute temperature

m = mass of the atmospheric constituent

g = acceleration due to gravity.

The maximum value of q, q_m is then given by

$$q_m = q_o \cos \chi \qquad (30)$$

and occurs at a height given by

$$z(q_m) = \log_e \sec \chi \qquad (31)$$

If equation (23) is to be used for the variation of the maximum electron density, N, then the assumption made is that the difference in height between $z(q_m)$ and z(N) is small. One wonders in many cases whether this assumption is justified. Due to the finite value of α, the height at which q_m and N occurs differ. This has for example been called the "sluggishness" of the ionosphere by APPLETON (1953). If these heights differ, suppose their difference (in terms of z) is a. Then for example

$$z(N) = \log_e \sec \chi - a \qquad (32)$$

Thus from equation (27)

$$\begin{aligned} q\left[z(N)\right] &= q_o \exp(1 - \log_e \sec \chi + a - e^a) \\ &= q_o \cos \chi \exp(-\tfrac{1}{2}a^2 - \ldots) \\ &= q_o \cos \chi \, (1 - \tfrac{1}{2}a^2) \end{aligned} \qquad (33)$$

providing a is less than unity.

Thus equation (23) must more correctly be written

$$\frac{dN}{dt} = q_o \cos \chi (1 - \tfrac{1}{2}a^2) - \alpha N^2 \qquad (34)$$

For equation (23) to be a valid approximation then $\frac{a^2}{2} \ll 1$. a has been termed the "height-lag" between the maximum rate of electron production and the maximum value of n. APPLETON and LYON (1955) have shown that a good approximation to a is given by

$$a = \frac{\tan \chi \frac{d\chi}{dt}}{2\alpha N} \qquad (35)$$

In terms of actual height h'

$$h(N) - h(q_m) = a \cdot H$$

$$= \frac{\tan \chi . \frac{d\chi}{dt} . H}{2\alpha N} \qquad (36)$$

Taking control day values at 0800, the time of mid-eclipse, $N = 1.04 \times 10^5$ electrons per cm^3, $\chi = 54^\circ 55'$, $\frac{d\chi}{dt} = 0.072$, and assuming $\alpha = 10^{-8} cm^3 sec^{-1}$, and H = 10 km (e.g. GERSON 1951) the value of a(h) = 0.43 km, and a(z) = 0.043. The error introduced into q from equation (32) would thus be $\frac{a^2}{2} = 0.001$, or one part in a thousand. Considering that N can only at best be determined to one part in a hundred, this is quite negligible. When considering the E region therefore, it is not necessary to determine n at various heights and quite legitimate to consider that N occurs at the same height as q_m.

Temperature variation.

From equation (30), equation (23) may be written

$$\frac{dN}{dt} = q_o \cos \chi - \alpha N^2 \qquad (37)$$

Since $\frac{dN}{dt}$ is small compared with αN^2 and $q_o \cos\chi$, being the difference between two much larger and nearly equal quantities, from equation (37),

$$N \propto \cos^{\frac{1}{2}}\chi \qquad (38)$$

A graph of log N versus log $\cos\chi$ should therefore give a straight line of slope $\frac{1}{2}$.

Fig. 51 shows such a plot, the resulting slope of which is 0.59 instead of 0.5 for a "Chapman" layer.

This departure from Chapman's theory might possibly be due to a change of temperature. Such a change would affect the value of q and of α.

In equations (27) and (30) q_o is given more explicitly by the relation

$$q_o = \frac{\beta I_o}{HexpI} \qquad (39)$$

where β = number of electrons produced by absorption of unit quantity of radiation.

I_o = intensity of the radiation before it enters the atmosphere.

Thus q_o is inversely proportional to the scale height, and from equation (29) is thus inversely proportional to the temperature. Supposing that α is proportional to the rth power of the temperature, equation (37) may be written

$$\frac{dN}{dt} = \frac{q_o T_o}{T} \cos\chi - \alpha \left(\frac{T}{T_o}\right)^r N^2 \qquad (40)$$

which means that since $\frac{dN}{dt}$ is small:

$$N^2 \propto \left(\frac{T_o}{T}\right)^{1 + r} \cos \chi \qquad (41)$$

It is observed however that

$$N \propto \cos^n \chi \qquad (42)$$

where $n = \frac{1}{2}$ for a Chapman layer but is here found to be 0.59. Combining equations (41) and (42) then

$$T = T_o \left(\cos\chi\right)^{\frac{1 - 2n}{1 + r}} \qquad (43)$$

$$= T_o \left(\cos\chi\right)^{\frac{-0.18}{1 + r}} \qquad (44)$$

where T_o represents the temperature when the sun is overhead.

To satisfy the common-sense condition that the temperature rises during the middle part of the day, then the index of cos χ in equation (44) must be positive, and consequently $r < -1$.

The variation of α with temperature has been considered by many authors and values of r of 0.5, -1, and -3 have been suggested by GERSON (1951), BARAL and MITRA (1950) and SEATON (1948) respectively. The only possible value of r to give a rise in temperature towards midday is thus r = -3, which is in fact the relationship of J.J.THOMPSON (1928) between the recombination coefficient and the absolute temperature at low pressures. Thus equation (44) becomes:

$$T = T_o(\cos\chi)^{0.09} \qquad (45)$$

If T_o = 300°K, a reasonable value for the temperature in the E layer at noon (GERSON, 1951), then the temperature at 0630 and 1800 is 264°K, a reasonable rise of 35°K during the day-time period. Table 14 shows the temperature at various times during the day using equation (45).

Time (SAST)	cos χ	$T = T_o(\cos\chi)^{0.09}$
0630	0.273	264°K
0700	0.370	272
0730	0.468	278
0800	0.560	283
0830	0.647	288
0900	0.726	291
1000	0.858	295
1100	0.945	298
1200	0.983	299
1300	0.970	299
1400	0.904	297
1500	0.792	293
1600	0.642	287
1700	0.461	277
1800	0.265	264

Table 14: Diurnal variation in temperature in E region (T_o = 300°K)

From equation (40) if $\frac{dN}{dt} = 0$ and $r = -3$, then

$$\left(\frac{T}{T_o}\right)^2 = \frac{\alpha N^2}{q_o \cos\chi} \qquad (46)$$

During the eclipse q_o must be replaced by fq_o and

$$\left(\frac{T}{T_o}\right)^2 = \frac{\alpha N^2}{fq_o \cos\chi} \qquad (47)$$

This equation also applies to the minimum value of N during the eclipse when $\frac{dN}{dt} = 0$.

Now $N_m = 0.52 \times 10^5$ electrons per cm^3

$f = 0.142$

and $\cos\chi = 0.56$

$\frac{q_o}{\alpha}$ may be calculated from the control value of N at noon when $T \approx T_o$ and $\cos\chi \approx 1$, and $N^2 = \frac{q_o}{\alpha} = 211 \times 10^8 cm^{-6}$ (48)

Thus from equation (46)

$$\left(\frac{T}{T_o}\right)^2 = \frac{0.27 \times 10^{10}}{0.142 \times 0.56 \times 2.11 \times 10^{10}}$$

and $\frac{T}{T_o} = 1.27$, $T = 381^\circ K$

which indicates a rise of about $100^\circ K$ during the eclipse! Changing the value of r does not affect this basic conclusion, since providing the condition $r < -1$ is fulfilled, $\frac{T}{T_o} > 1$.

This surprising conclusion results from neglect of an important factor in the theory. It is well known that a temperature gradient exists in the E region, in fact the temperature probably rises quite rapidly from 100 km to 200 km height (THE ROCKET PANEL, 1952; GERSON, 1951). The

fact that such a temperature gradient exists will also affect the value of q, whether or not this gradient varies throughout the day or during the eclipse.

Suppose therefore, that the temperature gradient expressed in terms of the scale height H is

$$H = H_o + \gamma h \tag{49}$$

where h is the height, and $H = H_o$ when $h = 0$.

$$\text{then } \gamma = \frac{dH}{dh} \tag{50}$$

where γ is the "scale height gradient".

It is easily shown (NICOLET, 1951) that equation (30) must be modified to

$$q_m = q_o(\cos\chi)^{1+\gamma} \tag{51}$$

Equation (40) thus becomes:

$$\frac{dN}{dt} = \frac{q_o T_o}{T}(\cos\chi)^{1+\gamma} - \alpha\left(\frac{T}{T_o}\right)^{r} N^2 \tag{52}$$

so that if $\frac{dN}{dt} = 0$,

$$T = T_o(\cos\chi)^{\frac{1+\gamma-2n}{1+r}} \tag{53}$$

Thus, providing $1 + \gamma \geq 2n$, positive values of r are acceptable in order to give a rise in temperature towards noon.

Values of γ have to be estimated from rocket measurements (THE ROCKET PANEL, 1952). Taking the published figures for the range 110 to 120 km which might apply to the E layer, the temperature rises by 60°K from 270°K to 330°K, giving a temperature gradient of 6°K per

km for a mean molecluar mass of 29 atomic mass units.

The scale height gradient can be calculated taking Boltzmann's constant to be 1.38×10^{-16} erg.deg.$^{-1}$, and g to be 950 cm.sec^{-2} for 100 km height. This gives $\gamma = 0.18$, and gives the result from equation (53) that $T = T_o$ and the temperature is constant during the day and independent of the value of r. The result is probably a coincidence, but γ is unlikely to differ very greatly from this value and thus it can reasonably be concluded that T is constant throughout the day.

However, during the eclipse taking $\frac{dN}{dt} = 0$, and replacing q_o by fq_o,

$$\left(\frac{T_o}{T}\right)^{1+r} = \frac{\alpha N^2}{fq_o \cos\zeta}(1+\gamma)\chi \qquad (54)$$

Thus using the values for mid-eclipse as before and taking $\gamma = 0.18$,

$$\left(\frac{T_o}{T}\right)^{1+r} = 1.79 \qquad (55)$$

If it is supposed that r = 1 say,

$$\frac{T_o}{T} = 1.34$$

or $$\frac{T}{T_o} = 0.75 \qquad (56)$$

So that if $T_o = 300^\circ$K for example, the temperature will have dropped by 75° to 225°, assuming of course that γ

has remained constant during the eclipse. Other values of $r > -1$ will also indicate a drop in temperature. Fig. 52 shows the variation of $\frac{T}{T_o}$ during the eclipse where T_o will represent the approximately constant diurnal value. The interesting feature of the deduced temperature change is the sudden rise in temperature from about 0715, which coincides with the rapid drop in N at this stage. It is interesting to note that this sudden drop in N coincides with the covering of a solitary sunspot visible on the eclipse day. This sunspot was uncovered about 0815 corresponding to the rapid rise in N at that time. The non-uniform distribution of solar radiation will not be considered in detail now, but if it is supposed that say 10% of the radiation is emitted from the spot, the resulting curve for $\frac{T}{T_o}$ which is also shown in Fig. 52, has a less pronounced rise in temperature at this stage and the value of $\frac{T}{T_o}$ now drops to 0.71 during the middle of the eclipse.

It must be pointed out that the resulting curves only give a qualitative picture of the possible temperature change since the theory assumes that $\frac{dN}{dt} = 0$ or that $\frac{fq_o T_o}{T}(\cos\chi)^{1+\gamma} \gg \frac{dN}{dt}$ and $\alpha\left(\frac{T}{T_o}\right)^{N^2} \gg \frac{dN}{dt}$. One cannot really procede further in the analysis without an idea of the value of α. However the condition $\frac{dN}{dt} = 0$ is satisfied during the annular phase and one at least can

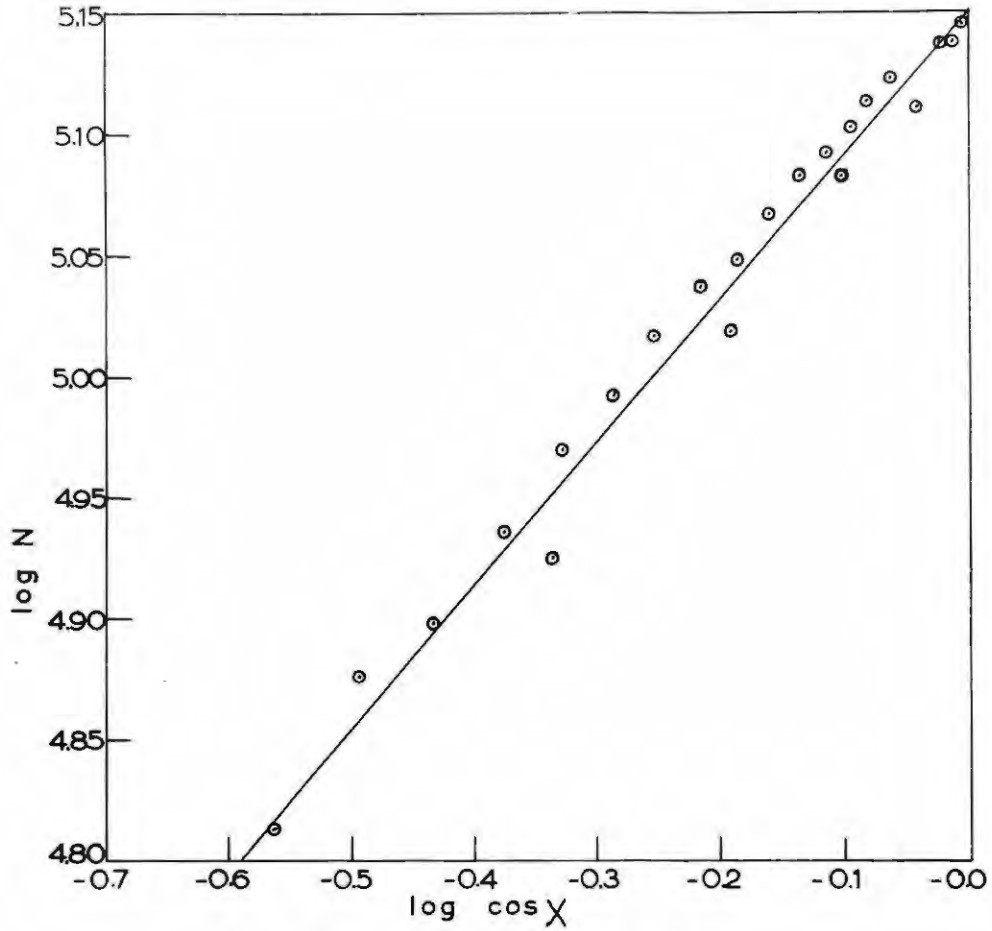

FIG: 51 log N vs log cos χ

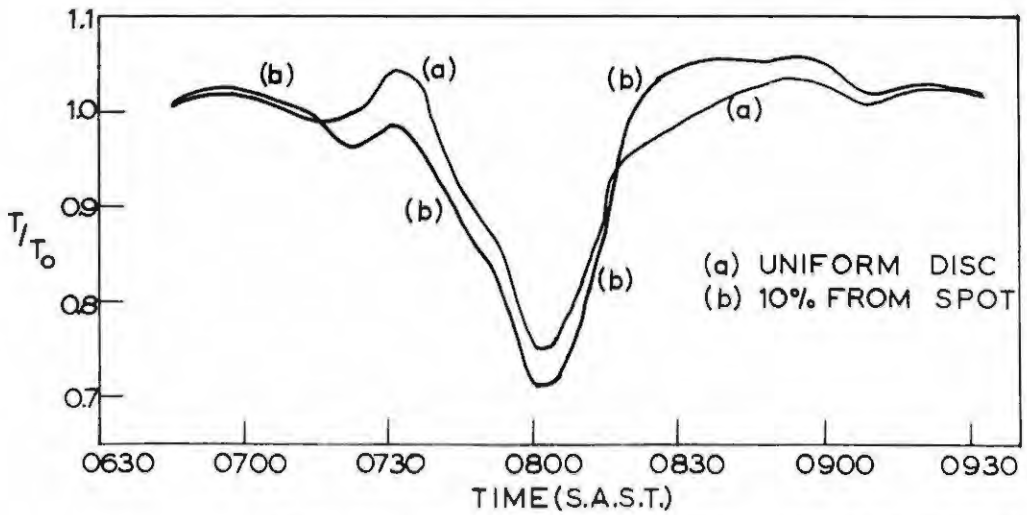

FIG: 52 ECLIPSE VARIATION OF TEMPERATURE

conclude that the $N_m - \delta t$ anomaly can be at least partly explained by a drop in temperature to $\frac{3}{4}$ of its normal value during the eclipse.

BATES (1951) in considering the thermal balance in the upper atmosphere has concluded that the thermal relaxation time in the F region to be of the order of a few days, so that temperature variations were thus unlikely to occur at that height. LOWAN (1955) has considered the cooling of the atmosphere above 100 km after sunset. Using the temperature values of the Rocket Panel, he concluded that there was no change in temperature below 160 km two hours after sunset. This would seem to indicate that it was unlikely that any temperature change in the E layer would occur during an eclipse.

BURKARD (1956) has analysed the results of MINNIS (1955) from Khartoum during the eclipse of 25 February, 1952 on the basis of a temperature change. In a more complicated analysis, he assumed that α was a function of temperature and pressure. He assumed that α was directly proportional to the temperature and that the temperature gradient was constant during the eclipse. Although his analysis is different in some ways to that presented here, the conclusions are roughly the same and he found that $\frac{T}{T_o}$ decreased to about 0.6 during the middle of the eclipse.

It seems likely that although little variation of temperature may be expected in the E layer during the daytime period, an eclipse may produce a drop in temperature to about 0.75 of the normal daily value, and provide a possible explanation of the $N_m - \delta t$ anomaly. The analysis however, makes some simplifying assumptions and it is not possible to determine a value of α.

The distribution of solar ionising radiation.

Most analyses up to 1940 of the effect of solar eclipses on the E layer have been made on the assumption that the sun is a uniformly radiating disc, and attempts were made to deduce the recombination coefficient on this basis. However, the $N_m - \delta t$ anomaly makes this method inconclusive, especially when on several occasions δt was observed to be zero or even negative. In addition, it was not unusual to observe abrupt changes in the rate of rise or fall of the electron density. These abrupt changes appeared to be associated with the covering or uncovering of sunspots, and implied that the distribution of the ionising radiation was not uniform over the sun's disc. In fact, it is well-known that chromospheric eruptions are associated with radio fade-outs and it is to be expected consequently that local "hot spots" might be temporary areas of increased emission of ionising radiation.

The first attempt to deduce the distribution of sources of ionising radiation from eclipse measurements

was that of HIGGS (1942), who found that the data obtained during the eclipse of October 1, 1940 could not be explained in terms of a uniformly radiating disc. Irregularities in the eclipse curves for the E and F_1 layers were found to be associated with four isolated areas of calcium flocculi which were visible at that time. By a method of least squares Higgs came to the conclusion that all the radiation must have come from these four areas and none from the disc. However, Higgs admitted that this was not a unique solution.

RYDBECK (1946) however, found that there was a correlation between sources of ionising radiation as deduced from E layer measurements during the eclipse of July 9, 1945 and areas of hydrogen faculae. However, WALDMEIER (1947) re-examined Rydbeck's data and pointed out that the E layer data suggested a link between the sources of ionising radiation and also areas from which the coronal line at 5303 Å was strongly emitted. A similar suggestion was made by OSAWA (1950) after the 1948 eclipse in Japan. During the eclipse of 25 February, 1952 MINNIS (1952, 1955) was also able to find a correlation between areas of 5303 Å emission and E layer ionising radiation. Table 15 below shows how some workers have had to postulate the existence of bright regions on the sun during some eclipses. The two most surprising results are those of

HIGGS (1942) who found that all the radiation came from four areas and DELOBEAU (1953) who found he had to attribute 54% of the radiation to a single area.

Eclipse & Observer	% obscured	α_E ($cm^3 sec^{-1}$)	% of radiation	
			Disc	Active areas
Oct 1,1940 Higgs (1942)	100	1.68×10^{-8}	0	36,33,20,11
Sept 1,1951 Delobeau (1954)	75	0.5×10^{-8}	55	37, 8
Feb 25,1952 Delobeau (1953)	45	0.7×10^{-8}	46	54
Feb 25,1952 Minnis (1956a) (Two places)	100 75	$1.2 \pm 0.1 \times 10^{-8}$	64	25,11
June 30,1954 Landmark & Leid(1956)	100	3.4×10^{-8}	71	14,10, 5
June 30,1954 Minnis (1956b) (Two places)	89 71	$>1.0 \times 10^{-8}$	92	15, 3, -6, -4
June 20,1955 Minnis (1957)	48	1.2×10^{-8}	62	21, 7, 6, 4

Table 15: Distribution of solar radiation during several eclipses

If the ionising radiation does not come uniformly from the sun's disc then equation (24) must be modified to

$$\frac{dN}{dt} = f'q - \alpha N^2 \qquad (57)$$

where f' = fraction of solar radiation left uncovered by the moon.

To determine the values of f' throughout the course of the eclipse, it is necessary to know the value of α since from equation (57)

$$f' = \frac{\frac{dN}{dt} + \alpha N^2}{q} \qquad (58)$$

and q can be calculated from control data knowing the value of α. Values of N and $\frac{dN}{dt}$ from the experimental data for the eclipse are used. MINNIS (1955, 1956 a, b) has used a refinement of this equation by supposing that during the course of the day

$$\frac{dN}{dt} = q_o \cos^n \chi - \alpha N^2 \qquad (59)$$

which is modified to

$$\frac{dN}{dt} = f' q_o \cos^n \chi - \alpha N^2 \qquad (60)$$

during an eclipse, where n represents the appropriate index by plotting log N^2 versus log cos χ. Rearranging the terms, Minnis obtained the relation

$$J = \frac{f' q_o}{\alpha} = \left(N^2 + \frac{1}{\alpha}\frac{dN}{dt}\right) \sec^n \chi \qquad (61)$$

Since q_o and α are assumed to be constants, J represents the relative intensity of the solar radiation. The method is essentially the same although Minnis avoids evaluating q from the control data by insertion of the index to cos χ.

Using equation (58) therefore, f' was evaluated from the eclipse values of N and $\frac{dN}{dt}$ for various values

of α from 10^{-8} to 10^{-7}. These are shown in Fig. 53 together with a plot of f. It is at once obvious from these curves that it is necessary to postulate the existence of a source on the West limb since for any value of the curves for f' lie below that for f. In addition, some source must have been covered about 0715 corresponding to the sharp drop in N and f' at this time. The curves indicate that whatever the value of α, the value of f' during the annular phase was about 0.23 to 0.24, or 10% more radiation than that due to a uniform disc. To explain this it is then necessary to postulate the existence of a further source on the East limb which would only be covered after the annular phase. Fig. 30 in Part I shows the path of the moon across the sun at various heights. By sliding a disc of appropriate size to represent the moon travelling across the sun, arcs of circles can be drawn at the appropriate times when irregularities occur in f'. The positions where these arcs intersect for the irregularities before and after the annular phase then fixes the position of the sources. However, because the moon travels across the middle of the sun it is not possible to say whether the sources so deduced lie in the northern or southern solar hemisphere. Irrespective of the value of α, however three sources have to be postulated, their positions varying slightly with different values of α. From Fig. 53 it is then possible to

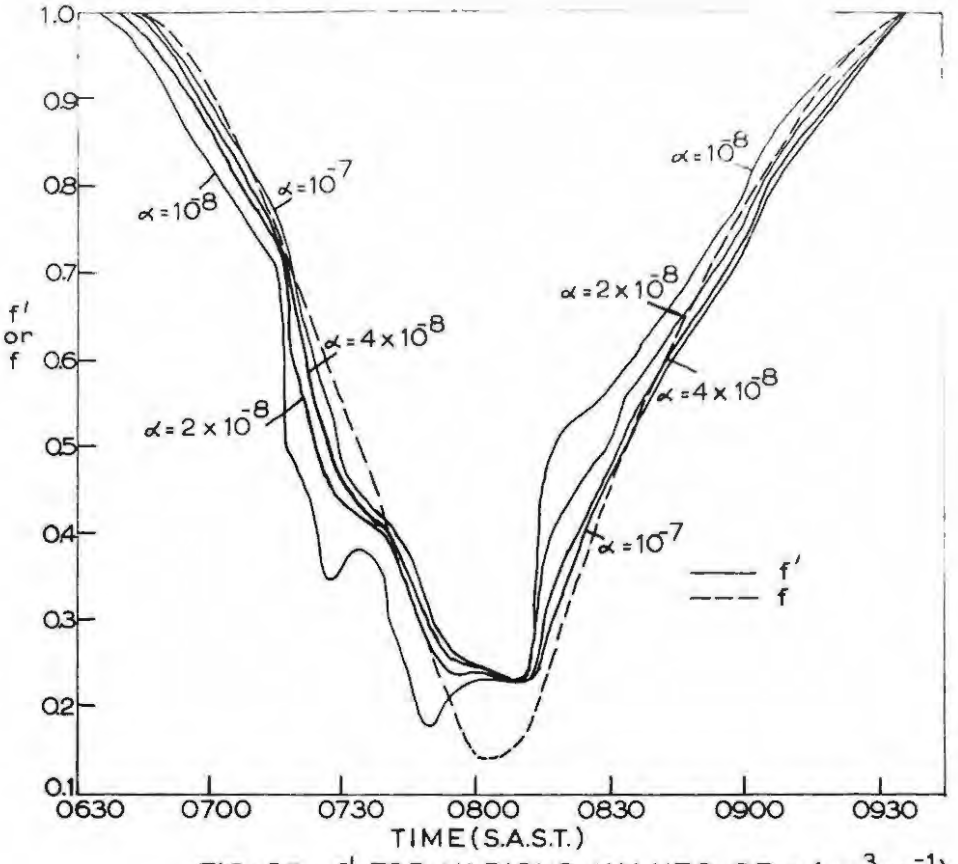

FIG: 53 f' FOR VARIOUS VALUES OF α ($cm^3 sec^{-1}$)

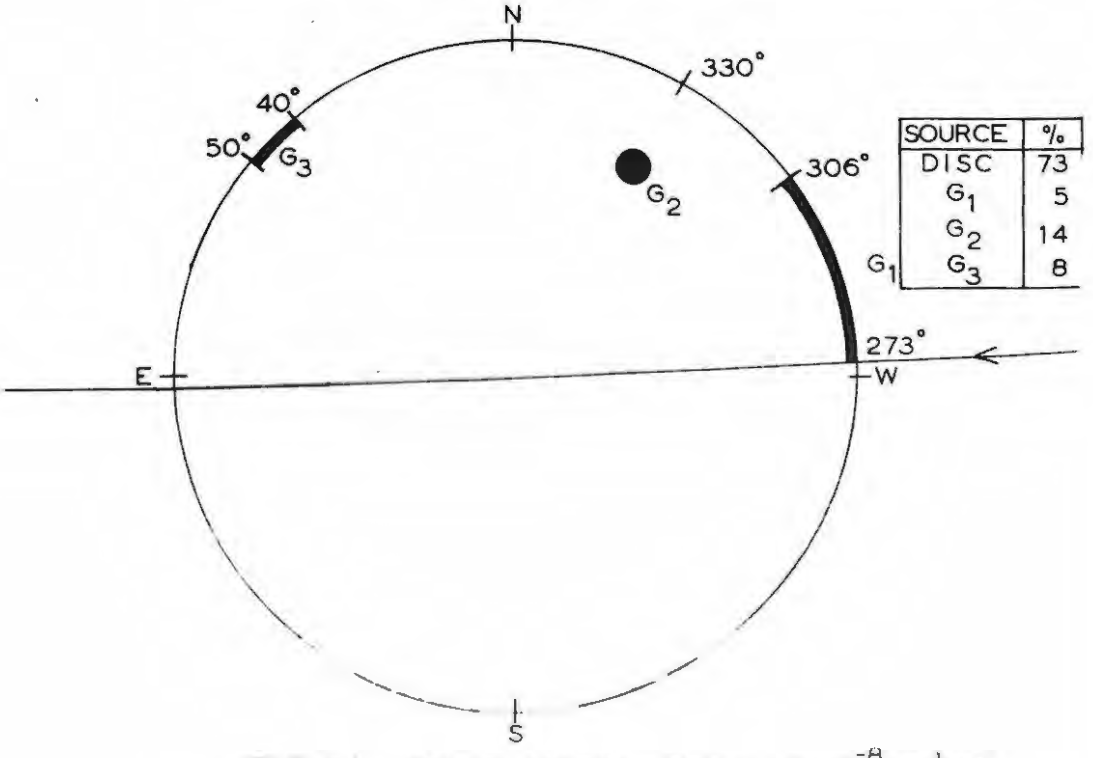

	SOURCE	%
	DISC	73
G_1	G_1	5
	G_2	14
	G_3	8

FIG: 54 SOLAR MODEL FOR $\alpha = 2 \times 10^{-8}$ $cm^3 sec^{-1}$

deduce by a process of trial and error the intensity of each of these sources for each value of α. The intensities so deduced are shown in Table 16.

Source	1.0×10^{-8}	1.5×10^{-8}	2.0×10^{-8}	4.0×10^{-8}	10^{-7}
Disc	65	70	73	78	80
West limb	12	8	5	4	3
East limb	3	6	8	8	9
Spot	20	16	14	10	8

Table 16: Variation of intensity of bright areas (% of total radiation) with α ($cm^3 sec^{-1}$)

Fig. 54 shows the solar model for $\alpha = 2.0 \times 10^{-8} cm^3 sec^{-1}$, with all the sources placed in the northern hemisphere, while Fig. 55 shows a plot of f' on this model against the observed values of f' for $\alpha = 2.0 \times 10^{-8} cm^3 sec^{-1}$. It is admittedly not good procedure to combine a mixture of theory with experiment as has been done here, and as was done by MINNIS (1955) for example. However, the method of deducing the sources from the experimental points is essentially a method of "working backwards" and it is difficult to see how one can avoid this.

Although the method of analysis cannot give a unique solution for the intensity of the sources and for α

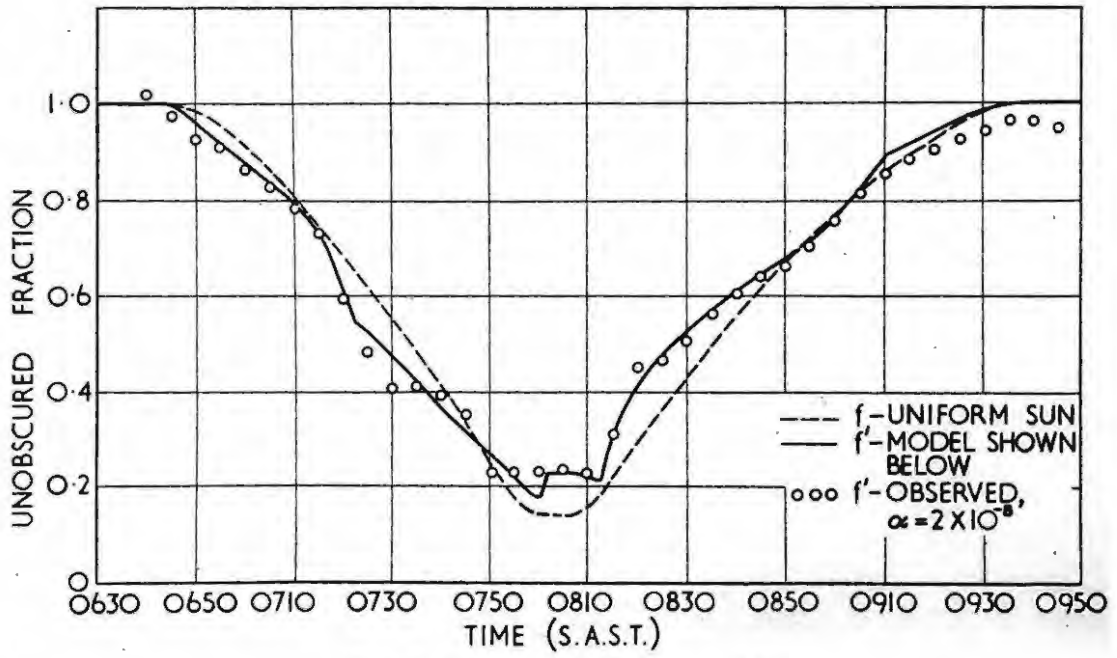

Fig. 55. Unobscured fractions of the sun.

CORONAL EMISSION IN 5303 Å SEEN AT LIMB

A VERY FAINT
B FAINT
C MODERATE
D BRIGHT
E VERY BRIGHT

CORONAL EMISSION IN 6374 Å SEEN AT LIMB

A' VERY FAINT
B' FAINT
C' MODERATE
D' BRIGHT
E' VERY BRIGHT

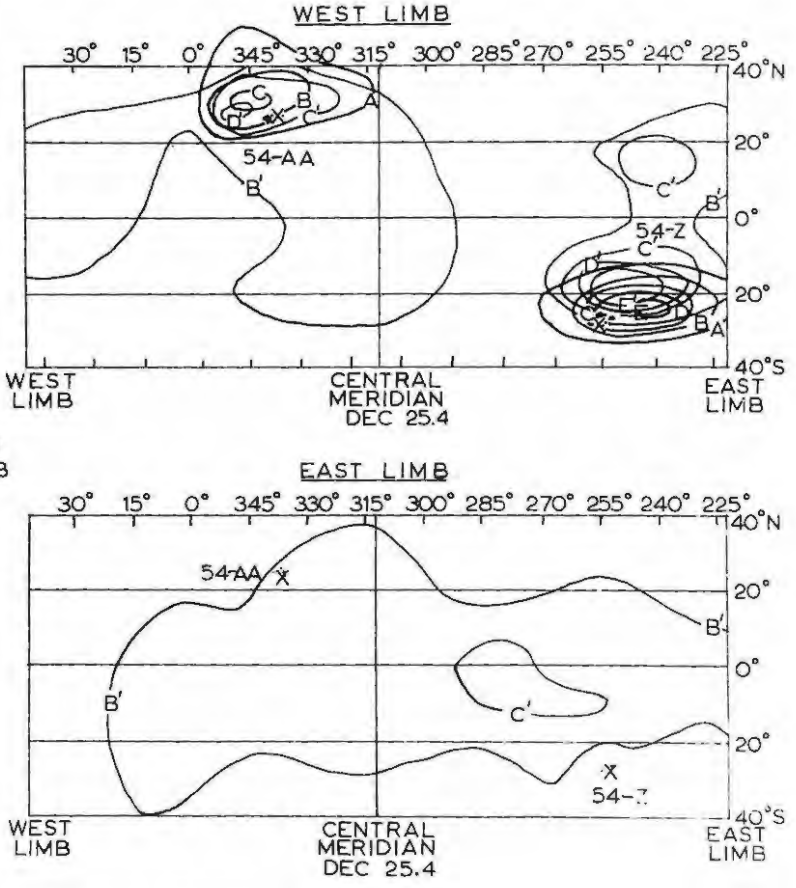

FIG: 56 CORONAL CONTOURS
(After Trotter & Roberts, 1955)

it does show that irrespective of the value of α, the position of the sources is roughly the same. It is interesting therefore, to compare the sources so deduced with those from spectroheliograms and other visual observations.

The author is grateful to Dr. A. K. Das of the Astrophysical Observatory, Kodaikanal, India, for supplying sketches of the sun made from spectrohelioscope and prominence spectroscope observations. Data on the distribution of the coronal green (5303Å) and red (6374Å) lines were kindly made available by Mr. C. M. Minnis of the D.S.I.R. Radio Research Station, Slough, England from the reports of TROTTER and ROBERTS (1955) on coronal activity around 25 December, 1954. Coronal emission intensities can only be measured at the limb. However, since the sun rotates once every 28 days, observations made on the West limb for a period of 14 days following the eclipse day may be compared with the observations made the 14 days prior to the eclipse day on the East limb. From this it is possible to gain a reasonably qualitative picture of the distribution of the coronal emission lines over the disc on the eclipse day. These limb intensities of the coronal green and red lines are shown in Fig. 56, which is a contour diagram of the intensities measured at the east and west limbs over a period of 14 days. The contours are plotted on lines of heliographic latitude and longtitude. The heliographic

co-ordinates of the centre of the disc and the sun's axis of rotation are given in the Nautical Almanac and for 25, December 1954 were:

Disc centre + 1.3° heliographic latitude

313° heliographic longtitude.

Position angle of axis of rotation of sun was 5.7° east of the North Point. Using this data it is then quite easy to transpose the heliographic co-ordinates to co-ordinates refering to the North Point. As can be seen the disc extends from 223° on the east limb to 043° heliographic longtitude on the west limb.

The sketches made by Dr. Das show only two features on the sun on the eclipse day,

(a) A solitary sunspot in the North-west quadrant of the disc, surrounded by a bright $H\alpha$ region.

(b) A prominence on the North-east limb.

From Fig. 56, it can be seen that the coronal contours as derived from each limb are quite different. They indicate that both limbs were very quiet in coronal emission with no enhancement in 5303Å. Radiation in 6374Å was observed on both limbs but was very faint. To gain a better picture of the corona over the disc, it is probably best to use the West limb data for the seven days after the eclipse for the Western half of the disc, and the East limb data for the seven days before the eclipse for the Eastern half of the disc. At once one can conclude that the eastern half

of the limb was almost completely inactive,whilst the solitary sunspot in the north-west quadrant of the disc was associated with a region of moderate intensity in 5303Å and was otherwise almost completely inactive. From the west limb data it can be seen that a sunspot whose position was about 30°S latitude and 255° longitude was observed on the west limb twelve days after the eclipse,associated with bright intensity in 5303Å. However, this spot was not observed when it should have been on the east limb two days before the eclipse. The data supplied by Dr. Das showed that this spot developed on the disc as the sun rotated. If it was present on the eclipse day its intensity in 5303Å must have been at most faint and just inside the east limb, roughly corresponding to the east limb source postulated from the E layer data, but in its corresponding position in the Southern hemisphere.

WALDMEIER (1955, 1956) has shown how to find a more quantitative aspect of the corona in front of the sun's disc, but it does not seem necessary to make such a detailed analysis.

The position of these active areas observed on the eclipse day together with the active areas deduced from the E layer measurements shown in both their northern and southern positions, are detailed in Fig. 57, which shows that:

(i) There is no correlation with either G1 or G1'

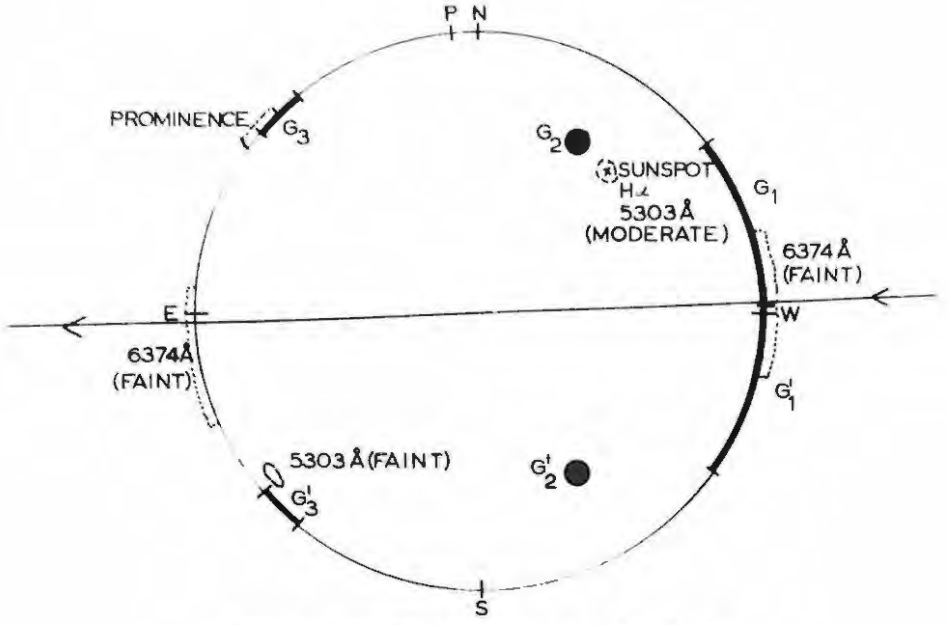

FIG: 57 SOLAR MODEL ($\alpha = 2 \times 10^{-8} cm^3 sec^{-1}$) COMPARISON WITH VISUAL AND OTHER OBSERVATIONS

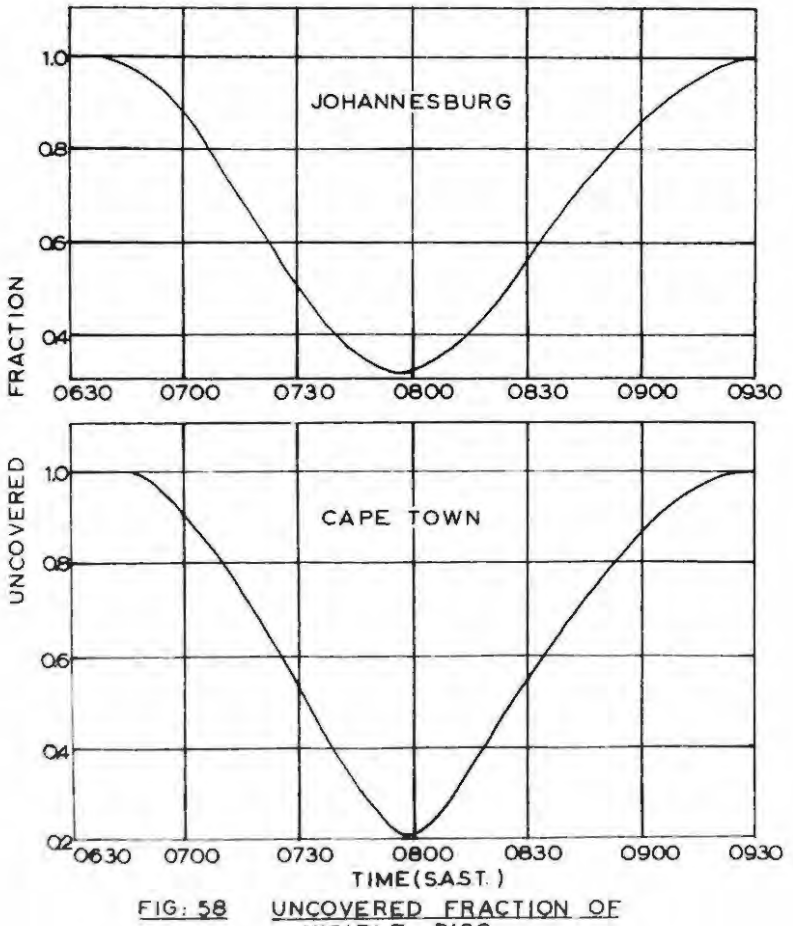

FIG: 58 UNCOVERED FRACTION OF VISIBLE DISC

as the Western limb was completely inactive except for faint 6374Å radiation.

(ii) The source G2 is close to a solitary sunspot surrounded by an Hα region, and a region of moderate intensity in 5303Å.

(iii) The source G3 almost coincides with the position of the solar prominence, whilst G3' is close to the faint area in 5303Å.

Comparison with measurements at Johannesburg and Cape Town.

Measurements were also made at Cape Town and Johannesburg during the eclipse on the ionosphere sounders operated by the National Telecommunications Research Laboratory of the South African Council for Scientific and Industrial Research. These measurements therefore, might help in deciding which of the models in Table 16 applies and consequently give an indication of the value of α. The measurements might also give an indication of whether the sources lie in their northern or southern positions.

The h'f records were made available to the Rhodes University Physics Department and the scaled values of critical frequencies were kindly made available to the author by Professor J. A. Gledhill. The measurements were made every minute during the eclipse and the critical frequencies were read to the nearest 0.01 Mc/s. However, at times during the eclipse the accuracy was only to the nearest 0.05 Mc/s. Control data were taken from the

"Monthly Bulletin of ionospheric characteristics recorded at Cape Town and Johannesburg during December, 1954", published by the National Telecommunications Research Laboratory. This data only gave critical frequencies to the nearest 0.1 Mc/s, and at hourly intervals. The mean values of N for the E layer covering the period 19 to 31 December, 1954 are shown in Table 17 together with the probable errors.

Time (Hours SAST)	Cape Town		Johannesburg	
	N	r	N	r
0600	0.40	0.02	0.47	0.04
0700	0.63	0.04	0.79	0.04
0800	0.89	0.04	1.04	0.01
0900	1.09	0.06	1.18	0.02
1000	1.22	0.04	1.32	0.04
1100	1.38	0.05	1.46	0.04
1200	1.45	0.02	1.50	0.04

Table 17: Mean Values of N ($\times 10^{-5}$ electrons per cm^3) for the E layer at Cape Town and Johannesburg, 19 to 31, December 1954.

The circumstances of the eclipse at these two places at a height of 100 km are shown in Table 18, where f-min represents the unobscured fraction of the visible disc at the maximum phase. For comparison figures for Grahamstown are also included.

Station	Begins	Middle	Ends	f-min
Grahamstown Lat: 33°19'S Long: 26°31'E	0646	0800 to 0807 (annular phase)	0935	0.142
Johannesburg Lat: 26°10'S Long: 28°05'S	0639	0758	0929	0.320
Cape Town Lat: 34°9'S Long: 18°19'E	0647	0758	0922	0.204

Table 18: Circumstances of eclipse at 100 km height (SAST) at three stations in South Africa

The unobscured fraction, f, of the visible disc at Cape Town and Johannesburg was calculated as detailed in Part I of the thesis. Fig. 58 shows the variation of f at a height of 100 km during the eclipse at these two places.

The usual first approximation was carried out as a first analysis using equation (24), assuming that the ionising radiation comes uniformly from the disc. However, it was found that the values of N at Johannesburg were lower on the eclipse day than the mean control values. Values of N at Cape Town were higher than the mean values before the eclipse and roughly the same afterwards. It was found necessary therefore, to adjust the values of q as deduced from the control values to account for these departures from the mean control values on the eclipse day.

This was probably not a real effect but the result of inadequate control data being available at only hourly intervals, and to the nearest 0.1 Mc/s. In any case one could hardly expect the eclipse to coincide exactly with the mean control values and providing any adjustments to q result in N falling within the probability belt for the control data, this procedure seems justified. As can be seen by comparison of Figs. 59 and 60 with Table 17, this condition is fulfilled. The two Figs. 59 and 60 show the resulting theoretical curves for Cape Town and Johannesburg. Using the minimum as the criterion, the values of α at Cape Town and Johannesburg are $8 \times 10^{-9} cm^3 sec^{-1}$ and $7 \times 10^{-9} cm^3 sec^{-1}$, which agree very well with the Grahamstown value of $7 \times 10^{-9} cm^3 sec^{-1}$.

MINNIS (1956a) has shown how it was possible from the measurements at two stations during the eclipse of 25 February, 1952 to solve for the intensity of the sources and α. Minnis found that the intensity of the sources could each be expressed as a linear function of α of the form $A + \frac{B}{\alpha}$. By solving simultaneous equations for each source at Khartoum and Ibadan, he was able to deduce both α and the intensity of the sources. However, the readings from Cape Town and Johannesburg exhibit many peculiar bumps which seem difficult to explain on the covering or uncovering of sources on the disc. The most striking peculiarity is that in the Cape Town curves between 0830 and 0850 when the

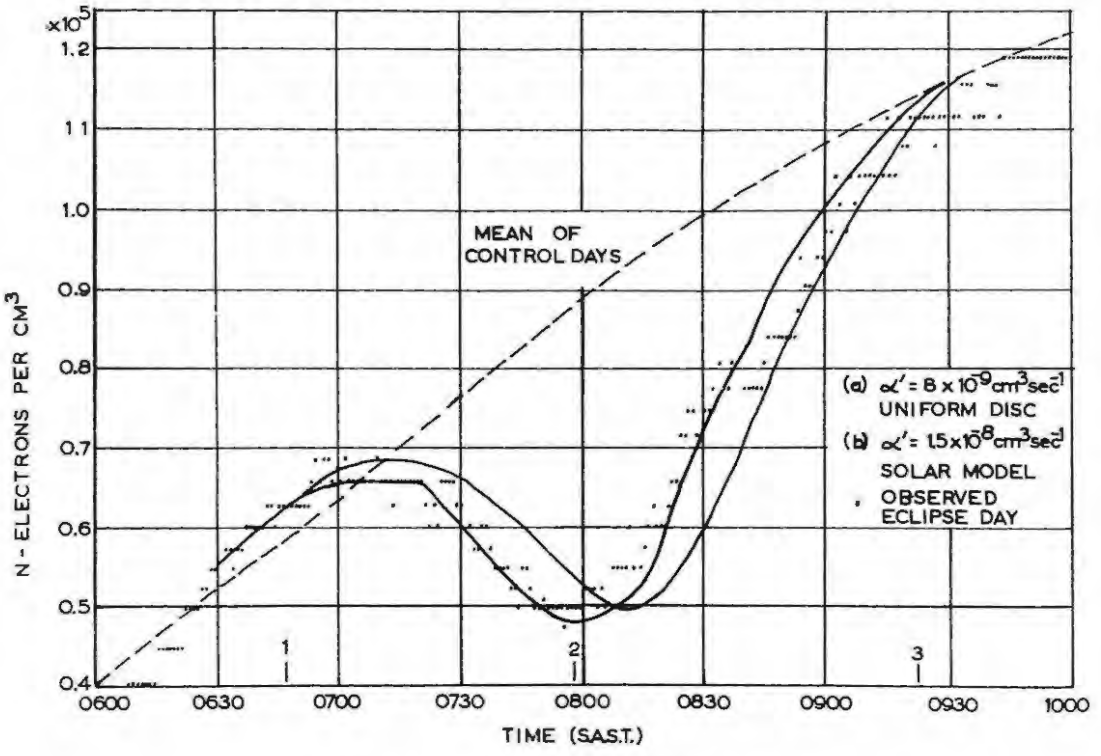

FIG: 59 CAPE TOWN, THEORETICAL CURVES
SOLAR MODEL: DISC 70%, SPOT 16%,
EAST LIMB 6%, WEST LIMB 8%

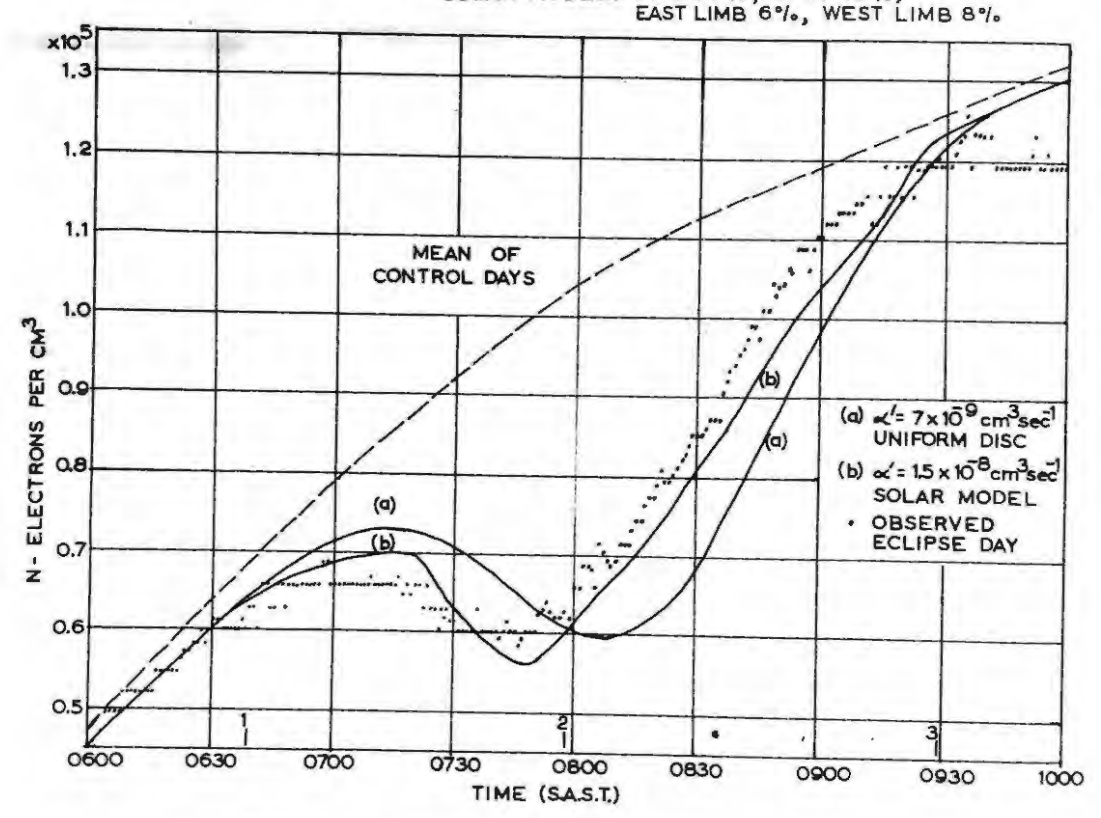

FIG: 60 JOHANNESBURG, THEORETICAL CURVES,
SOLAR MODEL: DISC 70%, SPOT 16%,
EAST LIMB 6%, WEST LIMB 8%.

upward slope is interrupted. However, to try and see if any of the Grahamstown models would fit the curves for Cape Town and Johannesburg, each of the 5 models were applied, not necessarily using the corresponding values of α. It was found that the model for Grahamstown corresponding to $\alpha = 1.5 \times 10^{-8} cm^3 sec^{-1}$ in Table 16 gave best agreement at the two stations with $\alpha = 1.5 \times 10^{-8} cm^3 sec^{-1}$ agreeing with the Grahamstown value. These curves are shown also in Figs. 59 and 60. Fig. 61 shows the resulting curve for this model for Grahamstown. It is necessary to place both the East and West limb sources in their Southern positions as is shown in the resulting model in Fig. 62. In fact, it does not alter the fit appreciably if the West limb source is in either its northerly or southern position, or if the source extends to include both positions. The fit to the observed points is reasonably good but by no means perfect and it seems likely that other facts must be involved. There seems to be some correlation between the east limb source and faint emission in 5303Å as well as an agreement with the solitary sunspot associated with moderate enhancement in 5303Å. However, there is no evidence for the existence of the west limb source. The only correlation is with a faint enhancement in 6374Å, which has never been found previously.

The recombination coefficient.

Up to now it has been assumed that the recombination

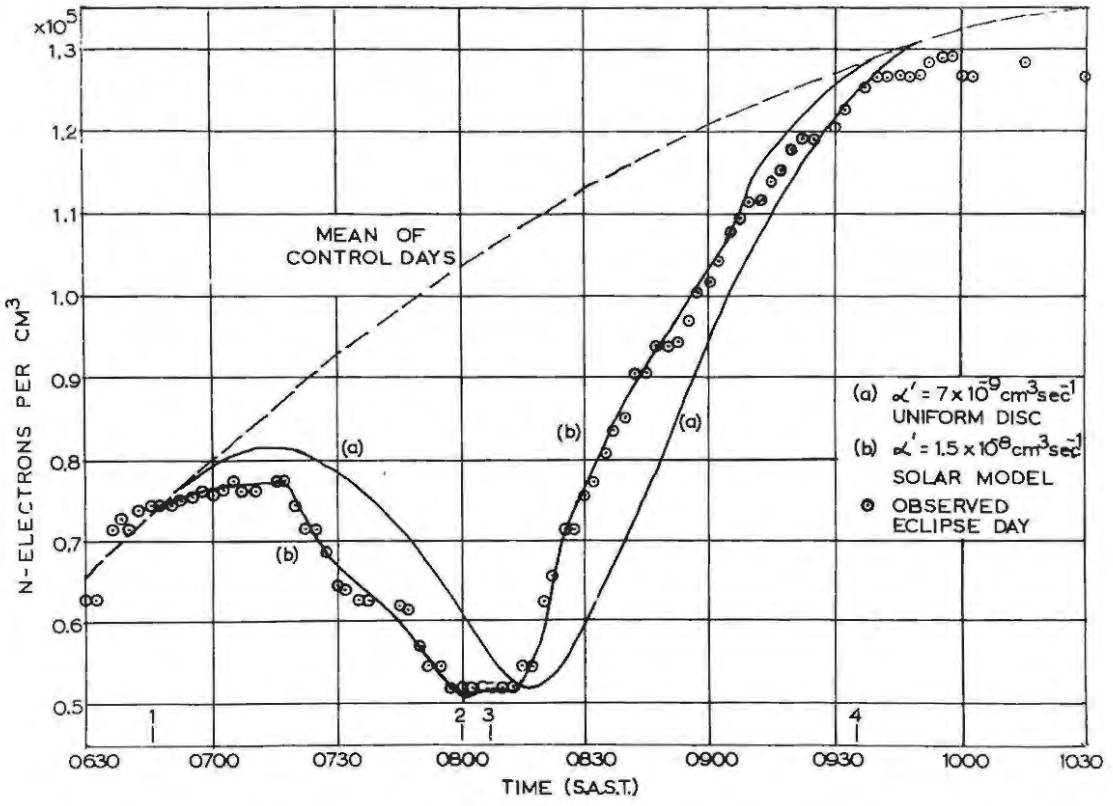

FIG: 61 GRAHAMSTOWN, THEORETICAL CURVES, SOLAR MODEL: DISC 70%, SPOT 16%, EAST LIMB 6%, WEST LIMB 8%.

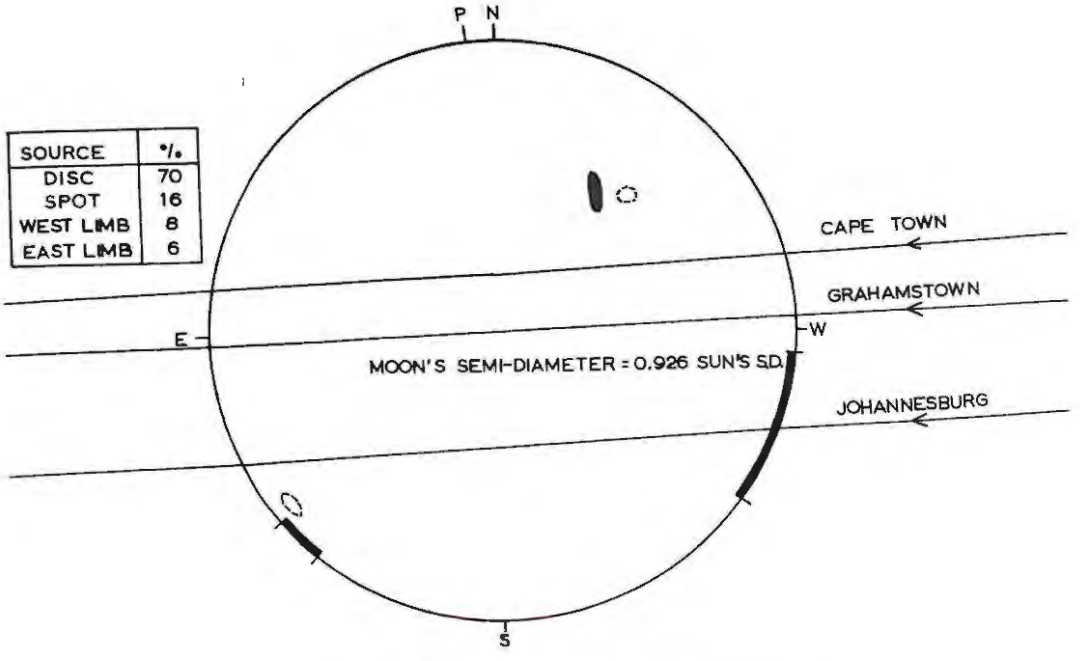

PATH OF MOON ACROSS SUN AT 100 KM

FIG: 62 SOLAR MODEL OBSERVED SUNSPOT + 5303 Å

CALCULATED

coefficient α in equation (23) is a constant. Before considering the possibility that it might vary it is necessary to consider its composition.

The early views on the process of recombination were those of ECKERSLEY (1933) for example, who favoured a process of recombination between electrons and positive-ions, so called radiative recombination. APPLETON and NAISMITH (1932), however, had previously inclined to the view that electrons disappeared mainly by attachment to neutral particles and the subsequent mutual neutralisation of positive and negative ions occurred. Later (APPLETON and NAISMITH, 1935) adduced their arguments in favour of a process of recombination in both the E and F regions. MARTYN and PULLEY (1936) then suggested that these two processes all occurred together and MASSEY (1937) and BATES et al (1939) have shown that this is probably a satisfactory picture of what occurs. In fact, it was able to account for the observed behaviour according to a recombination law when in fact important attachment and detachment processes were occurring together.

The resulting equation derived by BATES et al (1939) is

$$\frac{dN}{dt} = q - (\alpha_e + \lambda \alpha_i + \frac{1}{N^+} \frac{d\lambda}{dt}) N^2 \qquad (62)$$

where α_e = radiative recombination coefficient of electrons and ions.

$(O^+ + e \rightarrow O + h\nu)$

α_i = coefficient of mutual neutralisation of negative and positive ions - the ionic recombination coefficient. $(O^+ + O^- \rightarrow O^1 + O^1)$.

λ = ratio of negative ions to electrons

N^+ = positive ion density.

Theoretical values of these coefficients are $\alpha_e = 5 \times 10^{-12} cm^3 sec^{-1}$ and $\alpha_i = 2 \times 10^{-11} cm^3 sec^{-1}$. $\frac{d\lambda}{dt}$ was thought to be small and λ large, so that equation (62) reduces to

$$\frac{dN}{dt} = q - \lambda \alpha_i N^2 \qquad (63)$$

Thus if λ were of the order of 500 then the "effective" recombination coefficient would be of the order of 10^{-8} as observed. Certainly the value of the radiative recombination coefficient is too small.

MCLEISH (1948) was the first to notice that during the eclipse of July 9, 1945, the effective recombination coefficient appeared to vary during the eclipse from a high value of 4.2×10^{-8} soon after the beginning of the eclipse, to a low value of 0.8×10^{-8} at the maximum phase. He was able to account for this on the negative-ion theory by supposing that λ fell from 2,100 at the beginning of the eclipse to 400 at the maximum phase.

A detailed investigation of oxygen negative-ions by BATES and MASSEY (1943), led to the conclusion that α_i in fact had a much higher value of between 10^{-8} and 10^{-7},

the upper limit being 10^{-6}. Following this discovery, MASSEY and BATES (1943) were then able to show that λ was in fact small compared with unity. The resulting product $\lambda\alpha_i$ however, was still of the order of 10^{-8} and sufficient to account for the observed effective recombination coefficient. GHOSH (1944) has also considered the nature of the recombination coefficient and deduced the following expressions:

$$\frac{dN}{dt} = q - \alpha_e N N^+ - \beta N N_o + k N^- N_o + k_1 \beta N^- \qquad (64)$$

and

$$\frac{dN^-}{dt} = -\alpha_i N^- N^+ + \beta N N_o - k N^- N_o - k_1 \beta N^- \qquad (65)$$

where β = coefficient of attachment of electrons to neutral atoms and molecules ($O + e \longrightarrow O^- + h\nu$)

N_o = density of neutral particles.

N^- = density of negative ions

k = coefficient of detachment of electrons from negative ions by collision ($O^- + O \rightarrow O_2 + e$)

$k_1 \beta N^-$ is the rate of loss of negative ions by photo-detachment of electrons ($O^- + h\nu \rightarrow O + e$) according to TUDAKA (1937). If equations (64) and (65) are combined assuming that the ionosphere is electrically neutral and hence

$$N^+ = N + N^- \qquad (66)$$

then equation (64) becomes

$$\frac{dN}{dt} = \frac{q}{1+\lambda} - (\alpha_e + \lambda\alpha_i) N^2 - \frac{N}{1+\lambda} \frac{d\lambda}{dt} \qquad (67)$$

where $\lambda = \frac{N^-}{N}$ as before.

Since now $\lambda \ll 1$, λ can be found from equation (65) assuming that $\frac{dN^-}{dt} = 0$ and that $N^+ \approx N_+$, thus

$$\lambda = \frac{N^-}{N} = \frac{\beta N_o}{\alpha_i N + k N_o + k_1 \beta} \qquad (68)$$

assuming that $\frac{d}{dt}\lambda$ is small, then equation (67) becomes

$\frac{dN}{dt} = q - (\alpha_e + \lambda\alpha_i)N^2$, which is identical to equation (63). If each of the terms in the denominator in equation (68) is considered in turn greater than the remaining two, then the three resulting equations are

$$\frac{dN}{dt} = q - (\alpha_e + \alpha_i \frac{\beta}{k})N^2 \qquad (69)$$

$$\frac{dN}{dt} = q - (\alpha_e + \alpha_i \frac{N_o}{k_1})N^2 \qquad (70)$$

$$\frac{dN}{dt} = q - (\alpha_e + \alpha_i \frac{\beta N_o}{\alpha_i N})N^2 \qquad (71)$$

Now equations (69) and (70) reduce to the form

$$\frac{dN}{dt} = q - \alpha N^2 \qquad (72)$$

and equation (71) reduces to

$$\frac{dN}{dt} = q - \beta N_o N \qquad (73)$$

since α_e is small compared with $\beta N_o / N$.

A general equation might therefore take the form

$$\frac{dN}{dt} = q - \alpha N^2 - \beta N_o N \qquad (74)$$

This type of equation has been suggested by ESTRABAUD (1953) for example, to explain the fact that on control days $N \propto \cos^n \chi$ where $n \neq \frac{1}{2}$ according to Chapman's theory of layer formations.

It is interesting to see whether equations (72) or (73) more nearly describe the experimental curves during the eclipse. By replacing q by f_q during the eclipse as before, the curves which give the same minimum as the experimental curves are those for $\alpha = 7 \times 10^{-9} cm^3 sec^{-1}$ as before, and $\beta N_o = 2.5 \times 10^{-4} sec^{-1}$, and are shown in Fig. 63. The curves show that the "recombination" law is a better approximation to the observed than the"attachment" law.

However, BATES and MASSEY (1946, 1947) have since put forward potent arguments against the "negative-ion" recombination theory and proposed that the process responsible for the rapid disappearance of electrons might be dissociative recombination, which can be written

$$X Y^+ + e \rightarrow X' + Y' \qquad (75)$$

The process was highly speculative at that time since it was believed that atmospheric oxygen was completely dissociated above 100 km, and it was necessary to suppose that atomic ions were converted into molecular ions by charge transfer with subsequent dissociative recombination

i.e. $$Z^+ + XY \rightarrow Z + XY^+ \qquad (76)$$

Even so it was necessary to suppose that the molecule XY be identified as O_2.

NICOLET and MANGE (1954) however, have shown that,

because of mixing and diffusion, O_2 must be quite abundant even in the F layers. In fact, it is probable that O_2^+ ions must predominate in the E region (e.g. BATES, 1956a), and the rate limiting process is then as in equation (75) with XY^+ identified as O_2^+.

Since then laboratory measurements on dissociative recombination have been carried out and BIONDI and BROWN (1949) have measured the dissociative recombination coefficient of He_2^+ and found it to be about $10^{-8} cm^3 sec^{-1}$. Other measurements of the dissociative recombination coefficients have been made for example by BIONDI (1951) who found a value of about $10^{-6} cm^3 sec^{-1}$ for argon. Recent measurements on nitrogen (SAYERS, 1956) have given a value of $10^{-7} cm^3 sec^{-1}$ and even higher values have been reported (FAIRE, FUNDINGSLAND and ADEN, 1954). Measurement of the dissociative recombination coefficient of oxygen seems difficult because of the question of identifying the ion involved, but a tentative value of $4 \times 10^{-8} cm^3 sec^{-1}$ has been suggested (SAYERS, 1956).

The consequences of a high rate of dissociative recombination in the E layer has been considered by GERJUOY and BIONDI (1953), and the relation which emerges from their discussion is :-

$$\frac{dN}{dt} = \frac{q}{1+\lambda} - \left(\alpha_e + \frac{\lambda'}{1+\lambda}\alpha_d + \lambda\alpha_i\right)N^2 - \frac{N}{1+\lambda}\frac{d\lambda}{dt} \qquad (77)$$

where α_d = dissociative recombination coefficient

λ' = ratio of O_2 ions to free electrons.

If the usual assumptions are made that $\lambda \ll 1$, $\frac{d\lambda}{dt} \ll 1$, and α_e and α_i are small compared with α_d, equation (77) reduces to:

$$\frac{dN}{dt} = q - \lambda' \alpha_d N^2 \qquad (78)$$

It seems probable that $\lambda' \simeq 1$ and consequently the variation of the electron density in the E layer should follow a simple recombination law as in equation (23) where will represent the dissociative recombination coefficient of the effective ion in the E layer, which as has already been stated seems likely to be O_2^+.

The result of the discussion shows therefore, that on present theories of the recombination processes occurring in the E layer, it is unnecessary to suppose that the electron loss law is anything other than a recombination law as originally supposed in equation (23). The coefficient might vary during an eclipse due to changes of pressure and temperature, the latter case having already been considered.

HULBURT (1938) and VEGARD (1938) independently suggested that the E layer might be formed by the action of X-rays emitted by the sun. This suggestion has been well established by rocket measurements (BYRAM, CHUBB and FRIEDMAN, 1953, 1954: HAVENS, FRIEDMAN and HULBURT, 1955), and in fact, the intensities measured are sufficient to ionise all the atmospheric constituents (e.g. BATES, 1956b). This might therefore, complicate the recombination process since several

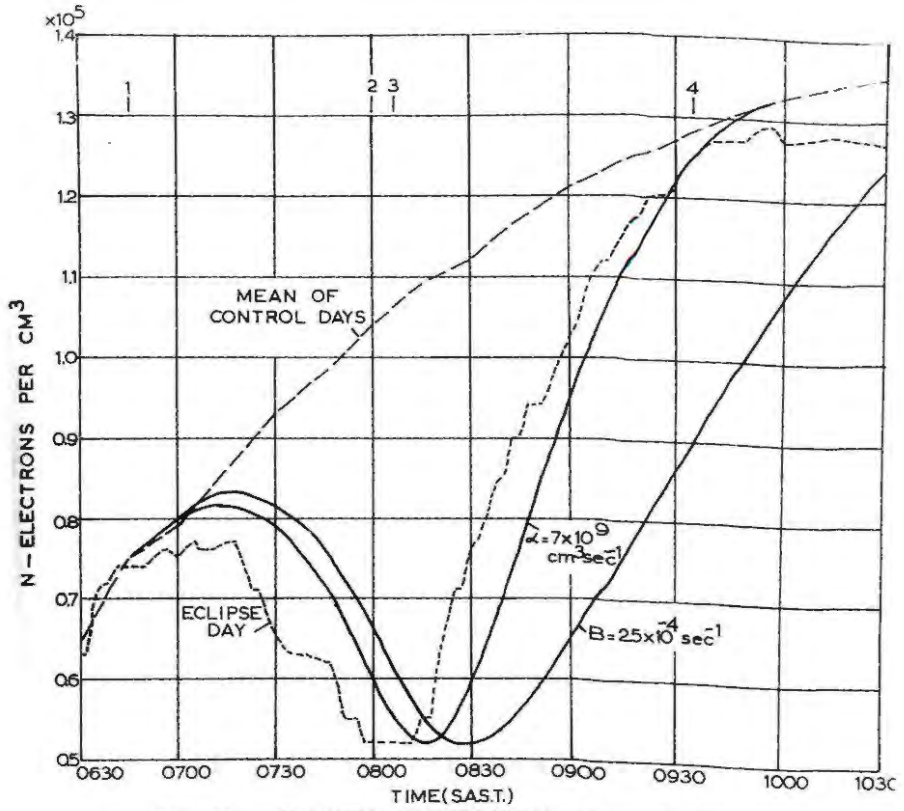

FIG: 63 E, LAYER THEORETICAL CURVES FOR α & B

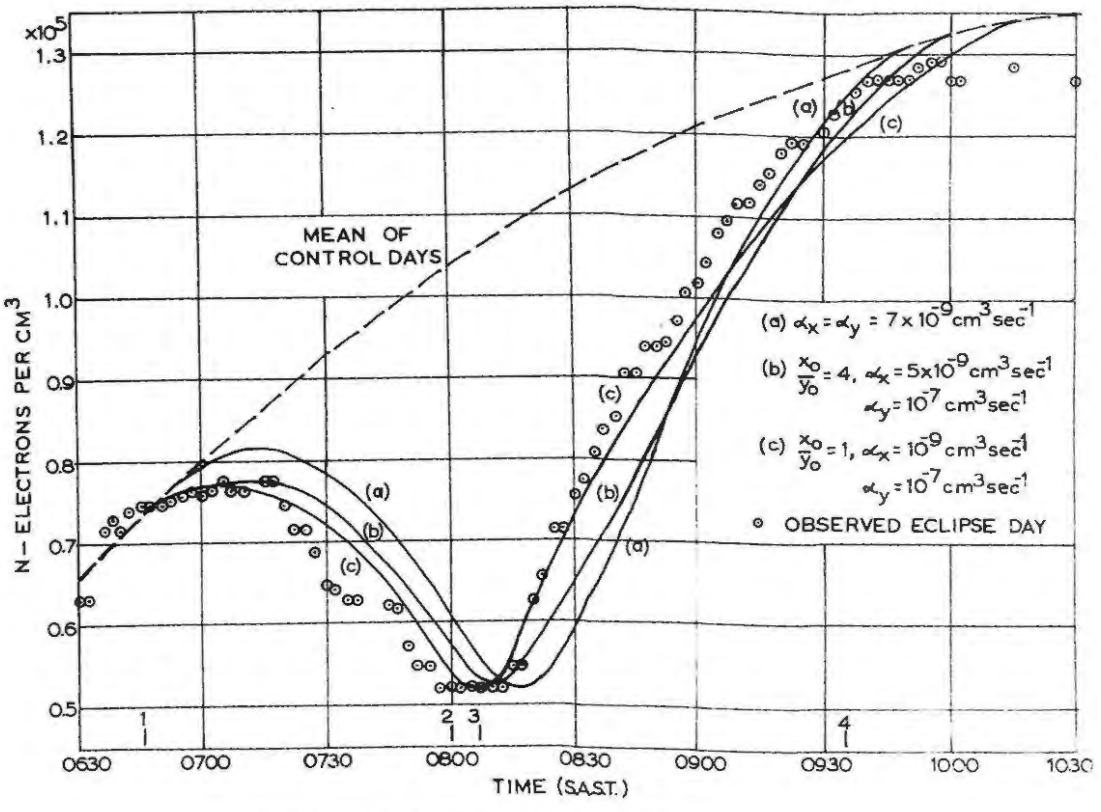

FIG: 64 E LAYER GRAHAMSTOWN,
VARIATION OF RECOMBINATION COEFFICIENT

species of ion will thus be present, each with its own recombination coefficient. BATES (1951) has shown that the diurnal variation of the electron density may be completely controlled by the more slowly recombining species of ion, and give no indication of a more rapidly recombining species.

Variation of the recombination coefficient.

The suggestion of BATES (1951) that the diurnal variation of electron density may only give an indication of the presence of the slower recombining species of ion, means that during an eclipse the faster recombining species might be indicated. This is exactly what happens during an eclipse. Many observers have noted that the ionospheric eclipse starts too quickly (e.g. HARANG, 1945: PIERCE, 1948: MINNIS, 1955, 1956b). If two species of ion were present, this is exactly what is to be expected; the more rapidly recombining species of ion will disappear first leaving the slower species. The value of N_m therefore, will be determined primarily by the slower species of ion and the time-lag δt by the more rapid species. This suggestion is clearly a plausible explanation of the $N_m - \delta t$ anomaly, and would account for the fact that during many eclipses the recombination coefficient apparently starts at a high value and to a low value during the maximum phase, (e.g. McLEISH, 1948). BATES and McDOWELL (1957) have considered this case theoretically for a hypothetical total eclipse. Following Bates and McDowell therefore, the sun will be considered a uniformly radiating disc, and it will

be supposed that there are two species of ion whose concentrations are x and y per cm^3 at any time. Let q_x and q_y be their rates of production per cm^3 and α_x and α_y their respective recombination coefficients. Indicating x_o and y_o for the control variation of x and y,

$$\frac{dx_o}{dt} = q_x - \alpha_x x_o N \qquad (79)$$

$$\frac{dy_o}{dt} = q_y - \alpha_y y_o N \qquad (80)$$

where $N = (x_o + y_o)$

Thus $$\frac{dN}{dt} = \frac{dx_o}{dt} + \frac{dy_o}{dt} = q_x + q_y - N(\alpha_x x_o + \alpha_y y_o) \qquad (81)$$

During the eclipse the equations for the variation of x and y will be

$$\frac{dx}{dt} = fq_x - \alpha_x x N \qquad (82)$$

$$\frac{dy}{dt} = fq_y - \alpha_y y N \qquad (83)$$

Bates and McDowell have advanced a rather complex mathematical method of solving these equations numerically according to HARTREE (1952). However, numerical solution for α_x and α_y may be carried out in the same way as that described previously for a single species recombination.

It is first necessary to establish q_x and q_y for insertion in equations (82) and (83). This is done by choosing the ratio $\frac{x_o}{y_o}$ in advance. For particular values of

α_x and α_y, q_x and q_y can be calculated from equations (79) and (80) assuming that $\frac{dx_o}{dt} = \frac{dy_o}{dt}$. Since $\frac{dN}{dt}$ is small, this does not materially affect the analysis. Using these values of q_x and q_y, the gradients $\frac{dx}{dt}$ and $\frac{dy}{dt}$ in equations (82) and (83) may be followed from stage to stage during the eclipse simultaneously. It is necessary to perform two computations at once, one for x and one for y, and at each stage the resulting value of N is of course (x+y). There are three variables which have to be fixed in advance, $\frac{x_o}{y_o}$, and α_x and α_y. Two values of $\frac{x_o}{y_o}$ were tried, $\frac{x_o}{y_o} = 4$ and $\frac{x_o}{y_o} = 1$. These two values are sufficient to indicate the possible effect of different concentrations of the two ions. It was then decided to fix the value of the more rapid ion, and a value of $\alpha_y = 10^{-7} cm^3 sec^{-1}$ was decided upon. The value was chosen as being the highest anyone has dared to suggest (e.g. PIDDINGTON, 1951), but in fact, the distinction between higher values and infinity is so small, that it was felt a value of 10^{-7} reasonably indicates an extreme case of the more rapid ion. For each of the chosen values of $\frac{x_o}{y_o}$, the value of α_x was determined by trial and error until a theoretical curve gave the same minimum as that observed. This gave three cases which are shown in Fig. 64. Case (a) $\alpha_x = \alpha_y = 7 \times 10^{-9} cm^3 sec^{-1}$ and the layer is a single species layer.

(b) $\frac{x_o}{y_o} = 4, \quad \alpha_x = 5 \times 10^{-9} cm^3 sec^{-1}$

$\alpha_y = 10^{-7} cm^3 sec^{-1}$

(c) $\frac{x_o}{y_o} = 1, \quad \alpha_x = 10^{-9} cm^3 sec^{-1}$

$\alpha_y = 10^{-7} cm^3 sec^{-1}$

As can be seen the cases (b) and (c) approach that observed more closely, but do not account for the rapid drop in N at 0717 SAST., which as has previously been mentioned is associated with the covering of the solitary sunspot in the north-west part of the disc. It was found that the best fit to that observed in cases (b) and (c) was found by supposing that 80% of the radiation came from the disc and 20% from the spot. The resulting curves are shown in Fig. 65. In case (b) the $N_m - \delta t$ anomaly is not sufficiently accounted for, and in case (c) where as the observed points are accounted for before and during annularity, the final recovery during the last stages of the eclipse is completely controlled by the more slowly recombining species $\alpha_x = 10^{-9} cm^3 sec^{-1}$, and does not account for that observed.

It is interesting to note that the "effective recombination coefficient", that is that which describes the diurnal variation of N as in equation (23) can be evaluated from equation (81), since

$$\alpha = \frac{\alpha_x x_o + \alpha_y y_o}{x_o + y_o} \qquad (84)$$

The values of α are -

Case (a) $\alpha = 2.4 \times 10^{-8} cm^3 sec^{-1}$

(b) $\alpha = 5.05 \times 10^{-8} cm^3 sec^{-1}$

Some evidence for the lower recombination coefficients may be provided from the fact that it is well-known that the E layer persists at night. The only apparent reference in the literature to measurements of α from E layer critical frequencies at night is that of BEST, FARMER and RATCLIFFE (1938) who obtained a value of $4 \times 10^{-9} cm^3 sec^{-1}$. Values as low as $10^{-9} cm^3 sec^{-1}$ have been reported by BARAL and MITRA (1950) using the assymetry method of APPLETON (1933) on E layer measurements at Calcutta. It is also interesting to note that the calculations of WAYNICK (1955) show that six hours after sunset the value of α at 120 km could be as low as $10^{-9} cm^3 sec^{-1}$. The higher values could be the dissociative recombination coefficient, which appears from preliminary laboratory experiments to have such a high value.

However, as Figs. 64 and 65 show the $N_m - \delta t$ anomaly cannot be completely accounted for by the presence of two species of ion with differing recombination coefficients, however the neglect of this factor, as will be seen later, may lead to the over-estimate of other factors, such as the distribution of solar radiation.

It is also possible that the recombination coefficient might vary through the layer, being a function of height. This will cause a distortion of the layer during the eclipse.

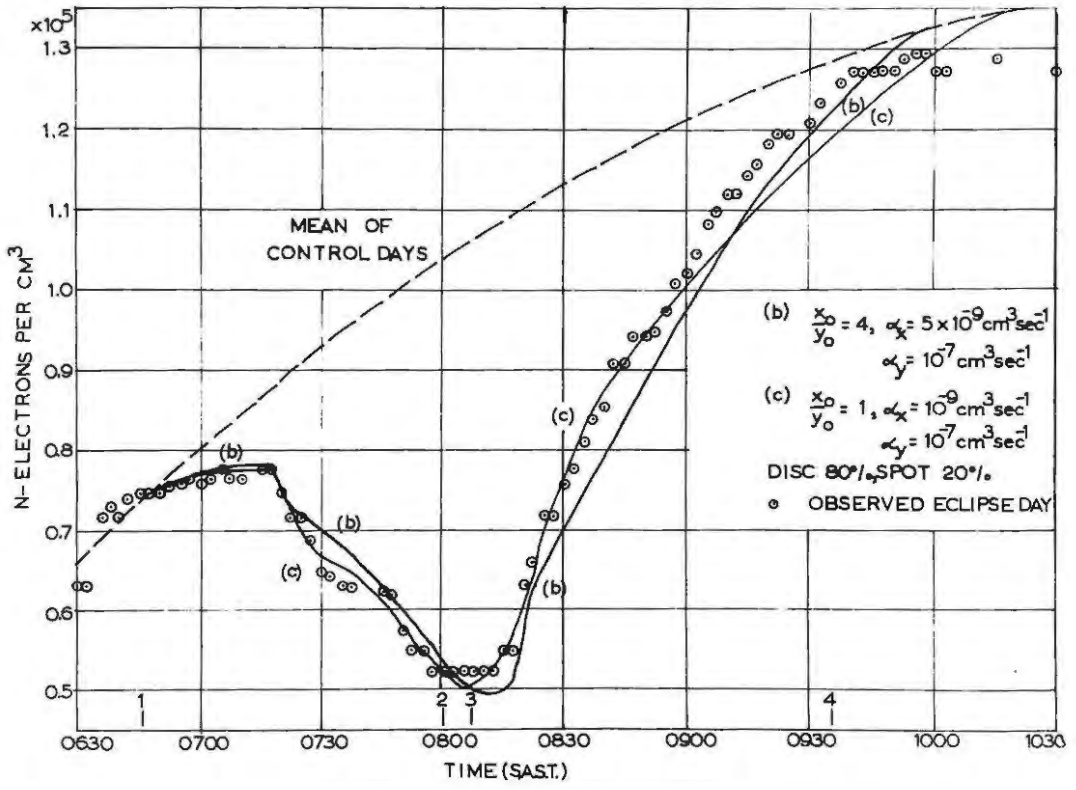

FIG: 65 E LAYER, GRAHAMSTOWN
VARIATION OF RECOMBINATION COEFFICIENT

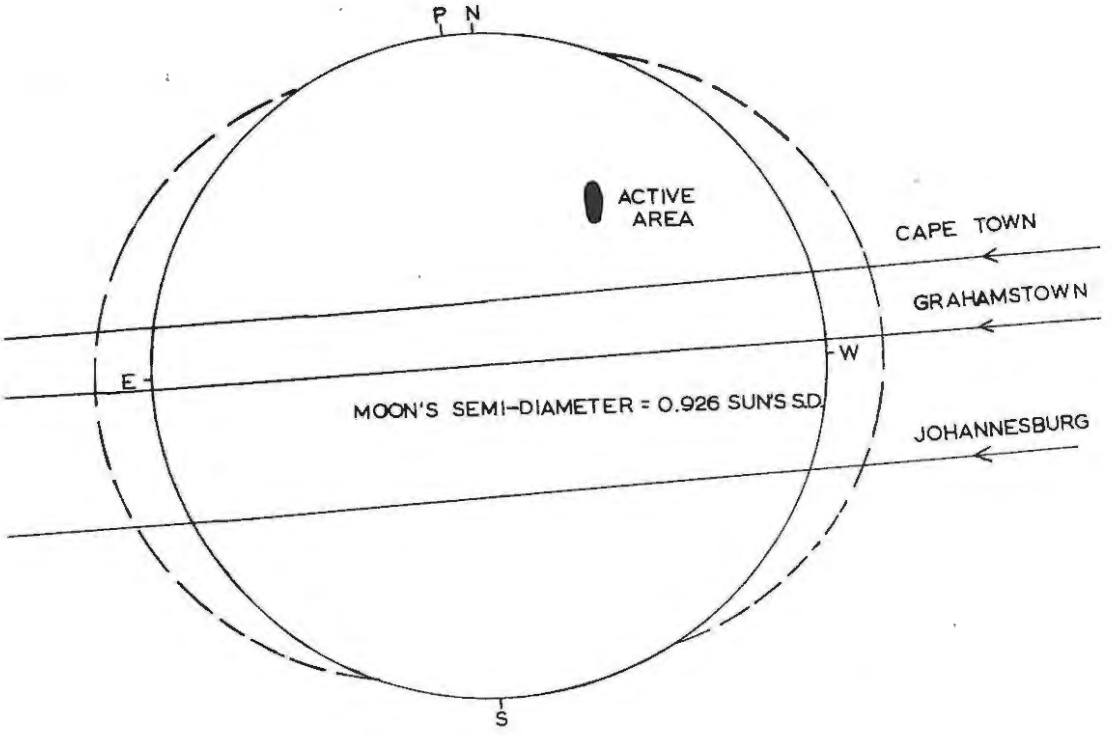

FIG: 66 SOLAR MODEL 15% OUTSIDE DISC
PATH OF MOON ACROSS SUN AT 100 KM

This case has been considered by LIED (1956) and he has shown that even in a rather exaggerated case of α varying with height, the error introduced is still negligible in the E layer.

Radiation from outside the visible disc.

It has been mentioned already that the preponderance of eclipse measurements in the E layer in which the minimum electron density occurs during the maximum phase but fails to reach its theoretical lowest value by 10 to 15%, makes it difficult to believe that the explanation is due to the distribution of active areas on the visible disc. As has been pointed out by RATCLIFFE (1956), one would expect such distribution to depend on chance. It would seem a remarkable coincidence if this was so. An attempt to explain this $N_m - \delta t$ anomaly by supposing that two species of ion exist has been partly, but not wholly successful. It seems likely as originally suggested by PIDDINGTON (1951) that some radiation must come from the corona outside the visible disc. In fact it seems almost certain that some of the ionising radiation comes at least from the lower corona (ALLEN, 1956). MINNIS (1956c) following the discussion at the London symposium on "Solar Eclipses and the Ionosphere", has been forced to admit the possibility of some radiation coming from outside the visible disc, and has calculated the resulting values of α according to how much residual radiation is present at totality. He gives the value of α as 9.2×10^{-8} if 10% were present at totality, and infinity for 12%. This conclusion is based on

a rather doubtful extrapolation of N and $\frac{dN}{dt}$ at second contact. BONNET, HUNAERTS and NICOLET (1957) have recently examined the measurements at six stations in Africa during the eclipse of 25 February, 1952, including those of MINNIS (1955) from Khartoum and Ibadan. It is interesting to note that in a model in which 15% of the radiation came from outside the visible disc, BONNET et al (1957) were able to obtain very good agreement with the measurements at Khartoum and Ibadan with $\alpha = 4 \times 10^{-8} cm^3 sec^{-1}$. It must be admitted, however, that the agreement with other stations is not so good. Nevertheless, it serves to indicate that the contention of MINNIS (1956a,c) that α would be infinite under these circumstances is erroneous.

It has been noted that on all the eclipses so far examined by Minnis, he has had to postulate the existence of a solar source on the west limb of the sun as well as on the east limb. In all cases he has been able to establish that a correlation with the limb intensities of 5303Å showed that the west limb was more active than the east. In fact, it would be easy to visualise the phenomenum of limb-brightening as calculated by WALDMEIER (1956). It would seem possible that this correlation was pure coincidence for it is easy to see from Table 16, that the west limb source exceeds the east limb source for $\alpha \geqslant 2.0 \times 10^{-8} cm^3 sec^{-1}$. In this eclipse there is little evidence for any limb-brightening in 5303Å, and whatever there might be would indicate the east limb to

be more active than the west. From table 16, one can conclude that $\alpha \gtrsim 2.0 \times 10^{-8} cm^3 sec^{-1}$, whereas the comparison of these models with Cape Town and Johannesburg gave α about $1.5 \times 10^{-8} cm^3 sec^{-1}$, although admittedly the agreement is not perfect.

The more likely explanation that some radiation comes from outside the disc seems plausible. In fact, there seems no reason to suppose the sun in solar ionising radiation to be the same as that in visible radiation, when for example, the sun in 21 cm wavelength (e.g. CHRISTIANSEN and WARBURTON, 1955) is elliptical in form and extending beyond the visible disc at the equator.

A solar model has therefore, been proposed in which 15% of the total radiation comes from outside the visible disc. The disc has been extended at the solar equator as shown in Fig. 66, by about 0.1 solar diameter in such a way that the intensity per unit area coming from outside the visible disc is the same as the disc itself. Suitable allowance must be made for the single active area in the north-west quadrant.

Fig. 67 shows the resulting curves for the variation of f', the unobscured fraction of the solar radiation on this model, as compared with that for a uniform disc. The circumstances of the eclipse for the three stations on this model is shown in Table 19, where f'min represents this time the unobscured fraction of the solar radiation at the maximum phase.

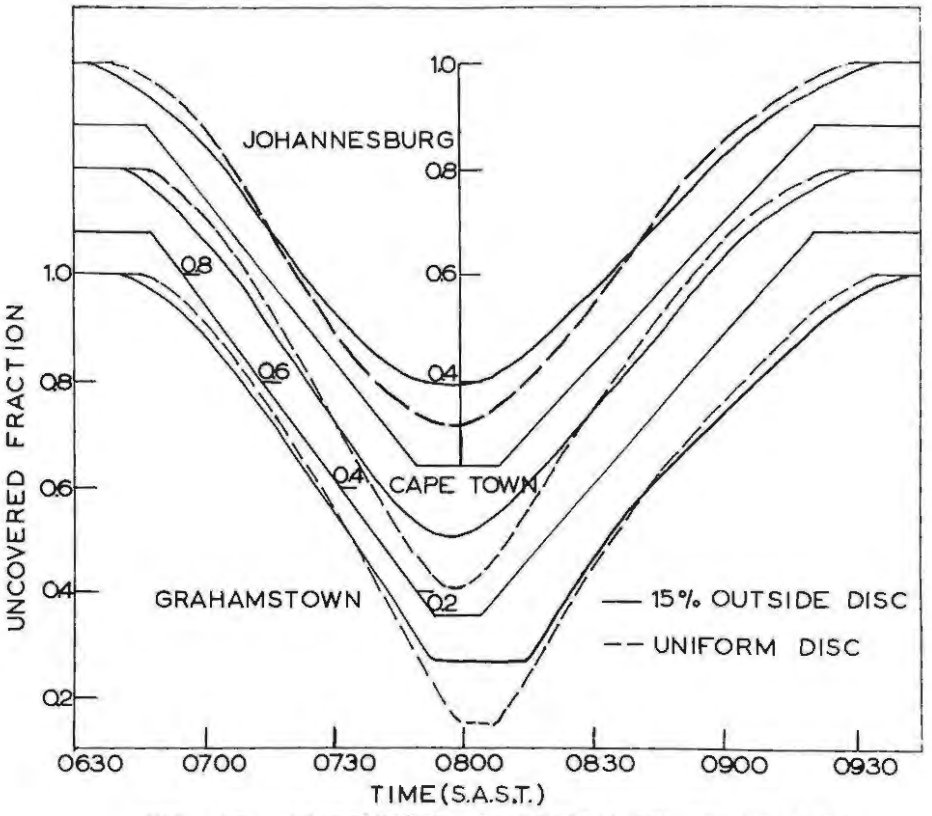

FIG: 67 UNCOVERED FRACTION OF SOLAR AREA

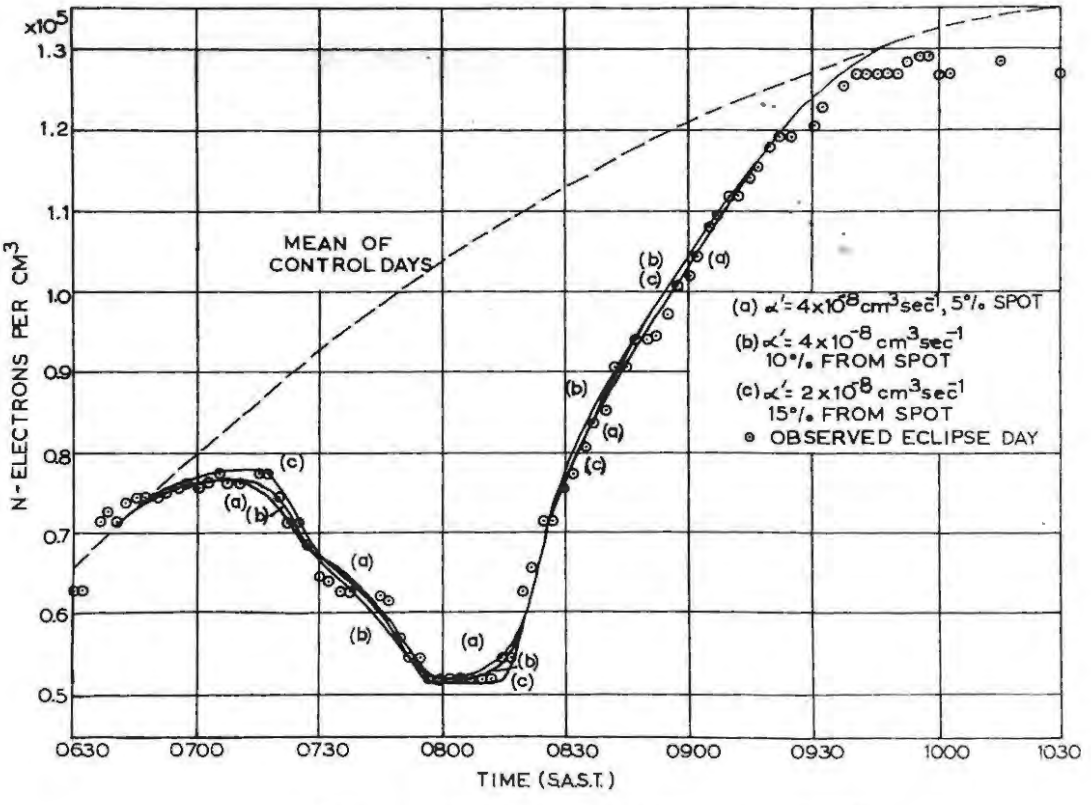

FIG: 68 GRAHAMSTOWN: THEORETICAL CURVES
15% OUTSIDE DISC

Station	Begins	Middle	Ends	f-min
Grahamstown	0639	0752 to 0815 (Annular Phase)	0946	0.270
Johannesburg	0641	0758	0930	0.396
Cape Town	0634	0758	0936	0.308

Table 19: Circumstances of eclipse of Solar Model (Fig. 66) at 100 km height

This model was applied to the three stations as shown in Figs. 68, 69 and 70. Allowing some contribution to the radiation from the active area in the north-west, the resulting curves are as follows:

(a) Grahamstown (Fig. 68)

$\alpha = 2.0 \times 10^{-8} cm^3 sec^{-1}$, Spot = 15%

$\alpha = 4.0 \times 10^{-8} cm^3 sec^{-1}$, Spot = 5 to 10%

$\alpha > 4.0 \times 10^{-8} cm^3 sec^{-1}$, less acceptable

(b) Johannesburg. (Fig. 69)

$\alpha = 4 \times 10^{-8} cm^3 sec^{-1}$, Spot = 5 to 10%

$\alpha > 4 \times 10^{-8} cm^3 sec^{-1}$, little difference

$\alpha < 4 \times 10^{-8} cm^3 sec^{-1}$, less acceptable

(c) Cape Town (Fig. 70)

$\alpha = 4.0 \times 10^{-8} cm^3 sec^{-1}$, Spot 5 to 10%

$\alpha > 4.0 \times 10^{-8} cm^3 sec^{-1}$, less acceptable

From the figures for the three stations it seems that the most acceptable model to give the best agreement to all three stations is a model with 5 to 10% attributed to the spot and $\alpha = 4 \times 10^{-8} cm^3 sec^{-1}$. The result is thus similar to that

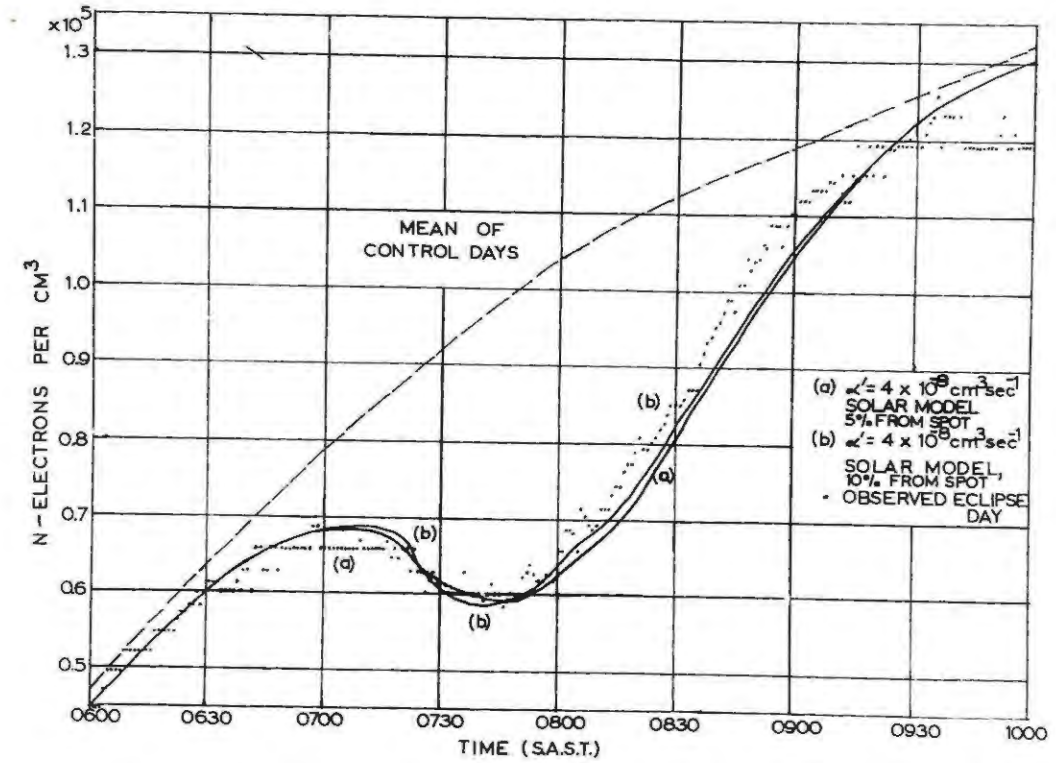

FIG: 69 JOHANNESBURG, THEORETICAL CURVES
SOLAR MODEL 15% OUTSIDE DISC

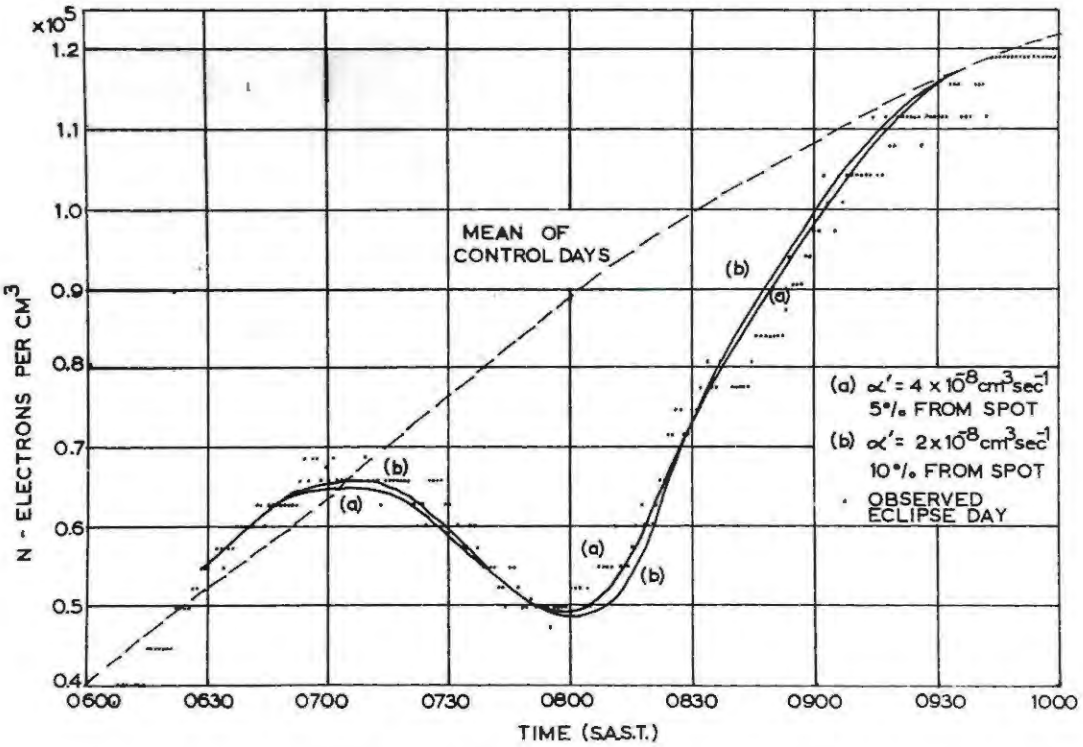

FIG: 70 CAPE TOWN, THEORETICAL CURVES
SOLAR MODEL 15% OUTSIDE DISC

obtained by BOWNET, HUVAERTS and NICOLET (1957) who also deduced $\alpha = 4 \times 10^{-8} cm^3 sec^{-1}$ and PIDDINGTON (1951) who concluded that α could be as high as $10^{-7} cm^3 sec^{-1}$.

Discussion of E layer results.

Attempts to explain the behaviour of the E layer during this eclipse on the usual hypothesis that the sun is a uniformly radiating solar disc have once again illustrated the so called $N_m - \delta t$ anomaly, which seems to occur in almost all analyses of E layer eclipse measurements on this simple theory. Various departures from this simple theory have been attempted to explain this anomaly. In the first place it is found that the anomaly can be explained in terms of a drop in temperature during the eclipse to about $\frac{3}{4}$ of its normal diurnal value. However, it is found that there must be little variation during the daylight hours on a normal day, and the result would thus seem surprising. In fact, most theoretical considerations of thermal balance in the upper atmosphere indicate that such a change is unlikely since the thermal relaxation time is of the order of a few days.

In the second case, it is assumed that the sun is not a uniformly radiating disc but that there are regions from which more radiation is emitted. By comparison with measurements from Cape Town and Johannesburg, it is found that reasonable, but by no means perfect agreement can be obtained with a model in which 70% of the radiation is attributed to the disc and $\alpha = 1.5 \times 10^{-8} cm^3 sec^{-1}$. Little visual evidence

can be found for the existence of two sources which have to be postulated on the limb. Extension of this case to include some radiation from outside the visible disc shows that quite good agreement can be obtained if 15% of the radiation comes from outside the disc and $\alpha = 4 \times 10^{-8} cm^3 sec.^{-1}$ In this case only 5 to 10% need be attributed to a solitary sunspot. It is interesting to compare the two cases. MINNIS (1956b) has pointed out that the absolute intensity of the uniform disc component is about the same for both the February 1952 and June 1954 eclipses. This conforms to the possibility suggested by ALLEN (1948, 1956) that there might be a component of radiation emitted uniformly from the disc which corresponds to the minimum possible level of solar activity, when the sunspot number would be zero.

It is interesting therefore, to compare the two hypothese that all the radiation comes from the visible disc and that 15% comes from outside the disc on this basis, assuming that the 15% outside the disc may be included in the minimum level.

Using the notation of Minnis, the diurnal variation of N may be expressed as

$$\frac{dN}{dt} = q_o \cos^n \chi - \alpha N^2 \qquad (84)$$

Rearranging the terms

$$J = \frac{q_o}{\alpha} = (N^2 + \frac{1}{\alpha}\frac{dN}{dt}) \sec^n \chi \qquad (85)$$

where q_o = rate of generation of electrons per cm^3 for an

overhead sun.

It has already been mentioned that the exponent $n = 1$ for a Chapman layer, but usually $n \neq 1$, and the appropriate value is used as deduced from control days. Using the noon values of N from the control days at the three stations when $\frac{dN}{dt} = 0$, values of J were deduced from equation (85) and are shown in Table 20 together with values of $\bar{n}$ for each station.

Station	n	J (10^8 cm^{-6})
Grahamstown	1.18	211
Cape Town	1.12	220
Johannesburg	1.20	229

Table 20: Values of n and J

Taking the mean value of J as 220 x 10^8cm^{-6}, $q_o = 220 \times 10^8$ cm^{-3}sec^{-1}. During the 1952 eclipse at Khartoum, $q_o = 258 \times 10^8$ cm^{-3}sec^{-1}. Using the result of BONNET, HUNAERTS and NICOLET (1957) for the 1952 eclipse, that when 15% of the radiation comes from outside the disc only 11% need be attributed to two spots, Table 21 shows the uniform component of q_o as deduced from the two models.

Eclipse	q_o	A ($cm^{-3}sec^{-1}$)	B ($cm^{-3}sec^{-1}$)
Feb. 1952	258α	198 ($\alpha = 1.2 \times 10^{-8}$) (64% uniform)	916 ($\alpha = 4 \times 10^{-8}$) (89% uniform)
Dec. 1954	220α	231 ($\alpha = 1.5 \times 10^{-8}$) (70% uniform)	836 ($\alpha = 4 \times 10^{-8}$) (95% uniform)

Table 21: Absolute intensity of uniform component of solar radiation

A = all radiation from visible disc

B = 15% radiation from outside visible disc.

The agreement for the values of (B) is better than that for (A), but the result is not conclusive, since the values of α and J for the 1954 eclipse are not as accurate as those of Minnis for the 1952 eclipse. It is interesting to note that MINNIS (1955, 1956a) has tried to justify the existence of a west limb source of intensity 25% of the total by following the changes in J several days after the eclipse. When the west limb source should have disappeared behind the disc due to the sun's rotation, he noticed a drop in J corresponding to 13% of its value on the eclipse day. If one can interpret changes in J in this way as Minnis did, the agreement with the value of 11% deduced by Bonnet, Hunaerts and Nicolet for the same limb on the (B) model is much better than that of Minnis of the (A) model.

According to ALLEN (1948), the intensity I_R of the E layer ionising radiation for a twelve-month mean sunspot

number $\bar{R}$ is given by

$$I_R = I_o \ (1 + 0.0097 \ \bar{R}) \qquad (86)$$

Now for December 1954, $\bar{R} = 10$ (J. Geophys. Res., 60, 108, 1955), and hence $I_R = 1.097 I_o$, where I_o will represent the intensity for zero sunspot and correspond to the permanent uniform component of solar ionising radiation. It is difficult to reconcile the fact that solar activity in E layer ionising radiation was only about 10% above its "zero" level with the solar model in which only 70% of the radiation is emitted uniformly from the visible disc. However, it agrees very well with the (B) model with only 5 to 10% attributed to a solitary active area. If this hypothesis of a minimum possible level of solar activity is to be accepted then the argument above points in favour of the hypothesis that about 15% of the radiation is emitted from outside the visible disc as a permanent feature of solar activity.

The effect of two species of ion with differing recombination coefficients has also been considered leading to a variation in the effective recombination coefficient during the eclipse. This analysis shows that the $N_m - \delta t$ anomaly cannot be completely accounted for on this basis, but clearly to neglect this factor must lead to an over-estimate of other factors, such as for example, the amount of radiation coming from outside the disc. However, if less than 15% of the radiation comes from outside the disc

and one were to take into account two species of ion the conclusion will be the same and α will probably have a value as high as $4 \times 10^{-8} cm^3 sec^{-1}$ or even higher.

Conclusion

The E layer measurements from Grahamstown have been compared with the measurements made at Cape Town and Johannesburg during the eclipse. Using equation (24)

$$\frac{dN}{dt} = fq - \alpha N^2 \quad \text{for the eclipse,}$$

the variation of each of the parameters, f, q and α have been considered in turn in order to explain the $N_m - \delta t$ anomaly which arises as the result of the application of simple theory.

It is not possible to consider the effect of varying all the parameters at once without some idea of their values. However, the results indicate that α_e, the effective recombination coefficient in the E layer, must be as high as $4 \times 10^{-8} cm^3 sec^{-1}$. Higher values than this are even possible. It was shown that the recombination coefficient should approximate closely to the value of the dissociative recombination coefficient of the active ion in the E layer. The high value obtained agrees with preliminary laboratory measurements of the dissociative recombination coefficient of some ions, which indicate values as high as $10^{-7} cm^3 sec^{-1}$.

Finally, it is noted that the work of MUNRO and HEISLER (1956) shows that cusplike anomalies which often appear in h'f records are due to travelling disturbances

of a wave-like nature producing tilts in the ionospheric layers and causing echoes to be returned from directions other than the vertical. Since an eclipse is essentially a travelling disturbance, MUNRO and HEISLER (1958) have shown that as a result of the curvature so produced, critical frequencies may not apply to points overhead. One of the features of the records from Cape Town was the number of "critical frequencies" which were observed. On occasions up to six critical frequencies could be seen on the h'f record, three of which were from the E region. It seems likely that these were oblique reflections. The presence of the E_2 layer, especially in the early morning, at Grahamstown might possibly owe its origin to oblique echoes.

GLEDHILL (1958) has made a preliminary analysis of the measurements at Grahamstown and has shown that it is unlikely that reflections during the middle of the eclipse are returned from points overhead. Since they would be returned from points where the electron density is necessarily higher, it seems likely that the apparent critical frequency will be higher than the true one. This would give the appearance of some radiation coming from outside the visible disc. Consequently, the electron density indicated during the maximum phase is higher than the true one, but again this would support the contention that a value of α of $4 \times 10^{-8} cm^3 sec^{-1}$ or higher is quite possible

(c) F REGION

Introduction

In Part II (a), the variation of the maximum electron densities in both the F_1 and F_2 layers during the eclipse were considered on the assumption that the sun is a uniformly radiating disc. It was shown that there was a possibility that the height of the maximum in the F_1 layer may have varied. The result would be a change of shape of the layer and consequently the values of q would not refer to the same height as on control days. In the F_2 layer, whilst the variation of the height of the maximum during the eclipse was not significant, the layer is a fairly thick layer, and consequently it might be possible to deduce the value of α at various heights throughout the whole F region. Such an analysis would amongst others eliminate any errors which might occur due to the value of q refering to different heights during the eclipse. Using the "constant height" map of Fig. 39 in Part I, the variations at various fixed heights in the F_1 and F_2 layers were compared with the variations at fixed heights during the eclipse.

(1) F_1 layer.

Fixed heights of 160, 180 and 200 km were chosen and Fig. 71 shows the variation in electron density for the control days together with the readings on the eclipse day for each of these three heights. As the eclipse occurred very near the summer solstice, the F_1 layer critical frequency

was always defined by a sharp cusp in the h'f records. The F_1 layer began to show itself usually about 0630, and at 0645 it was present on thirteen of the thirty control days, whilst at 0700 it was present on twenty five of the thirty control days. On the eclipse day it began to appear just after 0630 and was already a sharp cusp on the record by the time the eclipse began at 0645.

During the middle of the eclipse from 0730 to 0830 approximately, the F_1 layer was slightly masked by Esp, making the determination of the Kelso distributions in the layer impossible. However, as has previously been mentioned, from the retardation produced on the F_2 layer, it was possible to extrapolate the h'f curve back and estimate that the maximum electron density in the layer reached a minimum of 0.94×10^5 electrons per cm^3 at 0807. From the Kelso distributions before 0730 and after 0830, it can be seen that the layer became very thick with the electron density at 160 and 180 km, being very near to the maximum in the layer. This was undoubtedly due to the fact that the height of the layer maximum fell slightly during the eclipse. Hence, in extrapolating the curves for these heights between 0730 and 0830, it is assumed that the electron density at these heights did not fall much below the maximum in the layer during that period.

(ii) F_2 layer.

True heights of 220, 240, 260 and 280 km were chosen

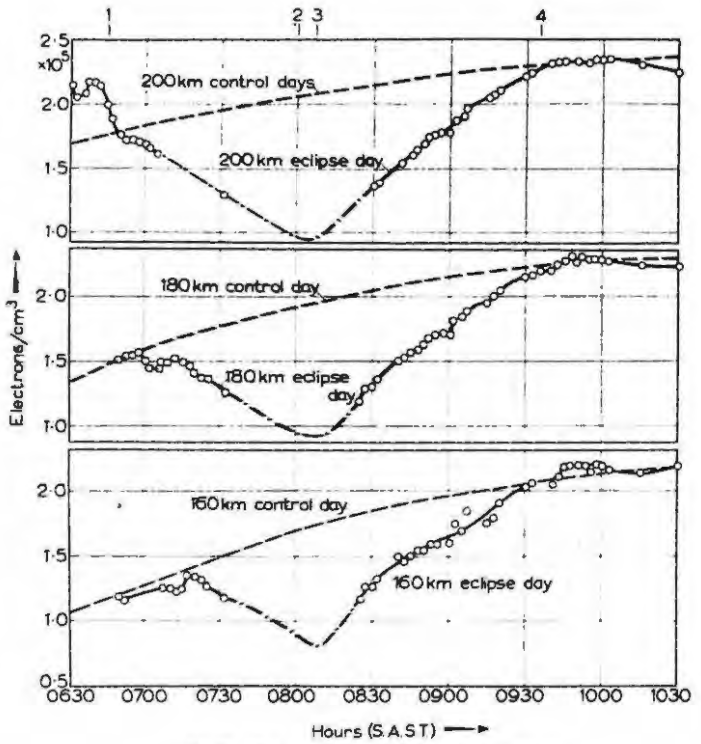

Fig. 71. *F1* layer, eclipse and control readings.

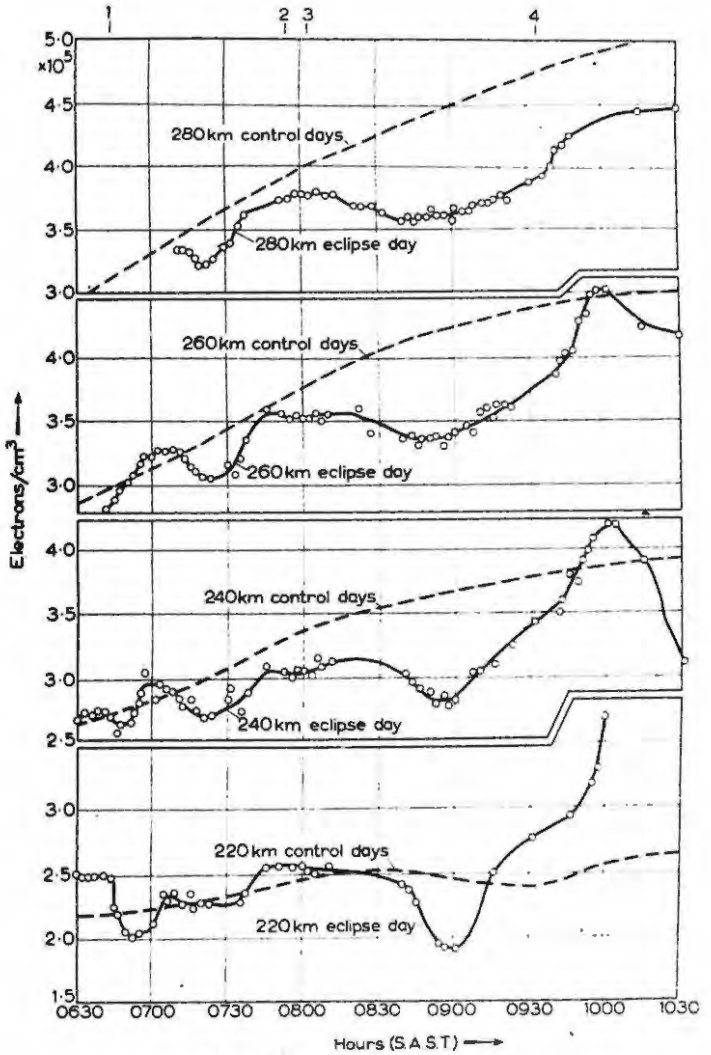

Fig. 72. *F2* layer, eclipse and control readings.

and Fig. 72 shows the mean variation in the electron density for the control days, together with the readings for the eclipse day for each of these four heights.

Electron-loss coefficient at constant height.

Several workers (KIRBY, GILLILAND and JUDSON, 1936; SAVITT, 1950; DOMINIC, 1955) have concluded from eclipse measurements in the F_2 layer that the electron-loss process in this region follows an attachment law, the loss-process being proportional to the electron density. It is interesting therefore, to test the resulting curves for the eclipse day to see if the decay during the eclipse simulates a recombination or attachment-like process.

It is assumed that the sun is a uniformly radiating disc and the two equations which will be used for the eclipse readings are:

$$\frac{dn}{dt} = f q - \alpha n^2 \qquad (87)$$

which follows a recombination law, and

$$\frac{dn}{dt} = f q - Bn^2 \qquad (88)$$

which follows an attachment law.

If attachment is the loss process, then $B = \beta N_o$ as in equation (88), where β is the attachment coefficient and N_o is the density of neutral particles.

Numerical solution of these two equations was carried out in the usual way for each of the selected heights in the F_1 and F_2 layers.

The minimum electron density during the eclipse at each height was used as the criterion for determining α or B. Various values for α and B were tried using equations (87) and (88), and when the theoretical curve gave the same minimum as that observed, it was assumed this determined α or B.

Fig. 73 shows the three experimental curves for 200, 180 and 160 km, together with the three curves plotted using equation (87). Fig. 74 shows similar curves using equation (88). It is at once seen that the curves for the recombination law (Fig. 73) approximate more closely to that observed than do the curves for the attachment law. It is concluded therefore, that a recombination type of law more nearly describes the process of electron removal in the F_1 layer. The values of α and B so found do not vary throughout the layer. Although the process of extrapolation means that the minimum for each height is uncertain, reference to Fig. 49 for the F_1 layer maximum shows that the values of α or B would not vary much with any reasonable variation of the minimum at each height. It can reasonably be concluded that α remains fairly constant throughout the F_1 layer. It is noted that the value of α found for the E_1 layer by this method gave $7 \times 10^{-9} cm^3 sec^{-1}$ whilst the F_1 layer gave $5 \times 10^{-9} cm^3 sec^{-1}$. It seems possible that there is little variation in α between the E and F_1 layers.

Similar calculations were made for each of the four

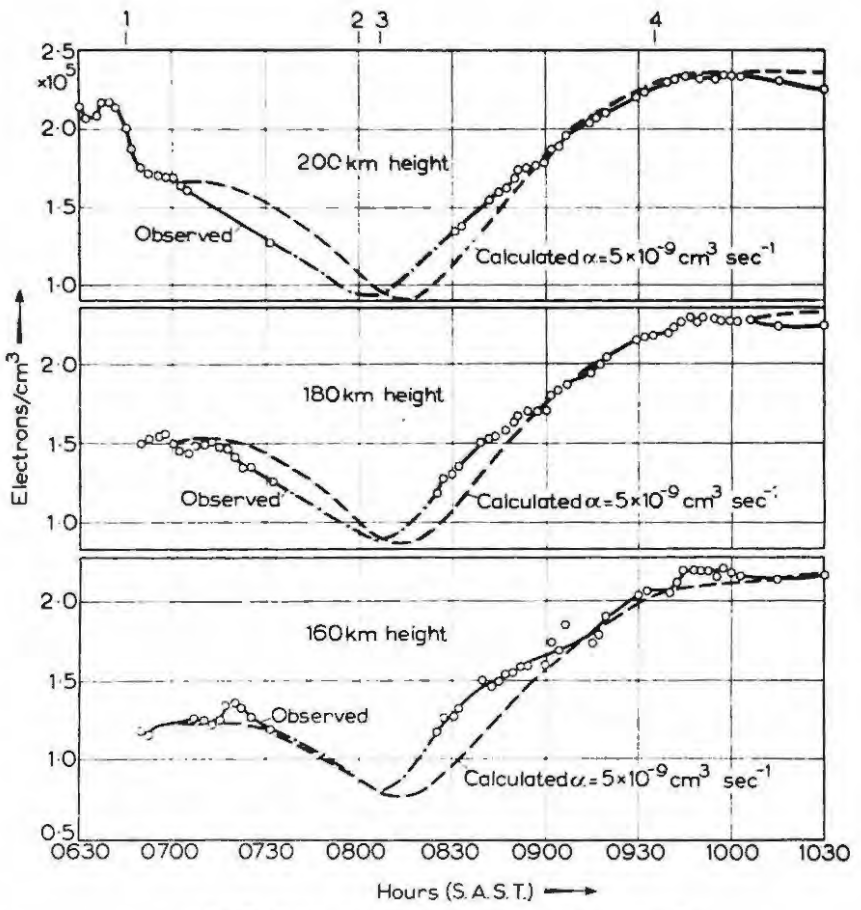

Fig. 73. *F1* layer, theoretical curves for values of α.

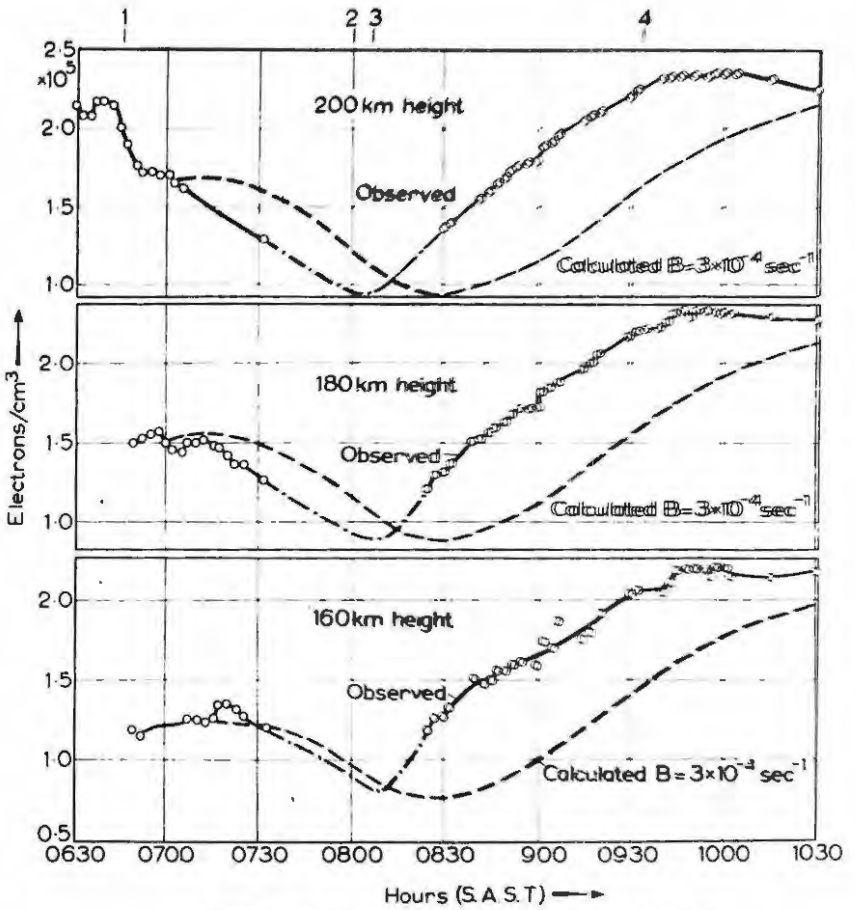

Fig. 74. *F1* layer, theoretical curves for values of B.

selected heights in the F_2 layer. The resulting theoretical curves are shown in Fig. 75 for values of α, and Fig. 76 for values of B. The agreement between the eclipse day results and the expected variation is not very good, but this can hardly be expected in view of the well-known irregularities of this layer. From the two sets of curves, there seems little to choose between the two types of electron-loss laws. It seems that either might be possible. Figs. 77 and 78 show how the values of α and B deduced for the F_2 layer vary systematically with height.

The great majority of workers in this field have limited their calculations and conclusions to the observation of critical frequencies. The diversity of the results obtained show that such analyses can hardly give even a qualitative explanation of the processes which take place in the ionosphere.

SAVITT (1950) undertook an analysis similar to that presented here and concluded that attachment was the more likely process than recombination in the F_2 layer. More recently MINNIS (1955, 1956d) has computed the variation of electron density at constant height in the F_2 layer. Although he was unable to make a detailed investigation of the electron density below the F_1 maximum, he was able to estimate that the value of α of $8.2 \times 10^{-9} cm^3 sec^{-1}$ applied to a height of 170 km.

The distribution of α with height has also been

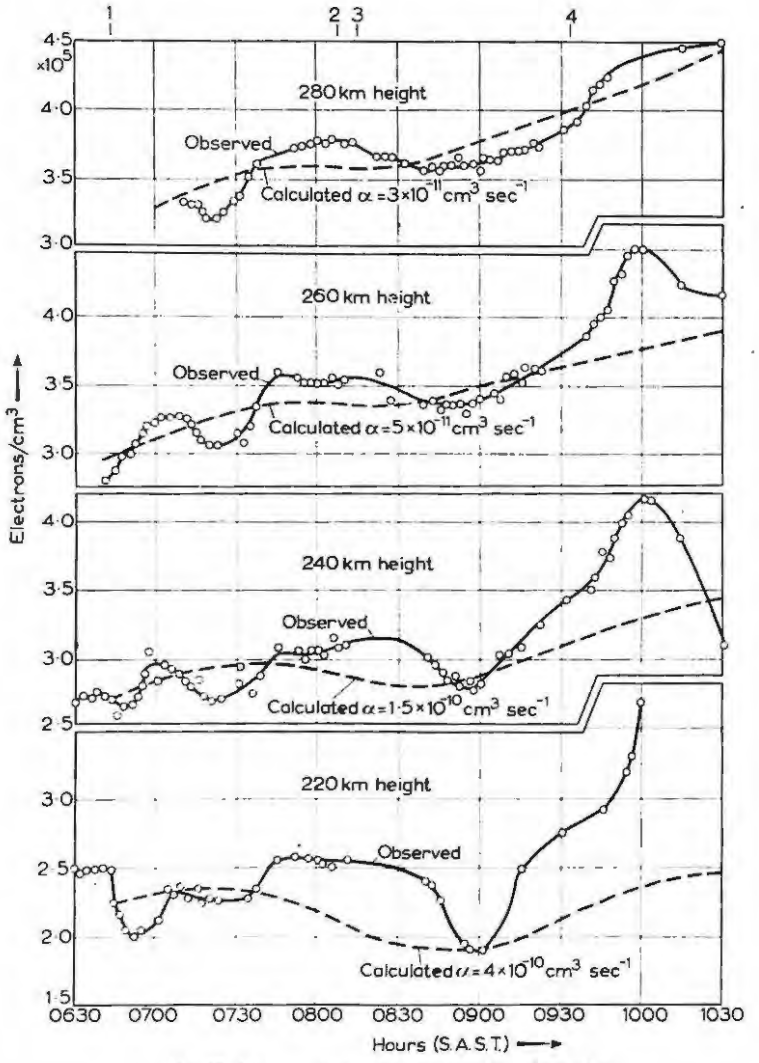

Fig. 75. *F2* layer, theoretical curves for values of α.

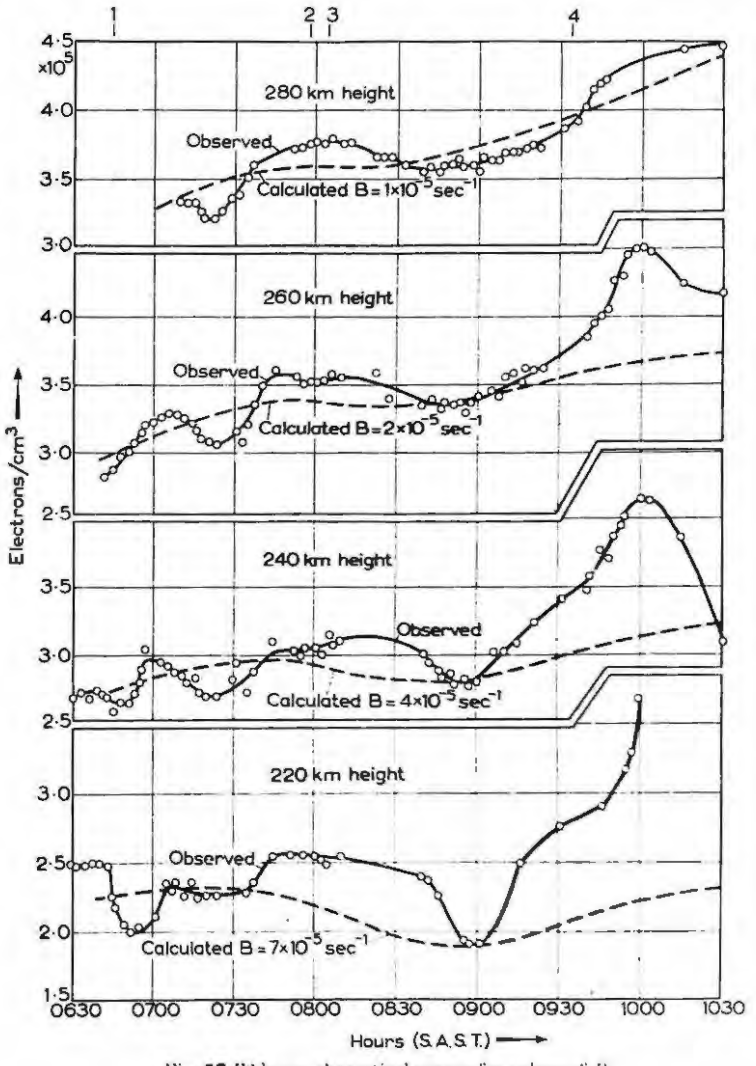

Fig. 76. *F2* layer, theoretical curves for values of B.

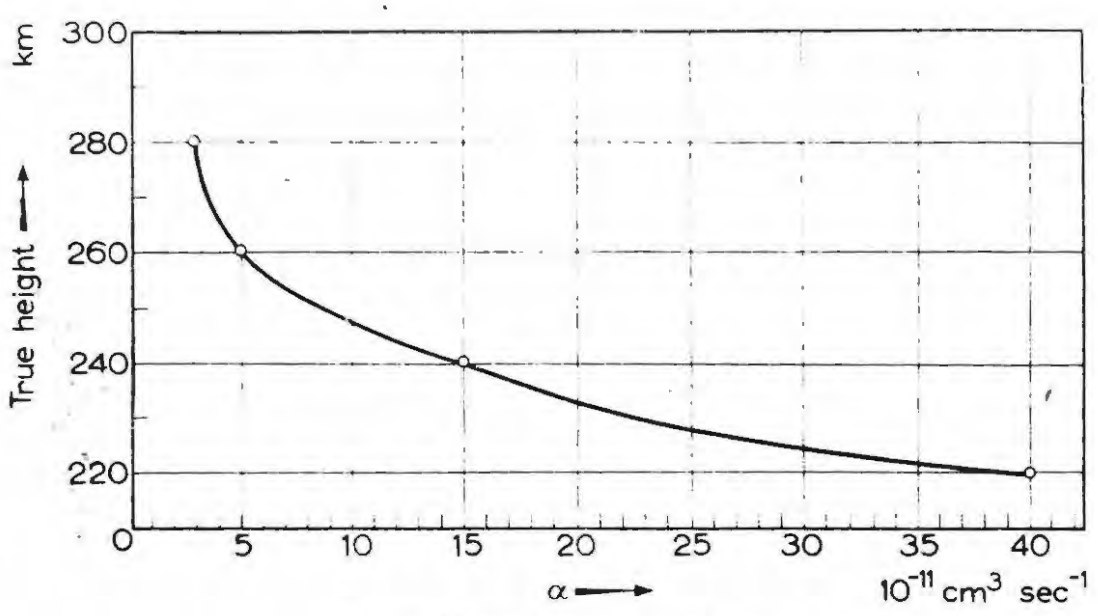

Fig: 77. Variation of α with height.

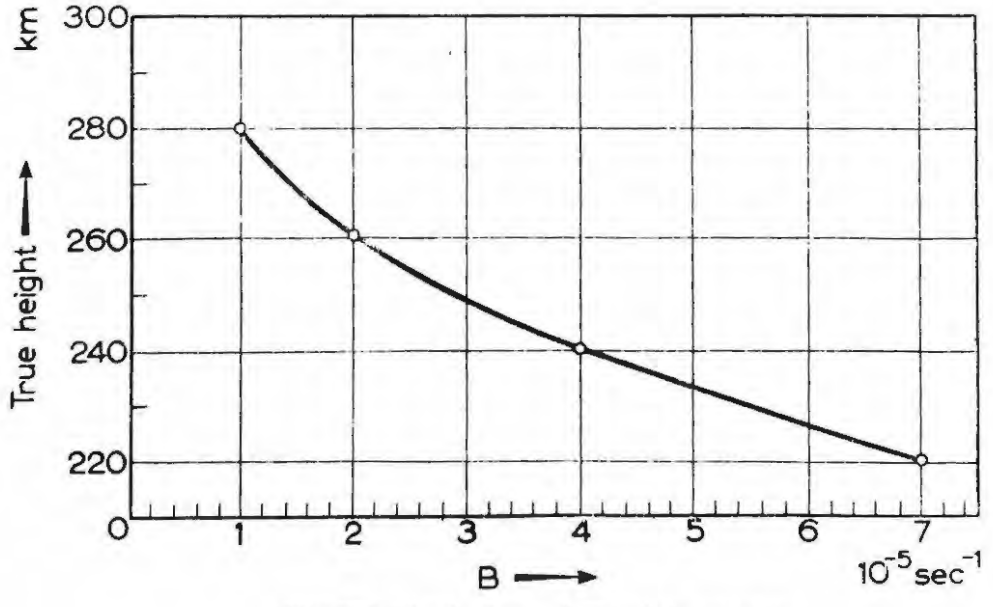

Fig: 78. Variation of B with height.

calculated by SEATON (1948) from the diurnal variation of N of the E_1, F_1 and F_2 layers. HAVENS, FRIEDMAN and HULBURT (1955) have estimated α at various heights from the result of rocket measurements. More recently RATCLIFFE, SCHMERLING, SETTY and THOMAS (1956) have deduced that the electron-loss process follows an attachment law in the F_2 layer and values of B have been deduced from the night-time distribution of electrons at various places. Tables 22 and 23 show the values of α and B as deduced here, compared with those deduced by other methods.

Height	Dec. 1954 Eclipse	Minnis, 1952 Eclipse	Seaton, diurnal change in N	Havens et al, rocket measurements
120	7×10^{-9}	8.0×10^{-9}	5×10^{-9}	1.6×10^{-8}
150				1.6×10^{-8}
160	5×10^{-9}			
170		8.2×10^{-9}		
180	5×10^{-9}	Savitt,		
200	5×10^{-9}	1947 eclipse		2×10^{-9}
220	4×10^{-10}	3×10^{-9}	1.3×10^{-9}	
240	1.5×10^{-10}	1.5×10^{-9}	(Max F_1)	
250				1.3×10^{-10}
260	5×10^{-11}	1×10^{-9}		
280	3×10^{-11}	6×10^{-10}		
300		4×10^{-10}		1.6×10^{-11}
320		2.5×10^{-10}	8×10^{-11} (Max F_2)	

Table 21: Values of α ($cm^3 sec^{-1}$) at various heights as deduced by several workers.

Height	Dec.1954 Eclipse	Savitt 1957 Eclipse	Minnis 1952 & June 1954 Eclipse	Ratcliffe et al, 1956
160-180	$3x10^{-4}$			
200	$3x10^{-4}$		$5.5x10^{-4}$	
220	$7x10^{-5}$	$6.5x10^{-4}$	$1.5x10^{-4}$) 1954 $2.4x10^{-4}$)eclipse	
240	$4x10^{-5}$	$5.8x10^{-4}$		$3.3x10^{-4}$
250			$5.0x10^{-4}$	$2.7x10^{-4}$
260	$2x10^{-5}$	$5.0x10^{-4}$		$2.2x10^{-4}$
280	$1x10^{-5}$	$4.2x10^{-4}$		$1.5x10^{-4}$
300		$3.5x10^{-4}$	$2.5x10^{-4}$	$1x10^{-4}$
320		$2.8x10^{-4}$		$7x10^{-5}$
350			$9.0x10^{-5}$	$4x10^{-5}$
400			$6;0x10^{-5}$	$1x10^{-5}$

Table 23: Values of $B(Sec^{-1})$ at various heights as deduced by several workers.

The values of α deduced here compare most favourably with those estimated from rocket measurements but are lower by a factor of 10 than those deduced by Savitt. The values of B are in all cases lower than those determined by other workers, on the whole by a factor of 10 again.

However, the most interesting feature of the values of α and B as deduced from this eclipse where it has been possible to evaluate the changes in electron density from 160 to 280 kms, is the rapid drop in α and B above 200 kms. The

value of α drops by a factor of 10 in the first 20 km and by a factor of 100 in the first 60 km. The values of B drop by a factor of 1 0 in the first 50 km.

This rapid drop in α or B suggests that the F_1 and F_2 layers might owe their origin to the same source of radiation ionising the same atmospheric constituent, the rapid decrease in α or B in the F_2 layer giving rise to a second maximum of electron density. This suggestion was first made by BRADBURY (1938), who suggested that the F_2 layer might arise as a second maximum of the F_1 layer due to the slower recombination at F_2 heights. BATES (1949) has shown that the source of radiation which produces the F_1 layer could produce the observed rate of ion production at F_2 heights. The results shown here are consistent with the theories of Bradbury and Bates.

There is the possibility that the rapid drop in α or B might be a consequence of Kelso's method of scaling, but it seems unlikely to affect much the values at 260 and 280 km. Certainly Kelso's method makes the electron density deduced for 220 km unreliable since it is so near the F_1 layer maximum. Another factor which might affect the values of and B is the fact that Kelso's method neglects the effect of the earth's magnetic field. SCHMERLING and THOMAS (1956) have suggested that a first order approximation for the effect of the earth's magnetic field to N(h) curves at Watheroo (30.3°S., 115.9°E.) and Slough (51.5°N., 0.5°W) deduced by KELSO'S (1952) method is obtained by reducing the heights deduced by 10 km. The

latitude of Grahamstown is $33^{\circ}19$ S., which corresponds roughly to that of Watheroo, and consequently such an approximation is probably valid here. However, the result would only be to reduce the heights to which the values of α and B refer at Grahamstown by 10 km. This would make them even lower than those deduced by other measurements, but would still indicate that the variation with height is the same.

Electron-loss process in the F region.

In view of the observed variation of the loss coefficient with height in the F_2 layer, it is interesting to see how this can be accounted for on theoretical grounds. BATES and MASSEY (1946, 1947) have concluded that the loss coefficients could only be as great as those measured in the F region if dissociative recombination was important. In the higher parts of the atmosphere they supposed that atomic oxygen was the ionisable constituent and that there were molecules XY (which might possibly be O_2), to which positive charges could be transferred from the atomic ions. The processes operating would then be:-

Production	$O + h\nu \longrightarrow O^+ + e$	(i)
Loss	$O^+ + XY \longrightarrow O + XY^+$	(ii)
	$XY^+ + e \longrightarrow X + Y$	(iii)

If q as before, is the rate of production of electrons and positive ions by photoionisation, $\left(\text{process (i)}\right)$, let $\lambda_1\, n(O^+)n(XY)$ represent the rate of charge transfer in process (ii), and

$\lambda_2 n(XY^+)n(e)$ be the rate of the dissociative recombination in process (iii).

$n(e)$, $n(O^+)$, $n(XY^+)$ represent the density of electrons, positive atomic oxygen ions, and positive molecular ions respectively.

The equations for the variation of $n(e)$ and $n(O^+)$ are, following MASSEY and BURHOP (1952) and RATCLIFFE (1956),

$$\frac{dn(O^+)}{dt} = q - \lambda_1 n(O^+)n(XY) \tag{89}$$

$$\frac{dn(e)}{dt} = q - \lambda_2 n(e)n(XY^+) \tag{90}$$

Under equilibrium conditions $\frac{dn(O^+)}{dt} = \frac{dn(e)}{dt} = 0$, and since the numbers of positively and negatively charged particles are equal

$$n(O^+) + n(XY^+) = n(e) \tag{91}$$

Hence,

$$q = \frac{\lambda_1 \lambda_2 n(XY)\, n^2(e)}{\lambda_1 n(XY) + \lambda_2 n(e)} \tag{92}$$

If (i) $\lambda_1 n(XY) \gg \lambda_2 n(e)$

$$q = \lambda_2 n^2(e) \tag{93}$$

(ii) $\lambda_1 n(XY) \ll \lambda_2 n(e)$

$$q = \lambda_1 n(XY) n(e) \tag{94}$$

Case (i) shows the loss-process to be according to a recombination law since λ_2 is a constant, and this occurs at heights where $n(XY)$ is large, which is obviously at the lwer heights.

Case (ii) occurs where n(XY) is small, and applies to greater heights, when the loss processwill follow an attachment law, since n(XY) is constant at a given height.

The two equations show that low down the recombination coefficient is approximately independent of height, but higher up when an attachment law is followed, the loss coefficient will decrease with height as n(XY) decreases with height.

This is exactly what has been found on the analysis of the electron density at constant height. Case (i) will refer to the F_1 layer where the recombination law operates and α is independent of height. Case (ii) refers to the F_2 layer, and although it was not possible to distinguish between the recombination and attachment cases in this eclipse, clearly on theoretical grounds, the attachment law is favoured. This result also confirms the conclusions of other workers, previously mentioned, that the electron loss process in the F_2 layer followed an attachment law.

It is thought that the molecule XY might be O_2. In this case the loss coefficient would decrease with height in the same way as the number of oxygen molecules decreases with height.

RATCLIFFE et al (1956) have deduced that the loss coefficient k (attachment-like) has the form

$$k = k_o \exp\left(\frac{h - h_o}{50}\right) \qquad (95)$$

and thus decreases with height with a "scale height" of 50 km.

NICOLET and MANGE (1954) have suggested that under the joint effects of photo-dissociation and diffusion O_2 would be distributed with its normal scale height in the F region. BATES (1954) has extrapolated measurements made by rockets to the F region and has concluded that the scale height of N_2 (which would not be much different from O_2) is about 30 km. The value of 50 km obtained by Ratcliffe et al is more nearly that of O on the R model of Bates.

The loss-coefficients obtained from the eclipse measurements very nearly fit the equation

$$B = B_o \exp \frac{h - h_o}{28} \qquad (96)$$

thus decreasing with a "scale height" of 28, which agrees very well with that of O_2 or N_2 on the Bates R model.

The loss-coefficient deduced from night values.

It is possible to deduce the loss-coefficient, B, from the night time variation of n at constant height. At night $q = 0$, so

$$B = \frac{-N}{\frac{dn}{dt}} \qquad (97)$$

and consequently B may be calculated from the variation of n at fixed heights during the night.

A glance at Fig. 39 shown that during the night there were times when the electron density increased at some heights especially during the early morning hours.

Fig. 79(a) shows the variation of electron density during the night from 2000 to 0400 hours. In Fig. 79(b), the corresponding N(t) curve is drawn. This shows the variation of electron density at constant height found by averaging the variations from individual nights at each height. The increases in electron density are not so pronounced in these curves. From 2000 to 0000 hours the electron density at all heights fell fairly uniformly and using equation (97) values of B were calculated for each hour at each height and are shown in Table 24

Time	Height (km)				
	260	280	300	320	340
20/2100	7.34	8.45	6.89	6.10	7.95
21/2200	8.95	7.81	7.48	5.90	4.39
22/2300	-	4.27	3.14	3.58	4.30
23/0000	-	4.52	2.84	3.27	3.51
00/0100	-	-	-	-	1.94
Mean	8.1	6.2	5.1	4.7	4.4

Table 24: Variation of B (10^{-5} sec^{-1}) at constant height as deduced from night values.

Table 25 compares these results with those deduced from the eclipse and also those deduced by RATCLIFFE et al (1956) from similar night-time variations.

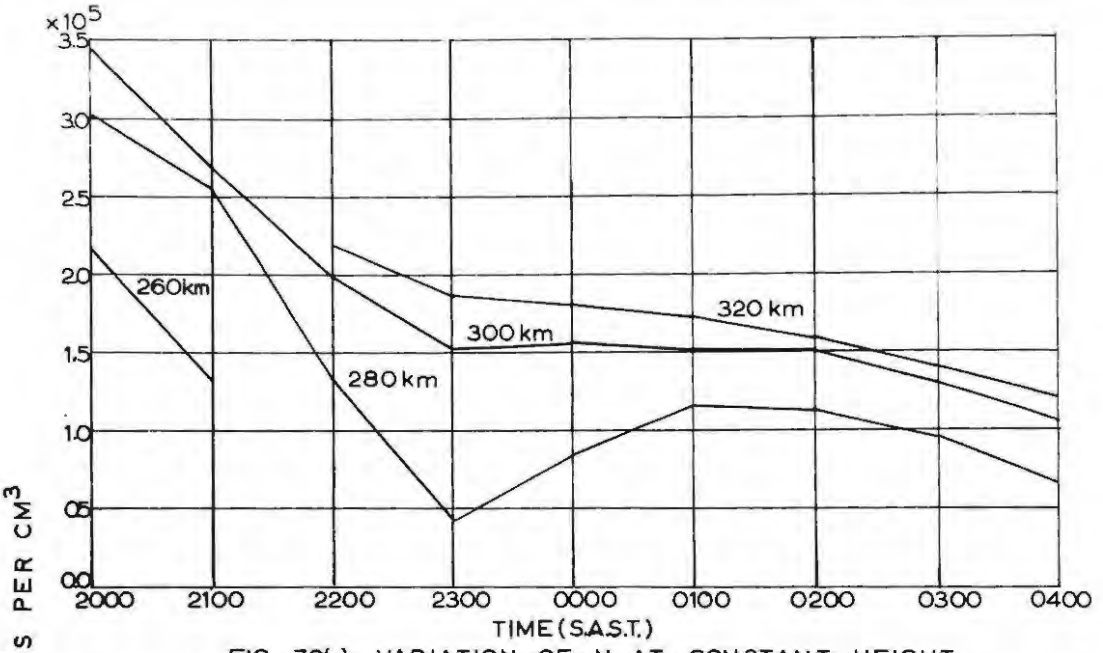

FIG: 79(a) VARIATION OF N AT CONSTANT HEIGHT DEDUCED FROM MEAN N(h) CURVES.

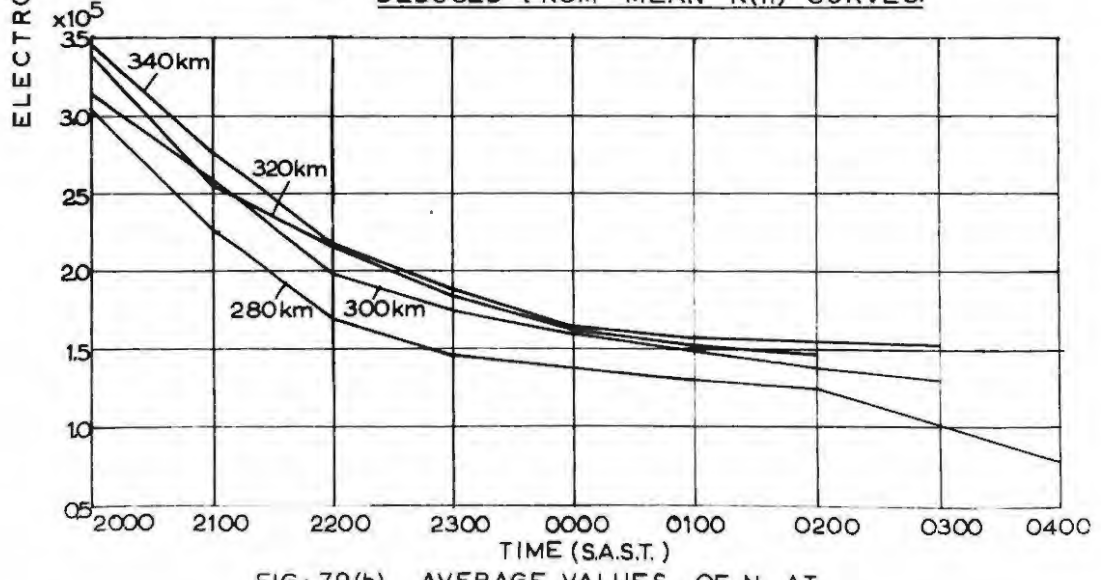

FIG: 79(b) AVERAGE VALUES OF N AT CONSTANT HEIGHT

Height (km)	Eclipse	Night	Ratcliffe et al.
220	7×10^{-5}		
240	4×10^{-5}		3.3×10^{-4}
260	2×10^{-5}	8.1×10^{-5}	2.2×10^{-4}
280	1×10^{-5}	6.2×10^{-5}	1.5×10^{-4}
300		5.1×10^{-5}	1×10^{-4}
320		4.7×10^{-5}	7×10^{-5}
340		4.4×10^{-5}	4.5×10^{-5}

Table 25: Comparison of values of B (sec^{-1}) at various heights.

The values deduced from the night-time variation of electron density are about 5 times higher than the eclipse values but still lower than the night values of Ratcliffe et al.

Ratcliffe et al have also noted that in years of sunspot minimum the electron density increased at some levels during some part of the night. Their results were therefore based on years of high sunspot number. Table 23 shows that the highest values of B from eclipse measurements are those of Savitt in 1947, a year of high sunspot number, whilst the lowest values of B are those found for this eclipse, a year of low sunspot number. Similar conclusions can be drawn from Table 24 for the night-time variation of electron density. It seems likely, therefore, that movements of electrons, which are known to play an important part in the F_2 layer (MARTYN, 1955) are considerably different in years of sunspot

maximum and sunspot minimum and might give the false impression that B varies with sunspot activity.

Comparison of E and F_1 measurements.

MINNIS (1955, 1956a, b, 1957) has noticed that the simultaneous changes in the E and F_1 layer critical frequencies during several eclipses are very similar. If such changes are to be attributed to the occultation or uncovering of bright regions on the solar disc, then it seems likely that the sources of solar ionising radiation for the two layers are very similar. In fact, Minnis has found that on several eclipses a solar model he has postulated to explain the E layer measurements, can also explain the F_1 layer measurements, the position and intensities of the sources being the same for each layer. MINNIS (1956 c) has shown that if this is so, it leads to important conclusion regarding the ratio of the recombination coefficients in the two layers.

If the diurnal variation of the critical frequencies in the E and F_1 layers are expressed in the form

$$f_oE = a \cos^m \chi \qquad (98)$$

and

$$f_oF_1 = b \cos^n \chi \qquad (99)$$

for a Chapman layer $m = n = \frac{1}{2}$, but it is well-known that the index m and n do not follow the simple Chapman relation. Providing χ is not too large, equations (98) and (99) can be modified to give a relation between $f_o E$ and f_oF_1

$$foE = \frac{am}{bn} foF_1 + a(1-\frac{m}{n})$$

$$= AfoF_1 + B \qquad (100)$$

Fig. 80 shows plots of log cosχ versus log foE and log foF_1 for the three South African stations, and from these graphs it is possible to deduce the constants a, b, m and n, and consequently A and B in equation (100). Table 26 below shows the values of these constants.

Station	a	b	m	n	a/b	m/n	A	B
Grahamstown	3.39	4.44	0.295	0.175	0.76	1.69	1.28	-2.34
Johannesburg	3.44	4.47	0.30	0.17	0.77	1.76	1.36	-2.62
Cape Town	3.44	4.41	0.28	0.13	0.78	2.15	1.68	-3.82

Table 26: Constants in equations (98), (99) and (100) deduced from diurnal variation of foE and foF_1

If during an eclipse the intensities and positions of the sources of ionisation is the same for the two layers, there should be a simple relation between foE and foF_1, as for example in equation (100). Minnis has found that equation (100) holds during an eclipse, but the constants A and B are altered. Fig. 81 therefore, shows plots of foE against foF_1 both for the eclipse and for the control days. It is noted that at all three stations the points for the values before the maximum phase do not seem to lie on the same line as those after the maximum phase. In fact, at Grahamstown and Johannesburg these points seem

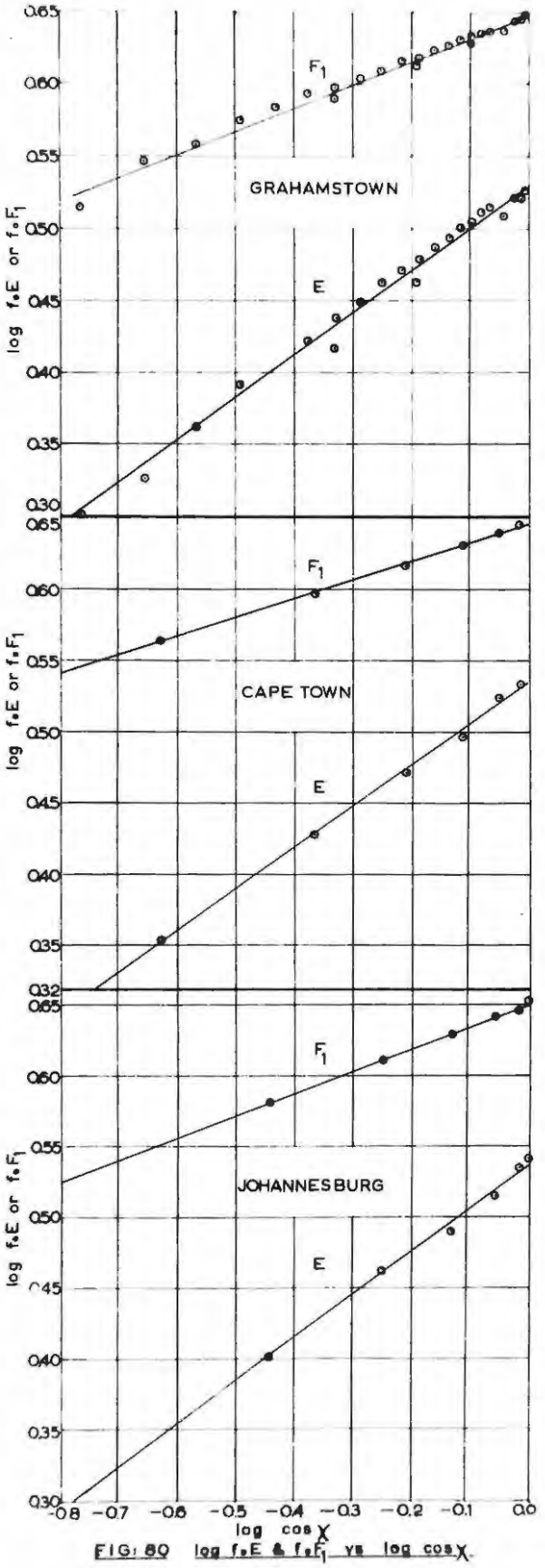

FIG: 80 log f_0E & f_0F_1 vs log cos χ

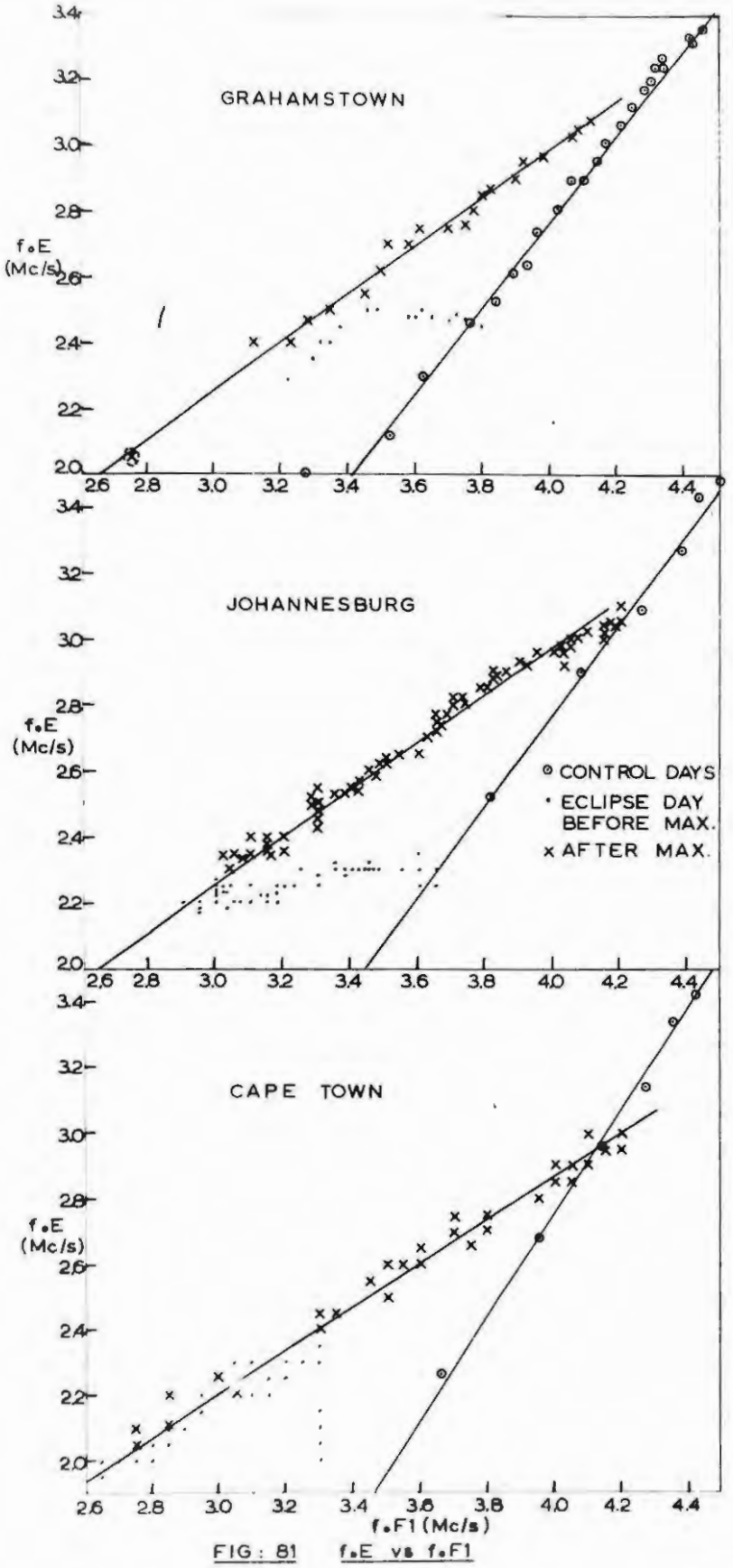

FIG : 81 f₀E vs f₀F1

strangely out of place. Thismay have been due to the fact that the F_1 layer at all the stations only just began to show itself at the start of the eclipse, and may not have been properly formed until the eclipse was well under way. However, the points after the maximum phase at all three stations lie very nicely on a straight line. It is at once noticed that the constants A and B for these lines are somewhat different from the control values. Using subscripts E and C to denote the eclipse and control valuesof A and B, Table 27 shows these values derived from Fig. 81.

Station	A_E	B_E	A_C	B_C
Grahamstown	0.75	+0.01	1.31	-2.46
Johannesburg	0.73	-0.03	1.38	-2.74
Cape Town	0.70	+0.12	1.60	-3.60

Table 27: Values of A and B deduced from eclipse and control data

During the eclipse the value of B has become almost negligible, which indicates that m = n, and Minnis has concluded that both layers respond in almost the same way to changes in the intensity of the ionising radiation. The fact that m = n during the eclipse indicates that the index of cos χ has become the same for each layer. This could perhaps be explained by a change in q_o in the F_1 layer due to the layer maximum changing its height. If q_o is assumed a constant, then the index of cos χ would

change. However, Minnis has assumed that the fractional obscuration of the ionising radiation is the same for both the E and F_1 layers as a result. Consequently, he has been able to show (MINNIS , 1956c) that the ratio of the recombination coefficients, the rates of electron production are given by

$$R = \frac{\alpha_E}{\alpha_{F_1}} = \frac{q_o F_1}{q_o E} = \sqrt{\frac{(q_o/\alpha)_{F_1}}{(q_o/\alpha)E}} = \frac{b^2}{a^2} \qquad (101)$$

Thus it may be concluded that

$$\alpha_{F_1} = \alpha_E \left(\frac{a}{b}\right)^2 \qquad (102)$$

Now a/b is tabulated in Table 26 for the three stations as deduced from the diurnal variation. Since B is almost zero, the value of A during the eclipse also corresponds to a/b. Table 27 shows that these values are not significantly different from those deduced from control data. Taking the average value of a/b as 0.75, thus

$$\alpha_{F_1} = 0.56 \alpha_E \qquad (103)$$

Two values of α_E were deduced in Part 1(a) according to two different solar models. In the first instance, if it is assumed that all the radiation comes from the visible disc, $\alpha_E = 1.5 \times 10^{-8} cm^3 sec^{-1}$, and consequently $\alpha_{F_1} = 8.4 \times 10^{-9} cm^3 sec^{-1}$. If 15% comes from outside the solar disc, $\alpha_E = 4 \times 10^{-8} cm^3 sec^{-1}$ and thus,

$\alpha_{F_1} = 2.2 \times 10^{-8} cm^3 sec^{-1}$. However, it seems that serious errors may be introduced when dealing only with critical frequencies in the F_1 and these would be eliminated to a certain extent by considering the changes in electron density at various heights. The results from Grahamstown are inconclusive since the values of foF_1 are extrapolated for an hour during the middle of the eclipse. N(h) curves were not deduced for the other two stations.

Radiation from outside the visible disc.

If the conclusions of Minnis that the fractional obscuration of the ionising radiation is the same for the E and F_1 layers is accepted, it seems that this conclusion should also apply to the F_2 region. It has already been mentioned that it seems likely that the F_1 and F_2 layers are formed by the same ionising radiation of the same ionisable constituent. Figs. 75 and 76 for the F_2 layer at various heights show that the solar model with west limb brightening would hardly account for the changes in electron density. In fact, it would seem more likely that these were darkening at the west limb! However, the model in which 15% of the radiation comes from outside the visible disc was applied to the F_2 region to see if any better fit to the results could be obtained. The resulting theoretical curves for various values of B were hardly different from those shown in Fig. 76, except that the values of B at each height were approximately twice as large as those deduced

for a uniformly radiating disc. No closer fit could be obtained and the resulting values of B are still lower than those of any other previous estimates. Since movements are known to play an important part in the F_2 layer, it seems clear that some considerable movement of electrons must have taken place. THOMAS and ROBBINS (1956) have shown that the movements in the F_2 layer during several eclipses were similar to those which took place during the 24 hours of the day.

Movements in the F_2 layer during the eclipse.

If movements of electrons take place in the F_2 layer, the ionospheric continuity equation at any height must be modified to

$$\frac{dn}{dt} = q_o - Bn - M \qquad (104)$$

where $M = \frac{d\,(nw)}{dh}$

and w represents the upward transport velocity of electrons.

As will be seen in Part III of this thesis, there is reason to believe from an analysis of the control data that the F_2 region is an isothermal region of constant scale height so that q will be given by Chapman's equation

$$q = q_o \exp\,(1 - Z - e^{-Z}\sec\chi) \qquad (105)$$

where q_o = rate of production of electrons for $\chi = 0^o$

and $Z = \frac{h - h_o}{H}$

where h_o is the height refering to q_o, and H is the saale height of the atmospheric constituent ionised.

By making assumptions as to q_o, h_o and H, and the variation of q_o during the eclipse, it is possible to deduce the magnitude of M. This has been considered for five different eclipses by THOMAS and ROBBINS (1956). The purpose of this section is to compare the movements that might have occurred during this eclipse with those deduced by Thomas and Robbins. It seems best, therefore, to make the same assumptions as they have made for the purpose of comparison with their results.

It is assumed that B has a variation with height determined by RATCLIFFE et al (1956).

$$B = 10^{-4} \exp\left(\frac{300 - h}{50}\right) \sec^{-1} \qquad (106)$$

$$Z = \frac{h - 180}{45} \qquad (107)$$

and $q_o = 280\ (1 + 1.4 \times 10^{-2}\ \bar{R})\ cm^{-3}sec^{-1}$ (108)

where $\bar{R}$ is the monthly average relative Zurich sunspot number.

These assumptions imply that the F_1 and F_2 layers owe their origin to the same source of ionising radiation whose peak of electron production occurs at the F_1 layer maximum. The values of q_o imply that $\alpha_{F_1} = 5 \times 10^{-9} cm^3 sec^{-1}$, and that the peak of the F_1 layer occurs at 180 km when $\chi = 0^\circ$. From the control data, using the noon values of N for the

F_1 layer, and $\alpha = 5 \times 10^{-9} cm^3 sec^{-1}$.

$q_o = 301\ cm^{-3} sec^{-1}$

and $h_o = 205$ km.

For December, 1954, $\bar{R} = 10$ and hence q_o as deduced from equation (108) is 319 $cm^{-3} sec^{-1}$. The absolute values of M may therefore not apply to the control and eclipse readings in this case if the values of Ratcliffe et al are used, but by evaluating $(M_E - M_C)$ the difference in the movement terms for the eclipse and control days, the assumptions made do not affect the analysis. During the eclipse it is assumed that the sun is a uniformly radiating disc and q must be replaced by fq.

Fig. 82 (a) shows the magnitudes of M for the control and eclipse days using equation (104), whilst Fig. 82(b) shows $\Delta M = M_E - M_C$, the difference in the movement term for the eclipse and control days. The resulting curves show that the movements which occurred during this eclipse are again similar to those analysed by Thomas and Robbins. This seems to indicate that such movements have some real significance.

Temperature variation during the eclipse.

The movements described in the previous section might possibly be attributed to temperature changes in the F_2 layer. Assuming that the loss coefficient follows an attachment law in the F_2 layer with values of B as in equation

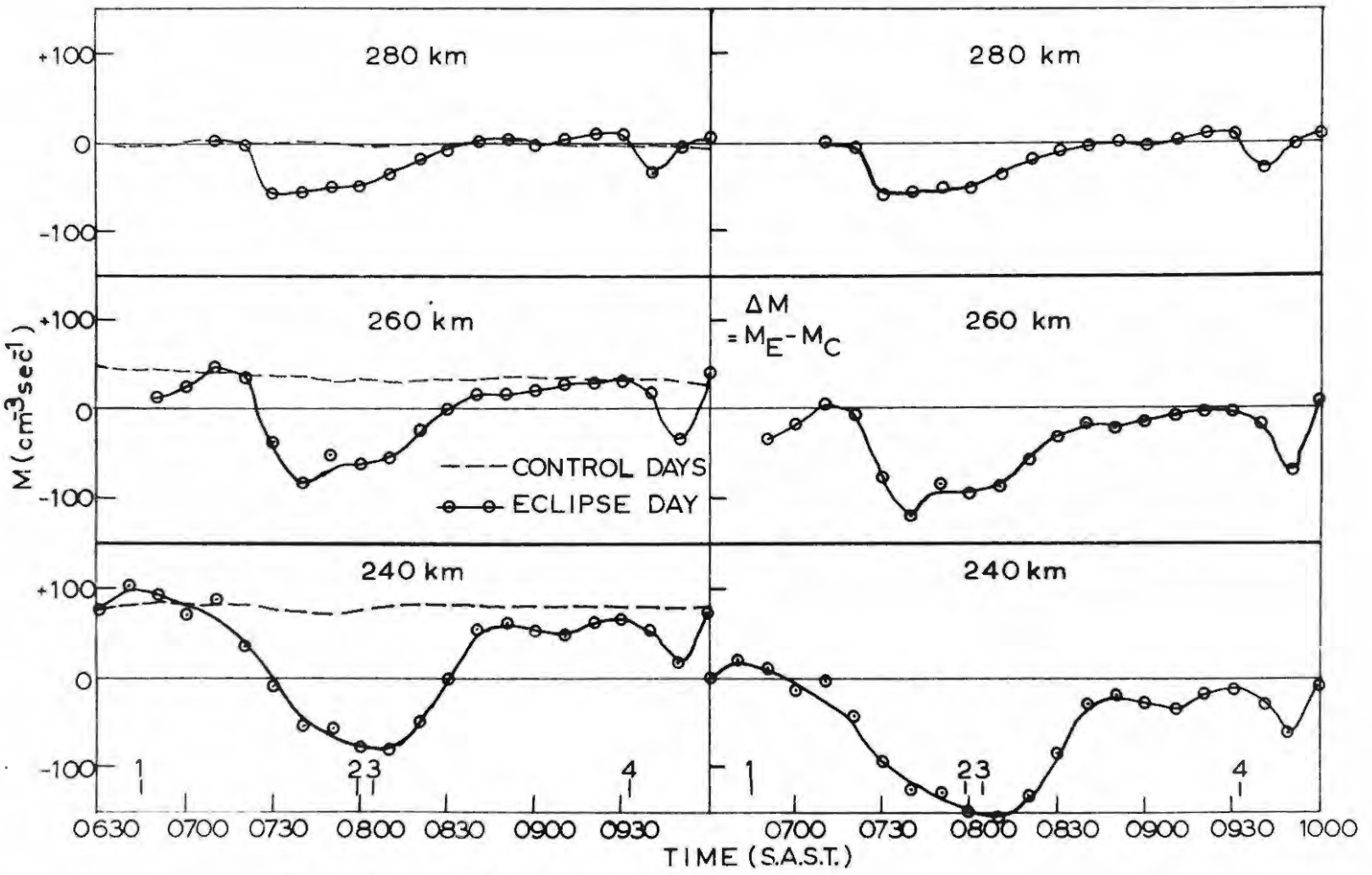

FIG: 82 MOVEMENTS IN THE F_2 LAYER

(106), and that α in the F_1 layer is $5 \times 10^{-9} cm^3 sec^{-1}$, it is possible to evaluate q for each height in the F region and consequently determine the "shape" of the ionising layer. Variations in q from simple Chapman theory might then be attributed to temperature changes. Fig, 83(a) shows q versus height curves for various times on the control days, and Fig. 83(b) shows the corresponding q(h) curves for the eclipse.

The control day q(h) curves show that the layer is somewhat similar to a Chapman layer. However, the eclipse curves show some remarkable features. Although the curves for 0745, 0800, and 0815 are extrapolated in the F_1 region, they show that during the eclipse the layer became very thick, and that the height of the maximum rate of electron production rose during the middle of the eclipse. GLEDHILL and SZENDREI (1947a, 1950) have considered the effect of a temperature gradient on a simple Chapman layer. A glance at the curves drawn by Gledhill and Szendrei shows that to distort the layer in this fashion would require (a) an increase in temperature at the base of the layer, and (b) a considerable increase in the temperature gradient.

To explain these movements therefore, on temperature changes means that there must have been a considerable increase of temperature during the eclipse, which must be rejected on grounds of common-sense. The alternative explanation put forward by Thomas and Robbins relates the movements to the

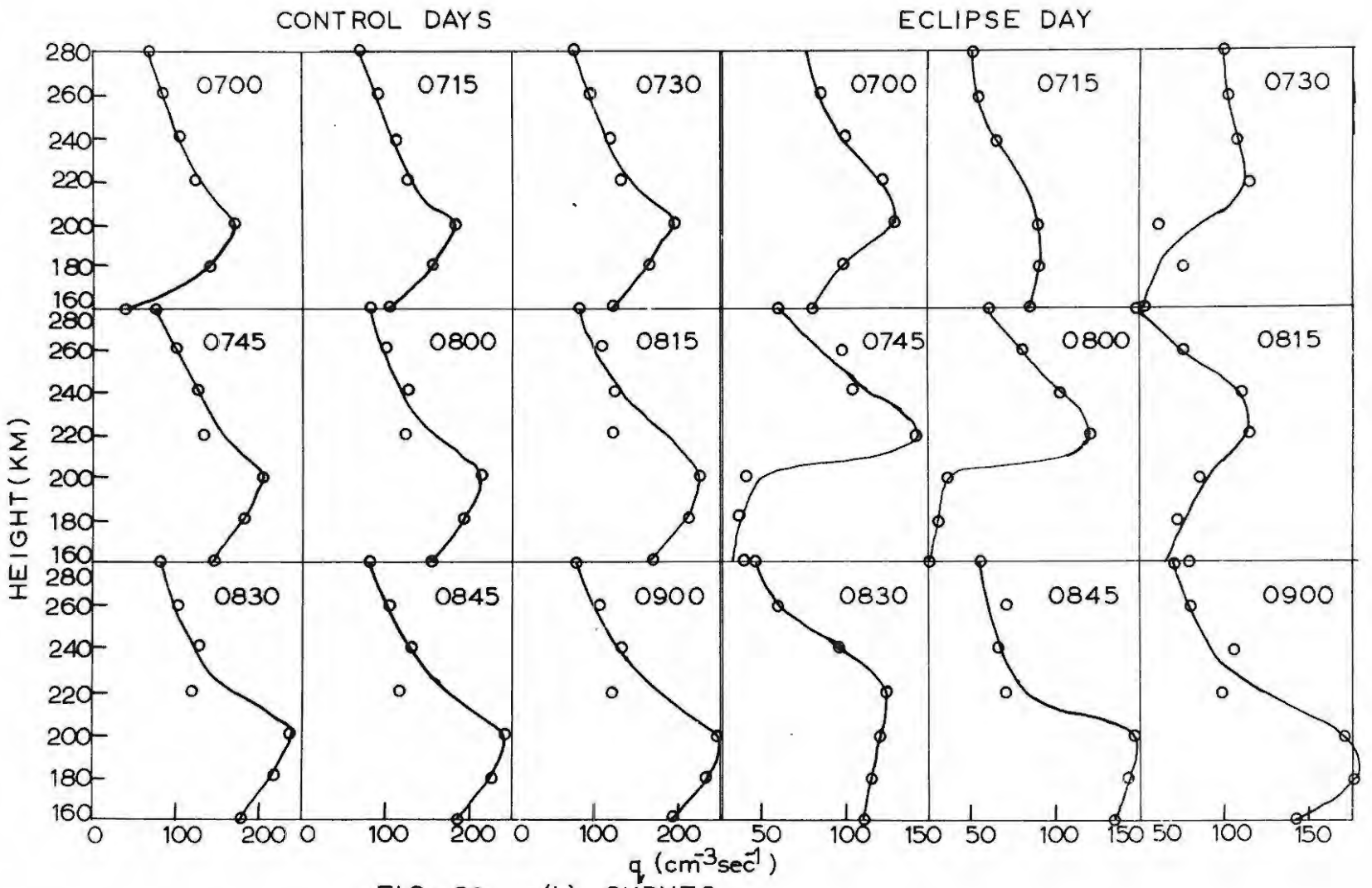

FIG: 83 q(h) CURVES

effect of the eclipse in the lower parts of the ionosphere. The eclipse might decrease the conductivity of that part of the ionosphere in which the geomagnetic S_q currents flow, and as a result, an electrostatic polarisation might be built up in this region which would produce a field in the F_2 layer. This field, crossed with the earth's magnetic field, would cause the layer to move.

However, such movements must be viewed with caution at the present time. The work of MUNRO and HEISLER (1958) has shown that due to the curvature produced in the ionosphere during an eclipse, reflections may be returned from points other than the vertical. GLEDHILL (1958) has shown that the reflections may quite reasonably have taken rather a devious path through the ionosphere. As has been pointed out by Munro and Heisler, and by Gledhill, this indicates that the scaling methods of KELSO (1952) and others are not valid during an eclipse. These apparent movements might therefore only be errors introduced by the application of Kelso's method of deducing N(h) profiles.

Conclusions.

An analysis of the variations in electron density at fixed heights in the F region has shown that in the F_1 layer a recombination type of electron-loss process is followed, the recombination coeffieient being independent of height. In the F_2 layer both a recombination and attachment law seem possible, and in both cases the

coefficients deduced decrease in a regular manner with height. On theoretical grounds the attachment law is favoured. Although the values deduced are somewhat lower than those of other workers, they indicate that it is possible that the F_1 and F_2 layers might be formed by the same radiation ionising the same constituent, but that a second maximum of electron density is produced above the F_1 layer due to the rapid decrease of the loss-coefficient with height. Comparison with the loss-coefficients deduced from the night-time variation of electron density at fixed heights again gives values lower than previously estimated.

Apparently considerable movement of electrons must taken place in the F_2 layer during the eclipse and it is found that they are similar to those estimated by Thomas and Robbins. An explanation of these movements in terms of temperature variations must be rejected.

Following the recent work of Munro and Heisler, and of Gledhill, it appears that the use of Kelso's method of deducing N(h) profiles during an eclipse is not valid, and therefore further analyses of F_2 layer eclipse measurements using this method must be viewed with caution.

PART III

(a) Theory of layer formation in an atmosphere in which the loss-coefficient varies with height.

Introduction.

The original theory of the formation of an ionised layer in the upper atmosphere is that due to CHAPMAN (1931a, b). Although this theory makes many simplifying assumptions, it has served as a basis for the study of the ionospheric layers. It is known that the E and F_1 layers approximate to a "Chapman" layer, but the behaviour of the F_2 layer cannot be accounted for on such a simple theory. Several modifications to Chapman's theory have been put forward to account for the behaviour of the F_2 layer. In particular, CLEDHILL and SZENDREI (1947a, 1950) ascribed the variations to expansion of the atmosphere due to heating by rejecting the assumption of an isothermal atmosphere, and assuming that the temperature increased linearly with height. MARTYN (1947a, b) has put forward a "drift theory" in which the abnormal behaviour of the F_2 layer is attributed to the polarisation S (electrostatic) field, associated with the production of the currents in the "dynamo" region of the ionosphere responsible for the observed magnetic variations.

The variation of the recombination coefficient with height has been considered theoretically by CHAPMAN (1954) and applied to the D and E regions. NICOLET (1951),

MITRA (1952) and APPLETON and LYON (1955) have considered the effect of the variation of the scale height and the recombination coefficient with height theoretically. Recently RATCLIFFE (1956) has considered the effect of the variation of an attachment-like loss coefficient with height, following the work of RATCLIFFE et al (1956) on the electron loss process in the F_2 region. The latter theory is most consistent with the current theoretical ideas on the mechanism of electron-loss in the F_2 region. However, Ratcliffe's theory has only served to show theoretically how some behaviour of the F region can be accounted for. In this section Chapman's theory of layer formation in an isothermal atmosphere will be extended to include the variation of both a recombination and attachment - like loss coefficient with height in the F_2 region. Equations are derived which are easily applied to the control data obtained for comparison with the eclipse measurements.

Chapman's Theory.

It is not necessary here to deduce the basic equations for Chapman's Theory, but the essential results show that for an isothermal atmosphere in which the number of molecules decreases exponentially with height, the density of molecules at a height h is given by

$$n' = n_o' \exp -\left(\frac{h-h_o}{H}\right) \qquad (109)$$

where n_o' is the number of molecules per cm^3 at height h_o, and H is the scale height of the atmospheric constituent, and

$$H = \frac{kT}{mg} \qquad (110)$$

where k = Boltzmann's constant

T = absolute temperature

m = molecular mass

g = acceleration due to gravity.

If I is the intensity of a beam of monochromatic radiation at a height h in such an atmosphere, then q, the number of ion pairs produced per cm^3 per sec at height h, is

$$q = \frac{\beta n' I}{W} \qquad (111)$$

where β = atomic absorption coefficient (in cm^2)

W = energy absorbed in ionising one molecule

Then it can easily be shown that

$$q = \beta n_o' I_\infty \exp\left\{-\frac{h-ho}{H} - n_o'\beta H \sec\chi \exp\left[-\frac{h-ho}{H}\right]\right\} \qquad (112)$$

where I_∞ = intensity of the radiation at $h = \infty$

χ = solar zenith distance.

Layer formation.

The rate of increase of electron density at a height h can be written as before

$$\frac{dn}{dt} = q - \alpha n^2 \qquad (113)$$

if the loss process follows a recombination law, or

$$\frac{dn}{dt} = q - Bn \qquad (114)$$

if the loss process follows an attachment law. According to Chapman these equations cannot be solved explicitly. It is necessary to impose the condition that $\frac{dn}{dt} = 0$, which will refer to the middle part of the day. It is also necessary to make some assumption regarding the manner in which α or B varies with height. The variation of these quantities with height as deduced from the eclipse measurements, very nearly follow an exponential variation with height.

Writing $\alpha = \alpha_o \exp - \delta(h - h_a)$ (115)

where α_o is the value of α at height h_a and δ is a constant, and

$$B = B_o \exp - \beta(h - h_b) \qquad (116)$$

where B_o is the value of B at height h_b, and β is a constant. Three cases may be considered.

Case I

$\alpha = \alpha_o$, which refers to the F_1 layer, and the layer is a simple Chapman layer, and thus

$$n_1^2 = \frac{q}{\alpha_o} = \frac{A}{\alpha_o} \exp\left[-\frac{h-h_o}{H} - \frac{1}{F}\exp\left(-\frac{h-h_o}{H}\right)\right] \qquad (117)$$

where $A = \frac{n_o' \beta I_\infty}{w}$ and $F = \frac{\cos \chi}{n_o' \beta H}$

The maximum electron is simply found by equating

$\frac{dn}{dh} = 0$ and the resulting equations deduced by Chapman are -

$$N_1^2 = \frac{AF}{\alpha_o} \exp(-1) \tag{118}$$

and $$h_{M1} = h_o - H \log_e F \tag{119}$$

where N_1 refers to the maximum electron density in Case I and h_{M1} is its corresponding height.

Case II

$$\alpha = \alpha_o \exp - (h-h_a)$$

Then $$n_2^2 = \frac{q}{\alpha} = \frac{A}{\alpha_o} \exp \delta(h-h_a) \exp\left[- \frac{h-h_o}{H} - \frac{1}{F} \exp\left(- \frac{h-h_o}{H}\right)\right] \tag{120}$$

$$\frac{dn}{dh} = \frac{n_2}{2}\left[\delta - \frac{1}{H} + \frac{1}{FH} \exp\left(- \frac{h-h_o}{H}\right)\right]$$

$$= 0$$

Thus $$\frac{1}{FH} \exp\left(- \frac{h-h_o}{H}\right) = \frac{1}{H} - \delta$$

$$\exp\left(- \frac{h-h_o}{H}\right) = F(1 - \delta H)$$

Since h refers to the height of the maximum thus,

$$\frac{h_{M2} - h_o}{H} = - \log_e F (1 - \delta H)$$

$$h_{M2} = h_o - H \log_e F (1 - \delta H) \tag{121}$$

Substituting this in equation (120)

$$N_2^2 = \frac{AF}{\alpha_o} (1 - \delta H) \exp\left[\delta (h_{M2}-h_a) - (1 - \delta H)\right] \tag{122}$$

Case III

$$B = B_o \exp - \beta (h - h_b)$$

$$n_3 = \frac{A}{B_o} \exp \beta (h-h_b) \exp \left[- \frac{h-h_o}{H} - \frac{1}{F} \exp\left(- \frac{h-h_o}{H} \right) \right] \quad (123$$

$$\frac{dn}{dh} = n_3 \left[\beta - \frac{1}{H} + \frac{1}{FH} \exp \left(- \frac{h-h_o}{H} \right) \right] = 0$$

Thus the equation for h_{M3} is the same as for h_{M2} except β replaces δ i.e.

$$h_{M3} = h_o - H \log_e F(1 - \beta H) \quad (124)$$

and

$$N_3 = \frac{AF}{B_o} (1 - \beta H) \exp \left[\beta (h_{M3} - h_b) - (1 - \beta H) \right] \quad (125)$$

Application of theory to control data

Three useful equations emerge from the theory, in each case considered, which give the values of three quantities which can be read off from the mean electron density-height distributions determined for each time of day in Part I. The three quantities are n, the electron density at height h, N, the maximum electron density, and h_M, its corresponding height. By taking the ratios of $\frac{n^2}{N^2}$ in cases I and II, and n/N in case III, most of the constants can be eliminated and the resulting equations are:

Case I

$$\log_e \left(\frac{n_1}{N_1} \right)^2 = 1 + \frac{h_{M1} - h}{H} - \exp \frac{h_{M1} - h}{H} \quad (126)$$

Case II

$$\log_e\left(\frac{n_2}{N_2}\right)^2 = \frac{h_{M2}-h}{H} + (1-\delta H)\left[1-\exp\frac{h_{M2}-h}{H}\right] - \delta(h_{M2}-h) \qquad (127)$$

Case III

$$\log_e\left(\frac{n_3}{N_3}\right) = \frac{h_{M3}-h}{H} + (1-\int H)\left[1-\exp\frac{h_{M3}-h}{H}\right] - \int(h_{M3}-h) \qquad (128)$$

In case I, which can be applied to the F_1 layer, all the parameters except H can be determined from the experimental data and consequently the value of H can be calculated.

In cases II and III there are two unknowns, δ or $\int$ and H. By making some assumption as to the value of δ or $\int$ H may again be determined. These two cases will apply to the F_2 layer.

Case I

By plotting a graph of $\log_e\left(\frac{n_1}{N_1}\right)^2$ versus $\frac{h_{M1}-h}{H}$ it is possible to deduce the value of H. For each time of day the value of n, corresponding to a height h can be read off the control distribution of electrons with height, as can N_1. The value of $\frac{h_{M1}-h}{H}$ is then read off the graph corresponding to $\log_e\left(\frac{n_1}{N_1}\right)^2$. Knowing h_{M1} and h, H can be ffound. A plot of $\log_e\left(\frac{n_1}{N_1}\right)^2$ versus $\frac{h_{M1}-h}{H}$ is shown

in Fig. 84.

This case was applied as a matter of interest to both the F_1 and F_2 layers. In both layers two values of h were chosen. In the F_1 layer the value of n_1 at h = 160, and 180 km were compared with N_1, and in the F_2 layer h = 240 and 260 km were used. Table 28 shows the values of H deduced by this method for the F_1 layer, and Table 29, the values of H for the F_2 layer.

Time	H(h = 160 km)	H(h = 180 km)	Mean H(km)
0700	45.6	43.1	44.4
0800	58.5	60.0	59.2
0900	65.0	57.5	61.3
1000	79.0	78.4	78.7
1100	80.3	74.5	77.4
1200	72.9	75.6	74.3
1300	69.3	59.5	64.4
1400	72.5	61.5	66.0
1500	59.0	75.4	67.2
1600	56.9	55.2	56.0
1700	45.1	39.2	42.1

Table 28: Values of H for F_1 layer, Case I

Time	H(h=240 km)	H(h=260 km)	Mean H(km)
0700	55.3	42.3	48.8
0800	62.9	54.1	58.5
0900	63.0	60.8	61.9
1000	63.7	63.4	63.5
1100	59.1	59.6	59.4
1200	58.4	65.5	61.9
1300	59.0	60.9	60.0
1400	55.1	52.6	53.8
1500	50.6	46.3	48.4
1600	54.1	54.1	54.1
1700	51.6	45.0	48.3

Table 29: Value of H for F_2 layer, Case I

Cases II and III

The value of δ and $\int$ must be established before the determination of H can be made in these two cases. The values of α and B deduced from the eclipse were found to follow the equations:

$$\alpha = \alpha_o \exp -\left(\frac{h-h_a}{25}\right) \qquad (129)$$

whence $\delta = 0.040 \text{ km}^{-1}$

and $B = B_o \exp -\left(\frac{h-h_b}{28}\right)$ (130)

whence $\int = 0.036 \text{ km}^{-1}$

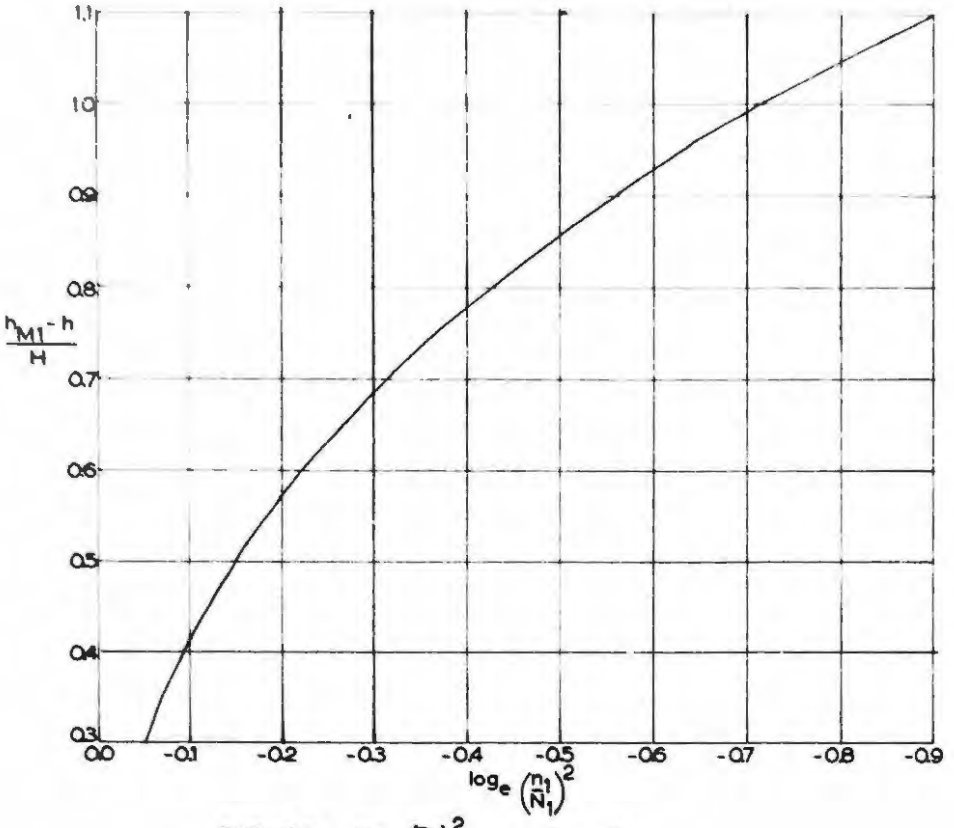

FIG: 84 $\log_e\left(\frac{n_1}{N_1}\right)^2$ vs $\frac{h_{M1}-h}{H}$

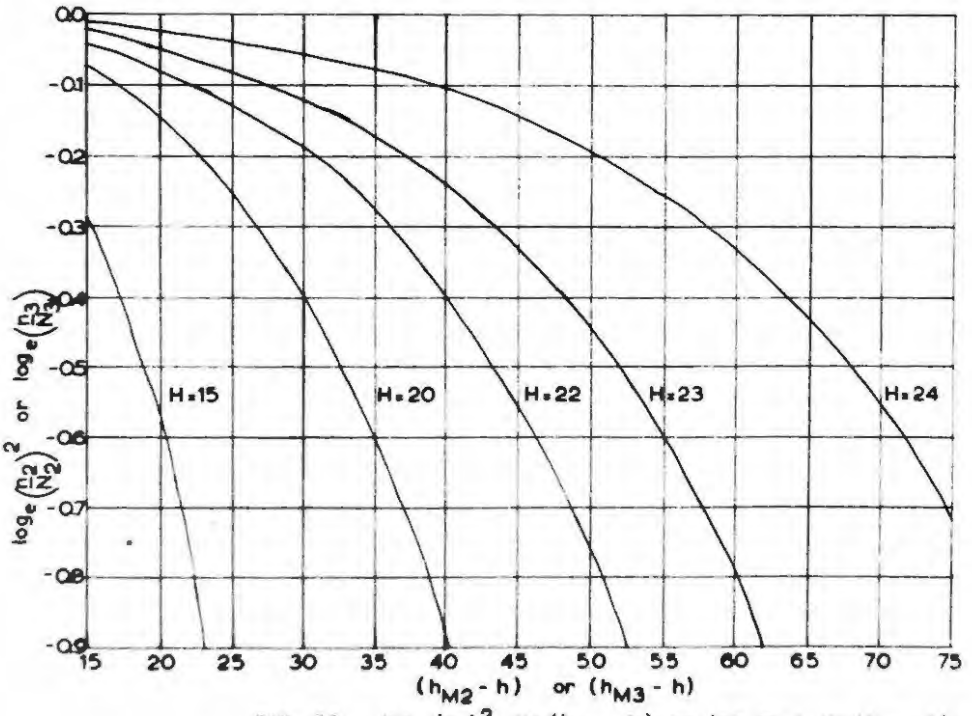

FIG: 85 $\log_e\left(\frac{n_2}{N_2}\right)^2$ vs $(h_{M2}-h)$ or $\log_e\left(\frac{n_3}{N_3}\right)$ vs $(h_{M3}-h)$

δ or f = 0.04

Time	H(h=240 km)	H(h=260 km)	Mean H(km)
0700	22.4	20.0	21.2
0800	23.0	21.8	22.4
0900	23.1	22.5	22.8
1000	23.2	22.9	23.0
1100	23.1	22.7	22.9
1200	23.0	23.0	23.0
1300	23.2	22.9	23.0
1400	22.6	22.0	22.3
1500	22.1	21.0	21.5
1600	22.3	21.6	21.9
1700	22.0	20.5	21.2

Table 30: Values of H for $\delta = 0.04$ km^{-1}, F_2 layer in Case II

Time	H(h=240 km)	H(h=260 km)	Mean H(km)
0700	23.5	22.5	23.0
0800	23.9	23.5	23.7
0900	23.9	23.7	23.8
1000	23.7	23.8	23.8
1100	23.9	23.7	23.8
1200	23.9	23.8	23.9
1300	24.0	23.8	23.9
1400	23.7	23.4	23.6
1500	23.3	23.0	23.2
1600	23.5	23.5	23.5
1700	23.3	22.9	23.1

Table 31: Values of H for $\delta = 0.04$ km^{-1}, F_2 layer in Case III

in the F_2 region than had previously been supposed. Therefore, it seems that as the values of the scale height deduced here are even lower than Bates' estimates, they are not acceptable. It is probable that the "gradient" of the loss coefficients δ and $\int$ have too large a value.

It is noted that the method of applying the theory deals only with the shape of the layer. It is not necessary to make any assumptions regarding the absolute values of the loss coefficient, but only the manner in which it decreases with height. In the F_1 layer, again no assumptions are made as to the value of the loss coefficient. In this case the scale heights deduced are at least twice as high as those for the F_2 layer. In addition, there is some evidence for an increase in temperature towards midday. The main point, however, is that the scale height appears to decrease with increasing altitude which is contrary to any model atmosphere yet proposed. For even if the temperature were constant in the F region as a whole, the mean molecular mass must decrease due to dissociation at higher altitudes causing an increase in the scale height. One can only conclude that the temperature decreases from the F_1 to the F_2regions. The more likely explanation seems to be that the values of δ and $\int$ deduced from the eclipse measurements are wrong. The value of $\int$ deduced by RATCLIFFE et al (1956) is 0.02 km^{-1}, and is more reliable than that

deduced from the eclipse measurements, since it is the mean of many readings at several places during different seasons and epochs of the solar cycle.

Taking β to be 0.02 km^{-1}, the control readings were applied in Case III again. However, Fig. 85 has to be redrawn for this different value of β. The resulting plots of $\log_e\left(\frac{n_3}{N_3}\right)$ versus $(h_{M3}-h)$ for different values of H are shown in Fig. 86. The control values were then applied as before and the resulting values of H are shown in Table 32.

Time	H(h=240 km)	H(h=260 km)	Mean H(km)
0700	39.2	35.0	37.1
0800	41.0	39.0	40.0
0900	41.4	40.0	40.7
1000	39.3	40.9	40.1
1100	40.6	40.0	40.3
1200	40.1	41.2	40.6
1300	40.7	40.4	40.6
1400	39.5	38.3	38.9
1500	38.0	36.4	37.2
1600	39.0	38.5	38.8
1700	38.3	36.3	37.3

Table 32: Values of H for β = 0.02 km^{-1}, F layer in Case III

The values deduced for β = 0.02 km^{-1} are somewhat higher than those for β = 0.04 km^{-1}, but are more consistent with the R model of Bates. RATCLIFFE et al

(1956) have deduced H = 45 km from F_2 measurements, and the values here are about 5 km lower. If it is assumed that atomic oxygen is the active ion in the F region then according to Bates' R model it will have a scale height of 52 km. N_2 will have a scale height of about 30 km, whereas the mean scale height on the R model is about 33 km. The reduction in the scale height as deduced here is probably due to the fact that some of the N_2 molecules are ionised, causing a reduction in the scale height of the ionisable constituent from that of atomic oxygen. The approximate value of 40 km obtained here would indicate that about 8% of the ions were N_2 ions, which is probably a not unreasonable value, since obviously some N_2 molecules are bound to be ionised. A mean scale height of 45 km would indicate that only about 4% of the ions were N_2 ions. The values of H obtained remain fairly constant throughout the day. Apparently H increases towards midday, but this is probably due to neglect of the term $\frac{dn}{dt}$ in the theory, which is not valid in the early morning or late afternoon. The results also show that the F_2 region approximates to an isothermal atmosphere which is also consistent with the R model of Bates.

However, the scale height is still lower in the F_2 region than in the F_1 region, which does not agree with Bates. This is in all likelihood due to the fact that the F_1 layer does not lie in an isothermal atmosphere, but there is a

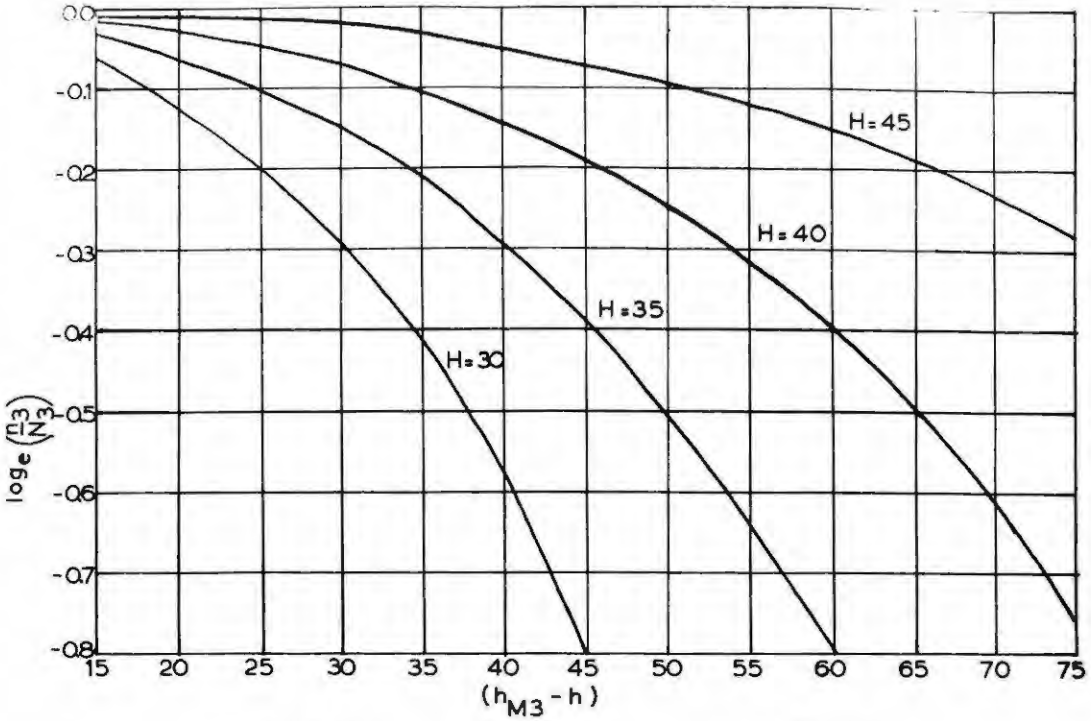

FIG: 86 $\log_e\left(\frac{n_3}{N_3}\right)$ vs $(h_{M3} - h)$ for $\int = 0.02$.

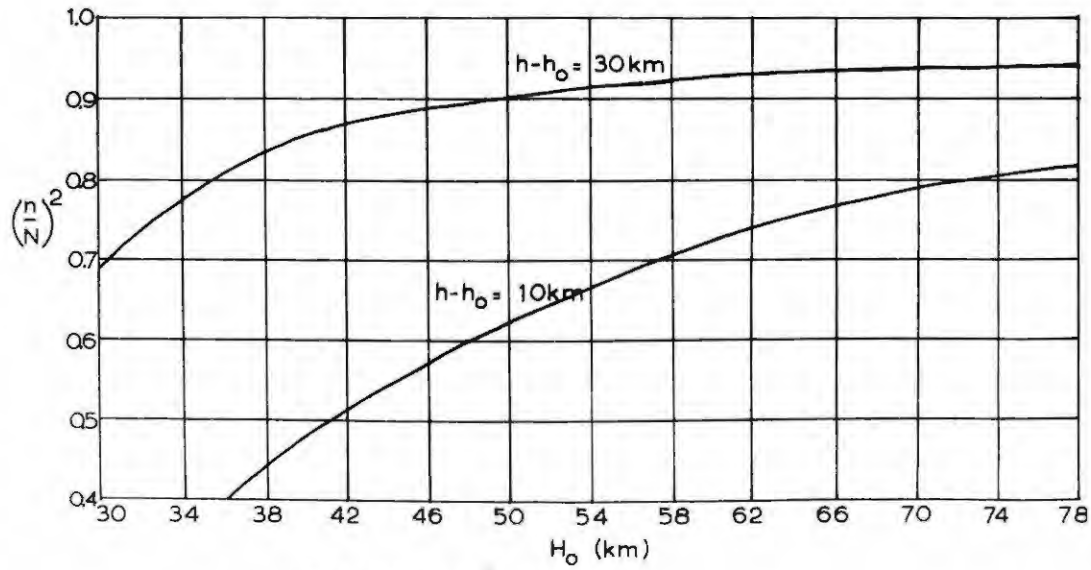

FIG: 87 $\left(\frac{n}{N}\right)^2$ vs H_o

temperature gradient in the layer. The R model of Bates indicates a gradient of 5°K per km in this region. In this case the modified form of Chapman's equations due to GLEDHILL and SZENDREI (1947a, 1950) will apply. To consider how such a gradient will affect the values of H deduced for the F_1 layer, a modified version of Gledhill and Szendrei's theory will be developed and applied to this region.

Temperature gradient in the F_1 layer.

The theory developed by Gledhill and Szendrei does not lend itself easily to the computation of the scale height in an ionospheric layer. The method involves the assumption of a mean molecular mass, with the consequent deduction of the temperature gradient and temperature at the base of the layer. The scale height so deduced thus only applied to the one particular value of the molecular mass. However, the theory can be modified so as to include the scale height and the "scale height gradient", and thus the temperature can be deduced for any value of the molecular mass. It is necessary therefore, to derive the equations of Gledhill and Szendrei on this basis.

Distribution of molecules with height.

The atmospheric pressure p is governed by the statical equation

$$dp = - gn'm \; dh \qquad (131)$$

where m is the mean molecular mass

n' is the molecular density

g is the acceleration due to gravity.

The pressure can also be expressed by the equation of a perfect gas

$$p = n'kT = \frac{\rho}{m} kT \tag{132}$$

where k = Boltzmann's constant

ρ = density of gas

T = absolute temperature

Thus $dp = kTdn' + kn'dT$

and $$\frac{dp}{p} = \frac{dn'}{n'} + \frac{dT}{T} \tag{133}$$

$$= - dh \frac{mg}{kT}$$

$$= - \frac{dh}{H} \tag{134}$$

Since $H = \frac{kT}{mg}$

$$dH = \frac{k}{mg} \quad dT = \frac{Hdt}{T}$$

$$\therefore \quad \frac{dH}{H} = \frac{dT}{T} \tag{135}$$

where m and g are considered to be constant, and from equations (133) and (135)

$$\frac{dn'}{n'} = - \left(\frac{dh}{H} + \frac{dH}{H} \right) \tag{136}$$

Let $$H = H_o + \gamma (h-h_o) \tag{137}$$

where γ = scale height gradient

H_o = scale height at $h = h_o$

$$\therefore \frac{dH}{dh} = \gamma$$

$$\text{and } \frac{dn'}{n'} = -\left(\frac{dH}{\gamma H} + \frac{dH}{H}\right)$$

$$= -\frac{dH}{H}\left(1 + \frac{1}{\gamma}\right) \qquad (138)$$

Integrating this equation gives the height distribution of molecules, i.e.

$$\int_{n_o'}^{n'} \frac{dn'}{n'} = -\int_{H_o}^{H} \frac{dH}{H}\left(1 + \frac{1}{\gamma}\right)$$

where n_o' is the molecular density at height h_o.

Thus $$\log_e \frac{n'}{n_o'} = -\left(1 + \frac{1}{\gamma}\right) \log_e \frac{H}{H_o}$$

and $$n' = n_o' \left(\frac{H}{H_o}\right)^{-(1+1/\gamma)} \qquad (139)$$

Intensity of radiation at height h

Assuming as usual that the radiation is monochromatic, at height h let the intensity be I and at height h + dh, I + dI. It follows that the fraction of I absorbed in passing through height dh is

$$dI = \beta n' I \sec\chi \, dh \qquad (140)$$

where β is the atomic absorption coefficient

χ is the solar zenith distance,

Thus $$\int_{I_\infty}^{I} \frac{dI}{I} = \beta \sec\chi \, n'_o \int_{\infty}^{h} \left(\frac{H}{H_o}\right)^{-\left(1 + \frac{1}{\gamma}\right)}$$

and $$I = I_\infty \exp\left\{\beta n'_o \sec\chi \int_\infty^h \left(1 + \gamma\frac{h-h_o}{H_o}\right)^{-\left(1+\frac{1}{\gamma}\right)} dh\right\}$$

$$= I_\infty \exp\left\{-\beta n_o' \sec\chi\, H_o \left(1+\gamma\frac{h-h_o}{H_o}\right)^{-1/\gamma}\right\} \quad (141)$$

Rate of ion production

Equation (111) shows as before that the rate of ion production q is given by

$$q = \frac{\beta n' I}{w}$$

$$= \frac{\beta I n_o'}{w}\ \frac{H}{H_o}^{-(1+\frac{1}{\gamma})} \exp\left\{-\frac{1}{F}\left(1+\gamma\frac{h-h_o}{H_o}\right)^{-1/\gamma}\right\}$$

$$= A\left(\frac{H}{H_o}\right)^{-(1+1/\gamma)} \exp\left\{-\frac{1}{F}\left(\frac{H}{H_o}\right)^{-1/\gamma}\right\} \quad (142)$$

where $A = \dfrac{\beta I_\infty n_o'}{w}$

and $F = \dfrac{\cos\chi}{n_o \beta H_o}$

Layer formation

In the F_1 layer the electron loss process follows a recombination law and consequently the rate of increase of electron density is given by

$$\frac{dn}{dt} = q - \alpha n^2$$

Assuming again that $\frac{dn}{dt} = 0$,

$$n^2 = \frac{A}{\alpha}\left(\frac{H}{H_o}\right)^{-\left(1+\frac{1}{\gamma}\right)} \exp\left\{-\frac{1}{F}\left(\frac{H}{H_o}\right)^{-1/\gamma}\right\} \quad (143)$$

The maximum value of n occurs when $\frac{dn}{dh} = 0$, so that

$$\frac{dn}{dh} = \frac{n}{2H}\left\{\frac{1}{F}\left(\frac{H}{H_o}\right)^{-1/\gamma} - \gamma\left(1+\frac{1}{\gamma}\right)\right\}$$

$$= 0$$

Thus the condition for a maximum is

$$\frac{1}{F}\left(\frac{H}{H_o}\right)^{-1/\gamma} = 1 + \gamma$$

and the height at which the maximum occurs is thus

$$h_M - h_o = \frac{H_o}{\gamma}\left[\left\{F(1+\gamma)\right\}^{-\gamma} - 1\right] \qquad (144)$$

The corresponding value of n is then given by

$$N^2 = \frac{A}{\alpha}\left\{F(1+\gamma)\right\}^{(1+\gamma)} \exp\left\{-(1+\gamma)\right\} \qquad (145)$$

The resulting equations for h_M, N and n are basically identical to those of Gledhill and Szendrei except that they are now expressed in terms of scale heights.

Application of theory to F_1 layer.

As before it is possible to eliminate the constants A and α by dividing n^2 by N^2, the resulting equation being

$$\left(\frac{n}{N}\right)^2 = \left(1+\gamma\frac{h-h_o}{H_o}\right)^{-\left(1+\frac{1}{\gamma}\right)}\left\{F(1+\gamma)\right\}^{-(1+\gamma)}$$

$$\cdot \exp\left\{(1+\gamma) - \frac{1}{F}\left(1+\gamma\frac{h-h_o}{H_o}\right)^{-1/\gamma}\right\} \qquad (146)$$

This leaves two equations with γ, H_o and F undetermined.

Now the purpose of this section is to determine whether the F_1 layer measurements are also consistent with the R model of Bates. No purpose will be served by an elaborate analysis such as that undertaken by Gledhill and Szendrei. It seems best, therefore, to fix γ at the value given in Bates' R model, thus leaving two equations with two unknowns. It will then be possible to determine values of H_o and compare them with the R model.

It is noted that the value of h_M in the F_1 layer is practically constant through the period 0800 to 1600 hours. In fact, the mean value over this period is 203 km and only varies by $\pm$ 2 km. The analysis is considerably simplified therefore, by taking h_M to be constant at 203 km. A variation of 2 km from this value is within the experimental error in any case.

Equation (144) may be written

$$F = \frac{\left(1 + \gamma \frac{h_M - h_o}{H_o}\right)^{-1/\gamma}}{1 + \gamma} \qquad (147)$$

Substituting this in equation (146)

$$\left(\frac{n}{N}\right)^2 = \left(1 + \gamma\frac{h-h_o}{H_o}\right)^{-(1+1/\gamma)} \left(1 + \gamma\frac{h_M - h_o}{H_o}\right)^{(1+1/\gamma)} \cdot \exp\left\{(1+\gamma) - \frac{(1+\gamma)\left(1+\gamma\frac{h-h_o}{H_o}\right)^{-1/\gamma}}{\left(1+\gamma\frac{h_M-h_o}{H_o}\right)^{-1/\gamma}}\right\} \qquad (148)$$

Taking h_o = 150 km, a graph of $\left(\frac{n}{N}\right)^2$ versus H_o may be plotted for any particular value of h. Two values of h were chosen, h = 160 km, and h = 180 km.

From Bates R model the scale height gradient for a mean molecular mass of 22, gives γ = 0.2 between 150 and 200 km.

Equation (148) then reduces to

$$\left(\frac{n}{N}\right)^2 = \left(1+ 0.2\ \frac{h-h_o}{H_o}\right)^{-6} \left(1+\frac{10.6}{H_o}\right)^{6} \exp\left\{1.2 - \frac{\left(1.2\ 1+\frac{0.2(h-h_o)}{H_o}\right)^{-5}}{\left(1+\frac{10.6}{H_o}\right)^{-5}}\right\} \qquad (149)$$

Fig. 87 shows a plot of $\left(\frac{n}{N}\right)^2$ versus H_o for $(h-h_o)$ = 10 and 30. Using the observed values of $\left(\frac{n}{N}\right)^2$, Table 33 shows the values of H_o deduced from Fig. 87.

The resulting values of H_o are not much different from Table 28 which refer to a simple Chapman layer. The values of H_o are far in excess of those on the R model where the greatest value of the scale height would refer to atomic oxygen which at 150 km has a value of about 27 km. The curves of Gledhill and Szendrei show that if such a low value of the scale height is applicable to the F_1 region, then the temperature or scale height gradient must be

Time	H_o (h=160 km)	H_o (h=180 km)	Mean H_o (km)
0800	55.4	37.6	46.5
0900	64.2	61.0	62.6
1000	80.6	78.4	79.5
1100	80.6	71.4	76.0
1200	74.4	80.2	77.3
1300	73.4	73.0	73.2
1400	72.0	55.0	63.5
1500	56.0	61.0	58.5
1600	55.4	52.0	53.7

Table 33: Values of H_o (150 km) for F_1 layer.

correspondingly higher than the value assumed here. This would not be compatible with the R model or with the values deduced for the F_2 layer. The scale height in the F_1 layer would be reduced if one were to assume that α decreased through the layer, but it would require a gradient of much the same as in the F_2 region to reduce H_o to a value compatible with the R model. It is improbable on present knowledge of α in the F_1 region that it decreases very much with height.

Conclusions.

In Part III (a) a theory has been developed which

takes into account the variation of the loss-coefficient with height in a simple Chapman layer. The theory has been applied to the control data for the F_2 region. It was found that if the loss-coefficient were to decrease with height as found from the eclipse measurements, the resulting values of the scale height in the F_2 region are only about a half of the present accepted values. However, the decrease of loss-coefficient with height as deduced by Ratcliffe and his workers gives values of H which agree well with the R model of Bates, deduced by extrapolating rocket measurements. However, in both cases it is found that the temperature must decrease with height above the F_1 layer, which is contrary to any current views. It was thought that the values of H deduced for the F_1 layer were in error due to the assumption of a simple Chapman layer. A slightly modified form of the theory of Gledhill and Szendrei which takes into account a temperature gradient in the layer, was then applied to the F_1 layer. Using the value of the scale height gradient on the R model it was found that the scale height at 150 km did not differ much from that deduced for a simple Chapman layer, and was at least twice as high as that in the R model. The conclusion is therefore the same and shows that the scale height above the F_1 must decrease

with height, which seems to be contrary to current ideas.

Finally, it is worth mentioning that the consistency of the values of H deduced for the F_2 layer on the variation of the loss-coefficient with height according to Ratcliffe et al would appear to indicate that movements in the F_2 region were small. The control period which was analysed here was particularly quiet magnetically. This is consistent with the views of Ratcliffe et al that movements are small on magnetically quiet days.

Summary & Discussion of Parts II and III

In Part II (a) the maximum electron density of each of the three layers was considered and compared with the results expected on simple theory that the sun is a uniformly radiating disc. The resulting curves again show the $N_m - \delta t$ anomaly in the E_1 and F_1 layers which is a feature of almost all eclipse readings. The E_1 layer measurements were considered in detail from several aspects. The conclusions drawn from all of these analyses depend essentially on the assumptions made in each case. It is shown, first of all, that the error introduced by considering only the maximum electron density in the E_1 layer, and consequently assuming that its height is the same as the height of the maximum electron production, is negligible.

An explanation in terms of a temperature variation during the eclipse indicates that the temperature would have to drop to about 3/4 of its value on control days. The surprising result is that the temperature on control days appears to have remained constant throughout the day. This would seem to indicate that the thermal relaxation time in the E_1 layer must be small, as has been shown by BATES (1951). Consequently, a drop in temperature during the eclipse would not be expected.

On the assumption that the sun is not a uniformly radiating disc, but that some of the radiation is concentrated in more active areas on the visible disc. It is found that the intensity and position of the sources which have to be postulated on this hypothesis varies with the value of α chosen. The intensity of the sources varies much more than their position. Little visual evidence of solar activity on the eclipse day can be found for two sources which have to be postulated on the ~~east~~ limb. Application of each of the solar models for different values of α to the measurements made at Cape Town and Johannesburg, shows that the best fit to the observed measurements is for the model corresponding to $\alpha = 1.5 \times 10^{-8} cm^3 sec^{-1}$, with α at all places having that same value. However, the fit to the observed points is by no means perfect.

Extension of this case to include some radiation from outside the visible disc, shows that with a model in which 15% of the radiation is assumed to be coming from outside the disc, only 5 to 10% need be attributed to a solitary sunspot, and $\alpha = 4 \times 10^{-8} cm^3 sec^{-1}$. The fit to the observed points is slightly better than before, but again is by no means perfect. This model is more consistent with solar activity at the time of the eclipse, and a comparison of the results from Khartoum and Ibadan during the 1952 eclipse, shows that

these results also appear to be more consistent with this type of model.

The variation of the recombination coefficient α, due to the presence of two species of ion is also considered, but the $N_m - \delta t$ anomaly cannot be completely accounted for on this basis. However, it is stressed that to neglect this fact may lead to an over-estimate of the amount of radiation coming from outside the disc, or of the intensity of sources on the limb. Again it is necessary to suppose that one of the ions has a recombination coefficient of $10^{-7} cm^3 sec^{-1}$.

Finally, the effect of oblique incidence echoes during the eclipse is mentioned but the conclusion is that should this be of any importance it will lead to higher values of α.

RATCLIFFE (1956) has pointed out that the analyses of Minnis during the 1952 and June 1954 eclipses are the most complete so far. However, Minnis has restricted his analyses to the one single case and has at all times tacitly assumed that all the radiation comes from the visible disc. He assumes further that any departues from the uniform disc theory are due solely to more intense regions on the disc.

Clearly, the conclusions one arrives at in analysing eclipse data depend basically on the assumptions from which one starts. On the analyses of Minnis, the recombination coefficient α, is usually found to lie between 1.0 and

$2.0 \times 10^{-8} cm^3 sec^{-1}$, but it has been shown here that the evidence seems to point in favour of a much higher value of α, and values as high as $10^{-7} cm^3 sec^{-1}$ would appear to be quite possible. The important point seems to be that there is not in the observations themselves enough to decide between any of several different conclusions. The difficulty lies in the uncertainty of the value of α, and it would appear from the analyses presented here that it may possibly be two or three times as high as the values found by Minnis.

In part II (c) the variations of the electron density at various fixed heights in the F_1 and F_2 layers are compared with the variations expected under the alternative assumptions that the process of electron-loss is recombination, or attachment-like. It was found that the predominant loss-process in the F_1 layer follows a recombination law, the coefficient α being independent of height. In the F_2 layer, it was not possible to decide between the two types of process but on theoretical grounds the attachment process is favoured. The coefficients deduced decrease systematically with height, but are somewhat lower than other estimates.

In Part III a theory was developed which takes into account the variation of the loss-coefficient with height on simple Chapman theory of layer formation. Application of the

theory to the control data for the F_2 layer, shows that the scale height in this region remains almost constant throughout the day and points to the fact that the region is possibly an isothermal region,as proposed on Bates' R model. The result also indicates that movements of electrons were small during the day, due in all probability to the low magnetic activity during this period. A modified version of the theory of GLEDHILL and SZENDREI (1947a, 1950) is applied to the F_1 layer, but the resulting values of the scale height at 150 km, are not consistent with Bates' R model, and indicate that the temperature decreases above the F_1 layer.

Application of Chapman's theory to the eclipse measurements on the basis of THOMAS and ROBBINS (1956) appear to show that considerable movement of electrons must have taken place during the eclipse in the F_2 region. Although movements were small on control days, the advent of the eclipse appeared to produce considerable movements. An attempt to explain these movements on temperature changes was unsuccessful. Whether or not these movements have any real significance cannot be certain, for it is again stressed as in the E_1 layer measurements that there is not in the observations themselves enough to decide. If oblique incidence echoes are important then it is apparent that the use of Kelso scaling

during eclipses is not valid. These movements, therefore, might be purely the result of the inapplicability of Kelso scaling.

It seems that in future eclipse measurements, it is important to determine the effect of oblique incidence echoes, for these surely cast doubt on the basic parameter used in all eclipse measurements. This could be done by having at least three fast sweeping ionosounders separated by 10 to 20 kilometers at the corner of a right angled triangle. In addition, as has been indicated by MUNRO and HEISLER (1958), h't characteristics should be recorded on several frequencies.

By this means it should be possible to make allowances for oblique incidence echoes and any travelling disturbances not connected with the eclipse.

Allen, C.W. 1948 Terr. Magn. Atmos. Elec., 53, 433

1956, Solar eclipses and the ionosphere, p. 204 (London, Pergamon Press)

Appleton, E.V., 1930, Proc. Phys. Soc., 42, 321

1932, J.I.E.E., 71, 642

1933, Proc. Phys. Soc., 45, 673

1937, Proc. Roy. Soc., A162, 451

1953, J. Atmos. Terr. Phys., 3, 282

Appleton, E.V., and Barnett, M.F., 1925, Proc. Roy. Soc., A109, 621

Appleton, E.V., and Lyon, A.J., 1955, Physics of the ionosphere, p. 20 (London, Phys. Soc.)

Appleton, E.V., and Naismith, R., 1932, Proc. Roy. Soc. A137, 36

1935, ibid, A150, 685

Appleton E.V., and Ratcliffe, J.A., 1927, Ibid, A115, 291

Baral, S.S., and Mitra, A.P. 1950, J. Atmos, Terr. Phys., 1, 95

Bates, D.R., 1949, Proc. Roy. Soc., A196, 562

1951, Proc. Phys. Soc., B64, 805

1954, Rocket exploration of the upper atmosphere, p. 347 (London, Pergamon Press).

1956 a, Solar Eclipses and the Ionosphere, p. 191 (London, Pergamon Press).

1956 b, ibid, p.184

Bates, D.R., Buckingham, R.A., Massey, H.S.W., and Unwin, J.J., 1939, Proc. Roy. Soc., A170, 322

Bates, D.R., and Massey, H.S.W., 1943, Phil Trans. Roy. Soc., A239, 269

Bates, D.R., and Massey, H.S.W., 1946, Proc. Roy. Soc., A187, 261

1947, Proc. Roy. Soc. A192, 1

Bates, D.R., and McDowell, M.R.C., 1957, J. Atmos. Terr. Phys., 10, 96

Berkner, L.V., 1939, Trans. Wash. Meeting Ass. Terr. Magn. & Elec., p. 502

Berkner, L.V. Wells, H.W., and Seaton, S.L., 1936, Trans. Edin. Meeting Ass. Terr. Magn. & Elec., p.340

Best. J.E., Farmer, F.T., and Ratcliffe, J.A., 1938, Trans. Edin. Meeting Ass. Terr. Magn. & Elec., p. 340.

Best. J.E., and Ratcliffe, J.A., 1938, Proc. Phys. Soc. 50, 223.

Biondi, M.A., 1951, Phys. Rev., 83, 1078

Biondi, M.A., and Brown, S.C., 1949, ibid, 76, 1697

Bonnet, G., Hunaerts, J., and Nicolet, M., 1957, Bull. des Sceances, academic royale des Sciences colonicles, N.S., III, 4

Booker, H.G., and Seaton, S.L., 1940, Phys. Rev., 57, 87

Bradbury, N.E., 1938, Terr. Magn. Atmos. Elec., 43, 55

Breit, G., and Tuve, M.A., 1926, Phys. Rev., 28, 554

Burkhard, O., 1956, Solar eclipses and the ionosphere, p. 69 (London, Pergamon Press)

Byram, E.T., Chubb, T., and Friedman, H., 1953, Phys. Rev., 92, 1066

1954, Rocket exploration of the upper atmosphere, p.274 (London, Pergamon Press).

Chapman, S., 1931 a, Proc. Phys. Soc., 43, 26

1931 b, ibid, 43, 483

1932, Mon, Not. Roy Astron. Soc., 92,413

Chapman, S., 1954, Proc. Phys. Soc., B67, 717

Christiansen, W.N., and Warburton, J.A., 1955, Observatory, 75, 9

Darwin, C.G., 1934, Proc. Roy. Soc., A146, 17

1943, ibid, A182, 152

Delobeau, F., 1953, Ann. Geophys., 9, 317

1954, ibid, 10, 148

Denisse, F., Seligman, P., and Gallet, R., 1947, C.R. Acad. Sci. Paris, 225, 1169

Dominici, P., 1955, Annali di Geofisica, 8, 1

1956, Solar eclipses and the ionosphere, p.26 (London, Pergamon Press).

Eckersley, T.L., 1933, Proc. Roy. Soc., A141, 708

Estraband, S., 1952, C.R. Acad. Sci. Paris, 235, 1521

1953, ibid, 236, 833

Faire, A.C., Fundingsland, O.T., and Aden, A.L., 1954, Phys. Rev., 93, 650

Gerjuoy, E., and Biondi, M.A., 1953, J. Geophys. Res., 58, 295

Gerson, N.C., 1951, Rep. Prog. Phys., 14, 316

Ghosh, S.N., 1944, Proc. Nat. Inst. Sci. of India., 10, 333

Gilliland, T.R., 1942, Nat. Geog. Soc. Solar Eclipse, Ser. No. 2, 88

Gledhill, J.A., 1958, Conference of South African Inst. of Phys. Pretoria, July 23 - 26

Gledhill, J.A., and Szendrei, M.E., 1947 a, PhD. thesis, Rhodes University College.

1947 b, Trans. Roy. Soc. S.A., 31, 315

1950, Proc. Phys. Soc., B63, 427

Halliday, E.C., 1936, Proc. Phys. Soc., 51, 747

Harang, L., 1945, Terr. Magn. Atmos. Elec., 50, 307

Hartree, D.R., 1933, Nature, 132, 929

1952, Numerical Analysis (Oxford, Clarendon Press)

Havens, R.J., Friedman, H., and Hulburt, E.O., 1955,
Physics of the ionosphere, p. 237
(London, Phys. Soc.)

Higgs, A.J., 1942, Mon. Not. Roy. Astron. Soc., 102, 24

Hulburt, E.O., 1938, Phys. Rev., 53, 344

1939, ibid, 55, 646

Kelso, J.M., 1952, J. Geophys. Res., 57, 357

1954, J. Atmos. Terr. Phys. 5, 11

1957, ibid, 10, 103

Kirby, S.S., Gilliland, T.R., and Judson, E.B., 1935
Phys. Rev., 47, 632

1936, J. Res. Nat. Bur. Stand., 16, 213

Kirby, S.S., Gilliland, T.R., Smith, N., and Reyner, S.E.,
1936, Phys. Rev., 50, 258

Landmark, B., and Lied, F., 1956, Elektroteknisk Tidsskrift,
69, 97

Ledig, P.G., Jones, M.W., Giesecke, A.A., and Chernosky, E.J.,
1946, Terr. Magn. Atmos. Elec. 51, 411

Lied, F., 1956, Solar Eclipses and the Ionosphere, p. 21
(London, Pergamon Press)

Lowan, A.N., 1955, J. Geophys. Res., 60, 421

Manning, L.A., 1947, Proc. I.R.E., 35, 1203

Martyn, D.F., 1947 a, Proc. Roy. Soc., A189, 241

1947 b, ibid, A190, 273

Martyn, D.F., 1955, Physics of the ionosphere, p.237 (London, Phys. Soc.)

Martyn, D.F., and Pulley, O.O., 1936, Proc. Roy. Soc. A154, 455

Massey, H.S.W., 1937, ibid, A163, 542

Massey, H.S.W., and Bates, D.R., 1943, Rep. Prog. Phys., 9, 62

Massey, H.S.W., and Burhop, E.H.S., 1952, Electronic and ionic impact phenomena, p.645

McLeish, C.W., 1948, Canad, J. Res., A26, 137

Minnis, C.M., 1952, Nature, 170, 453

1955, J. Atmos. Terr. Phys., 6, 91

1956 a, ibid, 9, 36

1956 b, ibid, 9, 201

1956 c, Solar eclipses and the ionosphere, p.204 (London, Pergamon Press)

1956, d, ibid, p.81

1957 J. Atmos. Terr. Phys., 10, 229

Mitra, A.P., 1952, Ind. J. Phys., 26, 79

Munro, G.H., and Heisler, L.H., 1956, Austr. J. Phys. 9, 343

1958, J. Atmos. Terr. Phys., 12, 57

Murray and Hoag, 1937, Phys. Rev., 51, 333

Naismith, R., 1937, Proc. Phys. Soc. 49, 214

Nakata, Y., 1950, Rep. Ionosphere Res. Japan, 4, 21

Nicolet, M., 1951, J. Atmos. Terr. Phys. 1, 141

Nicolet, M and Mange, P., 1954, J. Geophys. Res., 59, 15

Norton, K.A., 1933, Nature, 132, 676

Osawa, K., 1950, Rep. Ionosphere Res. Japan, 4, 53

Peckeris, C.L., 1940, Terr. Magn. Atmos. Elec. 42, 205

Piddington, J.H., 1951, J. Geophys. Res., 56, 409

Pierce, J.A., 1948, Proc. I.R.E., 36, 8

Pierce, J.A. Higgs, A.J. and Halliday, E.C., 1940a, Nature, 146, 747

1940b, Phys. Rev., 58, 1119

1942, Nature, 147, 701

Ratcliffe, J.A., 1939, Proc. Phys. Soc., 51, 747

1951, J. Geophys. Res., 56, 487

1956, J. Atmos. Terr. Phys., 8, 260

Ratcliffe, J.A., Schmerling, E.R., Setty, C.S.G.K., and Thomas, J.O., 1956, Phil. Trans. Roy. Soc., A248, 621

Rocket Panel, The, 1952, Phys. Rev., 88, 1027

Rydbeck, O.E.H., 1946, Trans. Chalmers, Univ., No. 53

Savitt, J., 1950, J. Geophys. Res., 55, 385

Sayers, J., 1956, Solar eclipses and the ionosphere, p.212 (London, Pergamon Press)

Schafer, J.P., and Goodall, W.M., 1936, Bell, Syst. Tech. J. 15, 162

Schmerling, E.R., and Thomas J.O., 1956, Phil. Trans. Roy. Soc. A248, 609

Seaton, S.L., 1948, J. Met., 5, 204

Seddon, J.C., Pickar, A.D., and Jackson, J.E., 1954, J. Geophys. Res., 59, 513

Shapley, A.H., 1946, Terr. Magn. Atmos. Elec., 51, 247

Stoffregen, W., 1956, Solar Eclipses and the Ionosphere, p.57 (London, Pergamon Press)

Thomas, J.O., and Robbins, A.R., 1956, ibid, p. 94

Thompson, J.J., 1928, Conduction of electricity through gases, Vol. 1. p.38 (C.U.P.)

Tenks, L., 1933, Nature, 132, 101 and 710

Trotter, D.E., and Roberts, W.O., 1955, High altitude observatory Colorado, Rep. NO. HAO - 26

Tukada, T. 1937, Rep. Radio Res. Japan, 7

Vegard, L., 1938, Geophys. Publ. Oslo., 12, No. 5

Wadley, T.L., 1947, C.S.I.R. Report, Series ETR 2

1949, J.I.E.E., pt. III, 96, 483

Waldmeier, M., 1947, Terr. Magn. Atmos. Elec., 52, 333

1955, Zeitschrift für Astrophysik, 38, 143

1956, Solar eclipses and the ionosphere, p.164 (London, Pergamon Press)

Wayrick, A.H., 1955, Physics of the ionosphere, p.1. (London, Phys. Soc.)

Wells, H.W., 1952, J. Geophys. Res., 57, 291

Wells, H.W., and Shapley, A.H., 1946, Terr. Magn. Atmos. Elec. 51, 401